USE OF THESES

SCALING PHOTOSYNTHESIS AND WATER USE

FROM LEAVES TO PADDOCKS

A thesis submitted for the degree of

Doctor of Philosophy

of

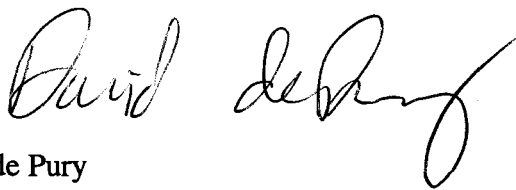The Australian National University

by

David Guillaume George de Pury

December, 1995

Statement

The work presented in this thesis is my own, using data I collected (leaf gas exchange and transect measurements) and data collected in collaboration with Dr. S.C. Wong of ANU (tent data), Dr. A.G. Condon (agronomic and seasonal water use data) and F.X. Dunin (Bowen ratio, lysimeter and meteorological data) of CSIRO, Division of Plant Industry and Drs. O.T. Denmead and R. Leuning (eddy correlation and turbulence data) of CSIRO, Centre for Environmental Mechanics. Contributions from individuals are credited with the description of techniques in Chapter Two.

David de Pury

Environmental Biology
Research School of Biological Sciences
Institute of Advanced Studies
Australian National University
Canberra

Acknowledgments

I thank my main supervisor, Graham Farquhar, for the opportunity to undertake this project through his financial support from an ANU scholarship and a National Greenhouse Advisory Committee (NGAC) grant and particularly for his intellectual rigour and questioning. I also thank my other supervisors, Chin Wong, for his assistance with field work, and Tom Denmead for providing an CSIRO-INRE (Institute of Natural Resources and Environment) scholarship and his revision of chapters.

I thank Frank Dunin and Wybe Reyenga for use of their Bowen ratio and lysimeter data and the general facilities that they provided at the Wagga Wagga field site from a Rural credits grant to GDF. I also thank Tony Condon for use of his agronomic data. I thank both John Evans and Ray Leuning for detailed discussions on drafts and for their encouragement and clear perspective. I thank Win Coupland and Peter Groeneveld for construction of the field equipment and for arranging the donation of the Smart-Modems from Netcomm Australia Pty. I appreciated the patient guidance from Mike Raupach, Helen Cleugh and Margi Böhm through the micrometeorological aspects of the thesis.

I thank Alison MacGregor, Kate Rockpool, Robin Davidson, David Stockwell and Anne Lyon for their encouragement and timely reminders of my abilities.

Finally, my perspective of my Ph.D. experience. From my early life on a mixed farm (sheep/cattle/vineyard) near Melbourne, I completed a B.Agr.Sc (Hons) degree at the University of Melbourne. My final year project supervisor, Prof. David Connor, inspired me to seek a future in computer modelling of crop physiology; a niche that seems to offer many opportunities. After twelve months in South America I decided to take on a Ph.D. and the ANU made a good offer that fitted with my goals.

My objectives for a Ph.D. were to undertake a process of intellectual challenge, which included both intensive numerical and computer modelling approaches to biological systems as well as fieldwork, to keep in touch with reality. I have met my objectives and more. While I expected the work to be difficult, and it was, I didn't anticipate the repercussions it would have on all aspects of my life. It challenged my existence and motivations, but I rediscovered tenacity and found my ability to learn from fundamentals intact. I am glad to be finished. It has been a tremendous learning experience. If I had my time over again, would I still do a Ph.D. with the knowledge I now have? Yes, but so differently!

Abstract

Plant breeders can select cultivars with physiological traits that confer a growth or yield advantage to individual plants. The extent to which single plant characters influence canopy performance depends on interactions between vegetation and the atmosphere and the non-linear response of physiological processes to the environment. Better understanding of the scaling of photosynthesis and water use will allow the assessment of changes to leaf scale physiological traits at the canopy scale and prediction of the response of vegetation to climate change. This thesis examines the relationship between reduced stomatal conductance and canopy scale water-use efficiency (ratio of instantaneous net canopy photosynthesis to total canopy evaporation).

A multi-disciplinary research project was established with two large paddocks of wheat with cultivars of contrasting leaf-scale water-use efficiency, due to inherent differences in stomatal conductance. Intensive measurements were made of CO_2 and H_2O fluxes at leaf and canopy scales. Different stomatal conductances at the leaf scale were reflected at the canopy scale, although their effects on transpiration were reduced due to canopy boundary layers and soil evaporation. Comparison of scaling from leaf to canopy in the two crops was complicated by their different leaf area indices. To facilitate scaling from leaves to canopies, models of stomatal conductance, leaf photosynthesis and radiation penetration in canopies were used.

A comparison of several models of conductance with field data found that using the correlation of conductance with photosynthesis was the best approach. The same model was found to work equally well at the canopy scale, using parameters derived from leaf scale data.

Canopy photosynthesis was modelled with a biochemical model of leaf photosynthesis incorporated into different integration schemes. A canopy model which divided the canopy into a single layer of sunlit and shaded leaves was found to be as accurate as a multi-layer model, but simpler and allowed incorporation of within-canopy profiles of photosynthetic capacity. A big-leaf model of canopy photosynthesis was found acceptable if tuned, but the uncertainties increased when it was used to predict responses of canopies with different properties. Photosynthetic capacity, the main parameter of the canopy photosynthesis model, was found to decrease during the day under conditions of mild water stress at both the leaf and canopy scale.

iv

Combined models of photosynthesis, conductance and energy balance accurately described diurnal variation of canopy gas exchange. The model predicted that a 40% reduction in stomatal conductance would result in 36% greater leaf transpiration efficiency and 19% greater canopy transpiration efficiency (ratio of gross canopy photosynthesis to canopy transpiration) which compared favourably with field measurements, but depended on the magnitude of the conductance and wind speed.

Measurements of air temperature, humidity and surface temperature along a transect across the interface between the two crops with different evaporation rates, showed that advection did occur, but that it had minimal impact on canopy fluxes.

It was concluded that reduced stomatal conductance does result in reduced transpiration and better transpiration efficiency at the canopy scale, but that canopy boundary layers and greater soil evaporation reduce the benefit. In this case reduced conductance was also accompanied by greater yield, although this result depends on the availability of soil water. The models presented were an effective tool for scaling non-linear physiological processes from leaves to canopies and provide a useful framework for assessing the impact of climate change on vegetation.

Contents

List of Figures

List of Tables

List of Symbols

Symbol	Units	Eq.	Description (constants at 25°C)
A	$\mu mol.m^{-2}.s^{-1}$	4.2	CO_2 assimilation rate (subscripts: l-per unit leaf area; c-canopy, per unit gnd area; V-Rubisco limited; J-light limited)
A_d	$mol.m^{-2}.day^{-1}$		daytime canopy photosynthesis (subscripts g-gross; n-net)
a	-	6.23	atmospheric transmission coefficient.
a_l	-	4.2	coefficient of Ball-Berry model.
C_p	$J.mol^{-1}.K^{-1}$	4.16	molar heat capacity of air at constant pressure (29.2).
c	$\mu mol.mol^{-1}$	4.1	CO_2 concentration (subscripts: a-air; i-intercellular; s-leaf surface).
D	m	7.8	damping depth of soil temperature oscillations, $(2\kappa/\omega)^{1/2}$ (0.15).
D	$mm^2.s^{-1}$	-	molecular diffusion coefficient in air (subscripts: v-water vapour (24.9); c-CO_2 (15.1)).
D	$mmol.mol^{-1}$	4.1	leaf-to-air water vapour concentration difference.
D_l	$mmol.mol^{-1}$	5.4	leaf-to-air water vapour concentration difference (1m above the canopy).
D_o	$mmol.mol^{-1}$	5.1	water vapour concentration deficit of the air at the nominal canopy surface.
D_r	$mmol.mol^{-1}$	5.1	water vapour concentration deficit at the reference height (1m above the canopy).
d	m	5.6	zero plane displacement height.
E	$kJ.mol^{-1}$	6.9	activation energy (subscripts: J-electron transport capacity (37); K_c & K_o-Michaelis-Menten constants of Rubisco (59.4, 36); R_c-canopy respiration (57.1); R_l-leaf respiration (66.4); R_s-soil respiration; V-Rubisco capacity (64.8))
E	$mmol.m^{-2}.s^{-1}$	5.5	evaporation rate (subscripts: , BB-derived from the Ball-Berry model; c-canopy transpiration; eq-equilibrium rate; s-soil; T-total evapotranspiration).
E_i	-	6.34	exponential integral.
E_t	min.	6.20	Equation of time.
e	kPa	4.15	water vapour pressure of air (subscripts: a-air; s-saturated).
f	-	6.25	forward scattering coefficient (subscripts: a-atmospheric (0.426); w-walls of tent ()).
f	-	6.26	fraction of diffuse light (subscripts; o-outside; t-tent).

Symbol	Units	Eq.	Description (constants at 25°C)
f	-	6.5	spectral correction factor (0.15).
f_l	-	6.15	fraction of leaf area in a leaf angle class.
f_{Sun}	-	6.44	fraction of leaves that are sunlit (subscript: c-canopy; l-layer; Sh-shaded leaves).
G	-	6.27	leaf area orientation function.
G	$W.m^{-2}$	5.14	ground heat flux.
G_c	$mol.m^{-2}.s^{-1}$	5.4	canopy conductance per unit ground area (subscripts: derived from-, BB-Ball-Berry model; D-evaporation flux/gradient equation; PM-Penman-Monteith equation).
g	-	6.13	distribution function of leaf area orientation.
g	$m.s^{-2}$	5.19	acceleration due to gravity (9.81)
g	$mol.m^{-2}.s^{-1}$	4.1	conductance to water vapour diffusion per unit leaf area (subscripts: b-boundary layer of both sides of leaf; t-total conductance, stomatal and boundary layer).
g_{aH}	$mol.m^{-2}.s^{-1}$	5.8	aerodynamic conductance to heat transfer ($1/r_{aH}$).
g_o	$mol.m^{-2}.s^{-1}$	5.1	intercept of stomatal model regressions.
H	$kJ.mol^{-1}$	6.11	curvature parameter of $J_{m(T)}$ (220).
H	$W.m^{-2}$	4.32	sensible heat flux (subscripts: f-foliage; s-soil)
h	-	4.2	relative humidity of the air at the leaf surface.
h	radians	6.17	hour angle of the sun $15\pi(t-t_o)/180$.
$I(L)$	$\mu mol.m^{-2}.s^{-1}$	6.23	PAR (0.4-0.7 μm) photon irradiance per unit ground area averaged over the horizontal area at depth L (Subscripts: b-beam; d-diffuse; t-tent; e-extra terrestrial; s-net downward scattered; $'$-including scattered light; sh-shaded; sun-sunlit).
$I_f(L)$	$\mu mol.m^{-2}.s^{-1}$	4.1	absorbed PAR per unit leaf area (subscripts: e-light effectively absorbed by PS II; b-beam; d-diffuse; sat-light saturation point of leaf photosynthesis, eq. 6.12; s-scattered; $'$-including scattered light; sh-shaded; sun-sunlit).
I_{lc}	$\mu mol.m^{-2}.s^{-1}$	6.60	absorbed PAR per unit area of canopy (subscripts: sh-shaded; sun-sunlit).
J	$\mu mol.m^{-2}.s^{-1}$	6.3	electron transport rate per unit leaf area (subscripts: m-maximum; T-temperature; 25-25°C).
K		5.16	turbulent transfer coefficient (subscripts: M-momentum).
K	$\mu mol.mol^{-1}$	4.9	Michaelis-Menten constant of Rubisco (subscripts: c-CO_2 (40.4); o-O_2 (24.8×10³)).

Symbol	Units	Eq.	Description (constants at 25°C)
K'	μmol.mol^{-1}	4.11	Effective Michaelis-Menten constant of carboxylation by Rubisco (73.8 at 25 °C).
k		5.6	von Karman's constant (0.41).
k	-	6.30	light extinction coefficient (subscripts: b-beam (0.5); d-diffuse (0.78); '-including scattered light (0.46)).
k	μmol.m^{-2}.s^{-1}	4.7	slope of the A-c_i response curve.
k	μmol.m^{-2}.s^{-1}	6.8	rate constant (subscripts: 25-at 25 °C; T-at T °C).
k	mmol.mol^{-1}	4.19	constant in the hyperbolic function of stomatal response to D.
L	kJ.mol^{-1}	4.17	molar latent heat of vaporisation of water (44.012 at 25°C).
L	m^{-2}.m^{-2}	5.2	cumulative leaf area index from top of canopy (subscripts: c-canopy leaf area index; l-leaf area of a layer; sun-sunlit; sh-shaded).
L_e	degrees	6.22	local longitude of field site (147°20.5' E).
L^M	J.mol^{-1}	5.5	molar latent heat of vaporisation of water.
L_{MO}	m	5.19	Monin-Obukhov stability length.
L_s	degrees	6.22	standard longitude of time zone (150° E).
M	g.mol^{-1}	5.7	molecular weight (subscripts: a-air = 29; w-water = 18; M_w/M_a = 0.622; 1 - M_w/M_a = 0.378).
m	-	6.23	optical air mass (1.5).
N_d	μmol.m^{-2}.sr^{-1}	6.31	diffuse photon radiance of the sky ($I_{d(0)}/2\pi$).
n	-	6.28	unit vector of orientation (subscripts: l-leaf).
O	μmol.mol^{-1}	4.9	oxygen partial pressure (205×10^3).
P	Pa	5.1	atmospheric air pressure (98.7×10^3).
p	Pa	4.9	CO_2 partial pressure (subscripts: a-air; i-intercellular).
Q	W.m^{-2}	4.13	available energy (R_n - G) (subscripts: f-foliage; o-isothermal; s-soil).
Q_{10}	-	6.8	coefficient for 10° increase in temperature.
R	J.mol^{-1}.K^{-1}	6.9	Universal gas constant (8.314).
R	μmol.m^{-2}.s^{-1}	6.1	respiration per unit ground area (subscripts: c-canopy; l-leaf, per unit leaf area; s-soil; (10)-at 10°C).
R	W.m^{-2}	4.13	absorbed radiation (subscripts: IR-infra-red; L-long-wave; n-net radiation; V-visible).
r	s.m^2.mol^{-1}	4.10	resistance to water vapour transfer ($1/g$) (subscripts: b-leaf boundary layer of both sides; s-stomatal).

Symbol	Units	Eq.	Description (constants at 25°C)
r^*_{bH}	s.m^2.mol^{-1}	4.10	combined resistance to radiative and sensible heat transfer in parallel.
r_a	m^2.s.mol^{-1}	5.5	aerodynamic resistance ($1/g_{aH}$) to transfer of (subscripts: H-heat; M-momentum; V-water vapour).
r_c	m^2.s.mol^{-1}	5.5	canopy resistance per unit ground area ($1/G_c$) (subscripts: PM-derived from the Penman-Monteith equation).
S	J.K^{-1}.mol^{-1}	6.11	electron transport temperature response parameter (710).
s	Pa.C^{-1}	4.13	change of saturated vapour pressure with temperature.
T	°C	4.1	temperature (subscripts: a-air; l-leaf; s,z,t-soil at depth z m and time, t; r-reference height; s-canopy surface).
t	day or hour	6.17	time (subscript: d-days since beginning of year; o-time of solar noon).
u_z	m.s^{-1}		wind speed (at height z).
u_*	m.s^{-1}	5.6	friction velocity.
V	µmol.m^{-2}.s^{-1}	4.9	photosynthetic Rubisco capacity (subscripts: c-canopy, per unit ground area; Sun-sunlit leaf fraction; Sh-shaded leaf fraction; l-leaf, per unit leaf area).
W	-	7.9	relative soil water availability.
w	mmol.mol^{-1}	4.34	water vapour concentration (subscripts: a-air; i-intercellular).
w_a'	mol.mol^{-1}	4.34	saturated water vapour concentration of air.
x	-	5.26	momentum stability correction function.
z	m	5.6	height above ground.
z_o	m	5.6	roughness length of surface for turbulent transfer (subscripts: H-heat; M-momentum).
α	radians	6.13	angle to the horizontal (subscript: l-leaf).
β	radians	6.17	solar elevation (subscript: max- midday maximum).
χ_n	mol.mol^{-1}.s^{-1}	6.59	ratio of photosynthetic capacity to leaf nitrogen.
ΔT	°C	4.16	difference between leaf and air temperature outside boundary layer.
δ	radians	6.17	solar declination.
ε	-	4.14	long-wave radiation emissivity (subscripts: $leaf$-leaf (0.95); sky-sky (0.78)).
ε	-	4.17	change of latent content of saturated air with a change of sensible heat ($sL^M/(C_pP)$).

Symbol	Units	Eq.	Description (constants at 25°C)
ϕ	-		stability corrections functions (subscripts: H-heat; M-momentum).
ϕ	radians	6.13	azimuth orientation (subscripts: s-sun).
Γ	$\mu mol.mol^{-1}$	4.8	CO_2 compensation point of photosynthesis (4.4) (subscripts: *-in the absence of mitochondrial respiration (3.69)).
Γ_d	radians	6.20	day angle.
λ	$mol.mol^{-1}$	4.3	a constant value of $\partial E/\partial A$.
λ	radians	6.17	latitude (-35°3.5'π/180 S at Wagga Wagga).
θ	-	4.1	relative leaf water content.
θ	-	6.4	light response curvature factor (subscripts: l-leaf (0.7); c-canopy).
ρ	-	6.38	reflection coefficient (subscripts: l-leaf (0.10); c-canopy; b-beam; d-diffuse (0.036); h-horizontal leaves (0.04)).
ρ_a	$kg.m^{-3}$	5.7	density of moist air.
ΣE	$mol.day^{-1}$	7.10	daily accumulated evaporation.
σ	-	6.37	scattering coefficient ($\rho_l + \tau_l = 0.15$).
σ	$W.m^{-2}.K^{-4}$	4.14	Stefan-Boltzmann constant (5.67×10^{-8}).
τ	$kg.m^{-1}.s^{-2}$		surface shearing stress.
τ_l	-		leaf transmissivity of radiation (0.05).
τ_p	s	7.8	period of temperature oscillation in soil (86400)
Ω	-		canopy-atmosphere decoupling coefficient.
ω	s^{-1}	7.8	angular frequency of temperature oscillation (2π/86400).
Ψ	-	5.6	atmospheric stability integral (subscripts: H-heat; M-momentum; V-water vapour).
ζ	-	5.6	ratio of reference height to the stability length (z/L_{MO}).

CHAPTER ONE:

GENERAL INTRODUCTION

Chapter Contents

1.1. Introduction

1.1.1. Overview

Plants use carbon dioxide (CO_2) from the atmosphere to build sugar molecules, in the process known as photosynthesis, which they ultimately use for growth and metabolism. Allowing enzymes of photosynthesis access to atmospheric CO_2 results in loss of water. If unabated, this loss of water can lead to desiccation and often death of plants. Higher plants have evolved over at least 400 millions of years to cope with this trade-off between water loss and CO_2 uptake (Thomas & Spicer, 1987). Physiologically they have developed vascular root systems, and waxy cuticles on aerially exposed surfaces with pores, called stomata, which regulate the exchange of gases between the inter-cellular space and the surrounding air. At the whole plant level, various growth and development strategies have evolved to cope with periodic drought. The competing objectives of carbon uptake while avoiding desiccation by plants have many implications for our immediate world through both climate regulation and food production.

. Plants are grown for food with often limited water supplies from either rain or irrigation. Better use of this limited resource may enhance food production, particularly in drier regions where food is most needed. Improved varieties of many major food crops are continually being released, with better traits and yields. Efficient utilisation of soil water supplies is one characteristic that has not been extensively exploited by plant breeders, primarily because water-use measurements in conjunction with yield measurements are difficult to make on a routine basis (Richards & Condon, 1993).

A promising alternative approach to direct water-use measurements, is through the use of carbon isotope discrimination (Δ) (Farquhar et al., 1982), which has been shown to be negatively correlated with water-use efficiency of plants grown in pots (Farquhar & Richards, 1984). However, this relationship does not necessarily translate into a correlation with yield in the field. At larger spatial scales it is possible that interactions between the atmosphere and the vegetation, due to the canopy boundary layer, may reduce or even reverse any advantage from more efficient water-use (Cowan, 1988).

To explore the scaling up of water-use efficiency and the interactions between canopies and the atmosphere, a multi-disciplinary research project was established with two large paddocks of wheat with cultivars of contrasting water-use efficiency.

Intensive physical and physiological measurements were made of the canopies, atmosphere and soil. As part of the larger project, the purpose of my work was to examine water-use efficiency at different spatial scales and the interactions with the atmosphere. This involved developing canopy models that incorporated the leaf level physiological processes of photosynthesis and water-use. This scaling of physiological processes from leaves to canopies also has implications for scaling physiological processes to assess global carbon cycling and its role in the mitigation of increasing atmospheric CO_2 concentration. Considering the global implications of this work, the modelling has been kept as simple as possible so that it may be used in the global context.

The following sections of this introduction elaborate on the concept of water-use efficiency and its components of photosynthesis, water-use and interactions with the atmosphere. Each section details the physiological process and its modelling, firstly at the leaf level and then at the canopy level. Inevitably the focus switches back and forth between leaf and canopy levels, but it is the nature of this scaling work, that it requires continual assessment of detail and a broader context. Each of the topics has mostly been covered in great detail in specific reviews, text books and research papers; it is not the intention of this review to repeat them. Rather, the scope of this work is to pull together many different themes of research and synthesise them into a useful framework on which to base the scaling-up of water-use efficiency from leaves to paddocks.

1.1.2. Modelling: A tool for scaling

Both the relationship between carbon isotope discrimination and water-use efficiency and the role of vegetation in global carbon cycling involve issues of scaling, both spatially and temporally. Carbon isotope discrimination occurs as a result of gas exchange at the scale of individual leaves on an instantaneous basis, but is used as a tool to evaluate water-use efficiency of whole crops over periods of several months. Similarly, carbon and water fluxes occur at the leaf scale, but collectively affect the global carbon and hydrological cycles. Both issues need answers, but progress has been slow in this field of integrative science (Berry, 1992).

There are several possible explanations for the dominance of the reductionist approach to science, including; the claimed successes of molecular biology; the difficulty of handling emergent properties at larger scales that can not simply be described from

small scale properties and interactions (Passioura, 1979); the debate of indeterminism versus determinism (Popper, 1982). The work presented in this thesis sets out to be integrative, to apply the successes of reductionism to broader issues, but in a new synthesis of those successes.

In moving between scales it is important to determine which interactions are significant, which should be considered and which can either be ignored or taken as independent variables (de Wit, 1970). While the reductionist approach reduces problems to a few manageable variables within a controlled system, scaling-up involves the integration or synthesis of the interactions of many variables (Norman, 1993). It is difficult to keep track of all such interactions and their relevance as the scope of research expands. Mathematical functions can be used to describe the effects of variables and their interactions in a model of the system. The behaviour of components of such a model can be compared with experiments in manageable systems, and the entire model can be compared with observations at larger spatial scales where experimental manipulations may not always be possible. Ultimately all models are just models or a simplification of a more complex system; otherwise they would no longer be models but a replica of the system itself. So the art or science of modelling is to decide which components are important and need to be included and which can be omitted.

Modelling can also serve to highlight deficiencies or gaps in the understanding of complex systems. In doing so, it can be used to assess the impact of individual components and direct future research to areas that are more likely to affect the system.

An important principle of modelling, as a component of scaling-up (rather than just modelling for whatever reason), is to use simple models developed at one scale, based on mechanistic processes, rather than statistical, empirical or detailed integrative approaches, and to apply these models to larger scales to avoid numerical integration. A mechanistic basis to modelling has several advantages: the extensive knowledge developed at one spatial scale can be extended to another scale; parameters can have physical meanings that can be interpreted at different spatial scales; understanding and familiarity of a system's behaviour can be applied at different scales; a mechanistic model is more likely to be able to make realistic predictions with combinations of variables that were not previously used to develop the model, *ie.*, altered climates, though this is not guaranteed, as new interactions may arise that were not previously apparent. By contrast

empirical or statistical models can be more accurate for particular situations, but are likely to break down very quickly in new situations.

On the other hand detailed integrative models, which consider each component separately and numerically integrate, can be very accurate, but are computationally very time consuming and difficult to parameterise in the detail required (Norman, 1993; Raupach & Finnigan, 1988). A good model for scaling will be based on mechanistic processes at a lower scale, have only the interactions that are relevant at the scale considered, be sufficiently simple that it can be used as a basis for further scaling, while still adequately describing the system with tangible parameters (Baldocchi, 1991).

While both spatial and temporal scaling are important, the focus of this thesis is on the spatial aspects. Temporal scaling, involving plant and crop growth is another important aspect, which is only considered in passing, not in detail. Agronomic aspects were covered by others involved in the project (Condon & Richards, 1993). The remainder of the introduction considers, in turn, regulation of water use and photosynthesis by plants, their scaling from leaves to canopies, water-use efficiency at leaf and canopy scales and the effect of vegetation-atmosphere interactions.

1.2. Water-Use

Water-use by vegetation can be considered at many different spatial and temporal scales: from the molecular perspective; as gas exchange from leaves and canopies; as crop water-use by agronomists; and in water catchment studies by hydrologists. This introduction will only consider water-use as a gas exchange process at the level of individual leaves and canopies. Many excellent reviews are available for information on other aspects (eg.; Jones, 1992, reviews physical aspects at the molecular level; Brutsaert, 1982, reviews the process of evaporation in to the atmosphere and; Stewart & Nielsen, 1990, review evaporation measurement methods).

Evaporation from leaves is known as transpiration. When combined with evaporation direct from the soil it has been called evapotranspiration or more simply total evaporation. In the following sections, leaf transpiration is first considered and then a description of canopy level transpiration and soil evaporation.

1.2.1.   Leaf Transpiration

Water loss from plants involves water moving down a water potential gradient from the soil, through roots, stems, leaves and boundary layer to the free air. At each step there is a gradient of water potential and some resistance to flow. The largest gradient occurs between the leaf and the atmosphere, where plants have developed specialised regulating structures, stomata. By conservation of mass and assuming no change in water content, the flow of water through plants must be equal at all points between the soil and the air. Plants exert the greatest control over water use at stomata on leaves, and this is often used as the point of measurement.

Gas exchange measurements on leaves use the diffusion equation to interpret transpiration in terms of a water vapour concentration difference and resistances (or conductances) across the stomata and leaf boundary layer. Use of the electrical resistance analogy, greatly simplifies the complex interactions between molecules of water vapour, CO_2, air and the walls of the stomatal opening (Cowan, 1977). However, at small stomatal apertures these interactions may not be adequately described by simple diffusion equations (Jarman, 1974; Leuning, 1983).

The leaf-to-air concentration gradient is determined from the humidity of the ambient air and the vapour concentration of the intercellular air spaces, which is assumed to be

the saturated vapour concentration at the measured leaf temperature. Leaf conductance is defined as the transpiration rate divided by the leaf-to-air vapour concentration gradient. It consists of both stomatal and boundary layer components. The boundary layer is the layer of air adjacent to the leaf that is modified by the leaf and its limit is commonly defined as the point at which the properties of the air are 99% of the values in ambient air. In the boundary layer wind speed, air temperature, humidity and CO_2 concentration are changed relative to the ambient air.

Leaf boundary layer resistance can be measured in gas exchange equipment by using leaf replicas made of wet filter paper, equivalent to a stomatal resistance of zero. More general relationships between leaf boundary layer resistance and leaf dimensions and wind speed have been established from metal leaf replicas that are heated electrically and their cooling rate measured (Bird *et al.*, 1960; Monteith, 1973; Grace, 1977). Despite extensive engineering analysis, models of boundary layer resistance do not accurately account for resistances over real leaves, where turbulence regimes are neither completely laminar or fully turbulent (Denmead, 1976), nor are leaf temperatures uniform, and the presence of leaf hairs and leaf curling further complicate matters. In practice, these models give leaf boundary layer conductances that are only about $^2/_3$ of those that are applicable for leaves in canopies (Jones, 1992).

1.2.1.1. Stomatal Conductance

The regulatory role of stomata results in their aperture responding to the environment in a complex manner (for recent reviews see; Zeiger *et al.*, 1987; Mansfield *et al.*, 1990; Grantz, 1990). Mechanistic models of stomatal behaviour have been too complex to be of use on a routine basis (eg.; Penning de Vries, 1972). Instead, stomatal behaviour has been successfully modelled empirically by a series of response functions to individual variables developed in controlled environments as proposed by Jarvis (1976). While the Jarvis stomatal model has been successfully applied to many data sets, there is often a considerable amount of unexplained variation in stomatal conductance (eg.; Kim & Verma, 1991b). Another modelling approach has been to consider the optimization of carbon gain with respect to water-use (Cowan, 1977; Cowan & Farquhar, 1977). This teleological approach, while very attractive for explanation of stomatal behaviour, has no mechanistic basis and further is not easily used for predictive purposes (Cowan, 1986). The observed correlation between stomatal conductance and leaf photosynthesis (Wong *et al.*, 1979) has been the basis for other stomatal models first proposed by Ball *et al.*,

(1987) and subsequently modified by others (Collatz *et al.*, 1991; Leuning, 1990; 1995). While this latter type of model is not mechanistic in the strict sense; it does take into account the duality of stomatal behaviour in regulating both water loss and CO_2 diffusion.

Most of these stomatal models have been developed from data sets obtained in controlled environments. Comparison of the models with field data may suggest which approaches are more successful.

1.2.2.   Canopy Evaporation

The above discussion of leaf transpiration is based on measurements in gas exchange systems. These systems usually involve enclosing the leaf in a well ventilated chamber, at an imposed temperature and humidity. In such systems the leaf boundary layer conductance is large and the transpiration rate has little effect on the conditions. However, leaves in the real world are often less well ventilated so that boundary layers have a significant effect on the transpiration rate. The air within the boundary layer is humidified and the leaf temperature departs from air temperature, either increasing or decreasing depending on the leaf energy balance, causing the vapour concentration gradient to change. It is apparent that in the real world transpiration is affected by both stomatal and boundary layer conductances.

Another perspective on transpiration is that it involves two processes: the phase change from liquid water to vapour; and diffusion of water vapour away from the evaporating surface. The first process, conversion from liquid to vapour, requires considerable energy known as the latent heat of vaporisation (44 $kJ.mol^{-1}$). This energy component of transpiration implicates the leaf energy balance as an integral part of transpiration. Through the leaf energy balance, stomata play a significant role in the partitioning of the energy of incident radiation into either sensible or latent heat.

The presence of the boundary layer reduces the transpiration rate in comparison to the rate that would be obtained if there were no boundary layer. In effect the boundary layer provides a negative feedback for transpiration, so that if stomata open incrementally, humidification of the air adjacent to the leaf and cooling of the leaf reduce the effect this change in stomatal conductance has on transpiration. As the scale of observation of transpiration increases from a single stoma to individual leaves, to canopies, to extensive regions, this feedback becomes more pronounced (Jarvis &

McNaughton, 1986). This only occurs if the change in stomatal conductance is uniform. The feedback through the effect of the boundary layer does not occur if the change is isolated to an individual.

While transpiration from isolated leaves can be adequately described by the diffusion expression, since leaf temperature is usually measured, transpiration from leaves in canopies requires consideration of both diffusion and the leaf energy balance. The dual processes of vaporisation and diffusion were first considered in an evaporation model by Penman (1948) and Penman & Schofield (1953). Their work was extended to include evaporation from vegetation by incorporation of a canopy conductance, in what became known as a big leaf model (Monteith, 1963; 1965; Thom, 1972). The Penman-Monteith model has been extensively used to describe evaporation from many different vegetated surfaces (Black *et al.*, 1989), despite the approximations involved (Finnigan & Raupach, 1987; McNaughton & Van den Hurk, 1995; Raupach, 1995). Subsequent modification led to the now widely used Penman-Monteith equation (Monteith, 1963; Thom, 1972; Cowan, 1977).

Multi-layer models of canopy transpiration have been developed (Cowan, 1968b; Shuttleworth, 1976; Lhomme, 1988), but there are difficulties in describing within-canopy turbulent transport. Many models have used *K*-theory, which assumes that turbulent transport is analogous to molecular diffusion in that fluxes occur along concentration gradients. Observations of counter-gradient fluxes within canopies have shown that *K*-theory doesn't work in canopies where fluxes are dominated by infrequent gusts of wind (Denmead & Bradley, 1985). Alternative theories of turbulent transport, which rely on higher-order closure (Meyers & Paw U, 1987b; Meyers & Paw U, 1987a; Paw U & Meyers, 1989) or Lagrangian schemes (Raupach, 1989), are being developed to more accurately describe the turbulence and concentration profiles, but their complexity remains a limitation to their use on a routine basis (Raupach & Finnigan, 1988). Comparisons of models using *K*-theory with those using the more physically realistic Lagrangian models of canopy turbulence have shown that errors from use of *K*-theory are negligible in practice in sparse canopies (Dolman & Wallace, 1991) and that use of resistances based on *K*-theory in a 2 layer model of soil and canopy evaporation are adequate (McNaughton & Van den Hurk, 1995; Van den Hurk & McNaughton, 1995). Definitive comparisons of predictions from *K*-theory with Lagrangian models have not been conducted, so despite the known flaws of *K*-theory in some situations it is still often used in practice.

1.2.2.1. Soil Evaporation

Water loss by canopies arises from both transpiration and evaporation direct from the soil. The soil component of evaporation is not under direct plant control, but is affected indirectly by the quantity of radiation that penetrates through the canopy to the soil surface. Soil evaporation also depends on many other factors, including: canopy leaf area, radiation penetration through the canopy, wetness of the soil surface, hydraulic conductivity of the soil and wind speed beneath the canopy.

When the soil surface is mosit, soil evaporation can be considered to be dependent on the available energy (Black *et al.*, 1970; Ritchie, 1972) and the surface mositure is replenished from soil water further down the profile. Evaporation continues in this manner as long as there is sufficient soil water and it can move to the surface fast enough to maintain the surface as mosit. When the supply of water from below is not sufficient the surface dries out, so that the point of evaporation moves deeper into the soil. This surface layer of dry soil offers further impedance to the diffusion of water vapour into the atmosphere, reducing the evaporation rate. The net result is that the rate of soil evaporation is rapid while the surface is wet and then declines as the surface dries.

Although some aspects of the physics of soil evaporation are fairly well understood, the complex and heterogeneous nature of soil has made it difficult to develop mechanistic models that can be used to predict bare soil evaporation (see recent review by; Jalota & Prihar, 1990). Presence of canopies over the soil adds even more difficulty to modelling evaporation from soil. Even obtaining separate measurements of soil evaporation and canopy transpiration is not easy.

Measurements of soil evaporation from beneath canopies have been achieved using mini-lysimeters (eg.; Leuning *et al.*, 1994). This approach is very labour intensive to get sufficient replicates and does not give temporal resolution better than daily soil evaporation. Simple estimates of soil evaporation can be obtained using the method of Cooper *et al.* (1983). This involves adjusting bare soil evaporation measurements by the radiation penetration through the canopy. Although crude this method is widely used by agronomists.

Canopies with complete or nearly complete cover, intercept most of the radiation so that soil evaporation is likely to be a small component of the total evaporation. If rain is infrequent and the soil surface dry then soil evaporation is often assumed to be insignificant and ignored. In canopies with intermediate levels of ground cover, simple

11

models are used to predict soil evaporation (eg.; Black *et al.*, 1970; Ritchie, 1972), which is added to canopy transpiration do obtain total evaporation. When soil evaporation is a larger component of total evaporation, in sparse canopies, it has been included in two-layer evaporation models (Shuttleworth & Wallace, 1985), although, realistic parameterisation of these models is difficult.

1.2.3. Scaling Conductance and Evaporation

Scaling conductance and evaporation from leaves to canopies has received considerable attention recently in recognition of the importance of the energy balance at the land-atmosphere interface in determining climate and its representation in general circulation models (Carlson, 1991; Ehleringer & Field, 1993). Several recent reviews have laid excellent groundwork for research into the scaling of conductance (Baldocchi, 1991; Baldocchi, 1993; Kelliher *et al.*, 1995). Actual experiments to test scaling principles, with data at both leaf and canopy levels as well as canopy leaf area, are far scarcer than discussion in the literature would suggest.

Much of the early field work with porometers was confounded by systematic biases in non-ventilated diffusion porometers (Körner *et al.*, 1978), incorrect interpretation of data from viscous flow porometers and lack of attention to variation of stomatal conductance within canopies. Spot measurements of stomatal conductance in canopies have often been assumed to apply to all leaves in a canopy (eg.; Monteith, 1965). In several experiments, it was probably fortuitous coincidence that the product of stomatal conductance by canopy leaf area matched the canopy conductance derived from the inverted Penman-Monteith equation.

In a comparison of scaling methods, Rochette (1991) found that simple scaling techniques such as multiplying by the canopy leaf area overestimated canopy conductance. Separate consideration of the conductance of sunlit and shaded leaves and their leaf area improved the scaling to the canopy, but use of a light penetration model and the leaf angle distribution was the best approach to scaling conductance from leaves to canopies. In another study, Kim & Verma (1991b) used leaf measurements to parameterise a model of stomatal conductance and found that driving the model with the average light of the sunlit and shaded fractions and weighting by the respective leaf areas gave good agreement with the canopy conductance under well-watered conditions, but overestimated canopy conductance under water-limiting conditions, since soil water

content was not used as a parameter. A companion paper (Kim & Verma, 1991a) showed that utilising the correlation between stomatal conductance and photosynthesis (Wong *et al.*, 1979) substantially improved the scaling of conductance from leaves to canopies under the water limiting conditions. This suggests that the stomatal model of Ball *et al.* (1987), which is based on the correlation between conductance and photosynthesis, may be a useful tool in the scaling of conductance.

1.3. Carbon Dioxide Fluxes

Carbon accumulation in vegetation involves exchange of carbon with both the atmosphere and the soil. Carbon is fixed in green parts of plants (predominantly leaves) from atmospheric CO_2 by photosynthesis during the day. Metabolic processes in all plant parts continue both day and night releasing CO_2 back to the atmosphere. CO_2 fluxes also occur from the soil as a result of microbial activity and root respiration. Each of these components are considered separately at both the leaf and canopy scale.

1.3.1. Leaf Photosynthesis

Photosynthesis is the dynamic process of CO_2 fixation into sugar molecules that is driven by energy from absorbed light. The rate of photosynthesis varies in response to both environmental and biotic factors. Many experiments have shown the non-linear response of photosynthesis to light, CO_2 concentration, temperature. The rate of photosynthesis also varies with plant nutrition, leaf age, growth environment and between species (see reviews; Berry & Björkman, 1980; Björkman, 1981).

Many mathematical models have been used to describe leaf photosynthesis, that vary in form depending on the application. Several empirical equations have been used to describe observations of the response of leaf photosynthesis to light, CO_2 concentration and temperature with varying degrees of success (see review in Chapter 4 of; Thornley, 1976). Ease of mathematical manipulation and integration are often criteria in choice of models. Empirical models are often adequate for interpretation or analysis of observations, but are of limited use for predictive purposes because their empirical nature limits the biological interpretation of the parameters.

Another approach has been to consider the biochemistry of the photosynthetic process and model the rate limiting steps (Farquhar et al., 1980). This model considers photosynthesis to be either Rubisco (ribulose bisphosphate carboxylase/oxygenase) limited or RuBP (ribulose bisphosphate) regeneration limited. The Rubisco-limited rate is described by Michaelis-Menten type reactions of CO_2 and O_2 with RuBP and Rubisco; while RuBP regeneration is described by light driven electron transport (for more details see; Farquhar & von Caemmerer, 1982; Woodrow & Berry, 1988; von Caemmerer et al., 1994). The apparent complexity of these models is simplified by the fact that many of the parameters do not vary between plants, but are in fact common features of

Rubisco found in all plants. This model has been validated by many experiments (von Caemmerer & Farquhar, 1981; Brooks & Farquhar, 1985; Kirschbaum & Farquhar, 1984) and is now widely accepted. Successful application of this photosynthesis model requires coupling with a stomatal diffusion model and a leaf energy balance.

1.3.1.1. Leaf Respiration

Respiration is the CO_2 release from mitochondria by the oxidation of carbohydrate. During daylight CO_2 released by respiration can be refixed by photosynthesis, so that respiration of photosynthetic tissues in the light is difficult to determine. Gas exchange of leaves in the dark measures respiration since no photosynthesis occurs. It has been argued that, in the light, ATP reduction is driven directly by electron transport and does not require oxidative phosphorylation, thus reducing leaf respiration in the light (Graham, 1980). Experiments to confirm this all have deficiencies, but it seems likely that leaf respiration is reduced in the light (Brooks & Farquhar, 1985; Kirschbaum & Farquhar, 1987; Amthor, 1989; Krömer, 1995); however see (Azcón-Bieto & Osmond, 1983).

Respiration is related to the metabolic activity of the tissue, so that growing tissues have much higher specific respiration rates than mature tissues (Amthor, 1989). Respiration rates of expanded leaves have been related to leaf nitrogen content (Hirose & Werger, 1987b), which is often incorporated into models so that leaf respiration is proportional to leaf photosynthetic capacity (Farquhar et al., 1980; Collatz et al., 1991). More detailed analysis of leaf respiration is not warranted since in the context of the carbon budget of the canopy, leaf respiration is relatively unimportant as leaves comprise only a small proportion of the canopy biomass (Amthor, 1989).

1.3.2. Canopy CO_2 Fluxes

Canopy carbon gain consists of carbon uptake by photosynthesis in leaves and respiratory losses from leaves, stems, roots and developing grain if present. There is a CO_2 flux from the soil, derived from root and microbial respiration.

Several techniques are available for measuring net CO_2 from canopies, utilising both chambers or micrometeorological approaches. Several recent reviews have described chamber techniques for leaf (Field & Mooney, 1990) and canopy CO_2 flux measurements (Reicosky, 1990; Garcia et al., 1990). Several comparisons of chambers with other flux

measurement techniques have demonstrated that despite the problems of the altered environment inside chambers they can be a useful measurement technique (Reicosky *et al.*, 1983; Dunin *et al.*, 1989b; Dugas *et al.*, 1991; Pickering *et al.*, 1993). Comparisons of micrometeorological techniques (Bowen ratio and eddy correlation) and lysimeters have shown that each of these also have limitations (Held *et al.*, 1990; Dugas *et al.*, 1991; Valentini *et al.*, 1991). Recent reviews have summarised the advantages and disadvantages of each of the techniques (Wesely *et al.*, 1989; Denmead & Raupach, 1993).

1.3.2.1. Canopy Photosynthesis

Canopy photosynthesis is the combined CO_2 uptake by all the leaves in a canopy. The canopy is a highly heterogeneous environment with light intensity varying from 0 to 110 % of the incident light above the canopy, caused by shading and scattering of light by other leaves.

Canopy Structure

The structure of plant canopies is determined by the distribution and orientation of leaves. The horizontal distribution of leaves is affected by the distance between individual plants, so that, for example, the leaves of row crops have a very non-uniform distribution. It is also affected by the individual plant structure, or branching pattern, so that some plants have highly clumped leaves, while others tend to more uniformly distributed leaves. Analysis and modelling of the horizontal distribution of leaves is very complex and will not be considered further here (for more details see; Ross, 1981). Research in this thesis has been restricted to canopies that can be considered homogeneous in their horizontal distribution of leaves.

Vertical distribution of leaves is also highly complex; however less research has been done in this field. High plant density and competition between plants for light results in an accumulation of leaves towards the top of a canopy and less leaves towards the bottom. New leaves are placed in positions of high light in the canopy (Field, 1981) and leaves in low light at the bottom of the canopy are the first to senesce. These vertical distributions are generally not explicitly described in models, but rather included implicitly by using the cumulative leaf area from the top of the canopy as the basis for describing position in the canopy. Cumulative leaf area is a more useful descriptor of

position than height since it is the light environment that produces most variation within the canopy and the light varies as a function of cumulative leaf area.

Orientation of leaves is considered in both horizontal (leaf azimuth) and vertical (leaf angle) aspects. Leaf orientation strongly affects both light absorption by individual leaves and light penetration in the canopy. The azimuthal distribution of leaves in many canopies is near to uniform, so that this component can be ignored. Leaf angle distributions vary widely and are often an adaptive strategy to optimize light absorption or avoid temperature stress (either heat or cold). They can be vertical, horizontal, a fixed angle in between, uniform or ellipsoidal. Wheat and many other crop canopies have leaf angle distributions that are close to uniform (Ross & Nilson, 1967), although there is tendency for leaf angle to be more horizontal deeper in the canopy and more vertical towards the top (Denmead, 1976). A uniform leaf angle distribution means that equal leaf area is oriented to all leaf angles, including both vertical and azimuth. This has also been called a spherical leaf angle distribution, because the leaves can be rearranged to form the surface of a sphere while maintaining their original orientations. This type of distribution means that the light intensity on the leaves is independent of the direction of the light *ie*. the solar position, although solar position does affect the penetration of light through the canopy.

Radiation Penetration and Absorption in Canopies

Radiation entering canopies is either direct beam from the sun or diffuse from the sky and clouds. Beam and diffuse radiation penetrate canopies differently because of the angle at which they enter the canopy. Radiation penetration through the canopy is affected by the projection of the leaves in the direction of the radiation source, which is determined by the leaf-angle distribution. In addition radiation is scattered by the leaves further complicating radiation penetration in canopies. Scattered radiation arises from either reflection or transmission through the leaves. These optical properties of leaves vary greatly with the wavelength, so that photosynthetically-active radiation (PAR, 0.4-0.7 μm) and near infra-red radiation (NIR, 0.7-3.0 μm) penetration and absorption are considered separately.

Early work by Monsi and Saeki (1953) showed that light penetration in canopies could be described by Bouguer's law, as an exponential decrease with cumulative leaf area from the top of the canopy. Much theoretical and experimental work has been done on light penetration for all types of canopies (see; Ross, 1975; 1981; Goudriaan, 1977).

17

While the average irradiance decreases down the canopy, consideration of sunflecks and shaded leaves mean that the instantaneous distribution of light is different to the average irradiance. For example, leaves in sunflecks at both the top and the bottom of the canopy receive the maximum irradiance, though there are more sunflecks near the top than at the bottom. Similarly there are shaded leaves both near the top and the bottom of the canopy, which will receive only diffuse light. Thus while the average penetration of light follows Bouguer's law, the actual distribution of irradiance is more binomial, either sunfleck or shaded.

Distribution of Photosynthetic Capacity in Canopies

Not all leaves in a canopy are the same. New leaves emerge in high light positions at the top of the canopy. In wheat canopies this results in a gradient of leaf age down through the canopy. As leaves age their photosynthetic capacity decreases and leaf nitrogen is remobilised from shaded leaves to leaves in high light positions. Together these phenomena cause leaf photosynthetic capacity to be highest at the top of the canopy and decrease towards the bottom.

Models of Canopy Photosynthesis

From the above description it can be seen that canopies are highly heterogeneous in both the radiation environment and leaf physiological properties. As well, photosynthesis and transpiration modify the air within canopies, so that gradients of temperature, CO_2 concentration and humidity are created. These gradients are usually much smaller than the variation of radiation and physiological properties that exist in canopies (Sinclair *et al.*, 1976). Each leaf in a canopy responds to its local environment. Thus by coupling a leaf photosynthesis model with models of radiation penetration and transport processes within the canopy, the flux from each leaf can be determined and then all leaves summed to give canopy photosynthesis. Such models are known as multi-layer models and have been successfully used to describe canopy photosynthesis (de Wit, 1965; Duncan *et al.*, 1967; Lemon *et al.*, 1971; Norman, 1979). Multi-layered models allow detailed analysis of sources and sinks of fluxes within the canopy, but also require considerable parameterisation to accurately reflect real canopies.

An alternative approach to scaling photosynthesis from leaves to canopies is to treat the canopy as though it were a single big leaf, with properties that match the bulk canopy properties. These models are known as 'big leaf' models. They have the advantage of

being much simpler to parameterise with far fewer calculations, which makes them attractive for embedding in models of larger scale processes such as crop growth or global carbon cycling. The main disadvantage of big leaf models is the errors introduced in deriving the bulk canopy properties (Sinclair *et al.*, 1976; Norman, 1980). In particular, the averaging of the gradients of light and photosynthetic capacity can introduce significant errors because of the non-linear response of photosynthesis to light (Smolander, 1984). Despite these limitations their simplicity is very attractive (Sellers *et al.*, 1992). It remains to be demonstrated how well big leaf models of canopy photosynthesis can reproduce measurements and secondly how useful they are for prediction (Amthor, 1994).

1.3.2.2. Canopy Respiration

Models of canopy photosynthesis account for the gross photosynthesis of a canopy. Measurements of CO_2 fluxes from canopies provide data of net photosynthesis, *ie.* gross photosynthesis less total respiration. This respiration comes from stems, heads and roots as well as from soil microbial activity. In an actively growing wheat crop, from 20 to 60% of carbon fixed during the day is re-released by respiration, depending on temperature and stage of growth (Evans & Rawson, 1970; Denmead, 1976; Gerbaud *et al.*, 1988; McCullough & Hunt, 1993).

Respiration in plant tissues is directly related to the metabolic activity or growth rate of the tissue and also to the carbohydrate status of the leaves (Azcón-Bieto & Osmond, 1983). Expanding leaves, new roots and developing grain are all tissues that have high specific respiration rates (Amthor, 1989). However, the biomass in each of these tissues is not very great so that their contribution to canopy respiration is not very large.

Soil respiration has plant and microbial components. Separation of these components is difficult because the rhizosphere is a very microbially rich environment where the main carbon source is root exudates from the plant. In the absence of plants soil respiration is considerably lower (Monteith *et al.*, 1964).

Microbial degradation of soil organic matter is strongly affected by both temperature and moisture content (Anderson, 1982). Field observations have shown a response of soil respiration to both temperature and soil moisture (Hall *et al.*, 1990; Norman *et al.*, 1992). Respiration from surface litter is often enhanced at night, because dew provides

moisture for microbial activity, but decreases during the day as the litter rapidly dries (Edwards & Sollins, 1973).

Soil is a highly heterogeneous substrate, so that variability in soil respiration occurs at a scale smaller than 15 cm, even in a seemingly uniform field (Rochette *et al.*, 1991). Part of this variability may be due to variation in soil porosity so that even though there is similar respiratory activity, measured CO_2 fluxes can be different. Indeed, the CO_2 concentration in soil air spaces can increase to several thousand ppm (Anderson, 1982). This poses problems for measurement of soil respiration, as small perturbations to the atmospheric pressure can alter the CO_2 flux from the soil (Kanemasu *et al.*, 1974).

Measurement of soil microbial activity and soil organic matter in a laboratory do not usually relate to measurements made in the field (Santrucková & Straskraba, 1991). This discrepancy arises because the contact between microbes and the organic matter is disturbed during sampling, and soil aeration is changed.

Although much research is continuing on respiration in relation to metabolic pathways and its association with physiological processes, understanding of whole canopy respiration is still very limited (Amthor, 1989). In actively growing crops canopy respiration is usually a small component of the total carbon budget, but in mature vegetation the carbon balance is much closer to zero net gain. Whether the carbon budget is slightly positive or slightly negative may have significant implications for global carbon cycling, and the response of the biosphere to climate change. Understanding of canopy respiration is limited but urgently needed.

1.4. Water-Use Efficiency

The stomatal controlled components of water-use efficiency are the instantaneous CO_2 and water vapour fluxes of leaves. The ratio of these fluxes, or the transpiration efficiency, is indirectly related to carbon isotope discrimination. Exploitation of this relationship as a tool in selection for water-use efficiency traits in plant breeding programs depends on the scaling of the instantaneous CO_2 and water fluxes from leaves to long term measurements at the canopy scale. In scaling to the canopy, carbon losses through respiration and water losses from soil evaporation, which are not related to carbon isotope discrimination, also need to be considered. These issues are discussed in more detail in the following sections.

1.4.1. Instantaneous Transpiration Efficiency

Diffusion of CO_2 and water vapour are described by Fick's law and depend on the concentration gradient and the diffusion coefficient. In plant and canopy systems it is simpler to make an analogy with Ohm's law, to express diffusion as the product of a concentration difference and a conductance (g), the reciprocal of resistance ($1/r$), as

$$A = g_c \left(p_a - p_i \right)/P \qquad (1.1)$$

$$E = g \left(e_i - e_a \right)/P \qquad (1.2)$$

where g_c and g are the leaf conductances to CO_2 and water vapour diffusion, respectively, p_a - p_i is the gradient of CO_2 partial pressures between the atmosphere and intercellular airspaces, e_i - e_a is the gradient of water vapour partial pressures between the intercellular spaces (assumed to be saturated at leaf temperature) and the ambient air and P is the total atmospheric pressure.

The ratio of photosynthesis to transpiration follows as (Farquhar & Richards, 1984)

$$\frac{A}{E} = \frac{p_a}{1.6v} \left(1 - p_i/p_a \right), \qquad (1.3)$$

21

where v is the leaf-to-air water vapour partial pressure gradient (e_i - e_a) and 1.6 is the ratio of diffusivities of CO_2 and water vapour in air. It can be seen that the *instantaneous* transpiration efficiency (A/E) is negatively related to the ratio of intercellular to atmospheric CO_2 partial pressures, p_i/p_a.

1.4.2. Carbon-Isotope Discrimination

The nature of carbon isotope discrimination in plants and its relationship to transpiration efficiency and water-use efficiency was recently reviewed in detail (Ehleringer *et al.*, 1993). An overview is given below.

Naturally occurring carbon atoms exist with several different atomic masses known as isotopes. The most abundant (98.9 %) is the carbon-12 isotope (^{12}C). About 1.1 % of all carbon atoms are carbon-13 (^{13}C) and a much smaller fraction are present as unstable radioactive isotopes, such as carbon-14. These carbon isotopes are incorporated into all carbon containing molecules. However, the heavier ^{13}C containing molecules behave differently to the ^{12}C molecules, so that different carbon pools have different isotopic compositions. Mass spectrometers used to measure carbon isotope ratios express compositions as a deviation (δ) from a standard, which for $^{13}C/^{12}C$ has been a fossil belemnite from the Pee Dee formation in South Carolina (denoted PDB). On this scale atmospheric CO_2 has a $\delta^{13}C$ of -8.0 ‰ (parts per mil), while plant material ranges from -8.9 to -30.1 ‰.

In analyses of the isotopic composition of plant material, it is the net isotopic discrimination relative to air (Δ) that is usually used, which is expressed as

$$\Delta = \frac{\delta_a - \delta_p}{1 + \delta_p},$$
(1.4)

where δ_a and δ_p are the relative $^{13}C/^{12}C$ ratios of air and plant dry matter, respectively (Farquhar & Richards, 1984). This measure has the advantage of being independent of the isotopic composition of the standard and of the air.

The heavier ^{13}C atoms have different reaction rates for most molecular interactions compared with ^{12}C, mostly slower (Farquhar *et al.*, 1989a). The net result of slower reactions is a discrimination against the heavier isotopes and an enrichment of ^{12}C in plant material. A simple theoretical analysis, of carbon isotope discrimination against

$^{13}CO_2$ during photosynthesis, partitioned the fractionation into components associated with diffusion (a) and carboxylation (b), ignoring fractionation associated with the boundary layer conductance, photorespiration and respiration (Farquhar $et\ al.$, 1982),

$$\Delta = a\frac{p_a - p_i}{p_a} + b\frac{p_i}{p_a} = a + (b - a)\frac{p_i}{p_a},$$

(1.5)

where p_i is the CO_2 partial pressure in the sub-stomatal cavities and p_a is the CO_2 partial pressure of the air. Direct measurements of discrimination in air passing over photosynthetically active leaves confirmed that discrimination in photosynthesis, against the heavier ^{13}C containing molecules, occurs in gaseous diffusion (a = 4.4 ‰) and carboxylation of ribulose bisphosphate (b = 29.0 ‰) (RuBP) (Evans $et\ al.$, 1986). More careful analysis can attribute isotope fractionation to each step of the carbon fixation pathway in plants (Farquhar $et\ al.$, 1989a).

1.4.3. Scaling Water-Use Efficiency

Extending the instantaneous transpiration efficiency to time scales of plant growth, requires that allowance be made for the proportion of carbon lost by respiration at night and from non-photosynthetic organs (ϕ_c), and the proportion of water loss that is not concurrent with photosynthesis, either by transpiration at night or soil evaporation (ϕ_w), so that whole-plant water-use efficiency (W) is (Farquhar & Richards, 1984)

$$W = \frac{p_a(1 - \phi_c)}{1.6v(1 + \phi_w)}(1 - p_i/p_a).$$

(1.6)

Thus, the relationship between carbon isotope discrimination and water-use efficiency is based on an indirect link through the ratio of intercellular to atmospheric CO_2 partial pressures (p_i/p_a). Combining the above expression with a simple model of ^{13}C discrimination (eq. 1.5) produces the relationship between W and Δ,

$$W = \frac{p_a(b - \Delta)(1 - \phi_c)}{1.6v(b - a)(1 + \phi_w)}.$$

(1.7)

Implicit in extension of this relationship to time scales of plant growth ($ie.$ weeks to months) is an averaging of all the variables involved with both Δ and W. In controlled

environments of glasshouses this presents few problems. In accordance with the theory, a negative correlation between Δ and W was observed in pot experiments with wheat (Farquhar & Richards, 1984) and subsequently with many other species (cited in; Ehleringer *et al.*, 1993).

For this relationship to be of use as a tool in breeding programs selecting for traits of water-use efficiency, a correlation of Δ with total dry matter production in the field is required as well as variation of Δ and W within the varieties, which can arise from differences in photosynthetic capacity or differences in stomatal conductance. However, there are complications when the relationship is applied to field situations where many of the components vary (Hall *et al.*, 1994): ϕ_c changes with phenology; ϕ_w varies with frequency of rain and canopy leaf area; v tends to increase as winter crops mature; and p_i changes with v. Additionally, at larger spatial scales v does not remain a truly independent variable; it is affected by the transpiration rate which partitions energy into either humidifying or heating the air and leaves (Cowan, 1977). This may complicate the relationship between Δ & W if the variation arises from stomatal conductance and evaporation rather than photosynthesis and carbon accumulation.

Contrary to expectations, a positive correlation between grain yield and Δ was observed in field trials of wheat (Condon *et al.*, 1987). Some of the previously mentioned complications were suspected as playing a role, but since water use was not measured in that trial no firm conclusions could be made. Trials with peanuts grown in pots embedded in fields did show a negative relationship between W and Δ (Wright *et al.*, 1988). These results, encouraging as they were, still did not rule out the possible feedback between transpiration rate and v caused by the canopy and leaf boundary layers (Cowan, 1988). These effects were thought to be possible explanations for results from further field trails that showed the correlation between grain yield and Δ was positive in wetter environments but negative in drier environments (Condon & Richards, 1993). Clearly, clarification of these canopy scale feedback effects could only be resolved by large scale field experiments where detailed measurements of carbon gain, water-use and carbon isotope discrimination were made concurrently at different scales.

1.5. Advection

As discussed earlier, the canopy boundary layer causes the air to be modified by the evaporation rate; the air above canopies with higher evaporation rates is more humid and cooler than air above canopies with low evaporation rates, under the same synoptic conditions. This modification of the air reduces the evaporation rate, compared to the evaporation rate that would have occurred if this feedback did not occur. This feedback reduces the sensitivity of evaporation to changes in stomatal conductance. At larger spatial scales the evaporation rate becomes less sensitive to changes in stomatal conductance (Jarvis & McNaughton, 1986).

This phenomenon of evaporation-atmosphere interaction, causes some doubt as to the value of selecting varieties of wheat with improved water-use efficiency through changed stomatal conductance (Cowan, 1988). The insensitivity of evaporation, at large scales, to changes in stomatal conductance suggests that if all crops had improved water-use efficiency through altered stomatal conductance, there would be no reduction in water-use (Jarvis & McNaughton, 1986). Given that variation in water-use efficiency also comes about as a result of changes in photosynthetic capacity, this change of evaporation rate will not occur.

A more immediate problem is the process of selection of wheat varieties with reduced stomatal conductance. It is unknown over what distances these canopy boundary layer effects continue to develop (Itier *et al.*, 1994), so selection of plot size for field trials may be critically important for evaluation of changes in stomatal conductance.

This process of the air equilibrating with vegetation with different stomatal conductance is called advection. It is defined as the horizontal flux of a scalar, *eg.*, heat, humidity, or CO_2. In the analysis and modelling of canopy fluxes discussed in earlier sections, the canopy was assumed horizontally uniform and extensive in all directions, so that it could be assumed that the air was in equilibrium with the surface. However, at the edges of plots this is no longer valid and advection may play a significant role.

Agronomists have had an awareness of edge effects and usually include a border of plants around their field trials, which are discarded in subsequent analyses. However, the basis for choosing the size of the border has often been arbitrary. In many cases where the main edge effects are caused only by an altered light environment, these assumptions

are probably sufficient, but where there is an interaction with the atmosphere as is the case with altered evaporation rates, then small borders may lead to erroneous conclusions.

Several experiments have been conducted where hot dry wind from an arid area blows across an irrigated crop (Rider *et al.*, 1963; Lang *et al.*, 1974). The observed advection is a result of changes in both surface roughness and surface conductance. As expected the air temperature decreases, humidity increases and water vapour deficit decreases with increasing distance downwind from the upwind edge of the irrigated field.

The situation of adjacent paddocks with different stomatal conductance is a less severe change than the arid-irrigation changes; the effect of the interactions between the vegetation and the atmosphere will be more subtle. It is likely that any horizontal gradients of air temperature or humidity will be one to two orders of magnitude smaller than the vertical gradients in the air above the canopy.

Several models have been developed to describe advection at step changes in surface properties, which have recently been reviewed (Brutsaert, 1982; Garratt, 1990; Itier *et al.*, 1994). They describe the development of the new boundary layer, scalar concentrations and fluxes as a function of distance downwind from the leading edge.

1.6. Thesis Hypothesis and Outline

The information presented above outlined the importance of understanding scaling from leaves to canopies for both improved agricultural production and understanding of global carbon and hydrological cycles. Current knowledge about scaling-up water-use efficiency and its components of photosynthesis and water use was reviewed. Concerns about the effect of vegetation-atmosphere interactions on improving water-use efficiency through changing stomatal conductance were also raised. It follows that a better understanding of scaling physiological processes is needed.

The objective of this thesis is to examine the scaling-up of water-use efficiency from leaves to paddocks. The hypothesis is that physiological and physical process operating on individual leaves can be scaled to describe canopy fluxes of CO_2 and H_2O. Many of these processes are non-linear with complex interactions. The hypothesis is tested by examining flux data at different spatial scales, by developing scaling models that can be used to examine the effect of physiological traits at the canopy scale, by examining advection of heat and water vapour as an additional complication at larger spatial scales.

Details of the field site and measurement techniques are presented in Chapter Two. Chapter Three addresses the scaling of water-use efficiency from leaves to canopies by examining flux data at different spatial scales and evaluates the measurement techniques. Further analysis of the flux data is aided by models of stomatal conductance and canopy photosynthesis that are developed in the subsequent four chapters. Chapter Four is an evaluation of several approaches to modelling stomatal conductance of leaves from both laboratory and field data. Chapter Five extends these models of leaf conductance to canopy conductance. Chapter Six compares a big leaf and multi-layer model of canopy photosynthesis and presents an improved simple canopy model, which treats sunlit and shaded leaves separately. Chapter Seven evaluates the sun/shade canopy photosynthesis model with the field data. The models of the previous four chapters are combined in Chapter Eight to examine the component interactions and are assessed with different parameterisation schemes against field data. It also readdresses the scaling of water-use efficiency from leaves to canopies with the aid of the models. Chapter Nine examines the advection issue. Finally, Chapter Ten presents a discussion and conclusions of the entire thesis.

CHAPTER TWO:

MATERIAL AND METHODS

Chapter Contents

Summary

This chapter describes the field site and techniques used in the experiments described in this thesis. A large field site was established at Wagga Wagga, to assess water-use efficiency in the field. Two varieties of wheat were grown, Matong and Quarrion, in adjacent paddocks. They were chosen for their contrasting water-use efficiencies, which was attributable to *ca.* 40 % difference in stomatal conductance.

Fortnightly harvests of the crop were made to measure leaf area and dry matter accumulation. Neutron probe measurements and time-domain reflectometry (TDR) monitored the changing soil water profile. Large lysimeters in each paddock measured evaporation continuously. A weather station continuously recorded meteorological data.

An intensive gas exchange campaign was conducted in the weeks pre- and post-anthesis. Measurements of leaf gas exchange were made with a Li-Cor 6200. Large ventilated chambers (Tents) measured gas exchange from sections of canopy. Bowen ratio systems measured fluxes from each paddock. An eddy correlation system made measurements, but less routinely.

Soil respiration was measured with a specially built chamber attached to the Li-Cor 6200. Soil evaporation was measured with mini-lysimeters beneath the canopy (Leuning *et al.*, 1994).

A system of travelling sensors was used to monitor the environment to detect advection at the interface between the canopies.

2.1. Laboratory Gas Exchange

Plants for gas exchange were grown in 5 litre pots in a glasshouse at Canberra during winter, 1991. Mean maximum temperatures were 26°C during the day and 20°C at night. Pots were flushed with half strength Hewitts solution (Hewitt & Smith, 1975), as modified by (Wong, 1979) (Table 2.1) three times a week. Gas exchange was performed on fully expanded flag leaves. Plants for gas exchange were left in the laboratory over night to equilibrate with room temperature.

Table 2.1 Composition of the nitrate-based Hewitt nutrient solution, which was used to fertilise glasshouse grown plants for laboratory gas exchange measurements.

Nutrients	Concentration (mM)	Micronutrients	Concentration (μM)
NO_3^-	4.0	FeNaEDTA	50
$H_2PO_4^{2-}$	1.33	$MnSO_4 \cdot 4H_2O$	10
K^+	4.0	$ZnSO_4 \cdot 7H_2O$	1
Mg^{2+}	1.5	$CuSO_4 \cdot 5H_2O$	1
Ca^{2+}	4.0	H_3BO_3	50
Na^+	1.33	$Na_2MoO_4 \cdot 2H_2O$	5
SO_4^{2-}	1.5	NaCl	100
Cl^-	8.0	$CoSO_4 \cdot 7H_2O$	0.2

2.1.1. Gas Exchange System

Gas exchange measurements were conducted at Environmental Biology, RSBS, ANU, as described by (Brugnoli et al., 1988) with the modifications described by (Hudson et al., 1992). The main features are described below and in figure 2.1.

A double-sided aluminium cuvette with a glass window was clamped around a leaf so that 2.4 cm² of lamina was exposed to the light and air flow. Independent air flow across the upper and lower leaf surfaces allowed separate gas exchange of each surface. Water circulating through the body of the chamber and embedded electrical heating elements regulated leaf temperature. Combined boundary layer conductance to water vapour transfer for both sides of the leaf was measured at 2 $mol.m^{-2}.s^{-1}$ from the evaporation rate

of a wet filter paper in the chamber. Calculated fluxes from the upper and lower leaf surfaces were combined to give whole leaf gas exchange.

The leaf was illuminated by a 250 W metal halide lamp. An infra-red mirror was place between the lamp and the leaf to reduce the heat load. Variation in light intensity was obtained 1). by varying the distance between the lamp and the leaf, 2). by a series of copper wire screens or 3). by a combination of neutral density filters (Balzer, Liechtenstein).

Ambient air was scrubbed of CO_2 by two 0.8 m soda-lime columns connected in series and an activated charcoal column. CO_2 free air flow was controlled by a mass flow controller. Air was saturated with water vapour through a series of two sintered bubblers in distilled water and then passed through a glass condenser column to set the humidity level. A temperature regulated water bath was used to circulate cooling water through the water jacket of the condenser to set the dew point of the air. A mass flow controller was used to inject 2% or 10% CO_2 in air to give the desired CO_2 concentration. Manual flow valves regulated the air flow to each side of both chambers at 0.8 L.min^{-1}.

Inlet and outlet vapour pressures of the air were measured with a relative humidity sensor (1518HM Humicap, Vaisala) set in an aluminium block. The temperature of the aluminium block was controlled at 35 ± 0.1 °C. The increase in humidity between the condenser and the air from the chamber was used to calculate the transpiration rate. Absolute CO_2 concentration of air before the chamber was measured with an absolute infra-red gas analyser (IRGA) (Fuji electric, model ZAR), while the change in CO_2 concentration before and after the chamber was measured with a differential IRGA (Beckman Instruments, model 865). Constant pressure was maintained throughout the system with overflow bubblers. A manometer was used to measure the pressure of the system with reference to the atmospheric pressure (approx. 350-450 mm of water over-pressure). Air pressure (typically 95 kPa at Canberra) was measured each morning from an aneroid barometer (Mechanism Ltd., Type No. M1991/A).

Leaf temperature was measured with a 100 μm copper/constantan thermocouple pressed against the lower leaf surface. Additional thermocouples measured the condenser and humidity sensor temperatures. Sensors were scanned by an analog to digital board in a standard IBM compatible PC. A chart recorder monitored instrument voltages. Calculations of gas exchange were based on those given by von Caemmerer & Farquhar (1981).
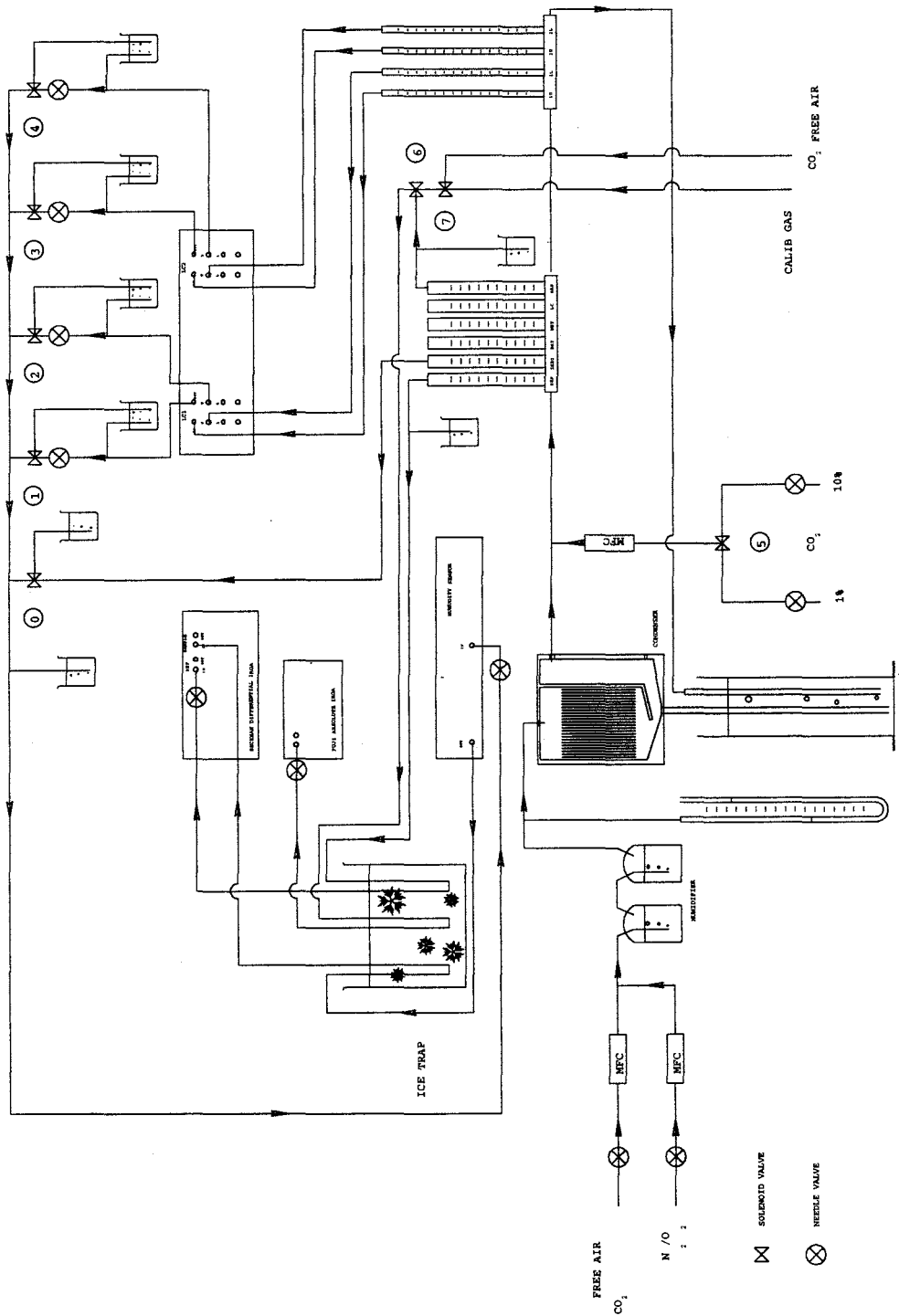
Figure 2.1 Flow diagram of laboratory gas exchange system, set up for concurrently measuring with two clamp-on leaf chambers by switching air streams with solenoid valves.

2.2. Field Site

Field work was conducted on wheat crops grown on 6 ha of land at the Experimental Farm of Charles Sturt University, 5 km north of Wagga Wagga, New South Wales, Australia (35° 3.5' S, 147° 20.5' E, 272 m asl). Wagga Wagga is on the wetter, eastern side of the cropping belt of south-eastern Australia. Land use in the surrounding district is wheat and other winter crops and pasture. The landscape rises to a peak in the east (+30 m), but is nearly flat for several kilometres in the other directions, from which the wind prevails.

The mean annual rainfall is 480 mm, occurring throughout the year, but heavier in winter. The mean rainfall during the growing season (May-November), is 308 mm. Frosts during winter restrict the sowing date for wheat crops, so that they flower after the last frost. Spring weather is characterised by, pre-dawn temperatures of a 1 - 5 °C, clear skies until late morning, followed by patchy cloud for the rest of the day. A diurnal temperature range of 20° is common. Occasionally during grain filling, there were hot days (35°C) with northerly winds before cold fronts moved in from the south-west.

The soil is a red earth. The profile has a disturbed shallow A horizon, a uniform B horizon to 1.80m. A hard layer was observed at 0.9-1.0m, with concretion of calcium carbonate below 1.0m.

2.2.1. Agronomy

Two wheat (*Triticum aestivum* L.) cultivars, Matong and Quarrion, were selected for this experiment from an extensive screening program (Condon, pers. comm.) based on carbon isotope discrimination as an indicator of water-use efficiency (WUE) (Farquhar & Richards, 1984). The cultivars were selected for contrasting WUE, which were derived from differences in stomatal conductance, rather than photosynthetic capacity, while having similar growth habit and development. Cultivar Matong was identified as having low WUE, and cultivar Quarrion has high WUE derived mostly from *ca.* 40% lower stomatal conductance.

Farm staff of the Charles Sturt University were responsible for the ground preparation and maintenance of the crops. A non-selective herbicide (glyphosate) was used prior to cultivation. A fine seed bed was prepared during May with a tyned cultivator.

In 1989 the crop was sown on 28 May. The crop suffered from an infestation of wild oats (*Avena negra*), a common weed of crops.

During the following summer the paddocks were left fallow and the stubble burnt in April, 1990. A pre-emergent herbicide (Triallate) was applied before sowing. The crops were sown on May 22, 1990 (Day 142) at 60 kg.ha^{-1} for cultivar Quarrion and 50 kg.ha^{-1} for cultivar Matong. The different sowing density was an attempt to compensate for the reduced early vigour of Quarrion. Nitrogen was applied at sowing as 130 kg.ha^{-1} of diammonium phosphate (20% P, 18% N). The crop was harvested on 14 December, 1990.

The 1991 crop was sown on 25 May. Post emergent herbicides were applied to the crops at 4 weeks. Selective herbicides were applied at 10 weeks to control wild oats (*Avena negra*). Additional nitrogen 25 kg.ha^{-1} was applied as urea 4 weeks prior to anthesis.

Fortnightly dry matter harvests of 8 × 0.5 m^2 quadrats were made by Dr. Tony Condon of CSIRO, Division of Plant Industry and staff of Charles Sturt University. These were sub-sampled to determine green leaf, dead leaf, stem, head and total biomass, and leaf area index. Final biomass and grain yield were measured at harvest.

2.3. Leaf gas exchange

In the field, leaf photosynthesis and stomatal conductance were measured with a portable photosynthesis system (Li-Cor 6200, Lincoln, NE, USA). The system operates in a closed circulation draw down mode for photosynthesis measurement. Stomatal conductance is calculated from the leaf-to-air vapour pressure difference calculated from leaf temperature, measured with a thermocouple, a humidity sensor and the flow rate of air through a $MgClO_4$ desiccant required to balance the transpiration and maintain a steady water vapour pressure in the chamber.

Accurate measurements with this system require that the leaves have no free surface water from either rain or dew. This limited the commencement of measurements in the morning, since heavy dews were a feature of the Wagga climate. Attempts to dry individual leaves for measurements were not reliable.

Leaves for measurement were selected at random from the youngest fully expanded, sunlit leaves at the top of the canopy. The chamber was enclosed around a 3.6 cm section of leaf that was perpendicular to the sun's rays and maintained at this angle throughout the measurement, thus ensuring that stomata were in an equilibrium state with the light regime. Partially cloudy weather, typical of Wagga Wagga during spring, made accurate measurements difficult due to the rapidly changing light conditions. Measurements were delayed until there had been at least 10 minutes of consistent light (< 10% variation). However despite these precautions, data from partially cloudy days were characteristically more scattered than on clear or overcast days. Several (5-8) replicate measurements were made on different plants of a cultivar before moving to the next cultivar. These measurements were made by myself and on some days by Peter Groeneveld and Mary Grealy of Environmental Biology, ANU.

2.4. Canopy fluxes

Three different canopy flux measurement techniques were used: ventilated chambers, Bowen ratio and eddy correlation as described below.

2.4.1.   Ventilated Chambers

These measurements were made by Dr. Chin Wong of Environmental Biology, ANU. Design and construction of the chambers was by him, Peter Groeneveld and Win Coupland of Environmental Biology, ANU.

Two ventilated chambers were placed over sections of each crop to simultaneously measure canopy gas exchange. Photosynthesis and transpiration were determined by measuring the change in carbon dioxide and water vapour concentrations of air as it was drawn from the ambient atmosphere and passed over the crop enclosed in the chamber. Samples of air from the inlet and outlet manifolds of both chambers were pumped through buried, heated tubing to a shed where the gases were analysed by IRGAs (figure 2.2).

2.4.1.1. Construction

The chamber covered 2.3 m^2 of crop, with a height of 1.25 m at the front, rising to 1.52 m at the rear wall, giving a total volume of approx. 3.2 m^3. The panels were constructed from sheets of 100 μm polyethylene stretched over 2.5 cm aluminium angle as a frame and sealed with a foam gasket. The chamber was attached to a 1.38 × 1.66 m frame of 50×100 mm angle steel that was hammered into the soil for an airtight seal. The southern wall of the chamber was made of clear 2 mm thick acrylic sheet for additional strength to mount four inlet manifolds at the bottom, four outlet manifolds at the top and two 25 cm exhaust fans for mixing. Air was forced into the tent by a 30 cm in-line fan at 200 $L.s^{-1}$ through the four inlet manifolds.

An air stream was drawn for analysis from the inlet and outlet manifolds and pumped at 8 $L.min^{-1}$ through approximately 150 m of buried, insulated 6 mm ID. polyethylene tubing heated with 13.1 $W.m^{-1}$ self temperature regulating (60 °C) heating cable to ensure there was no condensation of water vapour. The pumps were near the chambers

so that all remaining hoses were under pressure to eliminate problems of inward leaks and contamination.
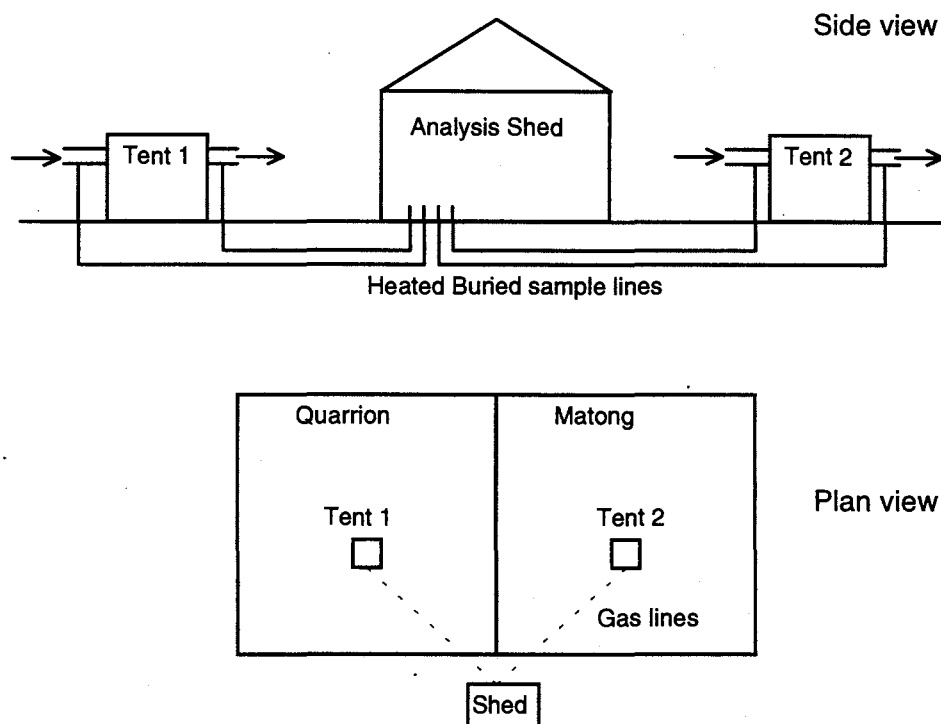
Figure 2.2 Layout of ventilated tents for measuring canopy gas exchange and underground gas lines for air sampling to measure CO_2 and H_2O.

2.4.1.2. Gas Analysis

A high flow rate through the tent was necessary to minimise the temperature increase, but this also minimised the CO_2 depletion and humidification. At maximum rates of photosynthesis a CO_2 differential of 1.2 Pa was observed and a change in water vapour pressure of 0.4 kPa between inlet and outlet air. To accurately measure these small differences a dual channel CO_2 and H_2O IRGA (BINOS, Inficon Leybold-Heraeus, Inc., E. Syracuse, NY) was used in differential mode, whereby the compositions of two air streams are compared by passing one stream through the reference cell and the other stream through the sample cell.

The absolute CO_2 concentration was measured with a single-channel BINOS-1 IRGA in absolute mode, which was checked with a bottle of compressed air of known CO_2 concentration each morning. The actual humidity of the air was measured with a psychrometer consisting of shielded, ventilated, wet and dry platinum resistors (Pt100) outside the tent.

The sample air streams arrived in the processing shed where a system of solenoid valves selected which air stream passed through the IRGAs. After switching between each stream a delay of 70 seconds was allowed for the system to purge. All the sensors were then logged by a Datataker (model DT100, Data Electronics Australia Pty. Ltd.) until thirty measurements were taken in approx. 30 seconds and an average calculated.

At the beginning of each measurement cycle a zero check on the differential IRGA was performed by passing the same air through both cells. Any drift in the zero value was incorporated into the calculations. Inlet and outlet air from the first tent was then measured, followed by air from the second tent and the process repeated with a zero check. In all, each cycle to measure both tents took approx. 12 minutes.

The path of air flow through the different gas analysers is shown in figure 2.3. From the solenoid valves the air was split and passed through the CO_2 and H_2O IRGA in parallel. The analysis of carbon dioxide concentration with an IRGA required a constant known water vapour concentration, which was achieved by passing the air through a water/ice trap. The air stream then split to the absolute IRGA and to the CO_2 differential IRGA. The pressure in each air line was maintained constant and equal by branching the air into a bubbler to provide a constant over-pressure.
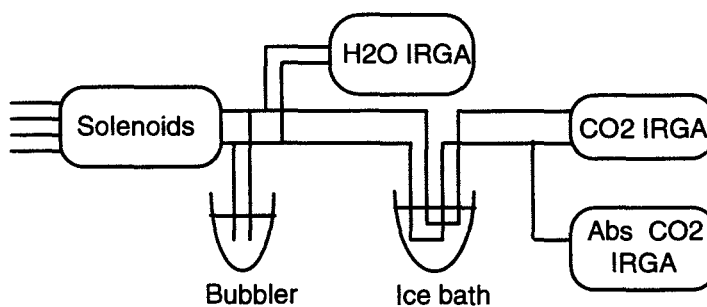
Figure 2.3. Layout of field gas analysis system used to measure canopy CO_2 and H_2O fluxes with the ventilated chamber.

The rate of photosynthesis was calculated from the flow rate through the tents and the CO_2 differential. An accurate measurement of the flow rate through the tent was determined by injecting a known flow rate of pure CO_2 into the inlet airstream before the fan and measuring the resultant increase in CO_2 concentration just before the tent.

Inside each tent was a quantum sensor (Li-190SB, Li-Cor, Lincoln, NE, USA) to measure photosynthetically active radiation (PAR, 0.4 - 0.7μm). Ten thermocouples (Copper/Constantan, 0.1 mm) in parallel were attached to leaves scattered through the canopy to measure leaf temperature. The reference junction of the thermocouples was embedded with a platinum resistor (Pt100) in a small aluminium block (1 × 1 × 2 cm), which was shielded with an aluminium can. The platinum resistor was used to provide the reference junction temperature. A separate thermocouple was used to measure air temperature inside the tent at the top of the canopy. Air temperature and water vapour pressure were measured outside the tent at 1.8 m above ground with aspirated (36 mm diameter fan, 280-360 L.min⁻¹) wet and dry bulb psychrometer using platinum resistors (Pt100) as temperature sensors.

At the commencement of a measurement period, the tent was placed over the canopy, where it remained for several days. Overnight condensation limited the use of evaporation and conductance data from early morning. If rain occurred while the tent was in place the tent was moved to a new site, to ensure that the chamber was covering a truly representative section of canopy.

Calculations for rate of photosynthesis and transpiration were based on the equations for gas exchange presented by (von Caemmerer & Farquhar, 1981).

2.4.2. Bowen ratio

The Bowen ratio technique assumes a zone above the crop where fluxes are constant with height, implying an arealy uniform flux. Measurements were made in the centre of each block to ensure at least 90 m fetch was available. These measurements were made by Frank Dunin and Wybe Reyenga of CSIRO, Division of Plant Industry, as described in detail by (Dunin *et al.*, 1989a).

This technique measures the finite differences of temperature and humidity above the crop and relates their ratio to that of the sensible and latent heat fluxes by the Bowen ratio (β) as calculated from

$$\beta = \frac{PC_p}{L\varepsilon} \frac{\Delta T}{\Delta e}.$$ (2.1)

The latent heat flux (LE, positive upwards) was calculated from

$$LE = \frac{R_n - G}{1 + \beta},$$ (2.2)

where net radiation (R_n) and ground heat flux (G) densities were positive downwards. where P is atmospheric pressure, C_p is specific heat of dry air, L is latent heat of vaporisation, ε is the ratio of molecular masses of water to dry air, and ΔT and Δe are finite differences of potential temperature and vapour pressure measured over a 1 m interval with the lowest sensor between 0.25 - 0.40 m above the canopy in the centre of each plot. Any potential bias in the wet and dry bulb sensors was eliminated by interchanging the upper and lower sensors every fifteen minutes and half hourly averages calculated.

The CO_2 gradient was measured at the same height above the canopy by pumping air to the shed through heated polyethylene tubing (as described for the tents) for analysis in a dual channel CO_2 and H_2O differential infra-red gas analyser (BINOS, Inficon Leybold-Heraeus, Inc., E. Syracuse, NY). The CO_2 gradient, combined with a transfer coefficient calculated from the water vapour transfer, was used to calculate the paddock CO_2 flux. R_n was measured with a net radiometer (Middleton & Co. Pty. Ltd., C.S.I.R.O., Division of Atmospheric Physics, Aspendale, Australia). Ground heat flux was measured with 3 heat flux plates (Middleton & Co. Pty. Ltd., C.S.I.R.O., Division of Atmospheric Physics, Aspendale, Australia) in series buried at 2 cm. No corrections for heat storage in the surface soil layer were made.

2.4.3. Eddy correlation

The eddy correlation technique was used by Dr. Tom Denmead, Dr. Ray Leuning, Alan Jackson and Gary Miller of CSIRO, Centre for Environmental Mechanics to obtain fluxes of CO_2, latent heat, sensible heat and the friction velocity, u_*. The principles of the technique are described in detail in texts such as (Haugen, 1973). Details of the sonic anemometer/thermometer system have been given elsewhere (Coppin & Taylor, 1983). A brief outline is give below.

Material and Methods

Three dimensional sonic anemometers of 20 cm path length were used together with a fine wire platinum resistor for measuring temperature, a Krypton hygrometer (Campbell Scientific, Logan, Utah) for measuring water vapour pressure and an open path CO_2 and H_2O sensor (E009 Advanced Systems Inc, Okayama, Japan). The sensors were logged at 20 Hz and covariances calculated in real time. Corrections for air density due to heat and water vapour fluxes were made using the standard equations (Webb *et al.*, 1980).

2.5. Soil fluxes

2.5.1. Gas exchange chamber

A stainless steel chamber was constructed for use with the Li-Cor 6200 system to measure soil respiration. The dimensions of the chamber (13 × 10 cm) allowed it to be pressed into the soil between the rows of wheat (17 cm spacing) to a depth of approximately 2 cm. The Li-Cor 6200 sensor head was attached to the top of the chamber. A small fan (100 L.min^{-1}) was used to stir the air within the chamber. An electric manometer was used during the initial setup to ensure that the differential pressure between the atmosphere and the chamber was below 10 Pa. Respiration rates were obtained by monitoring the rate of increase in carbon dioxide concentration. After inserting the chamber and placement of the sensor head approximately fifteen seconds was required to mix the air with the system and to observe a steady rate of CO_2 increase. Measurements were made over the next 20 seconds. Five replicate measurements were made under each crop on randomly selected soil.

2.5.2. Mini-lysimeters

During 1990 and 1991 Dr. Ray Leuning, CSIRO, Centre for Environmental Mechanics, measured soil evaporation by manually measuring the weight change in soil cores beneath the canopy. The 1990 trial consisted of measuring weight changes of soil cores over a period of a few days. The cores were encased in approx. 100 mm lengths of 40 mm diameter aluminium tubing and sealed at the bottom with laboratory plastic film (Parafilm, American Can Company). Cores were carried to the shed for weighing three times a day in a covered bucket to minimise water loss while away from the canopy, weighed and then returned to their locations beneath the canopy. After a few days these cores appeared drier than the soil and were replaced with new cores.

(Leuning et al., 1994) describes the more thorough 1991 experiment in detail, but a brief description is given here. At the beginning of the season 120 sleeves of 40 cm lengths of 200 mm diameter polyethylene piping were hammered into the soil in a randomised arrangement across the paddock. Throughout the season eight cores were extracted, sealed at the bottom and weighed at the beginning of each week. The cores were removed from the crop, weighed and returned, three times a day for one week and

then new cores were extracted. Between each weighing the cores were carefully reinserted beneath the canopy to minimise damage to the canopy. New cores were used each week to minimise the deviation in soil moisture content between the cores and the real soil between the canopy.

2.5.3. Neutron probes

Installation of neutron probe access tubes and measurements were made by Dr. Tony Condon of CSIRO, Division of Plant Industry and staff of Charles Sturt University. Details of the procedure are described by (Condon *et al.*, 1993), so only a brief description is given here. Sixteen neutron probe access tubes, of 40 mm diameter aluminium tubing, were installed to a depth of 1.8 m across the paddocks in a regular array shortly after sowing. The tubes were then probed fortnightly until harvest.

Soil water profiles from access tubes beneath the wheat crop were integrated to determine total water-use over the fortnight. Similar tubes were installed on bare land adjacent to the crop, from which bare soil evaporation was determined. The method of Cooper *et al.*, (1983) was used to then estimate soil evaporation from beneath the crop. This method entails measuring radiation penetration though the canopy, which is used as a correction factor to convert bare soil evaporation to soil evaporation beneath the crop. Radiation penetration was measured at midday with a linear ceptometer (Sunfleck Ceptometer, Decagon Devices Inc., Pullman Washington).

2.5.4. Time domain reflectometry

Installation and maintenance of the TDR equipment was by Steve Zegelin and Dr. Ian White of CSIRO, Centre for Environmental Mechanics. Details of the equipment, its installation and operation are given by (Zegelin *et al.*, 1992), but a brief description is given here. Probes were installed at four locations in both crops. Vertical probes were installed from the surface to 10, 20, 40, 50, 60, 80, 100 cm depth and were logged manually approximately once a month through the growing season. Horizontal probes of 53 cm length were installed at 5.5, 10, 20, 40, 60, 80 cm from a pit dug to 1 m. They were logged automatically every two hours from a central computer.

2.5.5. Lysimeters

A weighing lysimeter was installed in the centre of each plot, by Frank Dunin and Wybe Reyenga of CSIRO Division of Plant Industry, who maintained them. Details are given in (Dunin *et al.*, 1991). A monolithic core 2 × 2 m of 1.8 m depth was extracted and sealed with a steel case. A large pit was dug and a beam balance installed in the bottom. The lysimeters were logged continuously by counting the revolutions of a counterbalance required to maintain an equilibrium with the weight.

2.6. Transect Measurements

The two crops with inherently different stomatal conductances were expected to have different rates of evaporation. As the wind blew across the interface between the crops new canopy boundary layer conditions would develop reflecting the interaction between the evaporation surface and the atmosphere. Horizontal gradients of air temperature, humidity and leaf temperature were measured along a transect across the interface between the two crops using a set of travelling sensors. Two different systems were used as described below.

2.6.1. Flying fox

This equipment was designed and constructed by Mr. Peter Groeneveld and Mr. Win Coupland of Environmental Biology, ANU. I operated the system in the field during the spring of 1989 with assistance from Dr. Chin Wong also of Environmental Biology, ANU.

The expected changes in the environmental variables associated with the change in surface conductance between the two crops were very small, their magnitude being similar to the accuracy of the sensors. A series of sensors located at fixed distances from the interface were unlikely to resolve the small changes, since the variability between sensors may be as great as the changes expected. To overcome this dilemma the same sensors were used to measure the variables at all the locations by moving the sensors, since the precision was greater than the accuracy. Thus a system, the "flying fox", was constructed that could move sensors for measuring leaf and air temperatures and humidity along a transect above the crop canopy. Stationary sensors measured net radiation, wind speed and direction.

In creating such a system it was important to consider that the impact on the crop had to be minimal. Damage by trampling would significantly alter the micro environment above the crop. Suspending the sensors from a cable above the crop was a solution that was easy to erect and avoided damaging the crop.

2.6.1.1. Construction

The "flying fox" consisted of a cable strung between two posts 20 m apart, with a small trolley that moved along carrying the sensors. Since the horizontal gradients were 2 orders of magnitude smaller than the vertical gradients it was important to ensure that the height of the sensors above the crop was kept constant. This was achieved by keeping the cable very taut using a system of ratchets attached to the anchor posts at either end and a strain gauge to monitor the tension. The cable was high tensile 4 mm stainless steel, connected to the posts with marine U-bolts. The posts were 2 m lengths of 50 mm galvanised C-section, which were later strengthened with a strip of flat steel (figure 2.4).
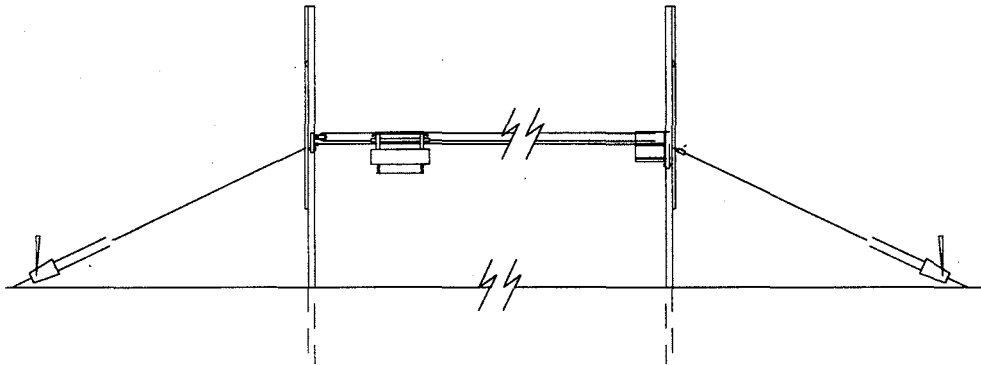
Figure 2.4 The 'flying fox' system of moving sensors; a small trolley with sensors for air and leaf temperature and humidity propelled along a 20 m transect above the crop canopy.

The trolley was a simple, split level, light-weight, aluminium, open platform suspended from the cable by two 50 mm aluminium wheels. A light aluminium roof shaded the instruments from direct solar radiation. The trolley was pulled by a towing cable looped to either end and driven by a windscreen wiper motor powered from a 12 V gel cell. Leads from the sensors were fed through a length of 13 mm nylon self coiling air hose, which was looped around the tension cable. It would stretch out as the trolley moved and recoil as it returned.

2.6.1.2. Sensors

Leaf temperature was monitored with two 15° field of view, infra-red surface temperature sensors (Model 4002, Everest) mounted at 45° to the horizontal, 0.5 m above the top of the canopy. These sensors were powered by a 12 V regulated power supply. Surface temperature was determined from the sum of a detector temperature and a temperature differential. The sensors were calibrated against a black body radiator, with an embedded platinum resistor (Pt100), over a range of temperatures generated by heating and cooling both the radiator and the sensors themselves. Surface radiative temperature was determined as an average of one east facing sensor and one west facing sensor with an assumed crop emissivity (ε_c) of 0.97.

Air temperature was measured with a 100 μm copper/constantan thermocouple referenced to a platinum resistor (Pt100) mounted in an aluminium block. Relative humidity was measured with a humidity sensor (1518HM Vaisala, Humicap). Both the thermocouple and the humidity sensor were mounted in a double shielded psychrometer with a 36 mm fan drawing air up past the sensors at 280-360 L.min^{-1} (approx. 5-7 m.s^{-1}). The humidity sensor was calibrated in the laboratory with an air stream saturated with water vapour at a dew point set on a condensor. The humidity sensor was found to have a different response to relative humidity at different air temperatures, so this was also included in the calibration function.

Distance traversed was measured by an idle wheel with an optical switch, which overcame uncertainties due to slippage on the cable, so that sensors could be scanned at regular intervals along the transect. A datalogger (Datataker DT100, Data Electronics Aust. Pty Ltd.) logged all the moving sensors as well as a Middleton net radiometer (Middleton & Co. Pty. Ltd., C.S.I.R.O., Division of Atmospheric Physics, Aspendale, Australia), a wind vane with an anemometer (model 1010 & 1005 Sierra/Misco Inc.) and two additional anemometers (Rimco 5 cm turning radius, 3 cm diameter cups).

2.6.1.3. Control

Switches at either end of the transect signalled when the fox had completed a traverse. A computer, located in a shed next to the paddock, communicated with the datalogger via an RS-232 cable, receiving data and sending commands to control the direction of the fox. Processed data were displayed on screen as received and stored at the end of each run. Observations were taken approximately every 60 cm and each

traverse took about 90 seconds; thus observations were taken at each location about every 5 minutes.

2.6.2. Mono-rail

This equipment was designed and constructed by Peter Groeneveld and Win Coupland of Plant Environmental Biology, ANU. From the results of 1989 using the "flying fox" system, it was apparent that changes were necessary, so the system was rebuilt and became the "monorail". The measurements and sensors used were the mostly the same, but the system of locomotion changed.

In 1989, the posts for the flying fox system became difficult to install as the soil dried. It was impossible to get sufficient penetration with the posts to support the tension to keep the cable taut. Additional stays and support posts were necessary. After a period of continuous heavy rain, the soil would not support any tension on the posts. In addition, analysis of the data revealed that the air above the crop had not reached a new equilibrium with the changed surface conductance within the length of the transect (20 m). (Finally, a cow entered the field and became entangled in the cables severely damaging the system). At the end of the season it was recognised that the system had become cumbersome and was no longer easy to move or install and there was considerable damage to the crop. A new system was needed.

2.6.2.1. Construction

The monorail consisted of a self-propelled sensor platform that traversed along a steel track erected across the paddock (figure 2.5). The rail was constructed from ten 6 m lengths of 50 × 100 mm galvanised steel C-section roofing beams connected end to end, giving a total length of 54.6 m. The rail was supported at the joints by stands that were made of 35 mm square steel tubing and consisted of three components; a base, a trunk and an adjustable arm, for levelling the rail and for different crop heights. Additional stays of 13 mm steel rod at the centre of each rail section were found to be necessary to prevent the rail from twisting with the weight of the train.

The train was an enclosed light aluminium box 800 × 300 × 40 mm hanging from the rail by two 75 mm diameter wheels. Propulsion was from a reversible roller door motor through a gearing mechanism pressing onto the axle of one of the wheels with an 'O'-ring and powered by a 12 V gel cell battery in the train. As with the 'flying fox', an idle wheel

with an optical counter was used to record the distance travelled. Break switches were mounted on the train at either end and closed when pressed against a block mounted at either end of the rail to mark the return point. These blocks were attached by magnets so they could easily be moved to restrict the train to any particular section of rail, depending on wind direction. Traction on the rail was enhanced by using neoprene 'O'-rings as tyres.
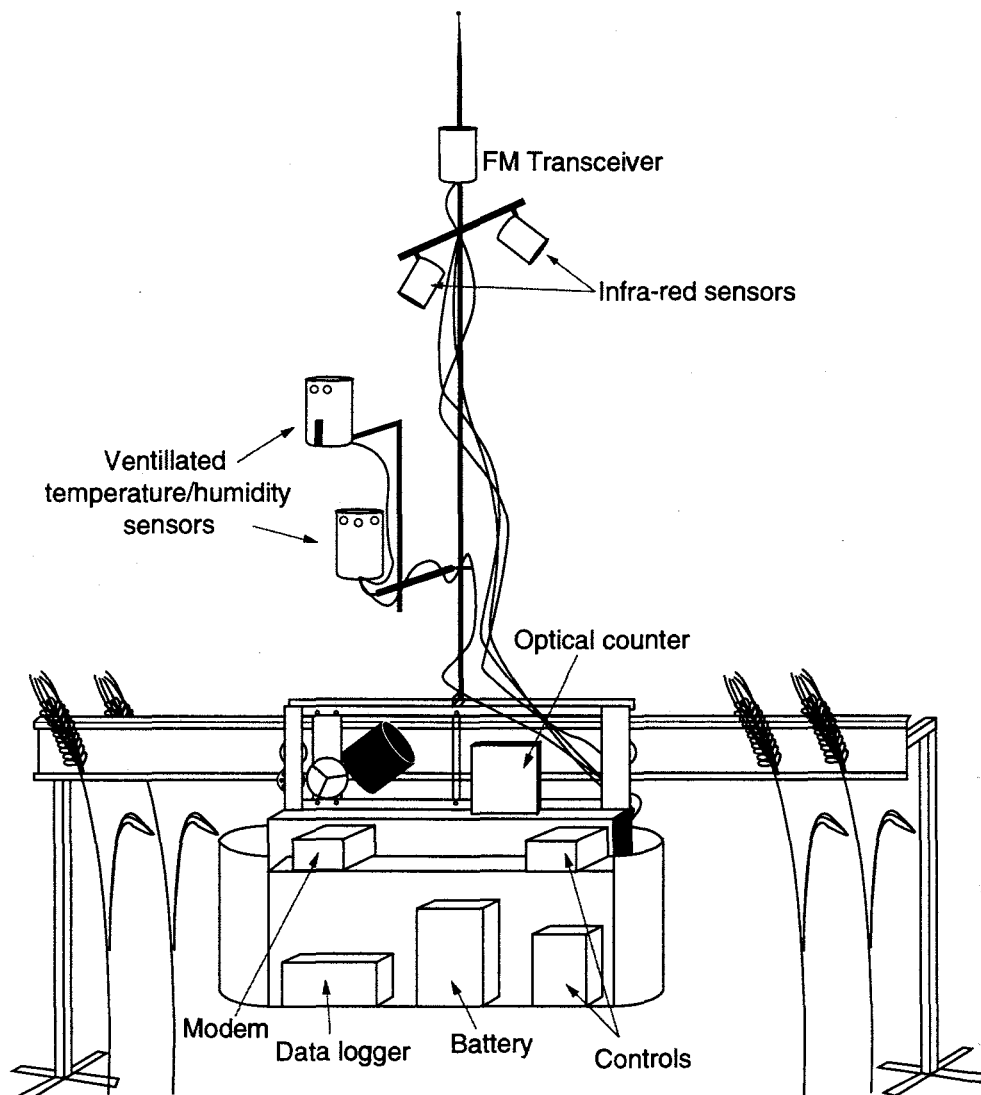
Figure 2.5 The monorail system of moving sensors; a self-propelled platform with sensors for air and surface temperature and humidity moved along a 58 m rail across the crop canopy.

2.6.2.2. Sensors

Sensors were mounted on a mast of 13 mm aluminium rod extending above the train. The humidity and temperature sensors were the same as used on the 'flying fox'. They were mounted 40 cm to the eastern side of the rail and adjusted to be 25 cm above the top of the crop. An additional thermocouple was installed in a similar psychrometer a further 25 cm higher. It was set up in series with the lower thermocouple to give a temperature differential relative to the Pt100 reference junction. The infra-red surface temperature sensors were mounted near the top of the mast at approx. 1 m above the crop and also pointed east and west. By geometrical analysis, it was estimated that they scanned an ellipsoid area approximately 2.3×1.8 m or 3.5 m². Sensors were scanned and logged at regular intervals along the rail by a datalogger (Datataker DT100, Data Electronics Aust. Pty Ltd.) mounted in the train.

A second datalogger (Datataker DT100, Data Electronics Aust. Pty Ltd.) scanned the net radiometer, wind vane and three cup anemometers as with the 'flying fox'. These signals were sent down an RS-232 cable to the shed.

2.6.2.3. Communications

It wasn't possible to use a fixed line communications cable so telemetry was used. The digitised data was sent down an RS-232 line to a Smart Radio Modem (Model RM100, CPU-100 v3.6, NetComm Australia, Pty Limited) and then transmitted by a low powered FM transceiver (Realistic, Tandy Corp.) at 55.05 MHz. Data were received by a similar FM transceiver approximately 50 m from the rail and reconverted by another Smart Radio Modem to a digital signal and sent down an RS-232 cable approx. 150 m to a computer in a shed outside the paddock. The Smart Radio Modem performed integrity checks on the data to ensure that they were all correct. The two dataloggers were daisy chained and used the same RS-232 line to communicate with the host computer.

Electrical interference, detected on the thermocouples, was traced back to an intermittent hum from the radios. This problem was overcome by cutting power to the train's radio prior to scanning the sensors. This was achieved by programming the scan schedule of the Datataker to trigger a relay to cut the power, wait 50 ms for the radio to fade, scan the sensors, re-trigger the power relay and then transmit the data. When atmospheric conditions were not ideal, there was some delay in the radio relay reconnecting. This occasionally caused some loss of data.

CHAPTER THREE:

WATER-USE EFFICIENCY OF

LEAVES AND CANOPIES

Table of Contents

Summary

A multi-disciplinary project was established to assess the relationship between Δ (discrimination against ^{13}C) and WUE (water-use efficiency) in the field. Two cultivars of wheat, Matong and Quarrion, were grown in large paddocks. These cultivars had contrasting WUE and Δ, due to ca. 40 % lower stomatal conductance in Quarrion than in Matong.

This chapter describes measurements of instantaneous water-use efficiency (including soil fluxes), transpiration efficiency (plant only) and their components of photosynthesis and transpiration at leaf, canopy and paddock scales. The objective of this work was to examine the scaling of gas exchange from leaves to paddocks and to explore the extent to which canopy boundary layers reduce any advantage of having lower leaf conductance.

Several canopy flux measurement techniques were compared: large ventilated chambers, Bowen ratio systems and lysimeters. All techniques had advantages and limitations. The chambers were limited by suitable site selection in a canopy of variable density, but provided day and night measurements of both water and CO_2 fluxes. The Bowen ratio system gave reliable CO_2 and water flux measurements during the day, but not at night. The lysimeters provided continual measurement of water-use, but not CO_2.

Field measurements of leaf gas exchange demonstrated that the cultivars did have different stomatal conductance and similar rates of leaf photosynthesis. The differences in stomatal conductance between the cultivars were reduced late in the season when Matong had greater soil water deficits than Quarrion.

Different stomatal conductances for the two crops at the leaf scale were reflected as different canopy conductances, but the difference between the canopy conductances was less than expected considering the differences in canopy leaf area. Differences in canopy transpiration between the two crops was further reduced due to the additional effects of the canopy boundary layer. Simple scaling of leaf photosynthesis by the leaf area was not reflected in the rates of gross canopy photosynthesis.

The distinct advantage of Quarrion in transpiration efficiency (excluding soil fluxes) over Matong at the leaf level (24%) was substantially reduced at the canopy level (5%), but nevertheless did result in more conservative total seasonal water-use (5%) and greater grain yield (23%) in 1990, a year with minimal rain after anthesis.

3.1. Introduction

Agricultural production in many parts of Australia is limited by available water. This is particularly true of winter wheat crops, where grain yield is closely related to rainfall (French & Schultz, 1984). Improvements in the ratio of biomass production to crop water-use have much potential to increase grain yield (Passioura, 1977). Although research into water-use efficiency has continued for many years, little progress has been made (Tanner & Sinclair, 1983). This slow progress is partly attributable to the difficulty and cost of measuring water-use over an entire growing season. Use of the relationship between carbon isotope discrimination and water-use efficiency offers a cheap alternative, although application of this tool to crops has complications (Farquhar *et al.*, 1989b).

Discrimination against ^{13}C in plants (Δ) has been shown to be related to the ratio of photosynthesis to transpiration of leaves (Evans *et al.*, 1986) and to the growth and water-use of individual plants (Farquhar & Richards, 1984). This suggests that Δ may be a useful tool in plant breeding programs for identifying cultivars with improved water-use efficiency (WUE) (Farquhar & Richards, 1984). Field trials showed some ambiguity in the relationship between Δ and WUE. In dry environments there was a negative correlation between Δ and WUE, as in the glasshouse trials, while in wetter environments the relationship was positive (Condon *et al.*, 1990; Condon & Richards, 1993). Where changes in WUE were due to altered photosynthetic capacity the relationship between WUE and Δ was similar in both glasshouse trials and field trials (Wright *et al.*, 1988; Wright *et al.*, 1993). It was speculated that where improvements in water-use efficiency were due to reduced stomatal conductance the benefits may be diminished at larger spatial scales due to the canopy boundary-layer (Cowan, 1988). Boundary layers of leaves and the canopy cause the humidity of the air to increase and the temperature to decrease, due to the transpiration, reducing the benefit of a reduction in stomatal conductance and causing a feedback on transpiration through these vegetation-atmosphere interactions (Jarvis & McNaughton, 1986; McNaughton & Jarvis, 1991). Reduced stomatal control can lead to similar transpiration in plants with differing stomatal conductances.

Little direct assessment has been made of stomatal control of evaporation from extensive vegetation, possibly due to the multi-disciplinary nature of such research. Indeed many researchers have found that evaporation is closely related to net radiation

(Penman, 1948; Priestley & Taylor, 1972), with no need to consider stomatal control at all. The degree of stomatal control of evaporation has been assessed indirectly by comparing evaporation from different types of vegetation (Denmead, 1969), comparing evaporation rates from periods with different water limitations (Tan & Black, 1976), measuring evaporation as canopy leaf area increased (Meinzer & Grantz, 1989), comparing evaporation before and after plant thinning (Whitehead *et al.*, 1984; Jarvis, 1993) and comparing evaporation from vegetation with different pathways of carbon metabolism (Baldocchi, 1994a). In all these experiments observed differences in evaporation were associated with changes in surface conductance. However, other changes also occurred to factors such as surface roughness and the weather, which makes it difficult to unequivocally confirm stomatal control of evaporation rate. Although, the aforementioned experiments confirm the theoretical analyses of evaporation, that show stomatal control of evaporation is reduced at larger spatial scales (Jarvis & McNaughton, 1986), it remains to be validated in actual experiments with direct changes in stomatal conductance in a range of vegetation.

A multi-disciplinary project was established to assess the relationship between Δ and WUE in the field. Two cultivars of wheat, Matong and Quarrion, were grown in large paddocks. These cultivars had contrasting WUE and Δ, due to ca. 40 % lower stomatal conductance in Quarrion than Matong. Water-use and biomass production over the entire growing season was discussed by Condon & Richards (1993). They found that differences in soil evaporation made a significant contribution to the crop WUE. Direct measurements of soil evaporation were pursued in a paper by Leuning *et al.*, (1994). This experimental set-up provided a unique opportunity to directly assess the effect of stomatal conductance on canopy evaporation, where the only change was the stomatal conductance; canopy structure and weather would be the same.

This chapter describes measurements of instantaneous water-use efficiency and its components of photosynthesis and transpiration at leaf, canopy and paddock scales. The objective of this work was to test the hypotheses that (1) stomata do contribute to the regulation of transpiration from canopies and (2) that although the canopy boundary layer may diminish the advantage of reduced stomatal conductance to transpiration efficiency, there is still an advantage at the canopy scale of selecting wheat cultivars that exhibit improved transpiration efficiency at the leaf level.

3.2. Experimental Methods

Details of many aspects of the field trials and measurements were presented in Chapter Two. A brief overview is reiterated here. The field experiments were conducted at Wagga Wagga, NSW. The chosen cultivars, Matong and Quarrion were selected with contrasting WUE and Δ, but similar in their developmental growth stages and canopy structure. The crops were sown on 28 May in 1989 and 22 May in 1990. Measurements of gas exchange were made throughout the growing season of 1989 and in the two weeks pre-anthesis and two weeks post-anthesis of 1990.

Leaf gas exchange measurements were made with a Li-Cor 6200 portable photosynthesis system. Sections of the uppermost fully expanded leaves (only flag leaves in 1990) were selected for measurement that were perpendicular to the solar beam, to ensure activation of the photosynthetic enzymes and maximum stomatal opening. Measurements were made throughout the day to follow the diurnal trends. However, measurements were not possible until after 10:00 when the dew had evaporated.

Large ventilated tents (2.3 m^2) were used to measure gas exchange from sections of canopy. A tent was placed over a section of canopy that was judged to be representative of the whole canopy. There was some variability in the canopy density, due to different germination rates and weed infestation. The tents measured continuously for several days of a week in the same position. They were removed over the weekends and replaced the following week. If showers of rain occurred while the tents were in place, they were moved to a new location.

Bowen ratio systems, with gas analysis for CO_2 gradients, were established in the centre of each paddock. Fetch was 130 m to the east and west and 100 m to the north and south. Differential gas analysers were used to measure both CO_2 and water vapour gradients.

Fortnightly harvests of 0.5 m^2 quadrats were used to measure leaf area index and biomass. The soil water profile was also measured fortnightly to determine total water-use.

3.2.1. Analysis

An important distinction needs to be made between gross and net fluxes, especially for evaluation of water-use efficiency by crops. In addition to transpiration through leaves, water is lost by direct evaporation from the soil. Benefits from increased transpiration efficiency can be greatly diminished by enhanced soil evaporation if greater transpiration efficiency is associated with lower canopy leaf area (Condon & Richards, 1993). An evaluation of scaling up WUE needs to compare gross fluxes of photosynthesis and transpiration as these are under plant control, but also total or net fluxes of evaporation including soil evaporation and net CO_2 flux including carbon simultaneously lost by respiration.

Measurements of fluxes by both tents and Bowen ratio systems are net fluxes. Transpiration is augmented by soil evaporation, while CO_2 uptake by canopy photosynthesis is reduced by CO_2 efflux from respiration of both soil and the canopy. However, there are subtle differences between the soil fluxes in tents and those measured by Bowen ratio systems. Over pressure in chambers can suppress soil CO_2 fluxes (Kanemasu et al., 1974) and possibly also water vapour fluxes. Enhanced turbulence, due to mixing fans in the tents, may increase the rate of soil evaporation compared to the undisturbed soil evaporation outside the tent. These effects were considered in calculation of gross canopy photosynthesis and transpiration as described below.

3.2.1.1. Canopy and Soil Respiration

Tent measurements of CO_2 fluxes at night were used to estimate total canopy respiration. These data were averaged over periods of one hour and found to be temperature dependent (see Chapter Seven). Respiration during the day was estimated from the night respiration measurements taking into account the higher temperatures during the day. Canopy respiration was reduced by 15 % during the day, to take into account the effect of light on the respiration of photosynthetic tissues (Graham, 1980; Brooks & Farquhar, 1985; Kirschbaum & Farquhar, 1987). Independent measurements of soil respiration were made with a chamber attached to a Li-Cor 6200. They were also temperature dependent (see Chapter Seven).

Gross photosynthesis in the tents was calculated by adding the canopy respiration to the measured net canopy flux. Paddock gross photosynthesis was calculated from the

Bowen ratio data with the extrapolated canopy respiration and an additional 30 % of the soil respiration to take into account the suppression of soil fluxes in the tent.

3.2.1.2. Soil Evaporation

Soil evaporation was estimated over intervals of two weeks, using the method of Cooper (1983). This involved measuring changes in the soil water profile both beneath the crop and under bare soil. Measurements of light interception by the canopy were used to then convert bare-soil evaporation to soil evaporation from beneath the crop. Measurements of pan evaporation were used as a scaling factor to interpolate to obtain daily soil evaporation. Diurnal variation of soil evaporation was assumed to be in proportion to the calculated equilibrium evaporation from the soil beneath the canopy while the soil surface was wet (Black et al., 1970; Ritchie, 1972). Cumulative evaporation and rainfall was used to model the water content of the top 5 cm of soil. As the soil surface dried below a threshold water content the evaporation rate from the soil was reduced in proportion to the surface moisture content. Soil evaporation from inside the tents was assumed to be the same as outside the tents, since the enhanced turbulence in the tent would tend to compensate for the chamber pressure suppression of soil fluxes.

3.2.1.3. Canopy and Surface Conductance from Bowen Ratio Data

Canopy conductance, G_c, was calculated by inverting the Penman-Monteith (PM) equation,

$$\frac{1}{G_c} = r_c = \frac{\varepsilon r_{aH} Q / L^M + D_r}{E_c} - (\varepsilon + 1) r_{aH}.$$ (3.1)

where ε is the change of latent heat of saturated air with a change in sensible heat as temperature changes ($sL^M/(PC_p)$), r_{aH} is the aerodynamic resistance to turbulent transfer of sensible heat between the surface and the reference height (1.0 m above the canopy), calculated from sonic anemometer measurements and stability corrections (see Chapter Five), Q is the available energy (R-G) absorbed by the canopy, L^M is the molar latent heat of evaporation, D_r is the water vapour concentration deficit of the air at the reference height, P is atmospheric air pressure and E_c is the measured canopy transpiration (total

evaporation less soil evaporation, E_T - E_s). Surface conductance, G_s, was calculated from the PM equation using E_T in place of E_c.

3.2.1.4. Canopy and Surface Conductance from Tent Data

Inside the ventilated tent, gradients typical of a normal canopy, are prevented from developing by mixing fans, rendering calculation of a suitable g_{aH} for the PM equation difficult. The transpiration rate can also be related to an equation describing the flux by a concentration gradient and resistances,

$$E_c = \frac{D_l}{\left(1/G_c + 1/g_{aH}\right)} .$$

(3.2)

where D_l is the leaf-to-air vapour concentration difference between the saturated vapour concentration at the measured canopy leaf temperature and the water vapour concentration of the air in the tent. This equation was rearranged to determine canopy conductance in the tents as,

$$\frac{1}{G_c} = \frac{D_l}{E_c} - \frac{1}{g_{aH}}$$

(3.3)

Canopy boundary layer conductance, g_{aH}, was set at 1.5 mol.m^{-2}.s^{-1} by comparing with the conductances obtained from the Bowen ratio data for both the Matong and Quarrion tents. Surface conductance, G_s, was calculated by using total evaporation, E_T, in place of E_c in eq. 3.3.

3.3. Results and Discussion

Leaf gas exchange measurements in the field demonstrated that stomatal conductance of Quarrion was on average 40 % lower than stomatal conductance of Matong (figure 3.1). Late in the season, stomatal conductance declined as the crop matured in both cultivars, but was more marked in Matong so that stomatal conductance was similar in both crops. Leaf photosynthesis was similar in both crops (figure 3.1) so that the ratio of intercellular to atmospheric CO_2 partial pressures (p_i/p_a) was lower in Quarrion than
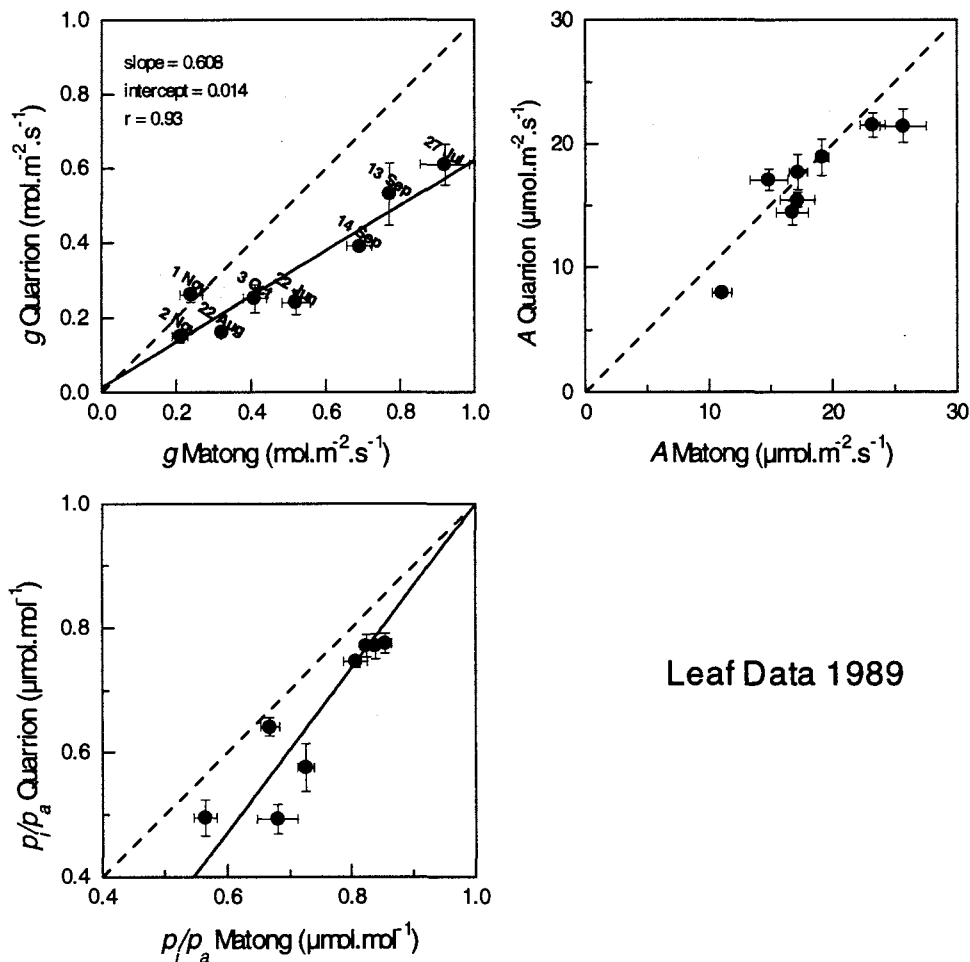
Figure 3.1 Comparison of spot measurements of stomatal conductance (g), leaf photosynthesis (A) and the ratio of intercellular to atmospheric CO_2 partial pressures (p_i/p_a) on fully expanded sunlit leaves at the top of the canopy of cultivars Matong and Quarrion in field crops throughout the 1989 season. Standard errors are shown as error bars.

Matong.

Canopy leaf area index (L_c) is the dominant scaling factor between leaves and canopies, at least until a closed canopy forms. While canopies are open, soil evaporation can dominate total evaporation, unless the soil surface is dry and the crop is growing on stored soil water. At Wagga Wagga rain occurred throughout the growing season so soil evaporation remained a large component until canopy closure (Condon & Richards, 1993).

In 1989 poor germination and low vigour of the Quarrion crop resulted in a significant difference in the canopy leaf area of the two crops (figure 3.2).
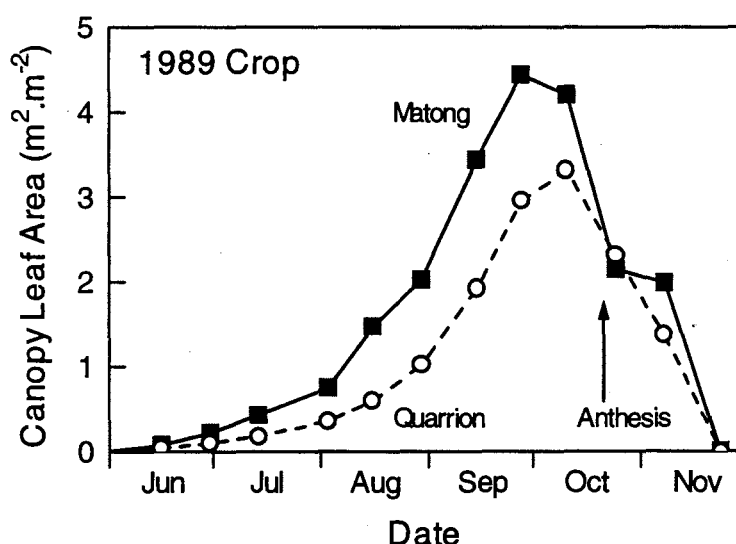
Figure 3.2 Canopy leaf area index (L_c) of the Matong and Quarrion crops in 1989.

The experiment was repeated the following year (1990) using the same two cultivars, but with the paddocks swapped. In this second year the sowing rate was increased 25% in the Quarrion crop, in an attempt to match the canopy leaf area of the two crops more closely. However, despite matching leaf area of the crops early in the season, maximum leaf area of the crops was still different (figure 3.3).
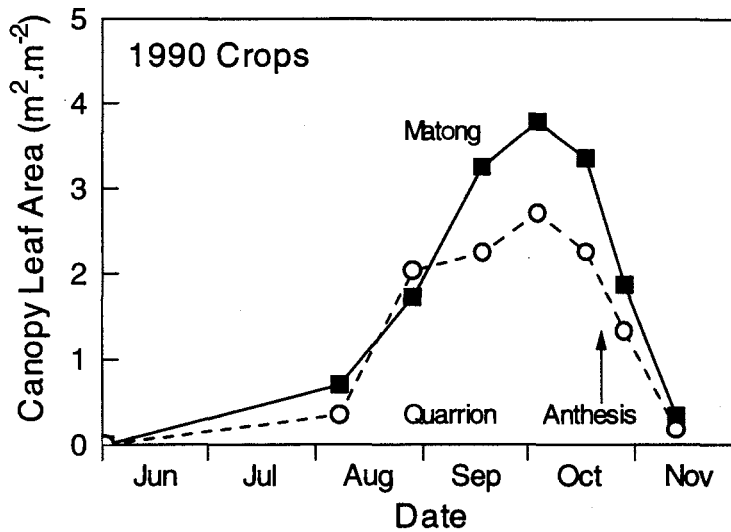
Figure 3.3 Canopy leaf area index (L_c) of Matong and Quarrion in 1990.

Total biomass of Matong was greater than that of Quarrion during October (figure 3.4). However, grain yield was 335 g.m^{-2} in Matong compared with 413 g.m^{-2} for Quarrion. The more conservative water-use by Quarrion allowed grain filling to continue longer.
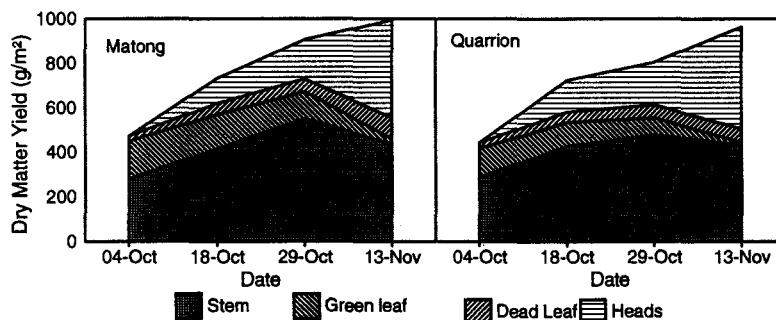
Figure 3.4 Partitioning of the crop biomass into stems, green leaves, dead leaves and heads for the Matong (left) and Quarrion crops (right) in 1990.

Differences in stomatal conductance between the cultivars were not always apparent in the second cropping year (figure 3.5). There was less rain and greater soil water depletion during 1990, which caused somewhat greater reductions in stomatal conductance of Matong than Quarrion, as the latter had more conservative water-use. On 23 October 1990 there was 33 mm of rain which restored the expected cultivar differences in stomatal conductance. Leaf photosynthesis was lower in Matong than Quarrion, except for the period immediately after rain, when they had similar rates. Similarly, p_i/p_a was lower in Quarrion when well watered (24-26 Oct), but similar to Matong under conditions of soil water deficit.
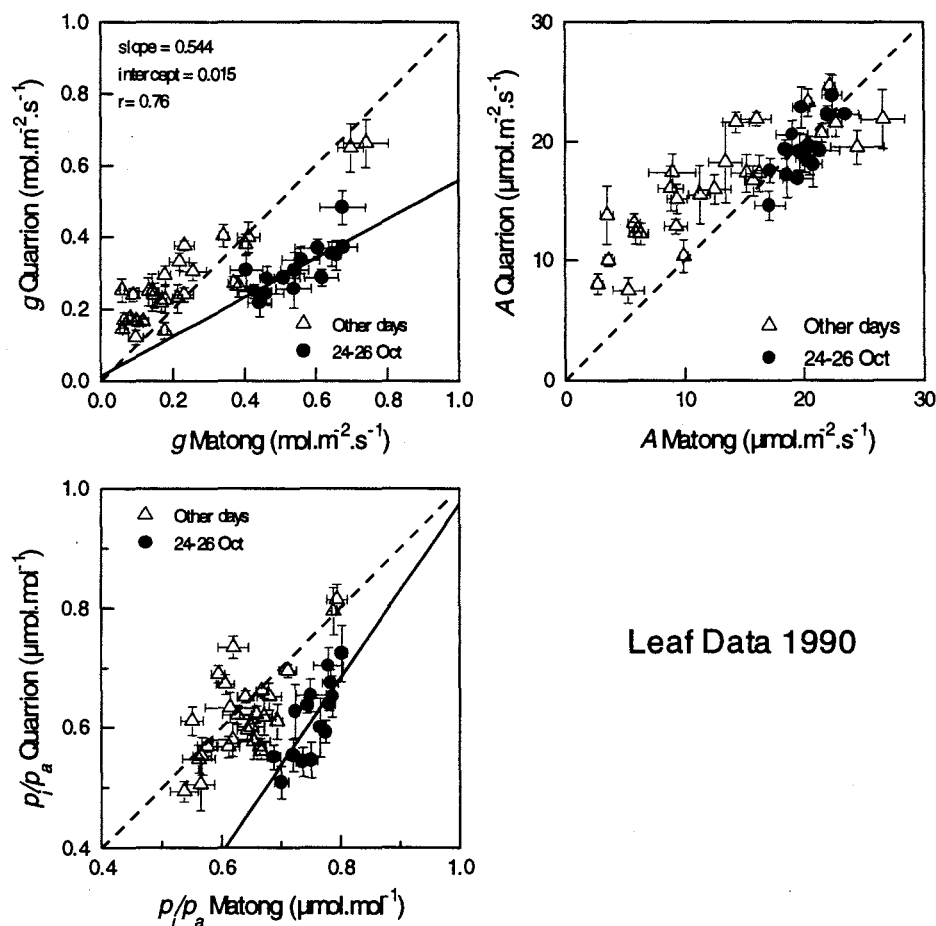
Figure 3.5 Comparison of spot measurements of stomatal conductance (g), leaf photosynthesis (A) and the ratio of intercellular to atmospheric CO_2 partial pressures (p/p_a) in field crops during October 1990. Standard errors are shown as error bars.

3.3.1. Comparison of Canopy Flux Measurement Techniques

Independent measurements by the tents, Bowen ratio systems and lysimeters in 1990 allowed a comparison of techniques and an evaluation of errors in measuring canopy photosynthesis and WUE. Weather conditions during 1989 were more cloudy with less clear days on which to make direct comparisons.

3.3.1.1. Comparison of Tents and Bowen ratio data with Lysimeters

Data from the tents and Bowen ratio systems were averaged to compare with hourly evaporation data from the lysimeters. Measured diurnal variation of evaporation was similar with the lysimeters, Bowen ratio systems and tents (figure 3.6). The Bowen ratio data at night were not used due to the difficulty of getting accurate measurements of the available energy and potential violation of the similarity assumption of equal turbulent diffusivities for heat and water vapour in stable conditions. The tents operated during the night, but the presence of the chamber and the air circulation prevented significant dew formation, which was recorded on the lysimeters as negative evaporation rates.
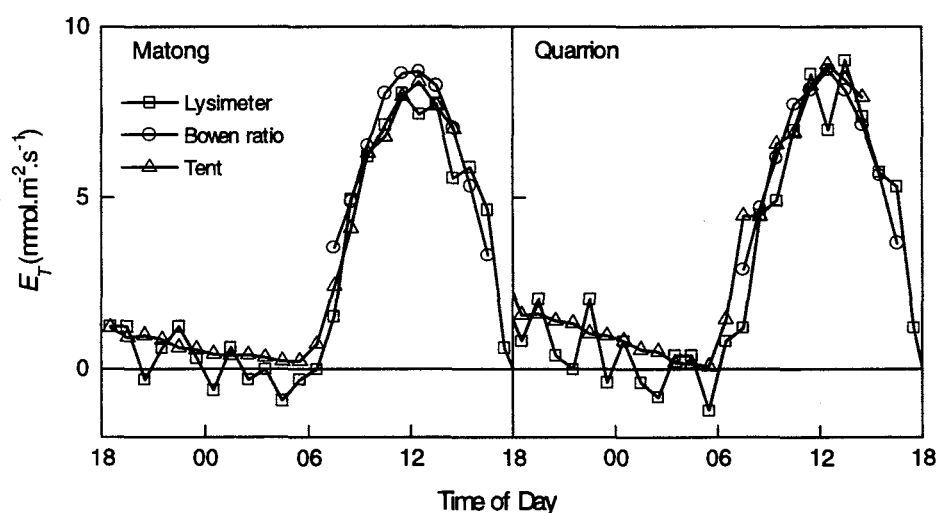
Figure 3.6 Comparison of diurnal variation of total evaporation measured by the lysimeters, Bowen ratio systems and tents in the Matong and Quarrion crops on the 12-13 October 1990.

For a more critical comparison, I have selected data from days between 12 October and 1 November when measurements were made at the leaf, canopy and paddock scales. During the period between 24 - 26 October there was good agreement between data of evaporation from the tents and the lysimeters (figure 3.7). On other days the agreement was poor, due to either underestimation by the lysimeters or overestimation by the tents.
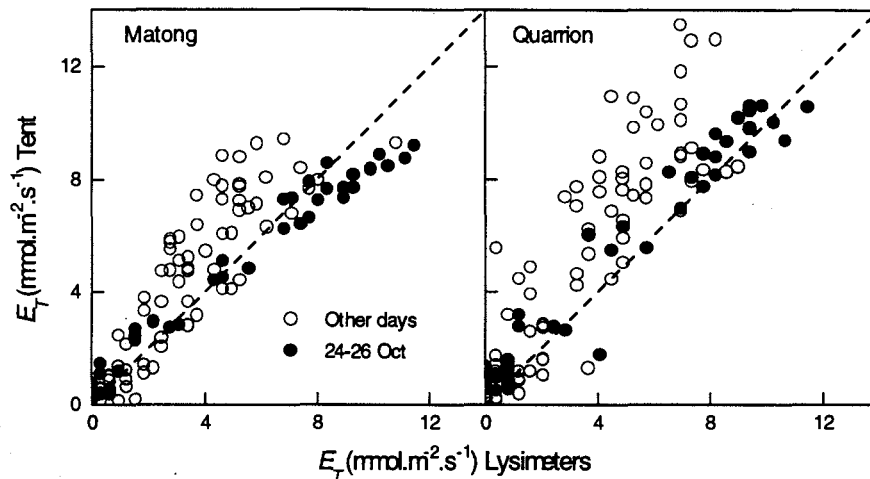
Figure 3.7 Comparison of total evaporation data from tents and lysimeters for the Matong and Quarrion crops in 1990.

A similar pattern was observed in the comparison of the Bowen ratio data with the lysimeters (figure 3.8), which suggests that evaporation from the lysimeters was not representative of the crop. The lysimeter crop was hand sown and had better seed germination and therefore higher plant density than the surrounding paddock. This resulted in faster water-use in the lysimeters early in the season and subsequent more severe water stress later in the season, which was observed as lower evaporation rates except for the days following rain (24- 26 Oct). Rate of evaporation from the lysimeters was greater than from the Bowen ratio measurements early in the season (data not shown).
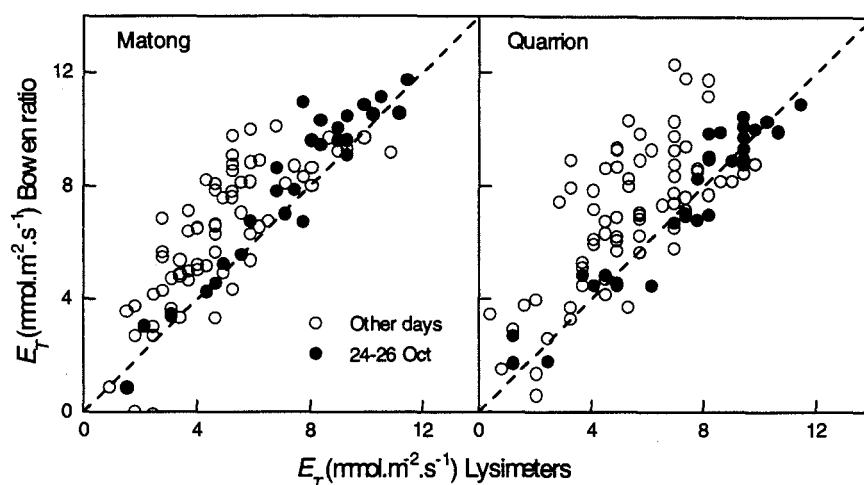
Figure 3.8 Comparison of total evaporation data from Bowen ratio systems and lysimeters for the Matong and Quarrion crops in 1990.

3.3.1.2. Comparison of Tents with Bowen ratio

Net Canopy Photosynthesis, Total Evaporation and Surface Conductance (Net Fluxes)

A comparison was made between the tent and the Bowen ratio data which allowed CO_2 flux measurements to be evaluated as well as evaporation data which were used in the comparison with the lysimeters. The Bowen ratio data were recorded as half hour running averages at 15 minute intervals. The tent data were recorded every 12 minutes and running averages of three measurements were used for this comparison. Surface conductance was calculated from the Bowen ratio data by inverting the Penman-Monteith equation. In the tents surface conductance was calculated from the measured evaporation rate, the leaf-to-air vapour concentration difference and an aerodynamic conductance of 1.5 $mol.m^{-2}.s^{-1}$, estimated by comparison with the Bowen ratio fluxes.

Both the tents and the Bowen ratio systems measured diurnal variations in net canopy CO_2 fluxes (figure 3.9). Bowen ratio data of CO_2 fluxes at night were not used,

for the reasons given earlier. Tent CO_2 flux data at night were used, although the data were sometimes erratic with the build up of CO_2. Bowen ratio net CO_2 fluxes were typically lower than the tent measurements due to suppression of soil respiration by over pressure in the tents, as discussed in the Methods section.
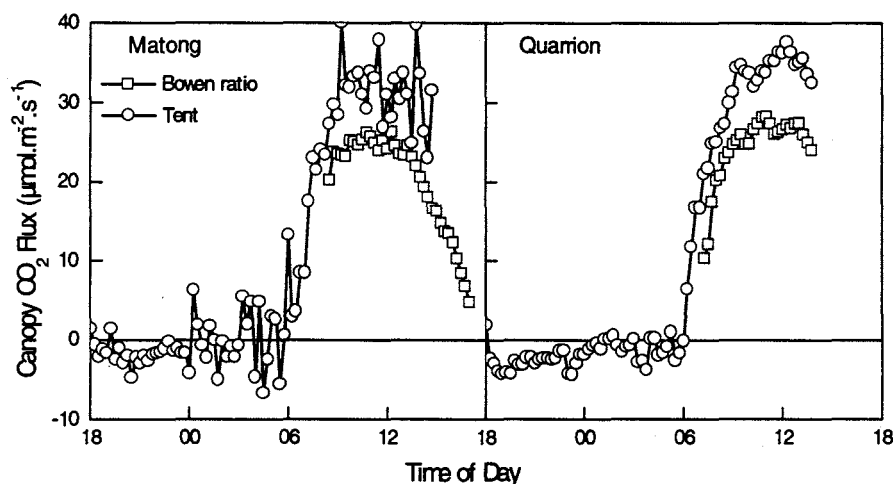
Figure 3.9 Diurnal variation of net canopy CO_2 fluxes measured with the tent and Bowen ratio systems of the Matong and Quarrion crops on 12-13 October, 1990.

Comparing data from the days selected above, measured net CO_2 fluxes from both the Matong and Quarrion crops were greater in the tent data than the Bowen ratio data (figures 3.10 & 3.11). There was better agreement between the tent and Bowen ratio system in the evaporation data; the tent measurements being slightly lower in Matong and slightly higher in Quarrion than the Bowen ratio data. There was poor agreement in the surface conductance data. Water-use efficiency (ratio of net CO_2 flux to total water-use) was greater in the tents than the Bowen ratio data.

Comparison of Techniques: Matong
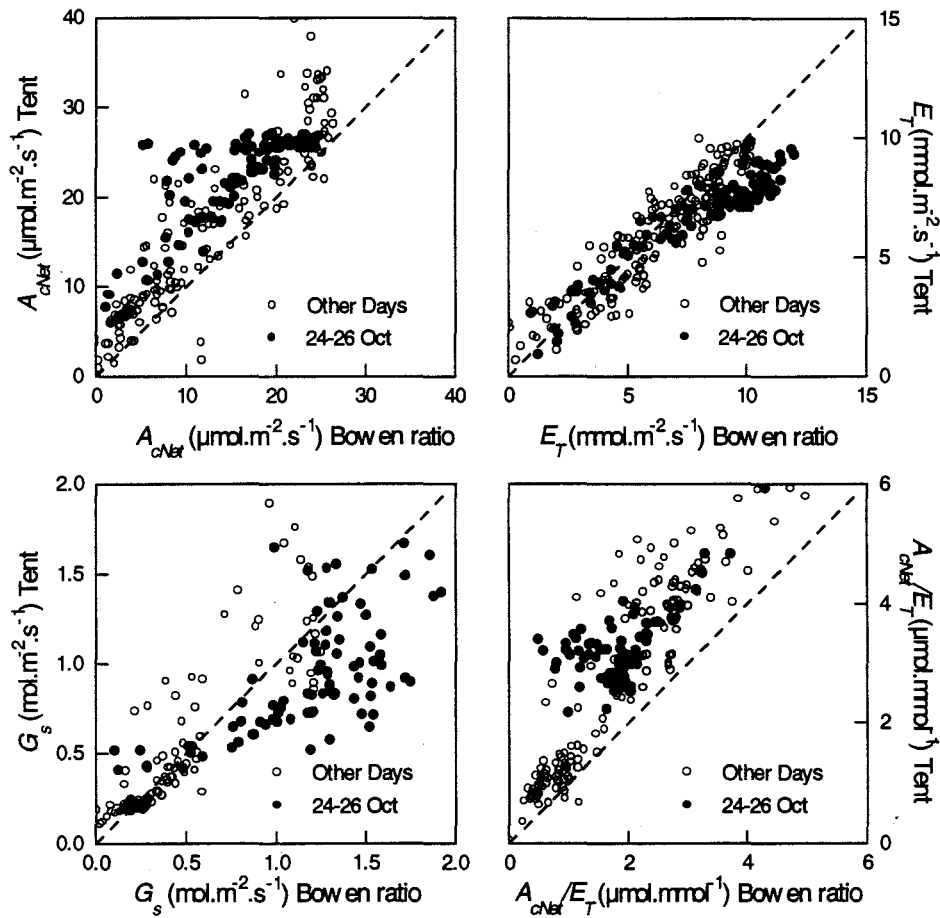
Figure 3.10 Comparison of the Bowen ratio and tent measurements of net photosynthesis (A_{cNet}), total evaporation (E_T), surface conductance (G_s) and water-use efficiency (A_{cNet}/E_T) for the Matong crop in 1990. The dashed lines are a 1:1 relationship.

There are several possible explanations for the differences in flux estimates between the tents and the Bowen ratio systems. Firstly the measurements are made at different spatial scales. The tent was placed over a 2.3 m² patch of canopy, while the Bowen ratio system measures fluxes that have evolved from an area of canopy up to 100 m distance. If the small patch of canopy in the tent was not representative of the entire paddock then the fluxes would be different. The Matong crop had a uniform plant density and therefore a homogeneous distribution of leaf area, whereas the Quarrion crop had a much more variable plant density with several patches that were nearly bare. The large

differences between the tent and Bowen ratio fluxes observed in the Quarrion crop are probably partly explained by the patch of canopy in the tent having more leaf area than the average of the entire paddock. It is unlikely that this would explain the observed differences in the Matong crop; other explanations are required.
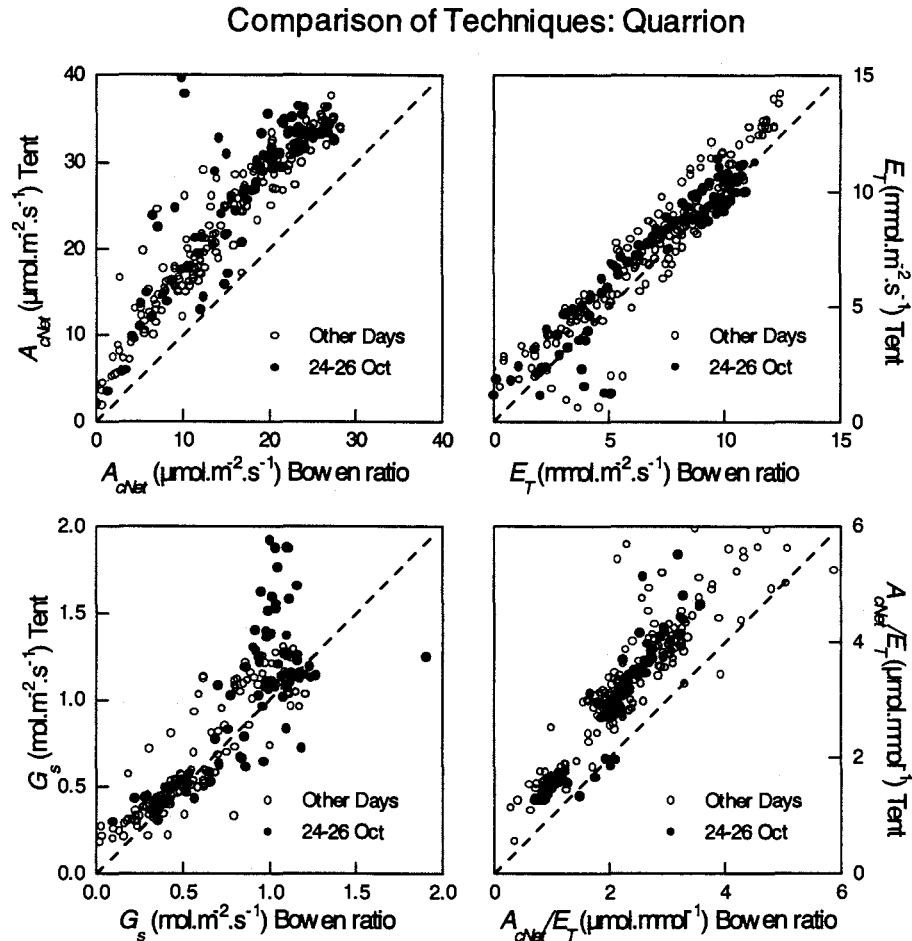
Figure 3.11 As in figure 3.10, but for the Quarrion crop.

The second explanation for the differences between the tent and Bowen ratio data is the effect of the chamber. Both the soil fluxes and the environment are affected by the chambers.

Pressurisation of chambers over soil is known to cause a reduction in soil CO_2 fluxes (Kanemasu *et al.*, 1974). The tents used in this experiment had air forced through at 200

L per minute, and so would have reduced soil CO_2 efflux compared with the undisturbed net CO_2 fluxes measured by the Bowen ratio system. Tests were conducted with these tents over bare soil, in which a second fan was used to exhaust air. When both fans were operating, with the speed adjusted so that the tent walls were slack, the CO_2 flux was 30 % greater than when the tent was pressurised. When only the exhaust fan was operating, so that the tent had a negative pressure compared with the free atmosphere, soil CO_2 flux was increased a further 30 %. It was concluded that when these tents were pressurised the soil CO_2 fluxes were reduced by 30 %. The flux of water vapour from the soil was assumed to be similarly affected by the chamber pressure.

The environment inside the chamber is altered compared with the ambient conditions; air temperature, humidity and the light quality all change. The amount of diffuse light was examined in detail and is discussed further in a later section. Changes to the air temperature and humidity were kept minimal by having high rates of air flow through the chambers (turnover time = 16s). The change in air composition was used as the basis for flux measurements in the tents, so that selection of the flow rate was a trade off between increasing changes to the air, and decreasing resolution of flux measurements. The draw down of CO_2 concentration was up to 1.5 Pa at maximum rates of canopy photosynthesis, whereas the humidity increase was up to 0.4 kPa. Air temperature increased inside the tent by up to 4°C, though more typically 1-2°C, above air temperature outside and was related to the sensible heat flux and (figure 3.12).

The lack of agreement between the surface conductance calculated from the tent and Bowen ratio data is not surprising given the different assumptions involved in the calculations and the effect of the chambers on the soil fluxes. Suppressed soil evaporation in the tents would result in lower calculated surface conductances in the tents as was observed.
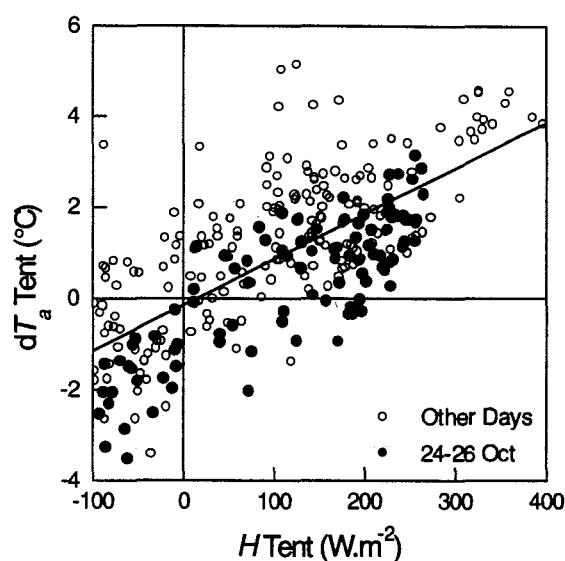
Figure 3.12 Increase of air temperature (dT_a) inside the Matong tent was correlated with the sensible heat flux (*H*). Linear regression shown.

Gross Canopy Photosynthesis, Transpiration and Conductance

Although it is possible to make a simple comparison of net fluxes measured by the tents and the Bowen ratio system, it is apparent that differences in the techniques, particularly with respect to soil fluxes complicate such a comparison. Independent measurements of soil respiration and soil evaporation allowed the calculation of gross canopy photosynthesis and canopy transpiration. With the soil components removed gross photosynthesis and transpiration were used to compare the tent and Bowen ratio techniques.

There was better agreement between data from the tents and Bowen ratio systems when the different soil fluxes in the two techniques were taken into account to compare gross photosynthesis and canopy transpiration than when net fluxes were compared (figures 3.13 & 3.14 cf. figures 3.10 & 3.11).
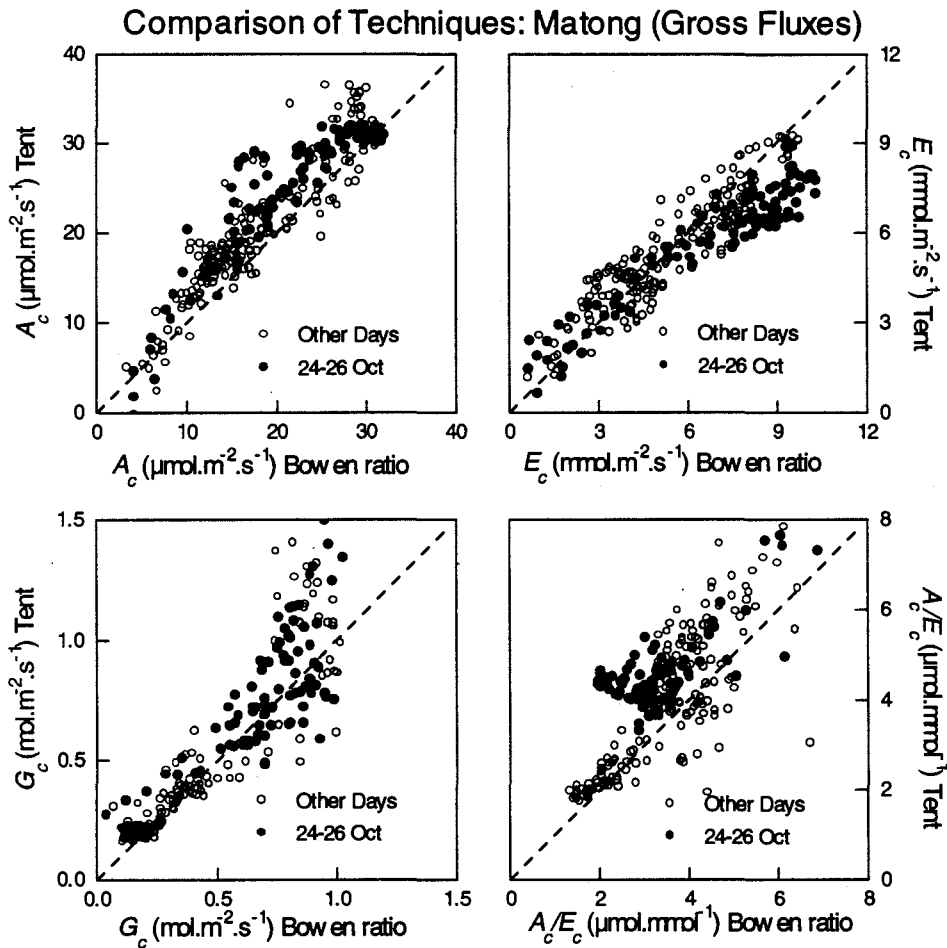
Figure 3.13 Comparison of tent and Bowen ratio data of gross canopy photosynthesis (A), canopy transpiration (E), canopy conductance (G) and transpiration efficiency (A/E) for the Matong crop in 1990. Canopy and soil respiration was added to the measured net canopy CO_2 flux. Soil evaporation was deducted from the measured total evaporation. The dashed lines are a 1:1 relationship. Data from the well watered conditions of 24-26 October are shown as solid dots.

Gross canopy photosynthesis was still greater in the tents than in the Bowen ratio data, suggesting that the different soil fluxes did not account for all the difference between the techniques and that the effects of more diffuse light and higher temperature and humidity in the tents enhanced the gross canopy photosynthesis. There remained a difference in the canopy conductance calculated from the tents and the Bowen ratio data, even after soil fluxes were deducted, but there was much better agreement between the two techniques. Transpiration efficiency remained greater in the tents than from the Bowen ratio data, though the difference was reduced compared to the comparison of water-use efficiency.
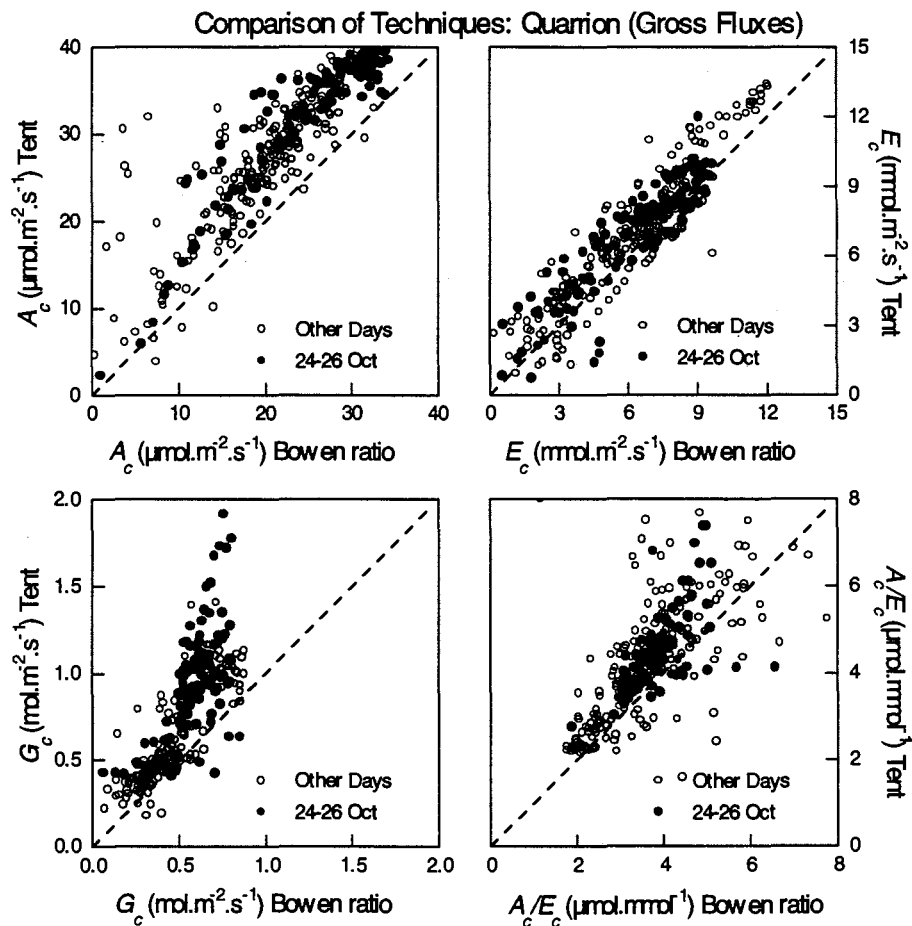
Figure 3.14 As in figure 3.13, but for the Quarrion crop.

3.3.1.3. Scattering of light by the tent

Another explanation for higher CO_2 fluxes in the tents compared with the Bowen ratio system, is the greater proportion of diffuse light in the tents than outside. Light is absorbed, scattered and reflected by the plastic walls of the tent, decreasing the total amount of light but increasing the proportion of diffuse light. Diffuse light is absorbed more efficiently by canopies resulting in higher rates of photosynthesis (Kumura, 1968). These effects were examined by measuring the proportion of diffuse light both inside and outside the tents as described below.

The plastic walls of the tent affected the proportion of beam and diffuse light by absorption and scattering. I quantified these effects by determining a transmission coefficient (τ_t) and a coefficient of forward scattering by the walls (f_w) from measurements of beam and diffuse light both outside and inside the tent (figure 3.15).
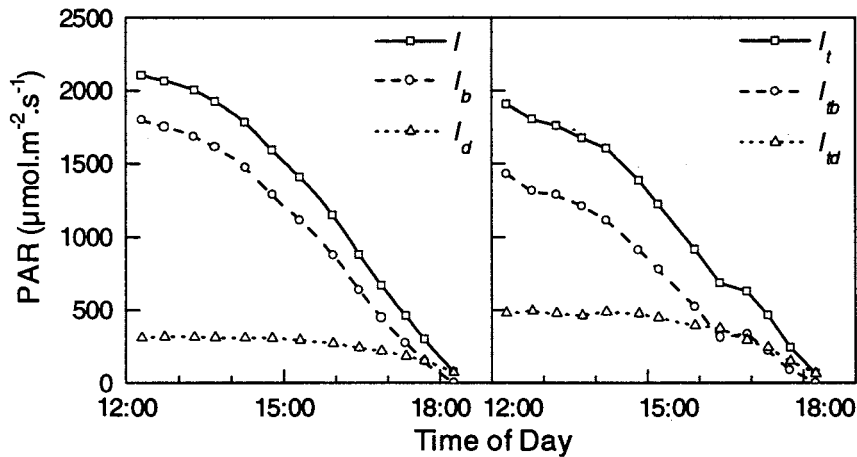
Figure 3.15 Measurements of beam and diffuse light on 5 Nov. 1991 both outside (left) and inside the tent (right). Each point is the mean of three measurements. Beam intensity was calculated as the difference between total and diffuse light.

Total PAR was measured with a PAR sensor (Sunfleck Ceptometer, Decagon Devices Inc., Pullman Washington). A black cardboard disk 20 cm in diameter was hand held at approx. 1.5 m to occult the sun from the sensor to obtain a measure of the diffuse PAR. Since simultaneous measurements both in the tent and outside were not possible, it was necessary to adjust the light intensity data for the time delay between

measurements, particularly at low light intensities. This was achieved by calculating the rate of change of light intensity over a half hour period, which was used to adjust for the time delay. Beam PAR was calculated as the difference between total and diffuse PAR after allowing for the time delay between measurements. No correction was made for the sky radiance blocked by the shading device, since it would have been very small.

In this analysis I define the tent transmission coefficient (τ_t) as the ratio of beam light in the tent (I_{bt}) to beam light outside (I_b):

$$\tau_t = I_{bt}/I_b .\tag{3.4}$$

This coefficient varies with the angle of incidence of the beam with the wall of the tent, since reflection increases as the angle decreases.

The transmission coefficient of diffuse light is assumed equal to that of beam light at the same angle, although it should more correctly be defined as the integral of radiance from all directions by the transmission coefficient of each direction summed over the entire sky. Light intercepted by the plastic is reflected out of the tent, scattered into the tent or absorbed. Light scattered into the tent is included in the diffuse light (I_{dt}) as the second part of the equation:

$$I_{dt} = I_d\tau_t + f_w I(1-\tau_t) ,\tag{3.5}$$

where f_w is the fraction of light intercepted by the tent walls scattered into the tent. An expression for this fraction is obtained by rearranging the above equation.

$$f_w = \frac{I_{dt} - I_d\tau_t}{I(1-\tau_t)} .\tag{3.6}$$

Values for the transmission coefficient (τ_t) were affected by solar elevation (figure 3.16). Beam light reached the sensor through the side wall of the chamber below a solar elevation of 22°, as indicated by the shadow of the frame cast across the sensor each morning and afternoon, while above 22° beam light reached the PAR sensor after entering the chamber through the top panel. Since the chamber was aligned north, the angle of incidence of beam light on the chamber top was calculated as

$$\angle(beam^\wedge top) = \beta - \arcsin\left(\frac{27}{167}\cos\phi_s\right),$$ (3.7)

where the fraction 27/167 is the sine of the slope of the chamber top, and β is solar elevation and ϕ_s is solar azimuth. When the beam reaches the sensor after entering the chamber through the wall of the tent, the sine of the angle of incidence is defined as;
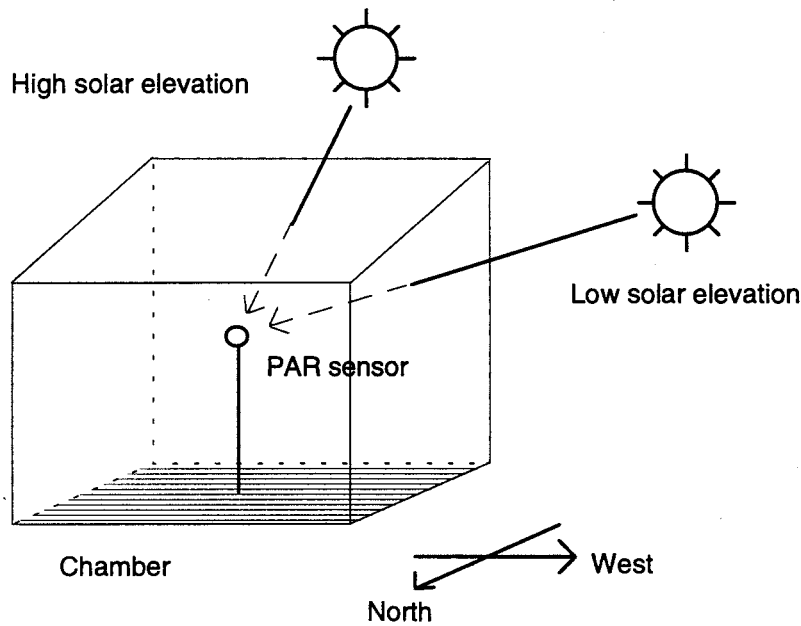
Figure 3.16 Diagram of tent with the beam path from the sun to PAR sensor highlighting the angle of incidence of the solar beam with chamber walls at high and low solar elevation.

$$\sin \angle(beam^\wedge side) = \cos\beta\sin\phi_s.$$ (3.8)

The sine of angle of incidence with the front panel is

$$\sin \angle\left(beam^\wedge front\right) = \cos\beta\cos\phi_s.$$ (3.9)

Calculated values for the coefficients are plotted (figure 3.17) as a function of the sine of the angle of incidence of the beam path with the chamber walls. Considering the

geometry of the chamber (figure 3.16), τ_t was best represented by a function of the angle of incidence of light on the chamber panels as in the equation;

$$\tau_t = \exp\left(-0.1811/\left(\sin\left(\angle_{beam}{}^{\wedge}{}_{panel}\right) - 0.2584\right)\right)$$

$$\left(\text{for } \sin\left(\angle_{beam}{}^{\wedge}{}_{panel}\right) < 0.27, \ \tau_t = 0\right)$$

(3.10)
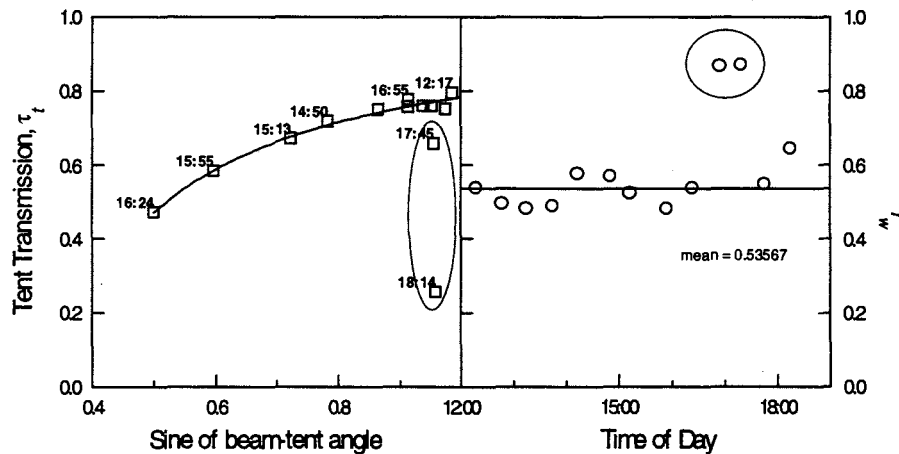
Figure 3.17 Tent transmission coefficient, τ_t, and coefficient of forward scattering by the tent walls, f_w, calculated using eqs. 3.4 & 3.6 from data in figure 3.15. Circled data points were excluded from the curve fitting.

where values of the coefficients were found by least squares fitting. The coefficient f_w was assumed unaffected by solar elevation and the mean value (excluding two extreme values) was calculated as 0.536.

Combining the expressions for transmission and scattering by the tent (eqs. 3.4 & 3.6) with the definition of fraction of diffuse light produces an expression for the fraction of diffuse light in the tent (f_t) as a function of the fraction of diffuse outside (f_o).

$$f_t = f_o + \left(1 - f_o\right)\frac{f_w\left(1 - \tau_t\right)}{\tau_t\left(1 - f_w\right) + f_w}$$

(3.11)

Modelled values of f_o and f_t are compared with data collected on 5 Nov. 1991 (figure 3.18). This comparison shows that the model accounts for much of the change in diffuse light as solar elevation varies.

However it is apparent in figure 3.18 that eq. 3.11 gives an abrupt change in f_t at $\sin\beta$ $\cong 0.4$, due to the altered beam path though the tent and the calculation of τ_t as a function of beam-panel angle (eq. 3.10). While this is true for the position of the sensor, it is not representative of the average light across the whole tent.
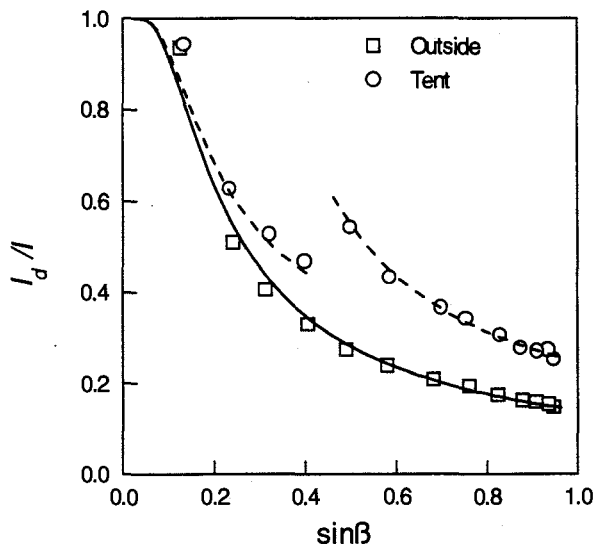
Figure 3.18 Comparison of the model (lines) of fraction of diffuse light outside, f_o, and inside the tent, f_t, with data (symbols) for 5 Nov. 1991.

Average f_t for the entire tent was calculated by determining an effective τ_t for the tent from the transmission coefficient of each panel and their contribution of light. Effective panel projection (P_s, P_t, P_f; side, top and front) was determined from panel dimensions, crop height (1.0 m) and the angle of beam incidence on each panel (eqs. 3.7 - 3.9) as;

$$P_s = (0.52 + 0.25)/2 \times 1.65 \times \sin \angle(beam^\wedge side)$$
$$P_t = 1.4 \times 1.65 \times \sin \angle(beam^\wedge top) \quad , \quad (3.12)$$
$$P_f = 0.25 \times 1.4 \times \sin \angle(beam^\wedge front)$$

The light contribution from each panel was calculated from their projection and their transmission coefficient $(P_s \tau_{ts})$, so that the effective τ_t was calculated from the weighted average transmission coefficient of each panel $(\tau_{ts}, \tau_{tt}, \tau_{tf}$; side, top and front) as in the equation;

$$\tau_t = \left(P_s \tau_{ts}{}^2 + P_t \tau_{tt}{}^2 + P_f \tau_{tf}{}^2\right) \Big/ \left(P_s \tau_{ts} + P_t \tau_{tt} + P_f \tau_{tf}\right).$$

(3.13)

The average tent transmission is used in eq. 3.11 to calculate the average fraction of diffuse light. An example of the application of these calculations is presented in figure 3.19 as the fraction of diffuse light outside the tent, fraction of diffuse light at the PAR sensor and the average fraction of diffuse light in the tent.
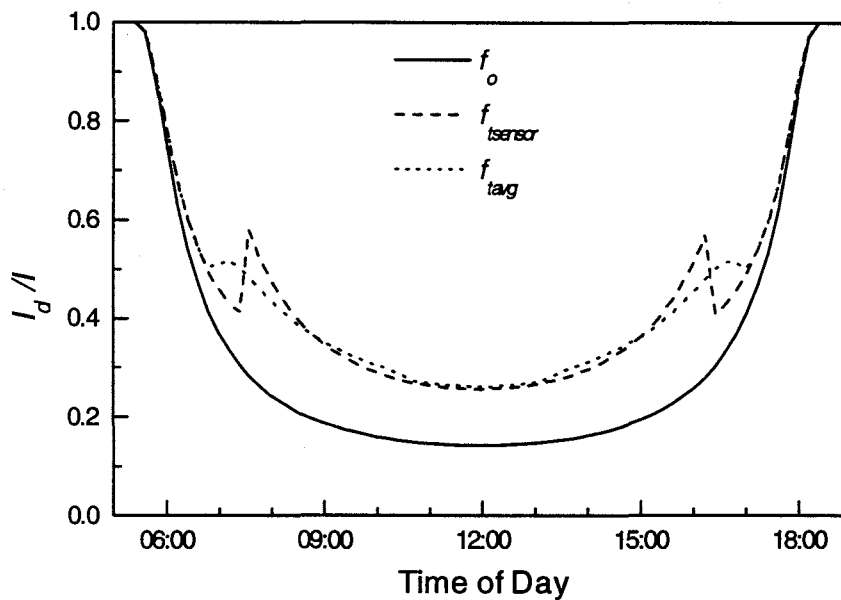
Figure 3.19 Fraction of diffuse light outside the tent, f_o, at the PAR sensor $(f_{tsensor})$ and the average of the tent (f_{tavg}), calculated using the model of light scattering by the tent. The discontinuity in the tent diffuse fraction is associated with a change in the path of beam light entering the tent through the side panel to entering the tent through the top panel.

It is necessary to use a model of radiation penetration and canopy photosynthesis to determine the effect of increased diffuse light on photosynthesis in the tents. The above

analysis of light scattering by the tent is used in subsequent chapters that examine modelling of canopy photosynthesis.

In conclusion, the comparison of measurement techniques has shown that all techniques have advantages and disadvantages. Lysimeters made continuous measurements of evaporation, but different crop densities on the lysimeters compared to the paddock caused an underestimate in the measured fluxes as soil water content declined. Bowen ratio systems provided reliable flux measurements of CO_2 and water, but only during the day. Tents provided flux measurements day and night, but were affected by higher air temperatures and humidity in the tent and a greater proportion of diffuse light. It is unlikely that the differences observed between the tent and Bowen ratio data for the Quarrion crop were all attributable to the effect of the chambers on the environment. It is more likely that the patch of crop in the Quarrion tent did indeed have a greater leaf area than the average of the whole Quarrion paddock.

3.3.2. Comparison of Crops

Comparison of canopy fluxes between the two crops was made with both the tent data and the Bowen ratio data for both the net fluxes and gross photosynthesis and transpiration. Comparison of the crops with the net tent data indicated that the Quarrion crop had greater CO_2 and water fluxes than the Matong crop (figure 3.20), whereas the Bowen ratio net flux data indicated that the fluxes from both crops were similar (figure 3.21). This is explained by the earlier observation that the Quarrion tent fluxes were greater than the Quarrion Bowen ratio fluxes, which was probably due to a denser patch
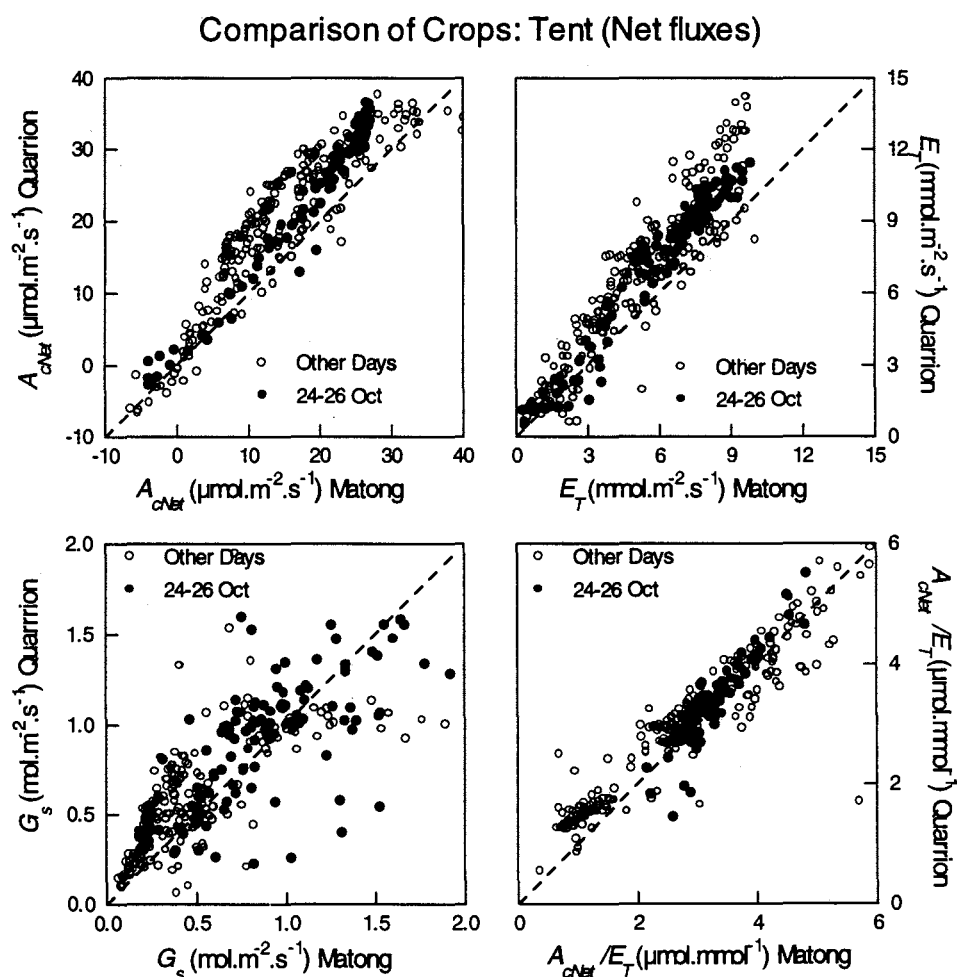
Figure 3.20 Comparison of net canopy CO_2 flux (A_{cNet}), total evaporation (E_T), surface conductance (G_s) and water-use efficiency (A_{cNet}/E_T) of the Matong and Quarrion crops measured with the tents. Data from the well watered conditions of 24-26 October are shown as solid dots

of canopy in that tent.

Surface conductance in the tents was similar for both crops for the period of 24-26 October, but was greater for Matong than Quarrion in the Bowen ratio data for the same period (figures 3.20 & 3.21). The ranking of cultivars in the surface conductance data from the Bowen ratio was in agreement with the observations of leaf conductance (cf figure 3.5), whereas that from the tent data was not. Similarly, the tent data indicated similar water-use efficiency for both crops for the 24-26 October, while the Bowen ratio data showed Quarrion more efficient than Matong.

Comparison of Crops: Bowen ratio (Net fluxes)
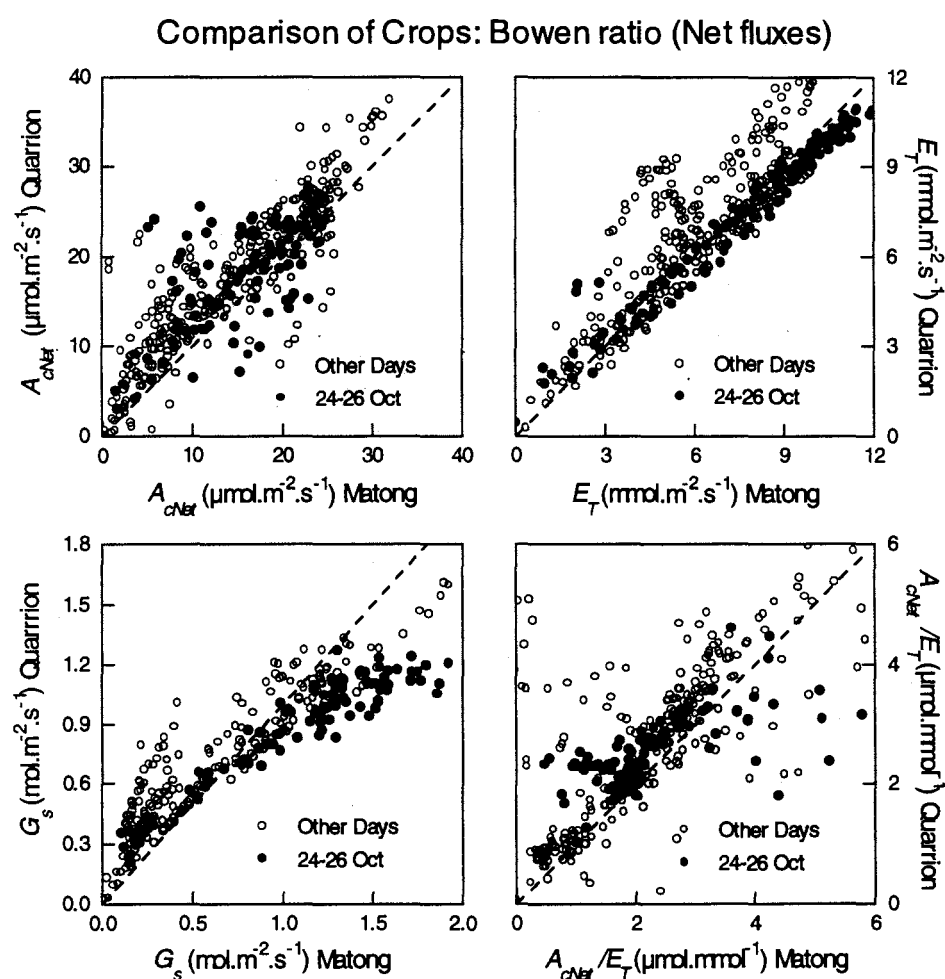
Figure 3.21 Comparison of canopy CO_2 flux, evaporation, surface conductance and water-use efficiency of the Matong and Quarrion crops measured with the Bowen ratio systems. Data from the well watered conditions of 24-26 October are shown as solid dots.

Comparisons of gross photosynthesis and transpiration for the two crops gave similar conclusions to the comparisons of net CO_2 flux and evaporation (figures 3.22 & 3.23 cf. figures 3.20 & 3.21). The tent data indicated greater gross canopy photosynthesis and transpiration from Quarrion than Matong for the period of 24-26 October, but the Bowen ratio data indicated similar gross photosynthesis and slightly greater transpiration from Matong than Quarrion.
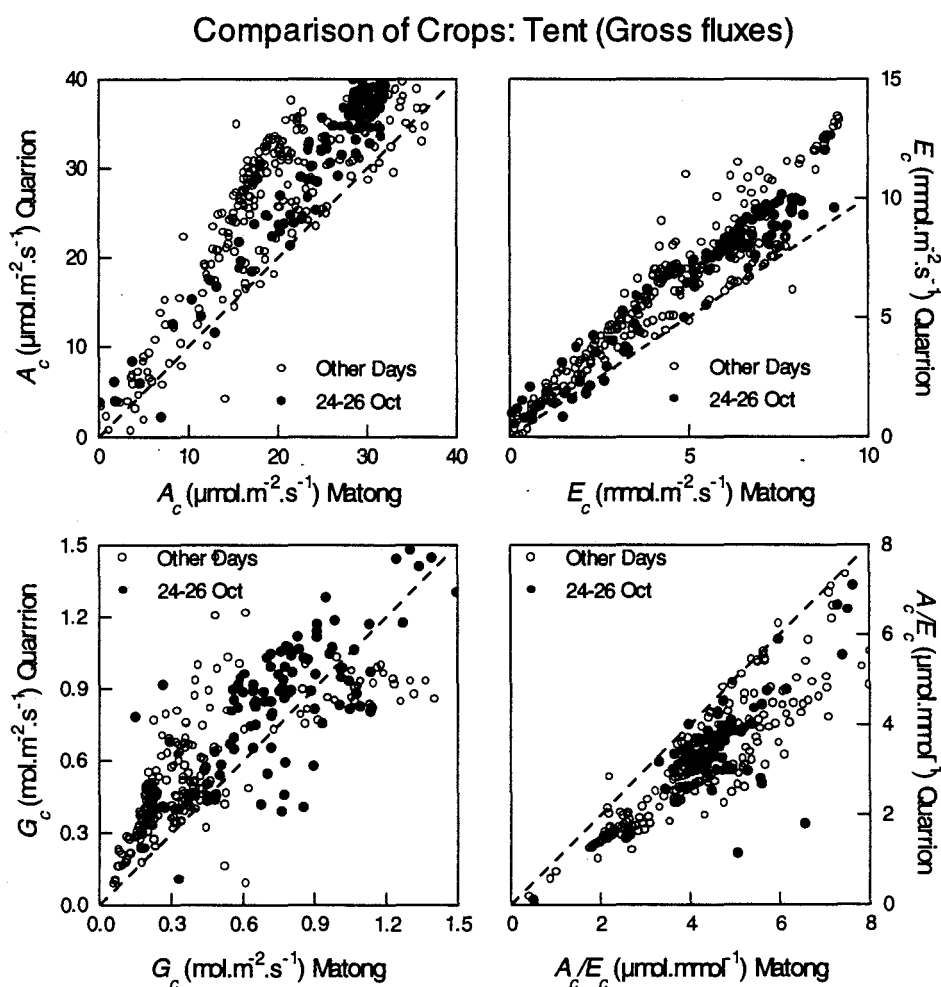
Figure 3.22 Comparison of gross canopy photosynthesis (A_c), transpiration (E_c), canopy conductance (G_c) and transpiration efficiency (A_c/E_c) of the Matong and Quarrion crops measured with the Bowen ratio systems. Data from the well watered conditions of 24-26 October are shown as solid dots.

As with the surface conductance the canopy conductance was similar for both crops in the tents, but greater for Matong than Quarrion in the Bowen ratio data for the period of 24-26 October. Transpiration efficiency was greater for Matong than Quarrion in the tents and the reverse in the Bowen ratio data.

Comparison of Crops: Bowen ratio (Gross fluxes)
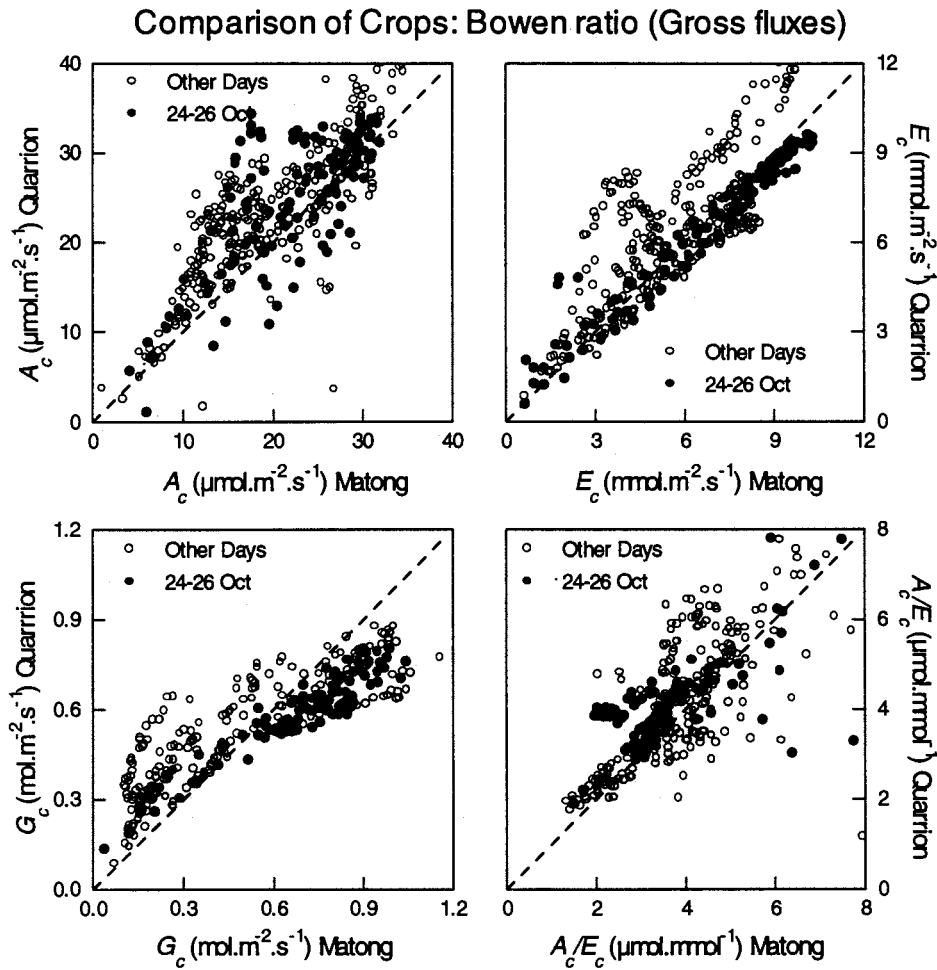
Figure 3.23 As in figure 3.22, but comparing Bowen ratio measured fluxes.

3.3.2.1. Scaling Conductance and Evaporation

Diurnal variation of the scaling of conductance from leaves to canopies was examined in more detail; two contrasting days are presented in figure 3.24. Different stomatal conductances in the two cultivars at the leaf level did translate into different canopy conductances, although the difference expressed as a percentage was reduced. For example, on 25 October leaf conductance of Quarrion was 46% lower than Matong, while canopy conductance of Quarrion was 31% lower than Matong. When the ranking of the cultivars in terms of their leaf conductance was reversed on the 30 October, a similar reversal was also observed in the canopy conductance. Precise conclusions should not be made about the scaling of conductance from this data, as there is considerable uncertainty in the canopy conductance data derived from the Penman-Monteith equation, which is examined further in Chapter Five.
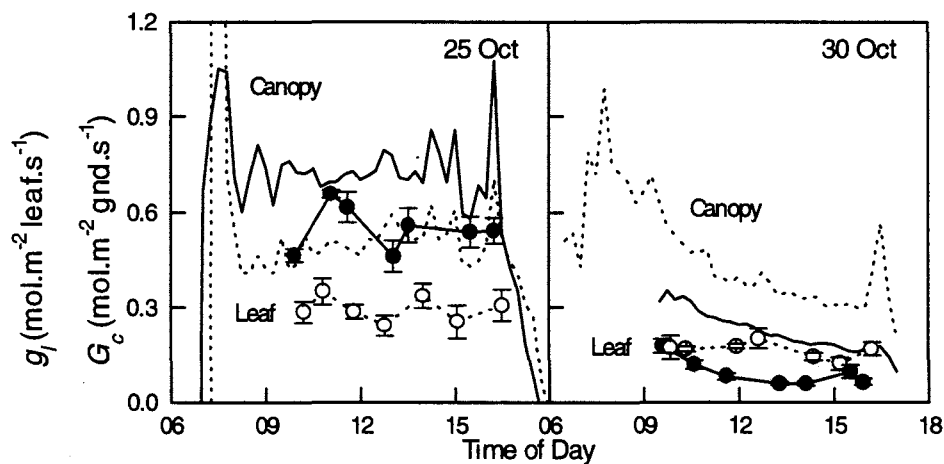
Figure 3.24 Comparison of the diurnal variation of leaf conductance and canopy conductance calculated from the transpiration rate measured with the Bowen ratio system and the inverted Penman-Monteith equation on the 25 October (left) and 30 October 1990 (right) for the Matong (—) and Quarrion (⋯⋯) crops.

The diminished difference between the cultivars in canopy conductance occurred despite a greater leaf area in the Matong than the Quarrion canopy (2.4 cf. 1.7 $m^2.m^{-2}$ on 25 Oct. and 1.8 cf. 1.25 $m^2.m^{-2}$ on 30 Oct. or 30% less leaf area in Quarrion). On the 25 October lower canopy conductance of Quarrion resulted in 7% less transpiration over

the whole day compared to Matong, which was offset by 26% more soil evaporation (E_s/E_T = 20% and 15%, for Quarrion and Matong respectively) so that total evaporation was 2% lower. On the 30 October the difference in the canopy conductance (figure 3.25) resulted in 23% more transpiration over the whole day from Quarrion than Matong, and 21% more total evaporation since soil evaporation was a much smaller component (E_s/E_T = 3% and 5%, for Quarrion and Matong respectively; soil evaporation was calculated to be 15% greater from Matong than Quarrion on 30 October, because the soil surface of Matong had not dried as rapidly as the more exposed soil beneath the Quarrion crop). These data clearly demonstrate the effect of differences in leaf stomatal conductance on canopy transpiration, yet it is unclear why the differences are reduced when comparing the cultivars at the canopy scale.
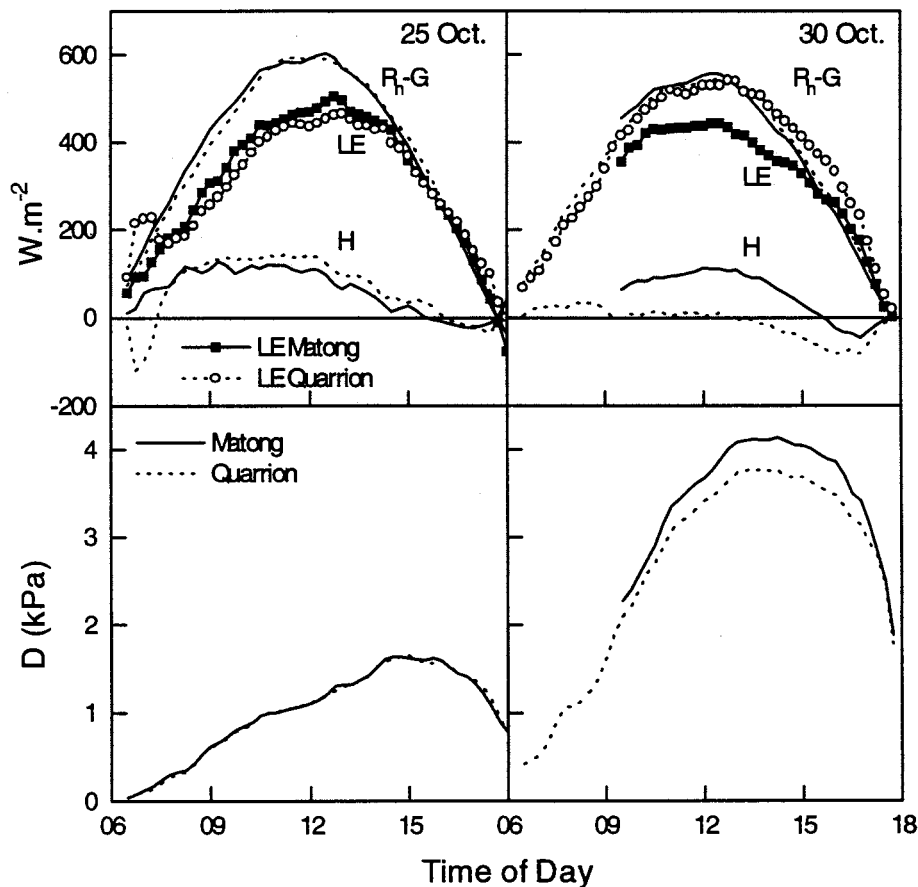
Figure 3.25 Diurnal energy balance of the Matong (——) and Quarrion (·····) crops on the 25 October (left) and 30 October 1990 (right): R_n - net radiation, G - ground heat flux, H - sensible heat, LE - latent heat, D - vapour pressure deficit.

It is also apparent that the atmospheric environment was altered by the energy balance of the crop so that the saturation deficit of the air above Quarrion was lower than the deficit above the Matong crop on the 30 October when Quarrion's transpiration rate was substantially greater than Matong's. This interaction between the vegetation and the atmosphere is explored further in a later chapter.

Simple scaling of leaf conductance by the leaf area index to obtain canopy conductance was inadequate compared to the observations. For example, on 25 October the ratio of Quarrion to Matong for leaf conductances was 0.54 and the ratio of leaf areas was 0.71, which combined is a ratio of 0.38, whereas the ratio of measured canopy conductances was 0.69. While such simple scaling was not expected to give reliable estimates of canopy conductance, because leaves deeper in the canopy would have lower conductances, it was expected that the ratio of the conductances would be scaled from leaves to canopies by the leaf area. There are several explanations for the inadequacy of this simple scaling. Firstly, the canopy conductance calculated from the Penman-Monteith equation has been shown, theoretically, to be different from the leaf-area weighted sum of the individual leaf conductances (Raupach, 1995; McNaughton, 1994). McNaughton (1994) suggested that weighting individual leaf conductances by the net radiation distribution as well as leaf area was required for integrating to the canopy scale; however I have demonstrated in a later chapter that radiation weighting made little difference to the total canopy conductance compared with the simpler leaf area weighting, as was also reported by Leuning et al. (1995).

Another problem with canopy conductance calculated from the Penman-Monteith equation is the sensitivity of the evaporation to canopy conductance. Canopies with small roughness elements such as wheat canopies can be aerodynamically decoupled from the free atmosphere so that evaporation rate is mostly driven by the available energy and is relatively insensitive to canopy conductance (Jarvis & McNaughton, 1986). When data from such smooth canopies are used to infer the canopy conductance any small errors in the evaporation data are propagated into larger errors in the canopy conductance. This makes the evaluation of scaling difficult, since there is potentially large error in the calculated canopy conductance. These errors are examined further in a later chapter.

Another complication in the comparison of leaf and canopy conductances presented here is the sampling of leaves for the leaf data; only sunlit leaves at the top of the canopy

perpendicular to the sun's rays were sampled. It is possible that the ratio of conductances between the two cultivars was not the same for older leaves and for leaves receiving less light deeper in the canopy.

3.3.2.2. Scaling Photosynthesis

Scaling of photosynthesis from leaves to canopies was examined for the same two days (figure 3.26). On 25-October leaf photosynthesis was the same for both cultivars, which was reflected in the same rates of gross canopy photosynthesis. In contrast, on 30-October leaf photosynthesis of Matong was lower than that of Quarrion and this was also reflected at the canopy scale.
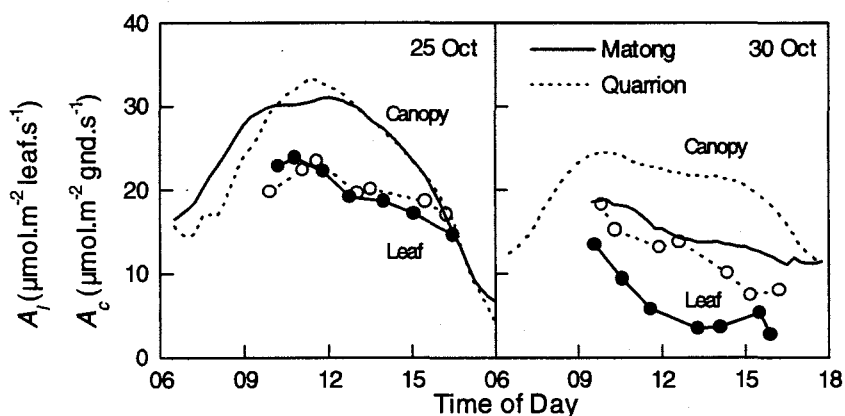
Figure 3.26 Comparison of diurnal variation in leaf (symbols) and gross canopy photosynthesis of the Matong (——) and Quarrion (·····) crops on the 25 October (left) and 30 October 1990 (right).

As with the scaling of conductance, photosynthesis was not simply scaled by the combined ratio of leaf photosynthesis of the two crops and the ratio of the canopy leaf areas. On the 25 October the Quarrion canopy had 30% less leaf area and similar rates of leaf photosynthesis, yet both crops had similar gross canopy photosynthesis. On 30 October the ratio of Quarrion to Matong in leaf photosynthesis was 2.3 and the ratio of the leaf areas was 0.69, which combined is 1.6, while the ratio of gross canopy photosynthesis was 1.4. While this is a reasonable match, there are obviously other factors involved in scaling up photosynthesis in addition to canopy leaf area. The

arguments given above for the problems in scaling of conductance also apply to scaling photosynthesis.

An alternative explanation for the similar rates of gross canopy photosynthesis from both crops when the leaf area of Matong was 30% greater than Quarrion's, is that the broadleaf selective herbicide (Igran) that was applied to the crops to control weeds impaired photosynthesis of leaves in Matong more than Quarrion. The spray was applied on August 29, so that leaves lower in the canopy would be affected but the flag leaf which would have emerged later would not be affected. Measurements of flag leaf photosynthesis would then not be representative of the whole canopy, if this were the case. Measurements of canopy CO_2 flux after the spray application were lower than CO_2 flux measurements before the spray, though no leaf gas exchange data were available for this period. Indeed, it was surprising that on the 12 October the Matong canopy, with a leaf area of 3.5 $m^2.m^{-2}$, had a net CO_2 flux of only 31 $\mu mol.m^{-2}.s^{-1}$ even though conditions were favourable for high rates of photosynthesis (PAR = 2200 $\mu mol.m^{-2}.s^{-1}$, D = 0.8 kPa, T_a = 16 °C).

3.3.2.3. Scaling Transpiration Efficiency

Transpiration efficiency of both crops was very similar despite expectations based on differences at the leaf scale (figure 3.27). On 25 October the transpiration efficiency of Quarrion was on average 49% greater than Matong at the leaf level, but only 5% at the canopy scale, while on the 30 October Quarrion had 24% greater transpiration efficiency than Matong but on average only 16% greater at the canopy level. Transpiration efficiency on the 25 October was higher than on the 30 October, due to higher air temperatures and hence greater leaf-to-air vapour pressure difference on the later day. The poor extrapolation of differences between the cultivars in transpiration efficiency from the leaf to canopy level is mainly a reflection of the insensitivity of canopy transpiration to canopy conductance, which is discussed further in later chapters. However, despite the diminished returns at the canopy scale there still was an advantage in the transpiration efficiency of Quarrion over Matong, which over the whole growing season could give a distinct advantage to the cultivar with more conservative water use.
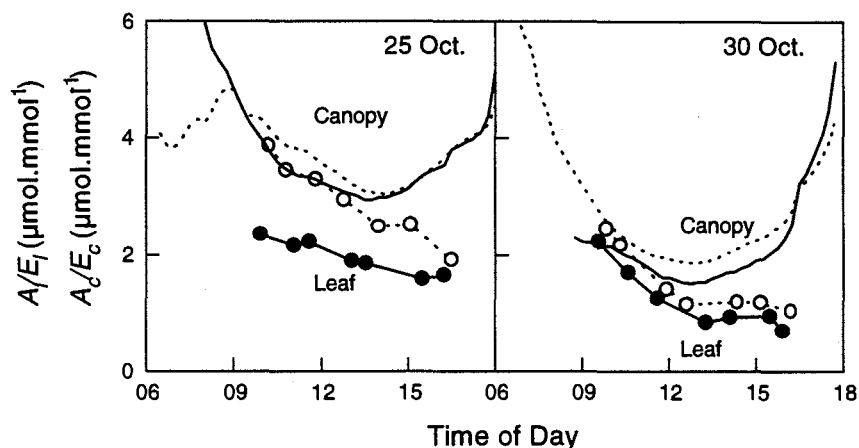
Figure 3.27 Diurnal variation of transpiration efficiency at the leaf (symbols) and canopy (lines) scales for the Matong (——) and Quarrion (·····) crops on the 25 October (left) and the 30 October 1990 (right).

3.3.2.4. Seasonal Water Use

Total water-use was greater from the Matong crop than the Quarrion crop in both years (figures 3.28 & 3.29) (Condon & Richards, 1993). In 1989 much of the water conserved from lower rates of transpiration in the Quarrion crop was lost as additional soil evaporation. This occurred because of the lower leaf area in the Quarrion crop (figure 3.2), which was a result of poor germination and low early vigour. Over the whole season the Matong crop had 21 mm more total water-use than Quarrion and 67 mm more transpiration.

In 1990 higher sowing rates were used in Quarrion to get the early leaf area of the two crops to match. However, the leaf area of Quarrion remained lower than that of Matong (figure 3.3). Again the reduced transpiration of Quarrion was offset by higher soil evaporation. At harvest total cumulative evaporation from Matong was 25 mm greater than from Quarrion, but 43 mm more transpiration.
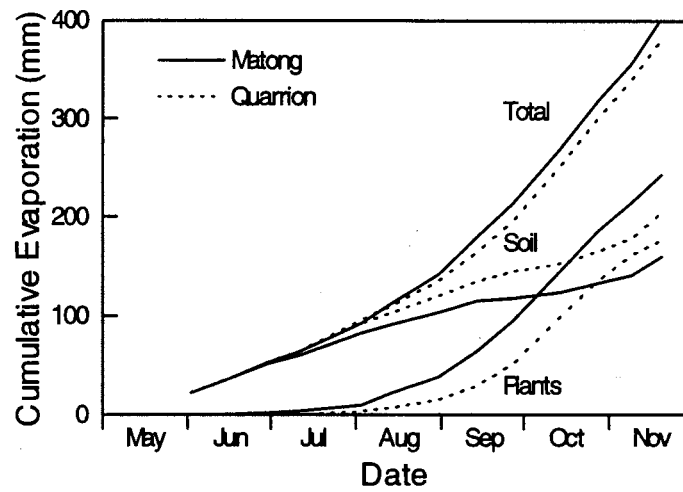
Figure 3.28 Cumulative water-use, transpiration and soil evaporation by the Matong (———) and Quarrion (·····) crops during 1989. Cumulative totals were calculated from the day of sowing (28 May).
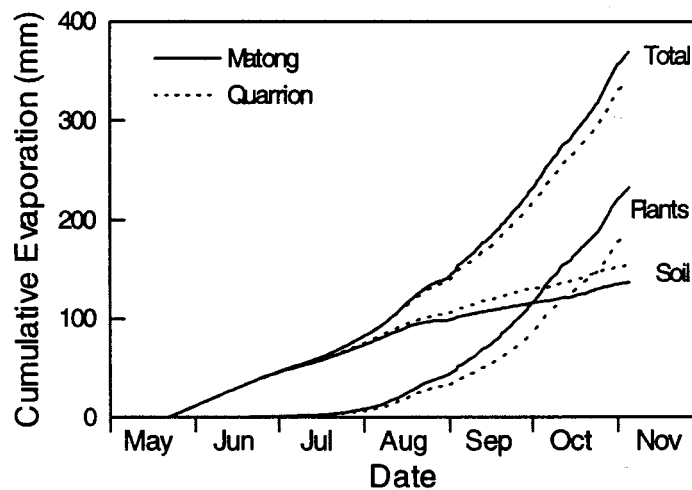
Figure 3.29 Cumulative water-use, transpiration and soil evaporation by the Matong and Quarrion crops during 1990. Cumulative totals were calculated from 28 August.

3.4. Further Discussion and Conclusions

3.4.1. Stomatal control of evaporation

The work presented in this chapter demonstrated that stomatal conductance does affect the transpiration rate of a crop, although differences in leaf area also had a significant impact on water-use over the growing season (figures 3.28 & 3.29). Jarvis & McNaughton (1986) theorised that the role of stomata in regulating evaporation decreases as the scale of observations increases from leaves to canopies to regions. At larger spatial scales boundary layer conductances become a more important factor in regulation of evaporation, than stomata. Canopy boundary layer conductance typically increases as the surface roughness and wind speed increase, so that rough canopies such as pine forests have relatively higher boundary layer conductances than smooth canopies of agricultural crops. Wheat crops, such as were examined in this work, are aerodynamically smooth so that their evaporation rate has low sensitivity to changes in stomatal conductance. This was confirmed in these experiments where large changes in stomatal conductance resulted in only small changes in evaporation rate (figure 3.25).

Despite the reduced effect of stomatal conductance on evaporation rate it was apparent that the energy balance of these wheat crops was affected by the stomatal conductance (figure 3.25). The different energy balance of the two contrasting wheat crops agrees with observed changes to the energy balance in other comparative studies of different canopies (Denmead, 1969; Tan & Black, 1976; Whitehead et al., 1984; Meinzer & Grantz, 1989; Jarvis, 1993; Baldocchi, 1994a). This confirms the importance of stomata, through their role in regulating water loss and CO_2 uptake, in determining the partitioning of energy from vegetation into sensible and latent heat, which is an important component of the global climate (Sud et al., 1990; Avissar & Pielke, 1991).

3.4.2. Scaling from leaves to canopies

In proposing the concept of canopy conductance, Monteith (1965) implicitly assumed that the conductances of individual leaves in a canopy act in parallel so that canopy conductance is determined by the leaf area weighted sum of leaf conductances (Monteith, 1973; Shuttleworth, 1976). Some experiments confirmed that canopy conductance was indeed related to the leaf conductance by a factor related to the leaf

area index (eg.; Tan & Black, 1976). However, other experiments found that simple scaling of leaf conductance by the leaf area index greatly overestimated canopy conductance so that a scaling factor less than the leaf area index was required (Munro, 1989; Rochette *et al.*, 1991). Theoretical analysis of the relationship between leaf and canopy conductance found that canopy conductance is influenced by the aerodynamic conductance and the radiation distribution, which are affected by the canopy structure, so that it is not an entirely physiological parameter (Thom, 1975; Shuttleworth, 1976; Finnigan & Raupach, 1987).

Despite these theoretical complications several studies have successfully demonstrated scaling between leaf and canopy conductances derived from flux measurements and the Penman-Monteith model. Bailey & Davies (1981) found that measurements of the adaxial and abaxial conductances scaled by the leaf area closely matched the canopy conductance. Similarly, Baldocchi (1987) found that sampling of stomatal conductance from sunlit and shaded leaves with weighting by the appropriate leaf areas matched the canopy conductance. Many of the earlier experiments which found scaling by the leaf area gave an overestimate of the canopy conductance, did not consider the variation of conductance between leaves in the canopy. Incomplete sampling of leaves throughout the canopy would lead to incorrect estimates of canopy conductance. Rochette *et al.*, (1991) compared several scaling approaches and found that consideration of the light distribution in the canopy was required to get agreement with the canopy conductance.

Several schemes have been proposed to account for the non-linear light response of stomata and radiation distribution in the canopy (Saugier & Katerji, 1991; Kelliher *et al.*, 1995). Such schemes are not simple and canopy models, which as a minimum account for light distribution, are required to accurately scale conductance from leaves to canopies. Scaling of photosynthesis from leaves to canopies also requires consideration of the non-linear light response of photosynthesis (Kim & Verma, 1991b; Norman, 1993). Scaling of stomatal conductance and leaf photosynthesis to canopy processes by means of models are considered further in subsequent chapters of this thesis.

Time and labour constraints prevented sampling all leaves in the canopy. This chapter emphasised the comparison of water-use efficiency of two cultivars at different spatial scales. It is apparent that large differences in stomatal conductance between the cultivars at the leaf level were diminished at the canopy level, although still present

(figure 3.24). This suggests that either the cultivar differences were not as large in the rest of the canopy (*ie.*, in the leaves not measured) or that some aspect of the scaling from leaves to canopies reduces the cultivar differences (*ie.*, not all leaf area contributes equally). The former explanation that cultivar differences were not present in all leaves could be explained by soil water deficits affecting leaves in the canopy differently (Dwyer & Stewart, 1986), so that the sampled flag leaves did not reflect the difference between the cultivars at the canopy scale. However, this effect must have been short lived since differences in carbon isotope ratios between cultivars were evident throughout the season (Condon & Richards, 1993) and were present in the penultimate leaves as well as flag leaves on the days sampled (data not shown), though this is not necessarily a reflection of the gas exchange taking place on those days.

Simple models of the light response of stomata and light extinction in canopies led to the suggestion that the ratio of maximum canopy to leaf conductance would asymptotically approach a value of 3 as leaf area of a canopy increases (Kelliher *et al.*, 1995). While these models suggest a diminishing return with increasing leaf area they do not explain why the difference between the cultivars should decrease at larger spatial scales.

Relative leaf photosynthesis of the cultivars was not reflected at the canopy scale considering the different leaf area of the crops (figure 3.26). As with the scaling of conductance, the comparison of cultivars in terms of canopy photosynthesis was expected to be related to the different leaf area of the crops, but this was not so.

These issues of scaling from leaves to canopies have been explored further by developing canopy models, which are presented in subsequent chapters of this thesis. I will return to these issues in the Chapter Eight to examine if some aspects of the scaling process are diminishing the cultivar differences at the canopy scale.

3.4.3. Comparison of canopy measurement techniques

There have been several comparisons of chambers with other techniques in the past. Canopy chambers have been demonstrated to give reliable canopy gas exchange so long as there is sufficient air mixing within the chamber and air flow is accurately measured (Nulsen, 1984). Chamber measurements were found to match lysimeter measurements (Reicosky *et al.*, 1983), but advective conditions at the edge of fields need to be avoided (Dugas *et al.*, 1991). Differences between chamber and Bowen ratio system

measurements were found to be between 40 to -80 $W.m^{-2}$ (0.9 to -1.8 $mmol.m^{-2}.s^{-1}$) and attributed to the different turbulent regime in chambers (Dunin *et al.*, 1989b). In the comparisons presented in this chapter, representative site selection was the greatest concern in getting reliable measurements of canopy gas exchange from the chambers. The lysimeter had the same problem, due to differences in canopy density. The Bowen ratio was the most reliable technique during the day, but did not operate at night, due to atmospheric stability which made measurements unreliable. Neutron probe measurements of the soil water profile gave the best integrated measurements of seasonal water-use.

Modification of the environment by the chambers limits their validity (Wesely *et al.*, 1989; Denmead & Raupach, 1993). For example, chambers have been shown to suppress soil fluxes (Kanemasu *et al.*, 1974). Denmead *et al.* (1993) attributed greater CO_2 fluxes in a chamber to enhanced utilisation of diffuse light by the canopy for photosynthesis; however they did not measure the diffuse light. The measurements of diffuse light presented in this chapter show that chambers do indeed increase the amount of diffuse light, but not all light in the chamber was diffuse. These effects of chambers on the quality of light in chambers will be examined further in subsequent chapters with models of canopy photosynthesis.

3.4.4. Canopy boundary layers

Associated with the canopy boundary layer is a modification of the air by the energy balance of the vegetated surface. The canopy boundary layer limits the mixing of air causing humidification and heating of the air close to the surface, which can result in a feedback from the atmosphere to the rate of evaporation from the surface (McNaughton & Jarvis, 1991). If stomatal conductance is reduced, the air adjacent to the surface becomes warmer and drier, increasing the saturation deficit of the air, which counteracts the effect of reduced conductance, so that the evaporation rate is not reduced by as much as it would have been if these feedbacks did not occur. Indeed, in this experiment the saturation deficit of the air was observed to increase when stomatal conductance was severely reduced (figure 3.25). Cowan (1988) suggested that the feedback associated with the canopy boundary layers may in fact reverse the benefit of reducing stomatal conductance, so that water-use efficiency may improve if stomata were to open more rather than close. Opening the stomata would cause the air to humidify reducing the saturation deficit of the air and increasing evaporation only slightly while allowing more

favourable conditions for photosynthesis. These experiments showed that although there was some modification of the air by the evaporation rate of the vegetated surface, the feedback was insufficient to completely negate or reverse the benefit of reducing stomatal conductance to improve canopy water-use efficiency (figure 3.27).

These feedback phenomena between the vegetation and the atmosphere have important implications for the size of plots used to examine water use by vegetation. If small plots are used with altered stomatal conductance to assess water use then the interactions with the atmosphere may not develop fully so that different results would be obtained than if extensive areas with reduced stomatal conductance were used. For these reasons this experiment was conducted in extensive paddocks of wheat with contrasting stomatal conductance. The issue of plot size was pursued by growing small plots of each of the cultivars Matong and Quarrion embedded in the large paddocks. Results of these comparisons will be presented in a paper by AG Condon *et al.* Another aspect of the same issue is the question of how large do plots need to be to observe the development of the atmosphere-vegetation interactions. This phenomenon of modifications to the atmosphere after a change in surface conductance or evaporation rate, is called advection and is pursued in Chapter Nine.

These experiments had an unexpected outcome in terms of approaches to improve water-use efficiency. It was apparent that much of the gain made through reduced transpiration could be offset by increased soil evaporation (Condon & Richards, 1993). This has led to a new line of plant breeding to obtain cultivars with low Δ, high water-use efficiency and high early vigour to reduce soil evaporation losses (Condon *et al.*, 1993 Richards, R.A., personal communication). This reinforces earlier work that showed canopy leaf area was a major determinant of crop water-use efficiency by balancing pre- and post-anthesis water use to maximise crop yields (Fischer, 1979). Improved water-use efficiency through use of Δ can only be effective so long as other crop attributes, such as early vigour, are not compromised. Use of cultivars selected on the basis of Δ to attain greater crop yields will require the incorporation of many other plant characteristics and altered management techniques, as was the case with incorporation of dwarfing genes into new wheat cultivars, where the alteration of a single trait by itself did not improve yield *per se* (Bush & Evans, 1988).

CHAPTER FOUR:

MODELLING STOMATAL CONDUCTANCE

Table of Contents

Summary

A comparison is made of three different approaches to modelling stomatal conductance based on either, 1) the response of stomata to environmental parameters, 2) the correlation of conductance with photosynthesis or 3) the optimisation of carbon gain with respect to water loss. The models were evaluated by comparison with field data from two canopies of wheat with contrasting leaf conductance.

In saturating light, a humidity response function in a Jarvis-type model accounted for much of the variation in stomatal conductance ($r^2 = 0.70$). Although there was little distinction between functions of relative humidity or leaf-to-air water vapour pressure difference (D), it was concluded that a function of $1/(k + D)$, the Lohammar function, were more appropriate given the response of stomata to evaporation rate rather than relative humidity. The Ball-Berry type model, using photosynthesis (A) as a variable improved the explanation of variation of leaf conductance over the Jarvis-type models ($r^2 = 0.75$). No other combination of variables in a Jarvis type model was as good as using A. No further functions of either light intensity, temperature, soil water availability or CO_2 concentration added any significant improvement to the models.

An analytical solution for leaf conductance was derived from the theory of optimisation of water loss with respect to carbon gain, $\partial E/\partial A$, using a linear response of photosynthesis to CO_2 concentration. This function explicitly contains photosynthesis, and a humidity response to $1/\sqrt{D}$. A simplified linear $\partial E/\partial A$ model was as good as the Ball-Berry model, with the Lohammar humidity function, at explaining the variation of leaf conductance. Fitting the linear $\partial E/\partial A$ model to data from each day separately improved the model ($r^2 = 0.87$), though many more parameters were used. Following 33 mm of rain, there was a large increase in values of $\partial E/\partial A$ from Matong, compared to little change of $\partial E/\partial A$ for Quarrion. The full $\partial E/\partial A$ model was poor at explaining the observed variance of leaf conductance ($r^2 = 0.36$ & 0.06 for Matong and Quarrion respectively), due to the sensitivity of the partial differentials of the model and the stochastic nature of stomatal conductance in the field.

The best model of stomatal response to the environment was the Leuning modified Ball-Berry model based on the correlation of stomatal conductance with photosynthesis and a hyperbolic response to D. Values of the model coefficients varied when the model was fitted to data from different days.

4.1. Introduction

Stomata are pores in the leaf surface that allow gaseous exchange between the atmosphere and the intercellular air spaces. They allow CO_2 to diffuse into the leaf, where it can be fixed by photosynthesis and they help prevent desiccation by regulating the efflux of water vapour. This conflict between CO_2 influx and water vapour efflux was one of the main problems that had to be overcome to allow plants to move away from permanent water onto land during the early Devonian era (Thomas & Spicer, 1987). Thus, the stomatal mechanism for this regulation has had approximately 400 millions of years of refinement through evolution.

The importance of stomata is reflected in the diverse areas of research that study stomatal response to the environment, including; photosynthesis (Farquhar & Sharkey, 1982), water use (Jarvis, 1976), energy partitioning (Avissar, 1993) and pollution uptake (Baldocchi et al., 1987). Many aspects of stomatal functioning and response to the environment have been extensively studied (for reviews see (Zeiger et al., 1987, and; Grantz, 1990). Yet despite all this work many mechanistic details remain elusive. Models of stomatal conductance reflect this state of affairs. Those that are based on known mechanistic functioning of stomata are too complex to parameterise and use (eg. (Penning de Vries, 1972). Other models are either based on empirical correlations, that may or may not be related to mechanisms, or on teleological theory.

Models of stomatal conductance can be divided into three categories: those that are based on regressions with environmental variables, referred to here as Jarvis-type models (Jarvis, 1976), those that are based on the correlation between stomatal conductance and photosynthesis (Wong et al., 1979; Farquhar & Wong, 1984), called Ball-Berry type models (Ball et al., 1987; Leuning, 1990; Leuning, 1995), and those based on the theory of optimisation of carbon gain with respect to water use (Cowan, 1977; Cowan & Farquhar, 1977), known as $\partial E/\partial A$ type models, where $\partial E/\partial A$ is the ratio of the sensitivities of transpiration and assimilation to changes in stomatal conductance ($(\partial E/\partial g)/(\partial A/\partial g)$)

The choice of functions used in the Jarvis or Ball-Berry models differ between experiments. In particular the nature of the stomatal response to leaf-to-air vapour pressure difference (D) has changed depending on whether vapour pressure (e_a) or leaf temperature (T_l) was varied (Collatz et al., 1991). This has caused consternation among

some researchers as to the mechanistic interpretation of such variation (Ball *et al.*, 1987; Aphalo & Jarvis, 1991). In field studies, variation in D is mostly attributable to the diurnal variation of T_a and to a lesser extent e_a.

The $\partial E/\partial A$ model as originally presented by Cowan and Farquhar (1977) required careful experimentation to determine the photosynthetic response surface to temperature and intercellular CO_2 concentration. While this is possible in controlled environments (Farquhar *et al.*, 1980; Hall & Schulze, 1980), it is yet to be achieved in natural environments. A simplification of the $\partial E/\partial A$ model, by assuming an infinite boundary layer conductance and a linear relationship between photosynthesis (A) and the intercellular CO_2 concentration (c_i), allowed an analytical expression to be obtained (Cowan, 1977), which was reflected in the shape of observed stomatal responses (Lloyd, 1991).

In this work I have taken another approach to implementing the $\partial E/\partial A$ model. Models of leaf photosynthesis, transpiration and the leaf energy balance were fitted to a data set of stomatal conductance (g) and environmental parameters. These models were then used to determine $\partial E/\partial g$ and $\partial A/\partial g$ numerically and hence calculate the value of $\partial E/\partial A$.

The broad objective of this work was to develop a scheme for spatial scaling of photosynthesis and evaporation, in particular from the leaf level of organisation to the canopy. In scaling physiological processes it is necessary to identify essential components at the smaller scale that influence the process at the larger scale. Stomatal conductance is a vital component that affects both photosynthesis and evaporation at the leaf level and at the canopy level. Since both photosynthesis and evaporation are driven by energy input from solar radiation and turbulent transfer, those leaves that intercept more light and are more exposed to the wind, *ie.* at the top of the canopy, are expected to make a greater contribution to the canopy level processes than shaded, sheltered leaves, lower in the canopy. This concept is supported by field studies using micro-meteorological techniques, which identified the upper level of canopies as the main source of water vapour and sink for CO_2 (Denmead & Bradley, 1985; Raupach *et al.*, 1992). In this context, the modelling of leaf level processes should reflect the relative importance of the upper leaves in a canopy, by giving emphasis to describing their behaviour.

Conductance of leaves lower in the canopy can be inferred from the conductance of leaves at the top using two consistently observed phenomena. 1) Conductance is correlated with photosynthesis, whether caused by leaf aging, nutrient status or light levels (Wong *et al.*, 1978; 1985a; 1985b; 1985c). 2) Leaves lower in the canopy are older, receive less light and have lower photosynthetic capacity (Field, 1983; Hirose & Werger, 1987b). Together these biological observations provide a sound basis for strategic modelling of upper leaves of the canopy, giving reasonable predictions of stomatal conductance of lower leaves. This strategy simplifies the stomatal model so that it can easily be parameterised, allowing it to be used for scaling up to the canopy.

It is important that a stomatal model, that is to be used to describe canopy processes, be developed using field data, since the dynamic environment of leaves in the field is different from the environment in laboratories. The environment in the field is dominated by diurnal changes in light and temperature, with little variation in CO_2 or water vapour concentration. The environment of leaves is also partially affected by the stomatal conductance itself. Wide-open stomata will tend to humidify the air and cool leaves, thus slightly reducing the leaf-to-air water vapour difference, *ie.* there is a degree of feedback in the evaporating system. In contrast, in many laboratory gas exchange systems leaf temperature or humidity is imposed upon a leaf, preventing any feedback. In some circumstances these interactions can result in apparently different stomatal responses to the environment between laboratory and field studies.

Models have typically not explained variation of stomatal conductance in field studies to the same degree as in laboratory studies (*eg.* (Lloyd, 1991; Lloyd *et al.*, 1991). This may be caused by the dynamic nature of the environment as already suggested, or by as yet unknown factors, or interactions between factors, or from the stochastic nature of stomatal conductance. In an attempt to account for this variability, many studies have attempted to monitor stomatal conductance in the field by random sampling of leaves from all positions in the canopy, yet have not necessarily included leaf age or position in the canopy as variables in the model. This strategy probably arose from the belief that a single unifying model of stomatal conductance should apply to all leaves. However, given the nature of degeneration of leaves with age and senescence, it is unlikely that a single model based on environmental parameters alone could account for this variation if leaf age or leaf nitrogen content (or photosynthetic capacity) is not included as a parameter itself. As already mentioned, gradients of leaf properties down a canopy are known to exist and have considerable effect on leaf physiology. Thus, this random

sampling strategy may have obscured better models of stomatal conductance from being identified. A focussed sampling effort aimed at leaves at the top of the canopy, may be a better use of limited resources and provide a better model of stomatal conductance in the context of scaling up to canopy processes.

This chapter describes the modelling of the stomatal conductance of fully sunlit leaves at the top of the canopy. The objective of the analysis was to determine the most suitable model to explain the variation of stomatal conductance in the field, that could also be used to extrapolate over a diurnal cycle and that could be incorporated into a scheme to scale up to the canopy. This involved a comparison of the models from both a theoretical and a statistical point. The next chapter uses these models to explore the scaling up of leaf measurements to the whole canopy and the determination of canopy transpiration.

4.2. Models

4.2.1. Jarvis type models

These models assume that stomatal conductance (g) can be described by several independent functions of environmental factors. Stomatal conductance is determined by their product:

$$g_l = f(I)f(D)f(T_l)f(c_a)f(\theta) \ , \tag{4.1}$$

where $f(I)$, $f(D)$, $f(T_l)$, $f(c_a)$, $f(\theta)$ are response functions to light intensity, leaf-to-air water vapour pressure difference, leaf temperature, CO_2 concentration and relative leaf water content, respectively. The form of the functions can be determined from controlled environment studies where environmental factors are varied separately, or by determining the best fit to a data set by statistics. Parameter values are determined by least squares regression of the functions on each data set.

The best choice of variables and response functions has varied with each data set examined, since they are based on regressions that may cover different ranges of the variables. The functions of I and D have been found to account for most of the variation and are considered a minimum set of variables (Thorpe et al., 1980; Jarvis et al., 1981). The response to I has been modelled as hyperbolic (Jarvis, 1976). The response to D has been linear, reciprocal or exponential (Jarvis, 1976; Lohammar et al., 1980; Jones, 1992). The temperature response functions reflect an optimum temperature for maximum stomatal conductance, and decreasing conductance to either side (Jarvis, 1976; Lloyd, 1991), but are often not significant (Jarvis et al., 1981). The CO_2 response reflects a linear decline above a certain threshold concentration. The effect of water status is modelled as a negative exponential function (Jarvis, 1976). However, in well-watered conditions or even under mild water stress a response to water status is not an important variable (Whitehead et al., 1981; Thorpe et al., 1980; Jarvis et al., 1985; Jones & Higgs, 1989).

A data set that covers the entire multi-dimensional environment space is required for these Jarvis-type correlation models, if the model is to be used confidently to predict new values of stomatal conductance. This is often difficult in field situations where many of

the environmental variables are strongly correlated. Strategic sampling is needed to overcome these correlations to determine the form of each function separately. Many data sets do not cover a broad range of some variables, which is probably the cause of the choice of best function varying between each experiment. Interpretation of the resulting best fit models to determine a mechanistic basis of stomatal response can be misleading (Aphalo & Jarvis, 1993). Some functions have asymptotic values of infinity or zero at extreme or particular values of the environmental variables. This should not be interpreted as a prediction of stomatal behaviour at these points, but rather that these functions are discontinuous $ie.$, they have limits to their applicability. Sometimes the discontinuities can be avoided by incorporating an additional constant (Leuning, 1995). Discontinuities are also present in some functions of the Ball-Berry and $\partial E/\partial A$ models.

4.2.2. Ball-Berry type model

These models take advantage of the observed coordination between leaf photosynthesis and conductance with changing light, CO_2 or nutrient levels, both in the short and long term (Wong $et\ al.$, 1978; 1985a; 1985b; 1985c). Ball $et\ al.$ (1987) used this correlation to model stomatal conductance by considering leaf photosynthesis as another variable in a Jarvis-type expression:

$$g = g_o + a_1 \frac{Ah}{c_s},$$ (4.2)

where A is leaf photosynthesis, and h and c_s are the humidity and CO_2 concentration of the air at the leaf surface. Simple linear regressions of g against the stomatal index, Ah/c_s, were used to determine the coefficient (a_1) and sometimes an intercept (g_o) representing a cuticular conductance. Leuning (1995) showed the importance of including the intercept term for correct modelling of intercellular CO_2 concentration (c_i) at low light. Modifications for particular data sets have included an offset of the CO_2 term by the CO_2 compensation point, Γ, which improves predictions at low CO_2 concentrations (Leuning, 1990), and replacement of h by a hyperbolic dependence on D (Leuning, 1995). Exploitation of the coordination between conductance and photosynthesis in models is based on the behaviour of c_i (Leuning, 1995). Other models have used the somewhat conservative behaviour of c_i explicitly in models of conductance

(de Wit & et al, 1978; Norman & Polley, 1989; Kim & Verma, 1991a), although this approach masks the subtle variations in c_i that do occur.

The Ball-Berry models can be considered a special case of a Jarvis type model, where one of the variables is leaf photosynthesis. However, this does have practical implications for use of the model, since photosynthesis must be known *a priori* or predicted from a model of photosynthesis. Thus the problem of knowing g is shifted to that of determining leaf photosynthesis. If photosynthesis is known by gas exchange then stomatal conductance is also easily measured. Alternatively, using a model of photosynthesis requires knowledge of the intercellular CO_2 concentration (c_i), which is determined by both photosynthesis and stomatal conductance. Thus, either conductance is measured and a model is not required or determining conductance becomes a circular problem. This circularity can be overcome and a solution found by iteratively solving the conductance and photosynthesis models, although the presence of leaf boundary layers mean that surface humidity, surface CO_2 concentration and the leaf energy balance must also be calculated iteratively. The Jarvis type models do not suffer from such circularity, but often do not reflect the reductions in stomatal conductance that occur when photosynthesis is reduced for endogenous reasons.

4.2.3. $\partial E/\partial A$ models

The $\partial E/\partial A$ concept is based on the optimisation of water use with respect to carbon gain. Cowan (1977) and Cowan & Farquhar (1977) developed this theory to demonstrate that leaf conductance would vary, in response to the environment during the day, so that the average rate of evaporation is a minimum for the particular average rate of assimilation. They showed that the 'optimum' stomatal behaviour is obtained when $\partial E/\partial A$ is constant (λ) with time and that a plant should operate such that λ is uniform amongst all leaves. Gas exchange in a controlled environment of a laboratory showed that stomatal response to the environment is consistent with the $\partial E/\partial A$ theory (Farquhar *et al.*, 1980; Hall & Schulze, 1980). Whether, stomatal behaviour in the field is consistent with $\partial E/\partial A$ theory remains to be demonstrated.

Analysis of $\partial E/\partial A$ requires division of the response surface into component interactions between photosynthesis, transpiration and the leaf energy balance (figure 4.1). Partial derivatives are used to describe the interactions so that
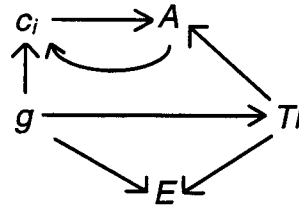
Figure 4.1 Component interactions of stomatal regulation of photosynthesis, transpiration and the leaf energy balance.

$$\lambda = \partial E/\partial A = \frac{\partial E/\partial g}{\partial A/\partial g}.$$

(4.3)

The response of photosynthesis and transpiration to leaf conductance can be further separated into that part which is caused directly by the change of conductance (*ie.* at constant temperature) and that which is a result of the change in temperature, a feedback from the leaf energy balance,

$$\frac{\partial E}{\partial g} = \left(\frac{\partial E}{\partial g}\right)_{T_l} + \left(\frac{\partial E}{\partial T_l}\right)_g \frac{\partial T_l}{\partial g},$$

(4.4)

$$\frac{\partial A}{\partial g} = \left(\frac{\partial A}{\partial g}\right)_{T_l} + \left(\frac{\partial A}{\partial T_l}\right)_g \frac{\partial T_l}{\partial g}.$$

(4.5)

The subscripts outside the brackets indicate the variables that remain constant with each partial derivative. The response of photosynthesis to conductance at constant temperature, $(\partial A/\partial g)_{T_l}$, can be further divided to demonstrate the direct effect of a change in leaf conductance on c_i, $(\partial c_i/\partial g)_A$, the effect of photosynthesis on c_i, $(\partial c_i/\partial A)_g$, and the physiological response of photosynthesis to c_i, $(\partial A/\partial c_i)_{T_l}$ (see Appendix for more details),

$$\left(\frac{\partial A}{\partial g}\right)_{T_l} = \frac{\left(\frac{\partial A}{\partial c_i}\right)_{T_l}\left(\frac{\partial c_i}{\partial g}\right)_A}{1 - \left(\frac{\partial A}{\partial c_i}\right)_{T_l}\left(\frac{\partial c_i}{\partial A}\right)_g}.$$

(4.6)

Solutions to these equations can be found by evaluating the partial derivatives by several different means; measurements in controlled environments, simplification to eliminate components or numerically with models. Considerable experimentation in a controlled environment is needed to measure the photosynthetic responses of $(\partial A/\partial c_i)_{T_l}$ and $(\partial A/\partial T_l)_g$. The results of such experiments depend on the measurement protocol (Collatz *et al.*, 1991; Lloyd, 1991) and consequently do not necessarily reflect the response in natural situations. This method has not been explored any further here. Simplifications, which allow an analytical solution to be obtained are explored in the next section. This is followed by a section describing a modelling approach to implement the full $\partial E/\partial A$ model to evaluate λ.

4.2.3.1. Linear form of $\partial E/\partial A$

There are various ways of simplifying the $\partial E/\partial A$ model. One way is to linearise components, which has been done in several different ways (Cowan, 1977). In well-ventilated situations the boundary layer conductance is large, so that $\partial T_l/\partial g = 0$ (*ie.* the leaf energy balance is ignored and $T_l = T_a$) and $(\partial E/\partial g)_{T_l} = D$. If light is sufficient to saturate photosynthesis and leaf conductance is small then the A-c_i curve can be approximated by a linear equation, so that

$$\left(\frac{\partial A}{\partial c_i}\right)_{T_i} = k = \frac{A}{c_i - \Gamma}. \tag{4.7}$$

An analytical solution was obtained for the optimal leaf conductance as a function of the 'internal resistance' to CO_2 transfer $(1/k)$ (Cowan, 1977, eq. 85 p. 203). However, I have chosen to replace k with $A/(c_i\text{-}\Gamma)$, which eliminates c_i and explicitly incorporates A, to give an analytical solution of leaf conductance, comparable with the Ball-Berry model,

$$g = A\sqrt{\frac{1.6\lambda}{(c_a - \Gamma)D}}. \tag{4.8}$$

This simple model can be extended to situations in which boundary layer conductance is finite by use of some approximations. In particular the leaf energy balance is used to determine T_l, but the feedback effects of the leaf energy balance are ignored $(\partial T_l/\partial g = 0)$ and to a first approximation $(\partial E/\partial g)_{T_l} \cong D$. Although this model is

not strictly correct for situations with a finite boundary layer conductance, it is still of use to give the general characteristics of the stomatal response.

The values of λ for this model were calculated from linear regressions. The linear form of $\partial E/\partial A$ model has a form similar to that of the Ball-Berry model, but with a stomatal response to $1/\sqrt{D}$. However, it is shown later that this equation has an unrealistic representation of stomatal response to CO_2, that does not concur with observations.

4.2.3.2. $\partial E/\partial A$ from Models of Transpiration and Photosynthesis

Cowan & Farquhar (1977) presented analytical solutions for the sensitivities of E and A to a change in leaf conductance, by differentiating models of the mass flow equations associated with E, A and the leaf energy balance (eqs. 4.17, 4.10 & 4.18). However, their expressions still require knowledge or measurements of $(\partial A/\partial c_i)_{T_l}$ and $(\partial A/\partial T_l)_g$, which are not easy. Alternatively, these expressions can be calculated numerically from models, which is the approach I have taken here. Since these calculations require implementation of entire models of E, A and the leaf energy balance, I have calculated all the differentials (eqs. 4.4 - 4.6) numerically rather than using their analytical solutions. Models were fitted to the data of E, A and the leaf energy balance, their sensitivities to a small change in g calculated and their ratio used to calculate λ.

Photosynthesis Model

The Farquhar *et al.* (1980) model of leaf photosynthesis was fitted to the data, assuming light saturation,

$$A = V \frac{c_i - \Gamma_*}{c_i + K_c (1 + O/K_c)},$$ (4.9)

where V is the Rubisco capacity of the leaf, c_i is the intercellular CO_2 concentration, Γ_* is the CO_2 compensation point in the absence of mitochondrial respiration, K_c and K_o are the Michaelis-Menten constants of Rubisco for CO_2 and O_2 respectively and O is the oxygen concentration. Temperature dependencies of V, K_c, K_o and Γ were described by the Arrhenius function (Farquhar *et al.*, 1980) and of Γ_* by a quadratic expression (Jordan & Ogren, 1984). Values of parameters are found in the List of Symbols.

111

The intercellular CO_2 partial pressure, c_i, was determined by the CO_2 supply function,

$$c_i = c_a - \frac{A}{1.6r_s + 1.37r_b},$$ (4.10)

where r_s and r_b are the stomatal and boundary layer conductances to water vapour, respectively and the factor 1.6 arises from the ratio of the diffusivities of water vapour and CO_2 in air (D_v/D_c) and 1.37 represents the ratio of the diffusivities in the boundary layer $(D_v/D_c)^{2/3}$ (Bird et al., 1960).

Combining eqs. 4.9 & 4.10 to eliminate p_i an expression was obtained for leaf photosynthesis in terms of combined leaf and boundary layer conductance $(g_t = 1/(1.6r_s + 1.37r_b))$,

$$A_l = \frac{V + g_t(c_a + K') - \sqrt{(V + g_t(c_a + K'))^2 - 4Vg_t(c_a - \Gamma_*)}}{2},$$ (4.11)

where K' is the effective Michaelis-Menten constant for carboxylation (mole fraction) and is given by

$$K' = K_c(1 + O/K_o).$$ (4.12)

Leaf Energy Balance

Available energy (Q) consists of several wavelength components that are differentially absorbed by leaves; photosynthetically active radiation (PAR, 0.4 - 0.7 µm), near infra-red (NIR, 0.7 - 3.0 µm) and long wave (3 - 100 µm), which can be summarised as

$$Q = R_V + R_{IR} + R_{Lsky} - R_{Lleaf},$$ (4.13)

where R_V and R_{IR} are the net absorbed PAR and NIR radiation, R_{Lsky} and R_{Lleaf} are the long wave radiation from the sky and leaf respectively. Long-wave radiation is dependent on the source temperature according to the Stefan-Boltzmann Law,

$$R_L = \varepsilon_s \sigma T_s^4,$$ (4.14)

where σ is the Stefan-Boltzmann constant, ε_s is the emissivity of the source and the temperature is degrees Kelvin. Long-wave radiation is absorbed by water vapour in the atmosphere so that an apparent emissivity of the sky (ε_{sky}) can be calculated from the air temperature (K) and water vapour pressure (mbar) (Brutsaert, 1982),

$$\varepsilon_{sky} = 1.24 \left(e_a / T_a \right)^{\frac{1}{7}}. \qquad (4.15)$$

Changes in leaf temperature affect the energy balance, through the emission of long wave radiation (R_{Lleaf}), which in turn affect the available energy for evaporation. The feedback between surface temperature and evaporation rate can be incorporated into the combination equation by use of the isothermal net radiation concept, in which Q has two components, Q_o the isothermal net radiation (the available energy if leaf temperature were equal to air) and a term that accounts for the additional radiation exchange as a result of the difference between leaf and air temperatures,

$$Q \cong Q_o - g_r C_p \Delta T, \qquad (4.16)$$

where g_r is a radiative conductance ($4\sigma\varepsilon_l T^3/C_p$), C_p is the molar specific heat content of air at constant pressure and ΔT is the difference between leaf temperature and air temperature outside the boundary layer ($T_l - T_a$). It was assumed that the lower leaf surface receives long-wave radiation from adjacent leaves at the same temperature and therefore has no net exchange of long-wave radiation, and that the upper leaf surface exchanges long-wave radiation with the sky. Net short-wave radiation absorbed by the leaf was calculated from the measured photosynthetically active radiation (PAR, 0.4-0.7μm) at the angle of the leaf, assuming that the ratio of short-wave radiation to PAR is 0.5 (MJ.mol^{-1}) and an absorption coefficient for solar radiation of 0.5.

Introducing this concept into the combination equation results in the expression (Cowan cited in Jones (1976)) (see appendix for details),

$$E = \frac{\varepsilon r_{bH}^* Q_o / L + D}{r_s + r_b + \varepsilon r_{bH}^*}. \qquad (4.17)$$

where ε is the change of latent heat content of saturated air with a change in sensible heat ($sL/(C_p P)$), L is the molar heat of vaporisation and r_{bH}^* is the combined resistance to sensible and radiative heat transfer in parallel ($1/(1/r_{bH} + g_r)$).

113

A similar equations can also be derived for the surface temperature (see appendix for details),

$$\Delta T = \frac{r_{bH}^{*}\left(Q_{o}(r_{s} + r_{b}) - LD\right)}{C_{p}\left(r_{s} + r_{b} + \varepsilon r_{bH}^{*}\right)} .$$ (4.18)

These models of transpiration and photosynthesis were used to implement the $\partial E/\partial A$ theory both to predict stomatal conductance and to interpret measurements as outlined below.

Estimation of $\partial E/\partial A$

The photosynthesis model was fitted to measured values of A, T_l and p_i to determine V. E was calculated using the Li-Cor measured g and values of T_a and e_a measured 25 cm above the canopy (eq. 4.17). Leaf temperature was then calculated from the leaf energy balance using the measured light intensity converted to radiant energy (eq. 4.18). A new value of A was then calculated using the new T_l and the ambient c_a (eq. 4.9). Leaf conductance was incremented by 0.05 mol.m^{-2}.s^{-1} and new values of E, T_l and A calculated. The ratio of the incremental changes in E and A was used to calculate $\partial E/\partial A$.

Leaf conductance predicted from λ

For optimal stomatal behaviour, $\partial E/\partial A$ is constant in time and space at a value λ, say. To calculate the value of g (and other parameters) at which $\partial E/\partial A = \lambda$, g was incremented in small steps from 0, and $\partial E/\partial A$ calculated as explained above. As g increased the value of $\partial E/\partial A$ also increased until the selected value of λ was reached and the combination of g, E, T_l, A and p_i noted as the values predicted by the model for any given combination of T_a, e_a, I and V. Predictions of g from several values of λ were obtained, which were then compared with the measured values.

As with the Ball-Berry model, the $\partial E/\partial A$ model requires knowledge of leaf photosynthesis. It does, however, then provide considerably more information than the Jarvis-type model. Interpretation of λ in an ecological context (Cowan, 1986) does give the $\partial E/\partial A$ model an advantage over the Ball-Berry and Jarvis models whose parameters do not necessarily have any physiological meaning.

4.3. Experimental Methods

Details of the experimental methods were given in chapter 3. A brief description is reiterated here.

4.3.1. Laboratory measurements

Plants of wheat cultivars Matong and Quarrion were grown in a glasshouse in Canberra from during May-July. Measurements of flag leaf gas exchange were conducted at 25°C, light intensity of 1500 µmol quanta.$m^{-2}.s^{-1}$, CO_2 concentration of 350 µmol per mol and average ambient air pressure of 95,100 Pa. Variation in D was generated by varying the humidity of the air stream passing over the leaf. At least 20 minutes was allowed for equilibration between each change of humidity, before steady state measurements were taken.

4.3.2. Field measurements

Two cultivars of wheat were grown in 5 hectare paddocks at Wagga Wagga. They were sown on May 22, 1990 and reached anthesis on the 20 and 22 October for Matong and Quarrion respectively. Measurements of leaf photosynthesis and conductance were made with a Li-Cor 6200 portable photosynthesis system. Sections of flag leaves for measurement were selected so that they were perpendicular to the solar beam, to ensure stomatal adjustment to saturating light. Average atmospheric pressure was 98.7 kPa.

Measurements were made on 10 days in the weeks before and after anthesis, which corresponded with a period of declining leaf area index. Ambient T_a and e_a were measured with ventilated wet- and dry-bulb psychrometers at 25 cm above the canopy. These sensors were part of a Bowen ratio system to measure canopy fluxes. Ambient c_a was measured in an air stream sampled from 25 cm above the canopy with an infra red gas analyser (Binos).

Soil water profiles were monitored fortnightly with a neutron probe to a depth of 1.8 m. The soil profile was saturated by rain at the end of July, which was used as a reference for subsequent measurements to calculate soil water depletion and relative soil water availability (W).

4.4. Results

4.4.1. Laboratory measurements

Leaf conductance, obtained from glasshouse grown plants measured with the laboratory gas exchange system, showed a strong response to D (figure 4.2). Photosynthesis also decreased with increasing D, but not as much as stomatal
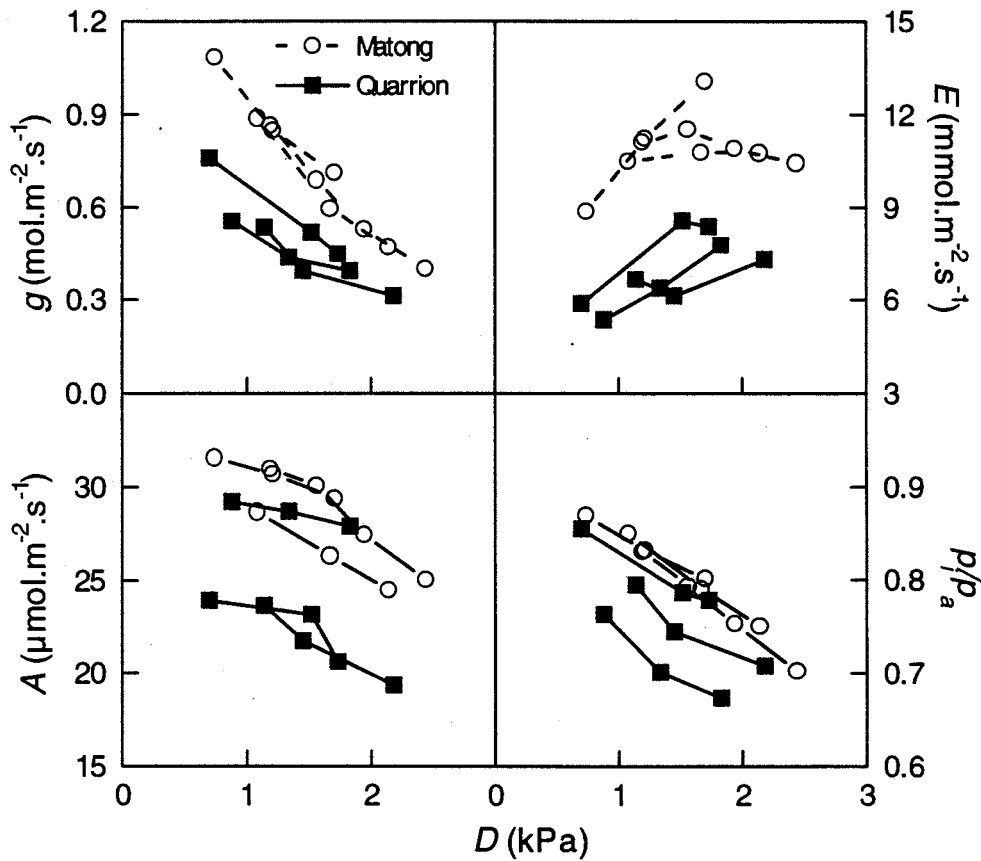
Figure 4.2 Variation in stomatal conductance (g), photosynthesis (A), transpiration (E) and ratio of intercellular to ambient CO_2 partial pressures (p_i/p_a) as a function of the leaf-to-air water vapour pressure difference (D). Measurements were made in the laboratory gas exchange system in order of increasing D on three different flag leaves of glasshouse grown wheat plants of the cultivars Matong and Quarrion (open circles and solid squares, respectively). Measurements made on the same leaf are connected by lines. Leaf boundary layer conductance was 3.5 $mol.m^{-2}.s^{-1}$. Leaf temperature was 25 ± 0.2 °C.

conductance, so that p_i/p_a decreased with increasing D. Transpiration increased with increasing D below 1.5 kPa, while at $D > 1.5$ kPa the response of E was variable. The response of transpiration to D has implications for inferring the mechanism by which stomata respond to humidity. When E increases with increasing D the stomatal response can be attributed to feedback behaviour, but when E decreases with increasing D a feedforward mechanism of sensing humidity is required (Farquhar, 1978; Cowan, 1977). There remains doubt about the existence of feedforward behaviour, as the response is usually not repeatable when D is decreased. In this experiment, some leaves showed evidence of feedforward behaviour, but reversibility was not checked.
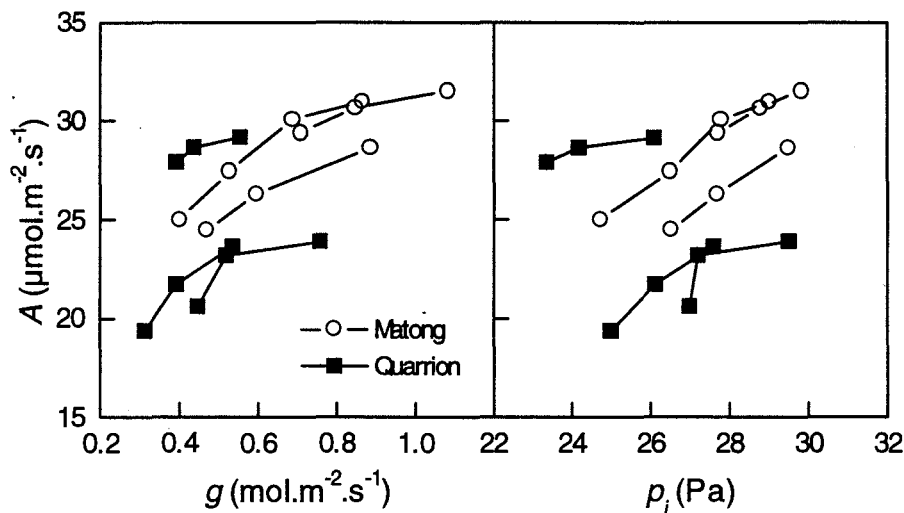
Figure 4.3 Variation of photosynthesis (A) with stomatal conductance (g) (*left*) and with intercellular CO_2 partial pressure (p_i) (*right*), caused by changing leaf-to-air water vapour pressure difference (D). Data were from the same measurements as in figure 4.2.

As expected the relationship between photosynthesis and stomatal conductance was not linear with variation in D (figure 4.3). However, significant variation was observed in the photosynthetic capacity; apparent in the A-p_i curves.

Table 4.1 Correlation coefficients (r^2) for the linear regressions of stomatal conductance (g) and the response functions of leaf-to-air water vapour pressure difference (D). Data were from the laboratory measurements presented in figure 4.2.

Function	Matong	Quarrion	Average
$1/D$	0.91	0.85	0.88
$1/\sqrt{D}$	0.95	0.84	0.90
D	0.97	0.77	0.87

Several stomatal response functions to D were fitted to both data sets. The fits with functions of $1/D$ and $1/\sqrt{D}$ (with non-zero intercepts) were just as good as a linear regression (Table 4.1). However, the predicted stomatal behaviour of these functions varied considerably when they were used to extrapolate to higher values of D (data not shown). A greater range of D was required to distinguish between these functions. The variation of D was generated by changing the water vapour pressure of the air. It was not possible to obtain data at higher values of D with these plants in the laboratory gas exchange system, as the stomata began to oscillate and did not stabilise sufficiently. This may have been due to the contrast between the steady, mild growth conditions ($T_a = 22$ °C, $h = 60\%$) and the higher temperatures required to get higher values of D.

4.4.2. Field measurements

Field measurements of stomatal conductance were made on ten days during 1990. Examples of the diurnal trend in g, A, p_i/p_a and D are presented in figure 4.4. The day of 25-Oct was typical of many days with adequate soil moisture and mild temperatures. On this day stomatal conductance of Quarrion was 45% less than that of Matong. Photosynthesis of both varieties was very similar, since Quarrion had a higher photosynthetic capacity per unit leaf area (Chapter Seven). As a result p_i/p_a was 20% lower in Quarrion than in Matong. There was a decline in photosynthesis during the day, which was not necessarily due to stomatal limitation, since p_i/p_a remained constant in Matong and increased during the day in Quarrion.
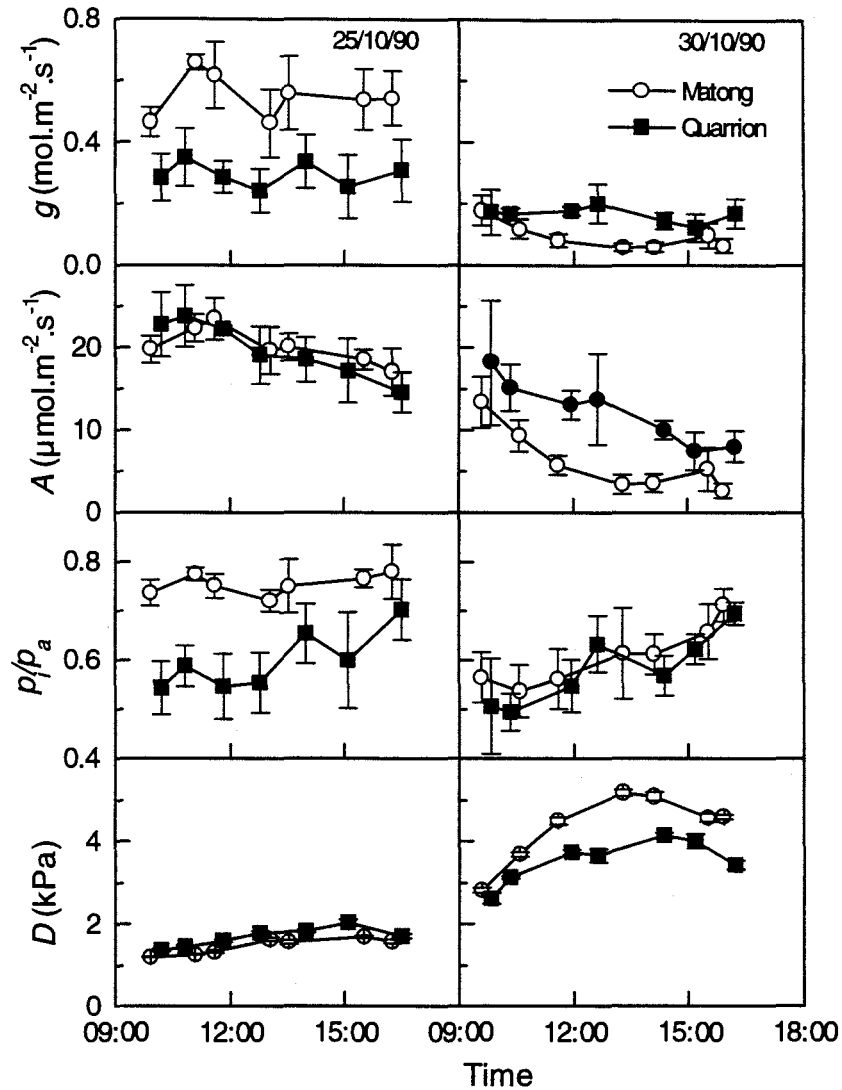
Figure 4.4 Field measurements stomatal conductance (g), photosynthesis (A), ratio of intercellular to ambient CO_2 partial pressures (p_i/p_a) and leaf-to-air water vapour pressure difference (D) on 25-Oct-90 (*left*) and 30-Oct-90 (*right*). Standard errors are shown as error bars. Each point is the average of five measurements.

The day of 30-Oct-90 was an extreme day of severe heat (35°C), high D and low soil water content. Matong which had been using soil water faster than Quarrion, because of the greater conductance, was more severely stressed with conductance on average 48% lower than that of Quarrion. Photosynthesis declined markedly in both varieties from mid-morning onwards, but this decline was not entirely due to stomatal limitation since

p_i/p_a increased during the day. Matong, as a result of the lower conductance, had higher leaf temperatures, drier air and greater D than Quarrion.
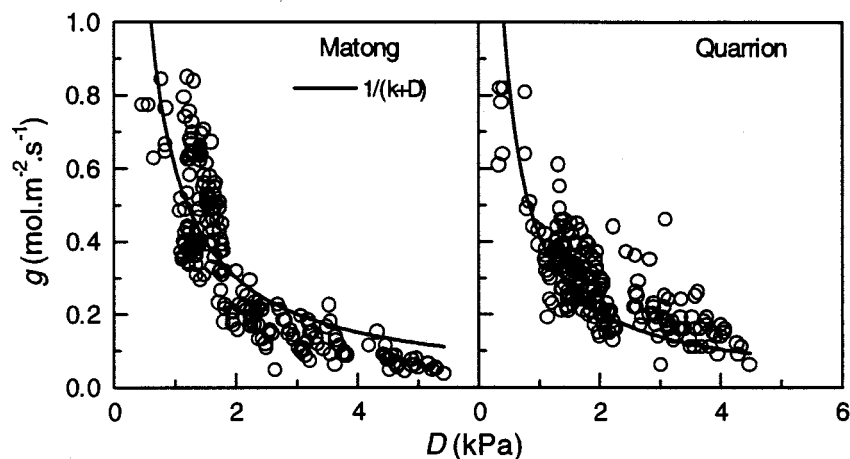
Figure 4.5 Stomatal conductance (g) measured in the field plotted as a function of leaf-to-air water vapour pressure difference (D). Data from 10 days are shown for Matong (*left*) and Quarrion (*right*). Also shown is the function of $1/(k+D)$ (line).

Combined data from all days showed a significant stomatal response to D in both varieties (figure 4.5). The function of $1/(k + D)$ is also plotted for comparison, which appears to account for much of the stomatal response to humidity. There was more unexplained variability in the Quarrion data than in Matong data.

4.4.3. Comparison of models

Different functions and combinations of functions have been used to model stomatal response to the environment. Several criteria are available for evaluating these models. Prior knowledge of variables which affect stomatal conductance was used to select suitable models which were then evaluated statistically. Common statistical criteria for rating regression equations are the residual mean squares or multiple correlation coefficient, r^2. However, inclusion of more fitted parameters inevitably causes a reduction in the residual mean squares and an increase in the r^2, which confounds comparisons between models with different numbers of parameters or variables. Using the adjusted-r^2 can account for inclusion or removal of independent variables, but has

defects when comparing models with different sets of variables (Snedecor & Cochran, 1980). When the proposed model is also to be used for prediction, each variable used introduces additional variance, so that the variance of the predictions increases monotonically with the number of variables used. Methods for quantifying the statistics in this trade-off, between increased explanation on the one hand and increasing variance of prediction on the other, are available (*eg*. Miller, 1990). Although they provide more accurate statistical criteria for evaluating models, they are complex to calculate. I have not used them in this analysis, but used instead the simple r^2 as a guide. Knowledge of stomatal behaviour outside the range of variables encountered in this study was also considered in the evaluation of stomatal models. For example, stomatal conductance decreases as CO_2 concentration increases and stomata do not continue opening at high humidity but reach a maximum aperture (Morison & Gifford, 1983).

4.4.3.1. Jarvis models

Several functions for the Jarvis models were fitted to the stomatal conductance data and the regression correlation coefficients compared (Table 4.2). Variables associated with the water vapour concentration *ie. h*, D or $\sqrt{D}$ were the most useful for explaining variation of g. Of these variables, h was the most useful explaining 69% of the variance

Table 4.2 Correlation coefficients (r^2) for the Jarvis type models with various functions fitted by linear regression to the field data of stomatal conductance.

Function	r^2 Matong	r^2 Quarrion	r^2 Average
h	0.735	0.646	0.691
h/c_a	0.792	0.665	0.728
$h/(c_a - \Gamma)$	0.780	0.636	0.708
$h[1 - \exp(-kW)]$	0.818	0.707	0.762
$1/D$	0.640	0.608	0.624
$1/(k + D)$	0.736	0.670	0.703
$1/[c_a(k + D)]$	0.765	0.676	0.721
$1/[(c_a - \Gamma)(k + D)]$	0.778	0.690	0.734
$1/\sqrt{D}$	0.683	0.609	0.646
$1/\sqrt{(k + D)}$	0.732	0.669	0.700
$1/[c_a\sqrt{(k + D)}]$	0.768	0.674	0.721
$1/[(c_a - \Gamma)\sqrt{(k + D)}]$	0.787	0.694	0.740

in g. However introducing a constant (k) in the denominator improved the functions of D and $\sqrt{D}$ (Lohammar et al., 1980), so that they were equally as good as h. Introducing a response to CO_2 (c_a) made only a small improvement in all three functions, which was expected since there was little variation in CO_2 concentration in the measurements. Adjusting the CO_2 function for the CO_2 compensation point of photosynthesis (Γ) improved the fit slightly for the D and $\sqrt{D}$ responses, but not for the h function. The best fit was obtained with h and an exponential function of relative available soil water (W). However, combining functions of W with other variables gave poorer fits than when W was not used (data not shown). Functions of light intensity, temperature or other variables did not improve the explanation of variance in g. There was more unexplained variation in data from Quarrion with all functions than with Matong.

4.4.3.2. Ball-Berry type models

All the functions that had been compared as Jarvis type models, with D or $\sqrt{D}$, were improved by incorporating leaf photosynthesis (A) as a variable (Table 4.3). Only the functions of D with the constant k are presented, since they all gave better fits than when k was omitted. Models with functions of W gave poor fits when A was included as a variable, reflecting the correlation between decreasing photosynthesis and decreasing soil water availability. Inclusion of c_a and Γ further improved both functions slightly. Functions with D or $\sqrt{D}$ were equally good in all combinations. It was noted earlier that

Table 4.3 Correlation coefficients (r^2) for the Ball-Berry type models with various functions fitted by linear regressions to the field data of stomatal conductance.

Function	r^2 Matong	r^2 Quarrion	r^2 Average
Ah	0.816	0.642	0.729
Ah/c_a	0.828	0.623	0.725
$Ah/(c_a - \Gamma)$	0.828	0.604	0.716
$A/(k + D)$	0.775	0.721	0.748
$A/[c_a(k + D)]$	0.787	0.721	0.754
$A/[(c_a - \Gamma)(k + D)]$	0.792	0.729	0.761
$A/\sqrt{(k + D)}$	0.771	0.724	0.747
$A/[c_a\sqrt{(k + D)}]$	0.785	0.723	0.754
$A/[(c_a-\Gamma)\sqrt{(k + D)}]$	0.788	0.726	0.757

functions h, $k + D$ and $1/\sqrt{(k + D)}$ were all equally good at explaining most of the variance in g. Adding a second variable to the model either c_a or A improved the model fit only slightly. Adding both c_a or c_a - Γ and A improved the model only incrementally.

These results and the response of stomata to CO_2 (Morison & Gifford, 1983; Mott, 1988), the response of stomata to evaporation rate rather than surface humidity (Mott & Parkhurst, 1991), which can be shown to be equivalent to a response function of $1/(k + D)$ (Farquhar, 1978; Monteith, 1995) and the behaviour of the functions beyond the range of variables encountered here, lead to the conclusion that the best combination of variables in a stomatal model was of the Ball-Berry type,

$$g = g_o + a_1 \frac{A}{(c_a - \Gamma)(k + D)}.$$

(4.19)

Careful attention to units is required in use of this model, such that all variables are in moles; g and g_o are expressed in $mol.m^{-2}.s^{-1}$, A is in $\mu mol.m^{-2}.s^{-1}$, c_a and Γ are in $\mu mol.mol^{-1}$ and k and D are $mmol.mol^{-1}$, which must all be scaled to moles to give the correct solution. This model was fitted to the field data from all days combined and for

Table 4.4 Coefficients for the stomatal model $g = g_0 + a_1 A/((c_a - \Gamma)(k + D)$ fitted to leaf data for Matong and Quarrion. A fixed intercept was used: $g_0 = 0.01$. All - indicates a fit to data from all days combined (as in Table 4.3). Individual dates indicate coefficients fitted for each day. Overall - is the regression correlation coefficient for all data with the model with coefficients for each day.

Date	Matong			Quarrion		
	k	a_1	r^2	k	a_1	r^2
All	10.0	0.162	0.80	5.68	0.100	0.73
06-Sep	3.69	0.093	0.89	8.45	0.139	0.76
12-Oct	14.9	0.151	0.51	9.86	0.101	0.47
17-Oct	14.7	0.138	0.58	32.1	0.200	0.39
18-Oct	14.7	0.142	0.75	32.1	0.198	0.77
24-Oct	2.60	0.113	0.81	4.82	0.093	0.66
25-Oct	2.60	0.127	0.10	4.82	0.081	0.32
26-Oct	2.60	0.136	0.60	4.82	0.099	0.49
30-Oct	43.9	0.260	0.80	36.0	0.231	0.57
31-Oct	43.9	0.279	0.77	36.0	0.272	0.85
01-Nov	43.9	0.276	0.82	36.0	0.228	0.51
Overall	-	-	0.92	-	-	0.82

each day separately. The model was over-parameterised for data of many individual days, so an intercept was assumed of $g_o = 0.01$. On days with a small range of D there was a mutual dependency between the parameters k and a_1, which was overcome by grouping data of consecutive days to fit k and independently fit a_1 for each day (Table 4.4). Direct comparison of the slopes between days and between cultivars is complicated by k varying, since k and a_1 are partially correlated. The values of k, which reflect stomatal sensitivity to D, were low following rain on the 24-26 October and increased as the soil water content decreased. The low regression coefficient in some data sets was due to little variation in conductance for those days, due to a small range of D.

4.4.3.3. $\partial E/\partial A$ Models

Linear form of $\partial E/\partial A$

The linear form of $\partial E/\partial A$ model was fitted to the data assuming a constant value of λ (Table 4.5). For the Matong data set the model fit accounted for only slightly less variation than any of the Jarvis or Ball-Berry models, whereas the Quarrion data set was better described by the linear $\partial E/\partial A$ model than the original Ball-Berry model, but less well than some of the other modified Ball-Berry type models. Overall the linear form of the $\partial E/\partial A$ model accounted for only slightly less variation in stomatal conductance than other models.

Fitting the linear form of $\partial E/\partial A$ model to data for each day separately improved the overall fit to the data (Table 4.5). However, as explained earlier, comparison between models with different numbers of parameters is not straight forward. The use of separate parameters for each day improves the explanation of variance in the data, but may not be of use for prediction unless the parameter values themselves can be predicted.

Table 4.5 Correlation coefficients of the linear form of $\partial E/\partial A$ model fitted to field data of stomatal conductance.

Function $A/\sqrt{[(c_a - \Gamma)D]}$	Matong λ	r^2	Quarrion λ	r^2	Average r^2
Constant λ	1544	0.782	869	0.667	0.724
Variable λ	-	0.929	-	0.807	0.868

Fitted values of λ seem to be related to availability of soil water (figure 4.6). After a large rain event (33 mm) the values of λ for the Matong data increased for a few days and then returned to values similar to those prior to the rain. There was only a small change in λ for Quarrion.
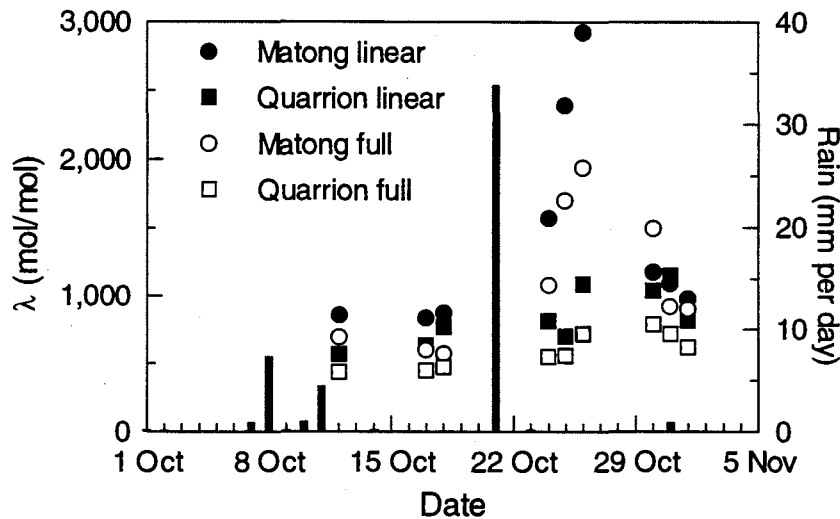
Figure 4.6 Day to day variation of λ calculated from the linear form of $\partial E/\partial A$ (solid symbols) or the averages of the full differential $\partial E/\partial A$ (open symbols) models of stomatal conductance fitted to field data for the wheat cultivars Matong (circles) and Quarrion (squares). Also shown is the daily rainfall (bars).

Full $\partial E/\partial A$

Values of the full differential of $\partial E/\partial A$ calculated from each data point using the models of transpiration, leaf energy balance and leaf photosynthesis were very variable (figure 4.7). No relationship with any variables was observed in either the Matong or Quarrion data (not shown).

Average values of λ were calculated from all data on each day for the full differential $\partial E/\partial A$ model. These averages were lower than those calculated by fitting the linear form of $\partial E/\partial A$ model, but varied in a similar manner (figure 4.6). This may seem contrary to expectations, since the linear model has larger values of $\partial A/\partial c_i$ than the full partial

differential model. However, the full model includes the leaf energy balance, so that $\partial E/\partial g$ and $\partial A/\partial g$ are altered by the subsequent change in leaf temperature.
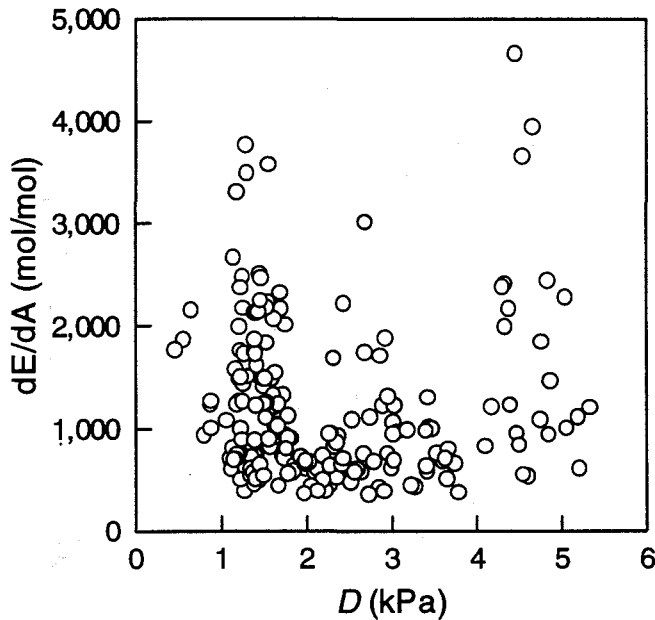
Figure 4.7 Values of $\partial E/\partial A$ calculated using the leaf transpiration, energy balance and photosynthesis models for the Matong field data.

The full $\partial E/\partial A$ model was unable to explain much of the observed variation in leaf conductance, with low regression correlation coefficients of predicted and observed g (Table 4.6). Allowing a separate value of λ for each day increased the r^2 for the Matong

Table 4.6 Regression correlation coefficients (r^2) of stomatal conductance predicted with the full $\partial E/\partial A$ model with a single λ for all days or a different value of λ for each day, with the data from Matong and Quarrion cultivars of wheat.

	Matong		Quarrion	
	λ	r^2	λ	r^2
Constant λ	1420	0.36	673	0.06
Variable λ	-	0.61	-	0.07

data, but made no change to the r^2 of the Quarrion data. Despite the extra detail included in the full $\partial E/\partial A$ model the regression correlation coefficients of predicted and observed g were lower than those obtained using the linear form of $\partial E/\partial A$ model (Table 4.5).

4.4.3.4. Predicted stomatal response to CO_2

Modelled stomatal response to CO_2 concentration was predicted for the Ball-Berry/Leuning model, the linear $\partial E/\partial A$ model and the full $\partial E/\partial A$ model (figure 4.8). Only the Ball-Berry/Leuning model gave predictions of stomatal response to CO_2 that matched experimental evidence (Morison & Gifford, 1983). The linear $\partial E/\partial A$ model predictions were unrealistic. The full $\partial E/\partial A$ model gave predictions that matched observations at low values of D, but unrealistic predictions at high D.
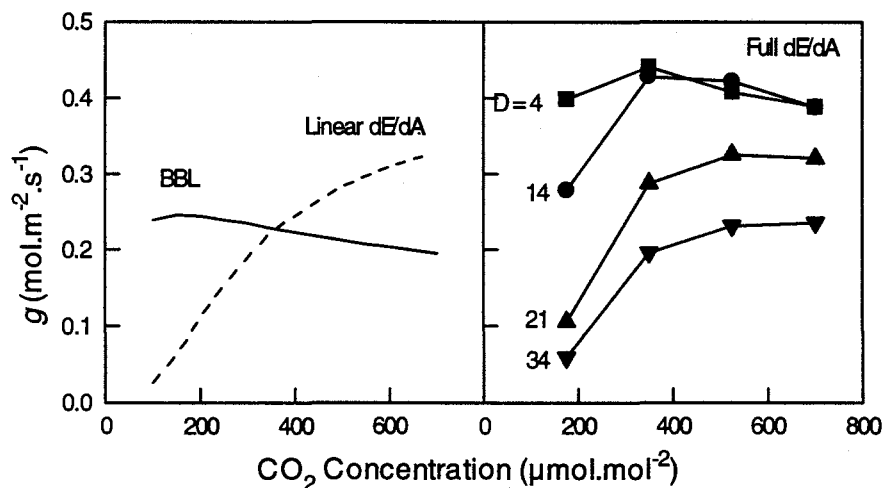
Figure 4.8 Modelled stomatal (g) response to CO_2 concentration as predicted by the Ball-Berry/Leuning model (BBL) and the Linear $\partial E/\partial A$ model (left) and the full $\partial E/\partial A$ model at different leaf-to-air vapour pressure differences (D) (right).

4.5. Discussion

4.5.1. Stomatal response to air humidity

There was little distinction between the various functions of D or h that were tried in the models of g, which accords with the conflicting results from other studies (Ball *et al.*, 1987; Leuning, 1990; 1995; Collatz *et al.*, 1991; Lloyd, 1991; Aphalo & Jarvis, 1993). Since the basis for these models is not mechanistic but only correlative, it is not surprising that different data sets are best explained by different variables. Nothing should be inferred from the variables selected in terms of a mechanistic basis of stomatal behaviour. Comparisons of D and h as the driving variables for stomatal response to humidity have shown that neither variable is entirely satisfactory (Aphalo & Jarvis, 1991; Collatz *et al.*, 1991). Indeed, studies in helium and oxygen (Helox) in place of air (Mott & Parkhurst, 1991), have shown that stomatal conductance is proportional to the transpiration rate, rather than any measure of the humidity at the surface. Given that transpiration is directly related to D rather than h, in a normal atmosphere, the former is a better choice where other criteria cannot distinguish between them. The ability of h to explain variation of stomatal conductance when water vapour concentration is varied at a constant temperature (Collatz *et al.*, 1991), is of little value in field situations where most diurnal variation of humidity is caused by changes in temperature rather than vapour concentration. In this context, the Lohammar (1980) function, $1/(k + D)$, was the best choice to describe the stomatal response to humidity, which concurs with the conclusions of Leuning (1995) in his appraisal of the Ball-Berry model.

Functions of humidity (either D or h) were the most significant in explaining the variation of g, which is not surprising since variation in CO_2 concentration and light intensity was minimised in the sampling strategy. Similar results were obtained by Thorpe (1980), who found that natural variations of CO_2 concentration were small compared to variations of D and I, allowing a simple model with only two variables to account for much of the variation of g, under well watered conditions. In many field situations, at least where canopy air is well mixed, such simple models may be sufficient, since diurnal variation is dominated by changes in light and temperature, while water vapour and CO_2 concentrations vary much less. In forests, however, these variables may be important although they are not always measured (Whitehead *et al.*, 1981).

4.5.2. Use of A to predict g

The results of this study confirm the general applicability of using A as a variable in models of g (Ball et al., 1987; Leuning, 1990; 1995; Collatz et al., 1991; Lloyd, 1991; Aphalo & Jarvis, 1993), which improved the model predictions more than any other variable after D or h. The basis of using A as a variable is the observed correlation between A and g, which is maintained with variation in light, nutrient levels or leaf age (Wong et al., 1979). A mechanistic basis for this correlation is unknown. Gas exchange studies with electron transport inhibitors have shown that stomatal conductance and photosynthesis can be decoupled (Sharkey & Raschke, 1981). Other studies with molecular antisense techniques directed at the ribulose-1,5-bisphosphate carboxylase/oxygenase (Rubisco) small subunit have shown that photosynthetic capacities of leaves could be reduced, without affecting stomatal conductance (Quick et al., 1991; Hudson et al., 1992). These results preclude a direct linkage between Rubisco photosynthetic capacity and stomatal conductance, requiring some other tightly coordinated link. Because such a link seems to occur in the field, models of the Ball-Berry type were significantly better than the Jarvis-type models, and are sufficiently simple to allow them to be easily incorporated into models of canopy photosynthesis and transpiration.

4.5.3. $\partial E/\partial A$ models

The linear form of $\partial E/\partial A$ model was only slightly worse at predicting leaf conductance than the other functions. Similarly Lloyd (1991) and Aphalo (1993) found that models with $1/\sqrt{D}$ were good predictors of leaf conductance.

Significant improvements were obtained by fitting separate values of λ for the linear form of the $\partial E/\partial A$ model for each day. Similar values of λ were obtained using the full $\partial E/\partial A$ model. Interpreting the cultivar differences in the values of λ is interesting. Quarrion, the cultivar with more conservative water use as a result of lower stomatal conductance, had lower values of λ than the cultivar Matong. The values of λ of Matong increased dramatically after the large rain event (October 22, 1990), but there was little response in Quarrion. The significance of these different responses is limited, since wheat cultivars have been selected for many traits other than adaptation to the environment. However this pattern fits with the speculated ecological significance of λ, which is expected to decrease with declining soil water availability (Cowan, 1982; 1986). An alternative explanation for the increase in λ is that it may have been somehow related

to physiological changes associated with anthesis which occurred on 20 October in both cultivars.

The $\partial E/\partial A$ models predict an increase in leaf conductance in response to increasing CO_2, which is contrary to observations (Morison & Gifford, 1983) and predictions of the Ball-Berry model (Leuning, 1995). This is not surprising, since there has been little selective pressure through evolution for plants to optimise water use with respect to carbon gain (and hence maintain a constant $\partial E/\partial A$) with changing CO_2 concentrations. It does not invalidate the use of the $\partial E/\partial A$ theory at steady CO_2 concentrations. However, it does render these models, as presented here, unsuitable for analysing or predicting leaf conductance with changing CO_2 concentrations.

The inability of the full $\partial E/\partial A$ model to describe the observed variation in stomatal conductance may be attributed to a combination of the stochastic nature of conductance and the highly sensitive partial differentials in the model. The $\partial E/\partial A$ model may have performed better if averages of the variables were used in place of the actual data. While the environment may fluctuate rapidly the biological response of stomata and photosynthesis is considerably slower, so that at an instant stomatal conductance may not reflect the current environment but reflect the average state of the environment over the preceding period, *eg.* 15 minutes. An extended optimisation model might include constraints associated with the dynamics of stomatal response.

Comparison of the performance of the chosen linear form of $\partial E/\partial A$ model with the full version, suggests that the ability of the former, to describe much of the variation in leaf conductance, was probably due to the coincidental form of the analytical solution containing essential elements. The assumptions made in the linear version are not trivial and indeed when they were realistically incorporated into the full version of the model, the model's performance was poor. Incorporation of the full $\partial E/\partial A$ model as a sub-process into canopy models is not warranted.

4.6. Conclusions

Comparison of several models identified water vapour concentration of the air as the most important variable for predicting leaf conductance in the field under conditions of saturating light. No distinction could be made between functions of D or h. However, based on results of other comparisons, functions of D are preferable to those of h.

Despite the additional complexity of using A as a variable, its inclusion in models of g is warranted if A is measured, since it encompasses effects of varying light intensity, temperature, plant nutrition and leaf age, which would otherwise be difficult to incorporate. However, in the absence of direct measurements of A, it remains to be seen how well models can predict photosynthesis in the field for use in models of stomatal conductance.

The linear form of $\partial E/\partial A$ model was as good at predicting leaf conductance as other functions. This ability was a fortuitous result of the form of the analytical solution, which contains the essential elements for describing the response of conductance to the environment. The full $\partial E/\partial A$ model was poor at explaining or predicting leaf conductance, due to the sensitive partial derivatives of the model and the stochastic nature of stomatal conductance.

From this work, it is concluded that the best model to describe leaf conductance was a modified Ball-Berry type model, that includes a hyperbolic response to D and c_a, and a linear function of A (eg. $g = g_o + a_l A/[(c_a - \Gamma)(k + D)]$).

4.7. Appendices:

4.7.1. Partial derivatives of the $\partial E/\partial A$ model

The response of photosynthesis to a change in leaf conductance is via the effect on the intercellular CO_2 concentration (c_i),

$$\left(\frac{\partial A}{\partial g}\right)_{T_l} = \left(\frac{\partial A}{\partial c_i}\right)_{T_l} \left(\frac{\partial c_i}{\partial g}\right)_{T_l},$$

(4.20)

where $(\partial c_i/\partial g)_{T_l}$ can be separated into components caused by the direct effect of a change in leaf conductance (at constant A) and the indirect effects via the change in photosynthesis (at constant g);

$$\left(\frac{\partial c_i}{\partial g}\right)_{T_l} = \left(\frac{\partial c_i}{\partial g}\right)_{T_l,A} + \left(\frac{\partial c_i}{\partial A}\right)_{T_l,g} \left(\frac{\partial A}{\partial g}\right)_{T_l}.$$

(4.21)

Combining these two expressions and rearranging, an expression is found that can easily be evaluated (Farquhar *et al.*, 1978; Cowan & Farquhar, 1977),

$$\left(\frac{\partial A}{\partial g}\right)_{T_l} = \frac{\left(\dfrac{\partial A}{\partial c_i}\right)_{T_l} \left(\dfrac{\partial c_i}{\partial g}\right)_{T_l,A}}{1 - \left(\dfrac{\partial A}{\partial c_i}\right)_{T_l} \left(\dfrac{\partial c_i}{\partial A}\right)_{T_l,g}},$$

(4.22)

where for the linear model (Cowan, 1977)

$$\left(\frac{\partial A}{\partial c_i}\right)_{T_l} = \frac{A}{c_i - \Gamma}$$

(4.23)

or for the full model at light saturation (Farquhar *et al.*, 1980)

$$\left(\frac{\partial A}{\partial c_i}\right)_{T_l} = V \frac{K' + \Gamma_*}{\left(K' + p_i\right)^2}.$$

(4.24)

In turn the variation of c_i in eq. 4.22 can be expanded according to the partial response of c_i to a change in leaf conductance

$$\left(\frac{\partial c_i}{\partial g}\right)_{T_i, A} = \frac{1.6A}{g^2},$$ (4.25)

and the partial response of c_i to a change in photosynthesis is

$$\left(\frac{\partial c_i}{\partial A}\right)_{T_i, g} = -\frac{1.6}{g}.$$ (4.26)

Also, the response of E to a change in leaf conductance (at constant temperature) is

$$\left(\frac{\partial E}{\partial g}\right)_{T_i} = D\left(\frac{1}{1 + g/g_b}\right)^2.$$ (4.27)

Equations incorporating the leaf energy balance are found in the Appendix I of Cowan & Farquhar (1977). (Note the typographical error in the numerator of their equation 17, where the terms should be subtracted rather than added.)

4.7.2. Derivation of the combination equation with isothermal net radiation.

The water vapour flux is given by

$$E = \frac{w_i - w_a}{r_s + r_b},$$ (4.28)

where w is the water vapour concentration (mol.mol^{-1}) of intercellular air spaces (w_i) and ambient air (w_a) outside the boundary layer of resistance r_b. r_s is the stomatal resistance. The sensible heat flux (H) is given by

$$H = C_p \Delta T / r_{bH}$$ (4.29)

where C_p is the molar heat capacity of air, r_{bH} is the boundary layer resistance to heat transfer and ΔT is the difference between leaf temperature and air temperature outside the boundary layer $(T_l - T_a)$. Available energy (Q) can be expressed as

$$Q \cong Q_o - 4\sigma\varepsilon_{leaf}T_a^3\Delta T \qquad (4.30)$$

where Q_o is the isothermal radiation (available energy if leaf temperature were equal to air) and the last term accounts for the radiation exchange as a result of the difference between leaf and air temperatures. Introducing the concept of radiative conductance $(g_r = 4\sigma\varepsilon_{leaf}T_a^3/C_p)$, the above equation can be rewritten as

$$Q \cong Q_o - g_r C_p \Delta T . \qquad (4.31)$$

Rearranging eq. 4.31 to obtain ΔT and using the energy balance $(Q = H + LE)$,

$$\Delta T = r_{bH}H/C_p = r_{bH}(Q - LE)/C_p , \qquad (4.32)$$

and, substituting for Q using eq. 4.16,

$$\Delta T = \frac{r_{bH}(Q_o - g_r C_p \Delta T - LE)}{C_p} = \frac{Q_o - LE}{C_p(g_{bH} + g_r)} = \frac{r_{bH}^*(Q_o - LE)}{C_p} , \qquad (4.33)$$

where g_{bH} is the boundary layer conductance to sensible heat transfer $(1/r_{bH})$ and r_{bH}^* is the combined resistance to sensible and radiative heat transfer in parallel $(1/(g_{bH} + g_r))$.

Using the approximation of $w_i \cong w_a' + (s/P)\Delta T$, where w' is the saturated vapour concentration and s is the change in saturated vapour pressure with temperature (de_s/dT), the combination equation is derived from eq. 4.28, and combined with the expression for ΔT (eq. 4.33),

$$E = \frac{w_a' + (s/P)\Delta T - w_a}{r_s + r_b} = \frac{w_a' + (s/P)r_{bH}^*(Q_o - LE)/C_p - w_a}{r_s + r_b} . \qquad (4.34)$$

Defining D as vapour concentration deficit $(w_a' - w_a)$ and ε as $sL/(C_pP)$, the above equation can be rearranged to give,

$$E = \frac{(\varepsilon/L)r_{bH}^{*}(Q_o - LE) + D}{r_s + r_b}.$$

(4.35)

Collecting terms of E, gives

$$E\left(r_s + r_b + \varepsilon r_{bH}^{*}\right) = (\varepsilon/L)r_{bH}^{*}Q_o - D,$$

(4.36)

which can be rearranged to

$$E = \frac{\varepsilon r_{bH}^{*}Q_o/L + D}{r_s + r_b + \varepsilon r_{bH}^{*}}.$$

(4.37)

Leaf temperature with isothermal radiation.

Combine expressions for ΔT (eq. 4.33) with the above isothermal combination equation,

$$\Delta T = \frac{r_{bH}^{*}}{C_p}\left(Q_o - L\frac{\varepsilon r_{bH}^{*}Q_o/L + D}{r_s + r_b + \varepsilon r_{bH}^{*}}\right),$$

(4.38)

which simplifies to

$$\Delta T = \frac{r_{bH}^{*}\left(Q_o(r_s + r_b) - LD\right)}{C_p\left(r_s + r_b + \varepsilon r_{bH}^{*}\right)}.$$

(4.39)

CHAPTER FIVE:

SCALING CONDUCTANCE AND TRANSPIRATION

Table of Contents

Summary

Stomatal conductance is well described by models that correlate conductance with photosynthesis. Extension of these models to describe and predict canopy conductance will improve the understanding of vegetation-atmosphere interactions.

Concurrent measurements of gas exchange at both the leaf and canopy scale were used to investigate the scaling of conductance from leaves to canopies. The Ball-Berry model was used to facilitate this scaling, since it can accommodate the within-canopy variation of light intensity and conductance. The model was fitted to data at both the leaf and canopy scale. Coefficients derived from fitting the model at the leaf level were used to predict canopy conductance.

The model accounted for much of the variation in canopy conductance. Coefficients derived from fitting the model to leaf and canopy scale data were different. Use of the coefficients derived from the leaf scale data allowed the model to predict the diurnal variation in canopy conductance, but the exact magnitude of canopy conductance was not accurately predicted. The disagreement was as much a reflection of the inherent uncertainty in data of canopy conductance as an inadequacy of the model.

Predictions of canopy transpiration were within 10% of measurements and often better, although the aerodynamically smooth canopies used in this experiment had low sensitivity of transpiration to changes in surface conductance.

The Ball-Berry model can be successfully used to model canopy conductance. The model provided a means to use leaf-scale data to predict canopy conductance. However, this model uses photosynthesis as a variable, which is not strictly independent. Simple and accurate models of canopy photosynthesis are required to make independent predictions of canopy conductance. Understanding the nature of the variation in the stomatal model coefficients will improve the utility of this approach.

5.1. Introduction

The study of evaporation from vegetation is an inter-disciplinary field of research encompassing meteorology and physiology. Both disciplines are aware of each other's work, yet the complexities are often greatly simplified to a 'black box' parameter in models of the process: for meteorologists this is a surface resistance and for physiologists a boundary layer conductance (usually in different units of $s.m^{-1}$ and $mol.m^{-2}.s^{-1}$, respectively).

Attempts to model climate and predict climate change has led to a recognition that an improved representation of surface resistance is needed. Similarly attempts by plant breeders to improve agricultural production through altered stomatal conductance has led to a need for better representation of canopy boundary layers and their effects on canopy evaporation (Farquhar *et al.*, 1989). Physiologists have long recognised the influence of CO_2 concentration (Morison & Gifford, 1983) and other environmental factors on stomatal conductance and have developed models to describe these responses. The challenge is to scale these physiological models to be applicable at the canopy level, while ensuring that they be sufficiently simple that they are useable.

A common link between physiology and meteorology in controlling canopy evaporation has been through the Penman-Monteith equation (Penman, 1953; Monteith, 1965) and several other forms of the combination equation (Stewart, 1983). They combine the processes of energy supply, turbulent transport and stomatal regulation into a single layer representation of canopy evaporation. The complexities of real canopies are disguised in the simplicity of the Penman-Monteith equation, but re-emerge when defining appropriate values for the parameters (Finnigan & Raupach, 1987; McNaughton, 1994; Raupach, 1995).

Three issues have led to modifications of the Penman-Monteith equation. 1). In the original formulation of the Penman-Monteith equation, Monteith (1965) proposed that the profiles of temperature and water vapour concentration be extended to an apparent source coinciding with the apparent sink for momentum at which wind speed would be zero. Thom (1972), however, demonstrated that there are differences in the level of the apparent sources and sinks for heat, water vapour and momentum transfer and that ignoring these differences would affect the definition of the surface resistance. Definition of the aerodynamic resistance to include the additional resistance to heat and water

vapour transfer that is not encountered by momentum transfer is preferable to having a significant aerodynamic component in the surface resistance (Brutsaert, 1982). 2). The single layer assumption of the Penman-Monteith equation is not valid in canopies where soil fluxes are significant. Shuttleworth & Wallace (1985) developed a two-layered model, which can be used in such situations. More recently, Raupach (1995) described definitions of the resistance parameters to include both plant and soil components for use in a single layered model. 3). From its inception the concept of surface resistance of a canopy was considered a mainly physiological parameter (Monteith, 1965), which was the summation of all the individual leaf conductances in parallel (Monteith, 1973). However, McNaughton (1994) showed that this was just one among many possible schemes available for averaging leaf parameters to obtain bulk canopy values, depending on the purpose of the scaling. Despite these different definitions, Raupach (1995) showed that several different schemes produce very similar results. Yet determining these resistances remains a serious limitation to using the Penman-Monteith equation as a predictive tool. It is to this latter point that this chapter is devoted.

In practice measuring the stomatal conductance of all leaves in a canopy or obtaining truly representative samples is impossible. Instead several aggregation schemes have been adopted and used in conjunction with different canopy sampling strategies (*eg.* (Bailey & Davies, 1981; Whitehead *et al.*, 1981; Avissar, 1993). A comparison of several methods found that these were unsatisfactory, since they did not account for seasonal changes in leaf area of the canopy or the distribution of light with leaf angle in the canopy (Rochette *et al.*, 1991). Another approach has been to parameterise models of leaf conductance (Jarvis, 1976) from measurements in canopies. A stomatal model combined with a model of the irradiance of sunlit and shaded leaves, was a significantly better approach than direct scaling of stomatal measurements (Rochette *et al.*, 1991). However, this approach overestimated canopy conductance when soil water content was low (Kim & Verma, 1991b), because soil water content was not explicitly included as a variable in the model.

The correlation between photosynthesis and conductance (Wong *et al.*, 1978) has led to improved models of stomatal conductance (Ball *et al.*, 1987; Leuning, 1990; 1995; Collatz *et al.*, 1991). These have been incorporated into several canopy models (Wang & Jarvis, 1990; Reynolds *et al.*, 1992; Leuning, 1995), but have not been tested with concurrent measurements of fluxes from both leaves and canopies. In only a few cases has this approach been used at the canopy level in conjunction with data. The

coordination between stomatal conductance and photosynthesis was used by Kim & Verma (1991a) to successfully model surface conductance in a grassland canopy using separate sunlit and shaded leaf fractions. It has been used in a multilayer canopy model, to explore the effects of increased atmospheric CO_2 concentration (Reynolds *et al.*, 1992) and in a big leaf model to predict daily water use in pine forests (McMurtrie *et al.*, 1992), but not compared with flux measurements. Further developments of big leaf models have been proposed by Sellers *et al.* (1992) and Amthor (1994). The applicability of these stomatal models to describe canopy conductance and the potential to use these models to scale from leaves to canopies remains to be demonstrated on a range of different vegetation types, with intensive concurrent measurements of leaf and canopy conductances and fluxes.

In the previous chapter (Four) several models of stomatal response to the environment were compared with a data set of leaf conductance measurements in a wheat paddock. Models that included leaf photosynthesis as a parameter were better able to explain the observed variation of stomatal conductance than models without leaf photosynthesis. It was concluded that the Leuning (1995) modified version of the Ball-Berry model was the best model.

The objective of this work was to demonstrate the applicability of leaf stomatal models to describe canopy conductance and to explore the scaling up of leaf stomatal measurements to canopy conductance and transpiration. The work presented in this chapter describes the application of the Leuning modified Ball-Berry stomatal model to a big leaf representation of a canopy. Predictions of canopy conductance were combined with the Penman-Monteith equation to predict canopy evaporation. Comparisons are made with measurements of evaporation, transpiration, and calculated surface and canopy conductances obtained with the Bowen ratio technique and ventilated chambers in a paddock of wheat.

5.2. Model

5.2.1. Scaling Conductance

The previous chapter (4) compared several models of stomatal conductance with different combinations of variables. It was concluded that the best model of stomatal conductance was the Ball-Berry model (Ball *et al.*, 1987) as modified by Leuning (1995) (referred to as the BBL model hereafter),

$$g_{lBB} = g_o + a_1 \frac{A_l}{(c_s - \Gamma)(k + D_o)},$$ (5.1)

where g_{lBB} is the leaf conductance modelled by the BBL model, A_l is leaf photosynthesis, c_s is the atmospheric CO_2 concentration at the leaf surface, Γ is the CO_2 compensation point of photosynthesis, D_o is the leaf-to-air vapour concentration difference (the difference between the saturated vapour concentration at leaf temperature and the vapour concentration of the air at the leaf surface), k is a constant, g_o and a_1 are the intercept and slope of the regressions respectively. Note that correct use of this equation and similar equations in this chapter require all variables in units of moles, so that scaling factors must be applied where the variables are typically given in μmol or mmol (refer to the List of Symbols for units of each variable).

The direct application of this stomatal conductance model to big leaf representations of canopies, is based on the conservation of the ratio of A_l/g_l, when either leaf age, nutrient status or light varies (Wong *et al.*, 1978; 1979; 1985c; 1985b; 1985a). The ratio does vary with c_s and D_o, which are explicitly incorporated in the stomatal model. Variation of leaf age and light are the principal sources of spatial variation of stomatal conductance in a canopy, while c_s and D_o vary much less. Thus it is assumed that these models describe the behaviour of all leaves in the canopy and therefore that the ratio of canopy photosynthesis to conductance will also be maintained, *ie.* A_c/g_c. A_c is defined as the sum of photosynthesis from all leaves of canopy leaf area index (L_c) (*ie.* gross canopy photosynthesis or net canopy CO_2 flux plus respiration),

$$A_c = \int_0^{L_c} A_l(L)dL,$$ (5.2)

and similarly for canopy conductance,

$$G_c = \int_0^{L_c} g_l(L)dL .$$

(5.3)

Combining these expressions with the BBL model and replacing the surface vapour deficit and CO_2 concentration with those of the air in the canopy results in the expression

$$G_{cBB} = g_o L_c + a_1 \frac{\int_0^{L_c} A_l(L)dL}{(c_a - \Gamma)(k + D_l)} = g_o L_c + a_1 \frac{A_c}{(c_a - \Gamma)(k + D_l)} ,$$

(5.4)

where values of c_a were obtained directly from measurements at the top of the canopy and were assumed to represent the values at the notional canopy surface. The response of Γ to temperature was calculated with an Arrhenius function of temperature with the activation energy given in the List of Symbols. D_l, the leaf-to-air vapour concentration difference, was calculated from measured canopy leaf temperature (T_s) and the water vapour concentration of the air (w_a) measured 0.25 m above the top of the canopy, assumed to be similar to w_a in the canopy. The stomatal model requires gross canopy photosynthesis as an input variable, which was calculated from measurements of net CO_2 flux and estimated respiration as described in the Experimental Methods section. In a subsequent chapter models of conductance, photosynthesis and the energy balance were combined and solved concurrently.

The model was applied to canopies by assuming a big leaf representation. Several different parameterisation schemes were compared. Parameters were obtained from fitting the model to either the leaf data from all days, leaf data from each day or from the canopy data for each day. The parameters g_o, a_1 and k obtained by fitting the models to the leaf data from each day and all days combined are given in Table 5.1.

Table 5.1 Coefficients for the stomatal model (eq. 5.1) fitted to leaf data for Matong and Quarrion. A fixed intercept was used: $g_0 = 0.01$. All - indicates a fit to data from all days combined. Individual dates indicate coefficients fitted for each day. (Reproduced from Table 4.4).

Date	Matong			Quarrion		
	k	a_1	r^2	k	a_1	r^2
All	10.0	0.162	0.80	5.68	0.100	0.73
06-Sep	3.69	0.093	0.89	8.45	0.139	0.76
12-Oct	14.9	0.151	0.51	9.86	0.101	0.47
17-Oct	14.7	0.138	0.58	32.1	0.200	0.39
18-Oct	14.7	0.142	0.75	32.1	0.198	0.77
24-Oct	2.60	0.113	0.81	4.82	0.093	0.66
25-Oct	2.60	0.127	0.10	4.82	0.081	0.32
26-Oct	2.60	0.136	0.60	4.82	0.099	0.49
30-Oct	43.9	0.260	0.80	36.0	0.231	0.57
31-Oct	43.9	0.279	0.77	36.0	0.272	0.85
01-Nov	43.9	0.276	0.82	36.0	0.228	0.51

5.2.1.1. Bowen Ratio Data

The calculated canopy conductance was compared with the surface conductance (G_{cPM}) calculated by inverting the Penman-Monteith (PM) equation,

$$\frac{1}{G_{cPM}} = r_{cPM} = \frac{\varepsilon r_{aH} Q / L^M + D_r}{E_c} - (\varepsilon + 1) r_{aH}. \tag{5.5}$$

where ε is the change of latent heat of saturated air with a change in sensible heat as temperature changes ($s L^M / (P C_p)$), s is the rate of change of saturated water vapour pressure with temperature, L^M is the molar latent heat of evaporation, P is atmospheric air pressure, C_p is the molar specific heat of air at constant pressure, r_{aH} is the aerodynamic resistance to turbulent transfer of sensible heat between the surface and the reference height (1.0 m above the canopy), calculated from sonic anemometer measurements and stability corrections as described in the appendix, Q is the available energy (R-G) absorbed by the canopy, D_r is the water vapour concentration deficit of the air at the reference height and E_c is the measured canopy transpiration (total evaporation less soil evaporation, E_T - E_s) (described in Experimental Methods section).

Aerodynamic conductance to sensible heat transfer ($g_{aH} = 1/r_{aH}$) from the canopy to the reference height was calculated from sonic anemometer data of wind speed (u) and friction velocity (u_*). Concurrent measurements of sensible heat flux were used to correct for atmospheric stability using the Monin-Obukhov theory, which results in the expression (see appendix for more details),

$$r_{aH} = \frac{1}{ku_*}\left[\ln\left(\frac{z-d}{z_{oH}}\right) - \Psi_H(\zeta)\right]\frac{RT}{P}, \tag{5.6}$$

where r_{aH} is the aerodynamic resistance, k is von Karman's constant, $z - d$ is height above the nominal crop surface, z_{oH} is the roughness length of the canopy for turbulent heat transfer, $\Psi_H(\zeta)$ is an integral function to describe atmospheric stability and RT/P is a conversion factor to molar units, which is derived from the universal gas equation, $PV = nRT$. Resistance in a flux equation responding to units of mole fraction (r^M) are related to resistance for a flux dependent on density difference (r^s) by several interchangeable expressions,

$$r^M = r^s\frac{RT}{P} = r^s\frac{M_a}{\rho_a} = r^s/C_a, \tag{5.7}$$

where M_a is the molecular mass of air (29 g.mol^{-1}), ρ_a is the actual density of air (including water vapour) and C_a is a molar concentration of air (ρ_a/M_a, mol.m^{-3}). I have chosen to express all resistances and conductances in molar units as this is the accepted practice in plant physiology. Use of units associated with density gradients, preferred by meteorologists, would have been equally valid.

The aerodynamic resistance to turbulent transfer of heat (r_{aH}) and water vapour (r_{aV}) are assumed equal, but are greater than the resistance to momentum transfer ($r_{aH} = r_{aV} > r_{aM}$) due to the bluff body forces encountered by momentum transfer that have no analogy in the transfer of other entities (see appendix) (Thom, 1972).

Direct comparisons of g_{cPM} with the modelled canopy conductance are complicated by the former not being an entirely physiological variable, when combined with the above definition of aerodynamic resistance (Raupach & Finnigan, 1988; Baldocchi, 1991; McNaughton, 1994). It contains some within-canopy resistance to transport and is affected to some extent by the wind speed and canopy structure as well as the radiation

regime. However in the canopy used in this study the physiological resistances are much greater than the within-canopy resistances so that these differences probably have little net effect (Finnigan & Raupach, 1987; Raupach, 1995). This is verified in Chapter Eight.

Values of the surface conductance (G_{cPM}) inferred from measurements of transpiration can be very variable in some situations. This problem arises when the aerodynamic resistance is large (*ie.* over smooth crops) and predictions of transpiration from the PM equation are relatively insensitive to the value of the surface conductance and so conversely the inferred surface conductance is very sensitive to small errors in the measured values of transpiration. Thus, this formulation of the PM equation makes it difficult to evaluate a model of canopy conductance. Comparisons of canopy conductance and surface conductance are subject to large influence from errors in the transpiration measurements, and comparisons of modelled and measured transpiration are relatively insensitive to the canopy conductance values. Comparisons of both conductance and transpiration have been used in this chapter.

5.2.1.2. Tent Data

Inside the ventilated tent, gradients typical of a normal canopy, are prevented from developing by mixing fans, rendering calculation of a suitable g_{aH} for the PM equation difficult. The evaporation rate can be related to an equation describing the flux by a concentration gradient and resistances,

$$E_c = \frac{D_l}{\left(1/G_c + 1/g_{aH}\right)}.$$
(5.8)

Rearrangement of this equation allows an alternative surface conductance (G_{cD}) to be calculated from the measured E_c, D_l and an assumed value of g_{aH}. A reasonable fit was obtained by assuming an infinite canopy boundary layer conductance, so no further assumptions regarding the value of g_{aH} were used. This surface conductance was used for comparison with the modelled canopy conductance in the tent.

147

5.2.2. Canopy Transpiration

Modelled canopy conductance was used in the Penman-Monteith equation to predict canopy transpiration,

$$E_c = \frac{\varepsilon r_{aH} Q / L^M + D_r}{r_c + (\varepsilon + 1) r_{aH}}.$$
(5.9)

Effects of the transpiration rate on surface temperature, the emmision of long wave radiaton and the energy balance were ignored, but are considered in Chapter Eight.

Equilibrium Evaporation

When the canopy aerodynamic conductance is very low, the surface and the atmosphere are said to be decoupled (McNaughton & Jarvis, 1983). The resultant evaporation rate is known as equilibrium evaporation (E_{eq}),

$$E_{eq} = \varepsilon Q / [L^M (\varepsilon + 1)].$$
(5.10)

However, the converse is not true. When the measured evaporation rate is the same as the equilibrium evaporation rate the surface is not necessarily decoupled. It is a biological coincidence that measured evaporation is often close to the equilibrium evaporation rate, that arises from the response of stomata to radiation. Such observations have occasionally been falsely interpreted as indicative of minimal control of evaporation by stomata.

The sensitivity of evaporation to changes in stomatal conductance is expressed in the decoupling coefficient (Ω), with values which range from zero for rough canopies, that are completely coupled to the atmosphere to one for canopies that are aerodynamically smooth and are completely decoupled (McNaughton & Jarvis, 1983; 1986). It is calculated as,

$$\Omega = 1 - (\partial E_c / E_c) / (\partial g_c / g_c) = (\varepsilon + 1) / (\varepsilon + 1 + g_{aH} / g_c).$$
(5.11)

148

5.3. Experimental Methods

Details of the experimental methods were given in chapter 3. A brief description is repeated here.

Concurrent measurements of stomatal conductance and photosynthesis on leaves and total canopy evaporation and net CO_2 flux were made in two paddocks of wheat in 1990. The two wheat cultivars used were similar, except for their stomatal conductance and hence transpiration efficiency (ratio of instantaneous photosynthesis to transpiration). Cultivar Matong had greater stomatal conductance than cultivar Quarrion. Measurements were made between 12 October and 1 November in the weeks around anthesis (20-22 October). Fortnightly harvests of 0.5 m^2 were used to determine the canopy leaf area.

Gas exchange measurements were made using a Li-Cor 6200 portable photosynthesis system on flag leaves oriented perpendicular to the sun's rays.

Canopy fluxes were measured by two methods in each paddock: Bowen ratio systems; and 2.3 m^2 ventilated chambers (tents). Half hour running means of two fifteen minute measurement intervals were available from the Bowen ratio systems and readings each 12 minutes from the tents.

Soil Evaporation

Soil evaporation was estimated over intervals of two weeks, using the method of Cooper (1983). This involves measuring changes in the soil water profile both beneath the crop and from bare soil. Measurements of light interception by the canopy are used to convert bare-soil evaporation to soil evaporation from beneath the crop.

Daily soil evaporation was calculated by interpolation of the fortnightly estimates using measurements of pan evaporation as a scaling factor. Diurnal variation of soil evaporation was assumed to be in proportion to the calculated equilibrium evaporation from the soil beneath the canopy while the soil surface was wet (Black *et al.*, 1970; Ritchie, 1972). Cumulative evaporation and rainfall was used to model the water content of the top 5 cm of soil. As the soil surface dried below a threshold water content the evaporation rate from the soil was reduced in proportion to the surface moisture content. Soil evaporation from inside the tents was assumed to be the same as outside the tents, since the enhanced turbulence in the tent would compensate for the chamber

149

pressure suppression of soil fluxes. Canopy transpiration was calculated by deducting soil evaporation from the measured total evaporation.

Gross Canopy Photosynthesis

Gross canopy photosynthesis was calculated from *measurements* of net canopy CO_2 flux with an estimate of canopy respiration added. Measurements of CO_2 flux at night were assumed to represent canopy respiration, which were corrected for the effect of temperature on respiration to determine daytime canopy respiration (see Chapter Seven). Soil respiration was calculated to be suppressed by 70% inside the tents due to over-pressure (Kanemasu *et al.*, 1974). Independent measurements of soil respiration were used to adjust the Bowen ratio data of CO_2 fluxes to determine gross canopy photosynthesis (see Chapter Seven). Gross canopy photosynthesis was calculated by adding an estimate of canopy plus soil respiration to the measured net canopy CO_2 flux.

5.4. Results

5.4.1. Aerodynamic Conductance

Data were available for parts of eight days during the measurement period. Data combined from all these days revealed that g_{aH} was strongly correlated with wind speed and that stability corrections (Ψ_H) were negligible compared to the height term (eq. 5.6, $\ln[(z-d)/z_{oH}] = 3.6$) for $u_l > 1.3$ m.s^{-1} (figure 5.1). Most of the corrections were for unstable conditions and hence positive, enhancing g_{aH}. A few corrections were for stable conditions, which occurred in late afternoon when $u_l < 1.3$ m.s^{-1}.
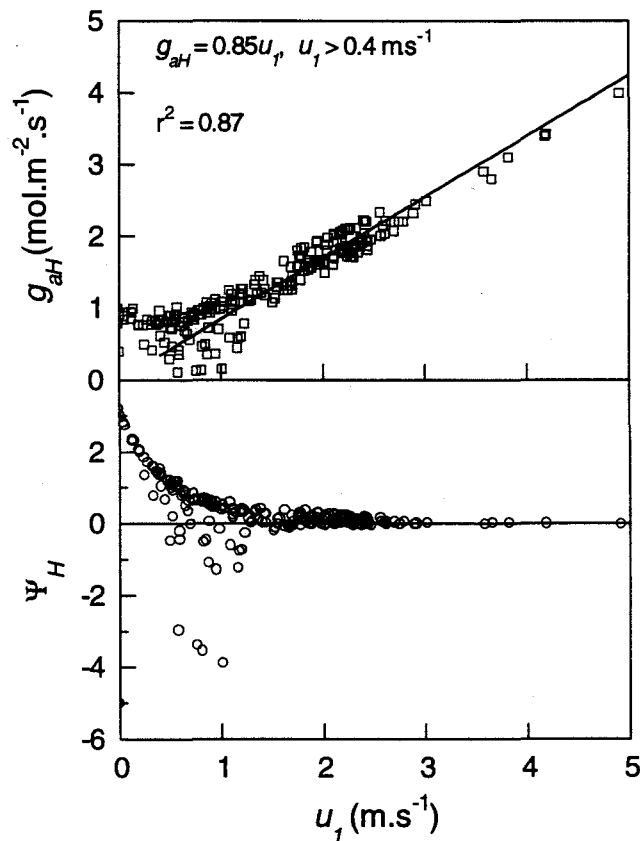
Figure 5.1 Aerodynamic conductance to sensible heat transfer from the canopy to the reference height (1 m above the canopy) (g_{aH}), calculated from sonic anemometer measurements of friction velocity and wind speed. Corrections for atmospheric stability (Ψ_H) were minimal at wind speeds greater than 1.3 m.s^{-1}, but sometimes significant at slower speeds.

Based on these observations a simple regression equation (g_{aH} = $0.85u_1$, for $u_1 > 0.4$ m·s^{-1}, r^2 = 0.87) was used to calculate g_{aH} from measurements of u for periods when direct measurements of u_* or H were not available. At these times data of u were obtained from either cup anemometer measurements or from hourly data of wind run from the weather station. Conversion from wind speed at the height of measurement to u_1 was achieved assuming neutral stability and a logarithmic wind profile (eq. 5.23).

5.4.2. Surface Temperature

An alternative expression to calculate the aerodynamic conductance to sensible heat transfer (g_{aH}) is obtained from that for the sensible heat flux

$$H = C_p g_{aH}(T_s - T_r),$$ (5.12)

$$g_{aH}(H) = H/(C_p(T_s - T_r)),$$ (5.13)

where T_s and T_r are the surface temperature and the air temperature at the reference height, respectively.

Values of the aerodynamic conductance to sensible heat transfer calculated from the sensible heat flux ($g_{aH}(H)$) (eq. 5.13) and from wind speed measurements ($g_{aH}(u)$) (eq. 5.6), were different (figure 5.2A). This highlights the difficulties of using surface temperature measurements in the calculation of g_{aH}, despite the accuracy of the measurements. Another manifestation of this problem appeared in the discrepancy between the time at which H became negative (15:30) and the time at which air and surface temperatures were equal (14:30) (figure 5.2C).

These discrepancies were resolved by separating H into soil and foliage components (figure 5.2B). Soil sensible heat flux (H_s) was calculated by an energy balance equation, from the soil evaporation (E_s) and soil net radiation (R_s) estimated from a canopy extinction coefficient for net radiation ($0.4/\sin\beta_{max}$) (Denmead, 1976), and the measured ground heat flux (G),

$$H_s = R_s - LE_s - G.$$ (5.14)

Sensible heat flux of the foliage (H_f) was calculated from the energy balance,

$$H_f(EB) = H - H_s,$$

(5.15)

and closely matched H calculated from the measured $g_{aH}(u)$ and surface temperature, $H_f(u)$ (eq. 5.12) (figure 5.2D). Calculation of $g_{aH}(H)$ from H_f and the surface temperature (eq. 5.13) was then in accordance with $g_{aH}(u)$ calculated from the wind speed measurements (figure 5.2A). Accounting for the sensible heat flux from the soil
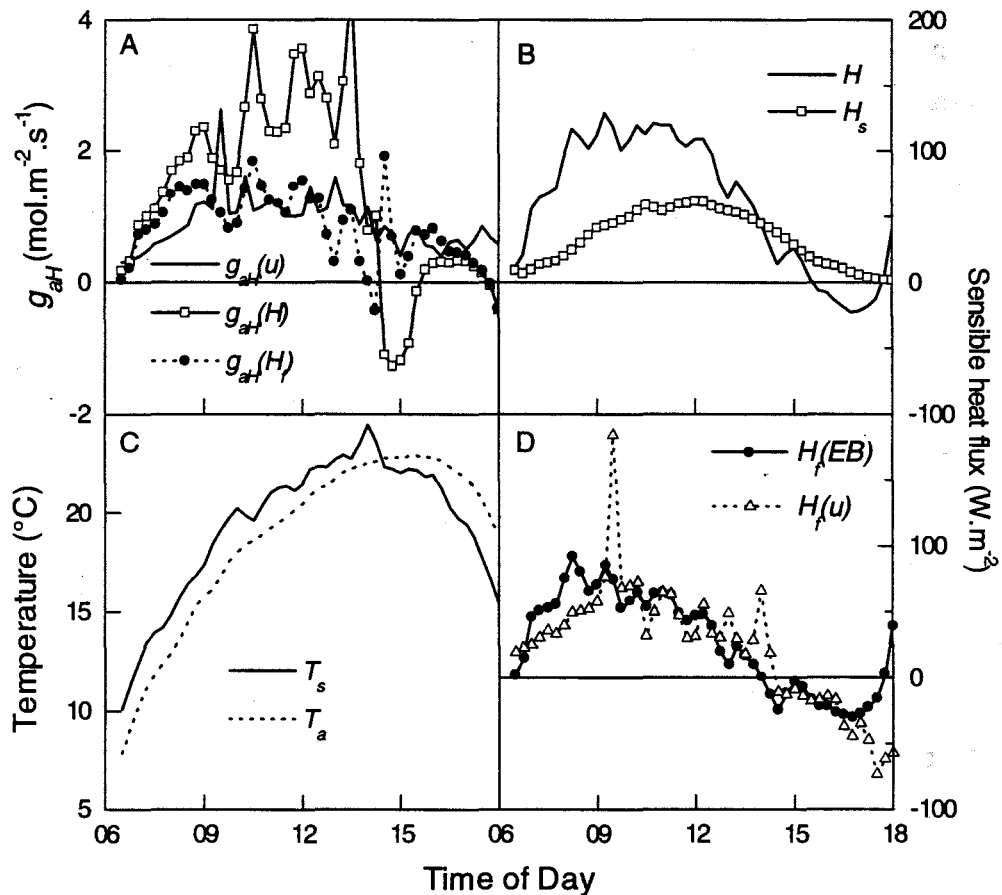
Figure 5.2 A. Comparison of aerodynamic conductance to sensible heat transfer (g_{aH}) calculated from wind speed measurements, $g_{aH}(u)$ (——), or surface temperature measurements and total sensible heat flux, $g_{aH}(H)$ (—□—), or the foliage sensible heat flux, $g_{aH}(H_f)$ (···•···). B. Measured total sensible heat flux (H) ( ) and soil sensible heat flux, H_s (—□—). C. Measured temperature of the canopy surface, T_s (——), and of the air 25 cm above the canopy, T_a (·····). D. Foliage sensible heat flux calculated from surface temperature and $g_{aH}(u)$, $H_f(u)$ (—△—) and from the energy balance, $H_f(EB)$ (—•—). Data are from the Matong crop on 25-Oct-90.

also resolved the discrepancy in the time of day at which surface and air temperatures were equal (figures 5.2C & D).

Similar discrepancies were observed in the data from other days, but were not always resolved so well. The data of g_{aH} calculated from wind speed measurements were assumed to be correct and were used for subsequent calculations.

5.4.3.   Modelling Canopy Conductance

The BBL stomatal model (eq. 5.4) was fitted to canopy data from the tents and the Bowen ratio systems by linear regressions of g_c against $A_c/((c_a + \Gamma)(k + D_l))$ assuming an intercept of $g_o = 0.01$. g_c was calculated from canopy transpiration and A_c was gross canopy photosynthesis (ie. including canopy respiration). Typically data of g_c before 9:00 did not fit the linear regression model and were discarded from the fitting process (figure 5.3). Similarly data from late in the day had high uncertainty and were not used in fitting. Anomalous data points such as those circled in figure 5.3 were also discarded.
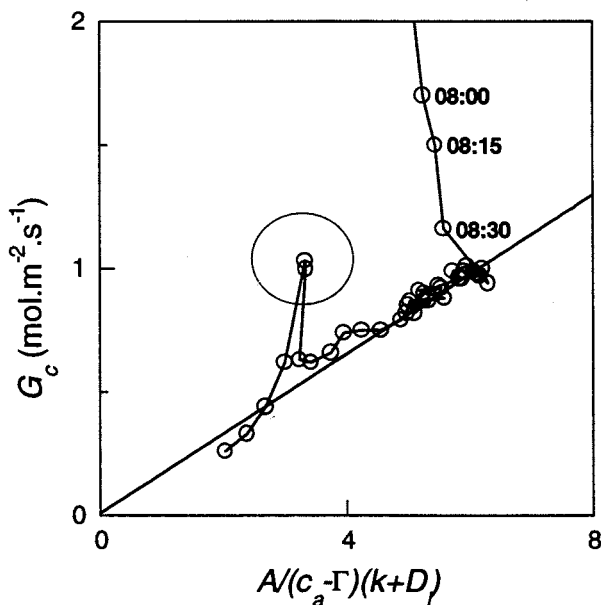
Figure 5.3 An example of canopy conductance from Bowen ratio measurements of transpiration plotted against the BBL stomatal model index. Data early in the morning were affected by evaporation of dew and were discarded from the fitting routine. Anomalous data points, circled were also discarded. The fitted regression shown is $g_c = 0.01 + 0.161A_c/((c_a - \Gamma)(6.78 + D_l))$. Data are from the Matong crop measured by the Bowen ratio system on 13-Oct-90.

Coefficients for the model fits are given in Tables 5.2 & 5.3 for the tent and Bowen ratio data, respectively.

Table 5.2 Coefficients for the stomatal model (eq. 5.4) fitted to Tent canopy data for Matong and Quarrion. A fixed intercept was used: $g_0 = 0.01$. Individual dates indicate coefficients fitted for each day.

Date	Matong		Quarrion	
	k	a_1	k	a_1
12-Oct	-	-	-	-
13-Oct	22.2	0.186	7.59	0.095
17-Oct	-	-	-	-
18-Oct	16.6	0.115	7.21	0.090
24-Oct	5.87	0.097	29.8	0.199
25-Oct	8.52	0.112	15.6	0.148
26-Oct	11.6	0.115	11.0	0.108
30-Oct	46.9	0.247	34.7	0.212
31-Oct	40.4	0.208	14.1	0.135
01-Nov	13.3	0.098	17.9	0.117
02-Nov	5.36	0.064	9.42	0.093

Table 5.3 Coefficients for the stomatal model (eq. 5.4) fitted to Bowen ratio canopy data for Matong and Quarrion. A fixed intercept was used: $g_0 = 0.01$. Individual dates indicate coefficients fitted for each day. *The coefficients were mutually dependent, so k was set by combining with the data of the previous day. +The coefficient was at the imposed limit of $k > 1.0$.

Date	Matong		Quarrion	
	k	a_1	k	a_1
12-Oct	3.78	0.125	4.95	0.078
13-Oct	6.78	0.161	5.13	0.119
17-Oct	2.16	0.075	13.0	0.154
18-Oct	4.01	0.096	7.08	0.122
24-Oct	8.49	0.162	17.1	0.179
25-Oct	9.02	0.178	4.07	0.087
26-Oct	11.9*	0.228	2.21*	0.081
30-Oct	24.0	0.229	2.41	0.165
31-Oct	34.4	0.209	12.3	0.173
01-Nov	1.22	0.062	1.00+	0.098
02-Nov	1.00+	0.065	11.5	0.156

The value of the coefficients obtained from fitting the model were different for the tent and Bowen ratio data and also varied between days. Mutual dependency of the coefficients makes comparison of the coefficients between data sets difficult. However, it is apparent that stomatal sensitivity to D_l was reduced on the hot days, 30-31 October, for Matong (*ie.* large values of k) as was observed with the leaf data (Table 5.1). No other trends in the coefficients could be determined. Different values for the coefficients for the tent and Bowen ratio data may partly be attributed to the inherent differences between the techniques.

Coefficients of the BBL stomatal model were different at the canopy scale compared to the leaf level (Tables 5.2 & 5.3 cf. Table 5.1). Standard errors of the coefficients were greater for the leaf data than at the canopy scale (data not shown), since the range of leaf conductances and variables was more limited.

The model of canopy conductance explained much of the observed variation in data sets from the tent and Bowen ratio systems for both Matong and Quarrion (*eg.* figure 5.4).
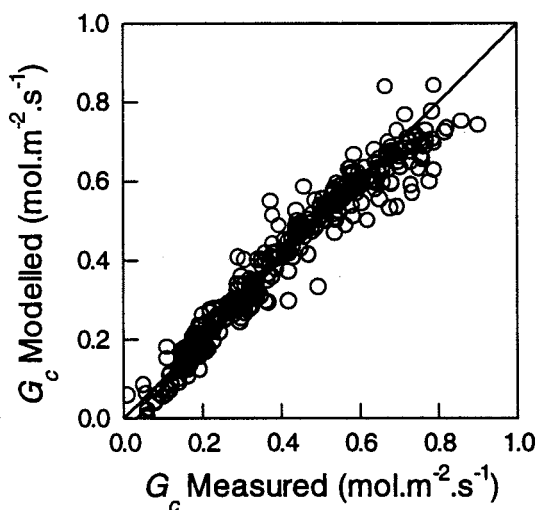
Figure 5.4 Comparison of modelled canopy conductance with the measured canopy conductance in the tent from the Matong crop.

5.4.4. Predicting Canopy Conductance from Leaf Data

5.4.4.1. Tent Data

With coefficients from individual days' leaf data (Table 5.1) the BBL model predicted canopy conductance that was in excellent agreement with the canopy conductance estimated from the tent measurements of transpiration (figure 5.5). The response of conductance to light was apparent both before 08:00 and again after 16:00. Between these times conductance was responding mostly to the leaf-to-air vapour concentration difference, D_l.

The lower conductance values, on the 30-Oct, were associated with low available soil moisture, which was more apparent in the Matong canopy than the Quarrion since the former had inherently more profligate water use (Chapter Three). Model predictions of canopy conductance were greater than the measured values for the Matong data on 25-Oct, which was attributable to the poor fit of the BBL model to the leaf data on that day ($r^2 = 0.10$, Table 5.1).

5.4.4.2. Bowen Ratio Data

Predictions of canopy conductance, using coefficients from leaf data, did not match the surface conductance derived from the Bowen ratio measurements of transpiration as well as the tent data (figure 5.6). A measure of the uncertainty in G_{cPM} was determined by combining errors of $\pm$ 0.01 °C of wet and dry bulb temperatures, $\pm$ 5% of available energy and $\pm$ 20% of g_{aH} in the calculations. The Penman-Monteith derived surface conductance provided a direct estimate of canopy conductance, but as described earlier it was very sensistive and magnified errors from the evaporation estimates (*ie.* large error bars), which were also apparent as large fluctuations in G_{cPM}, particularly in the late afternoon. Smaller error bars on the 30-Oct were due to greater coupling between the canopy and the atmosphere on that day.
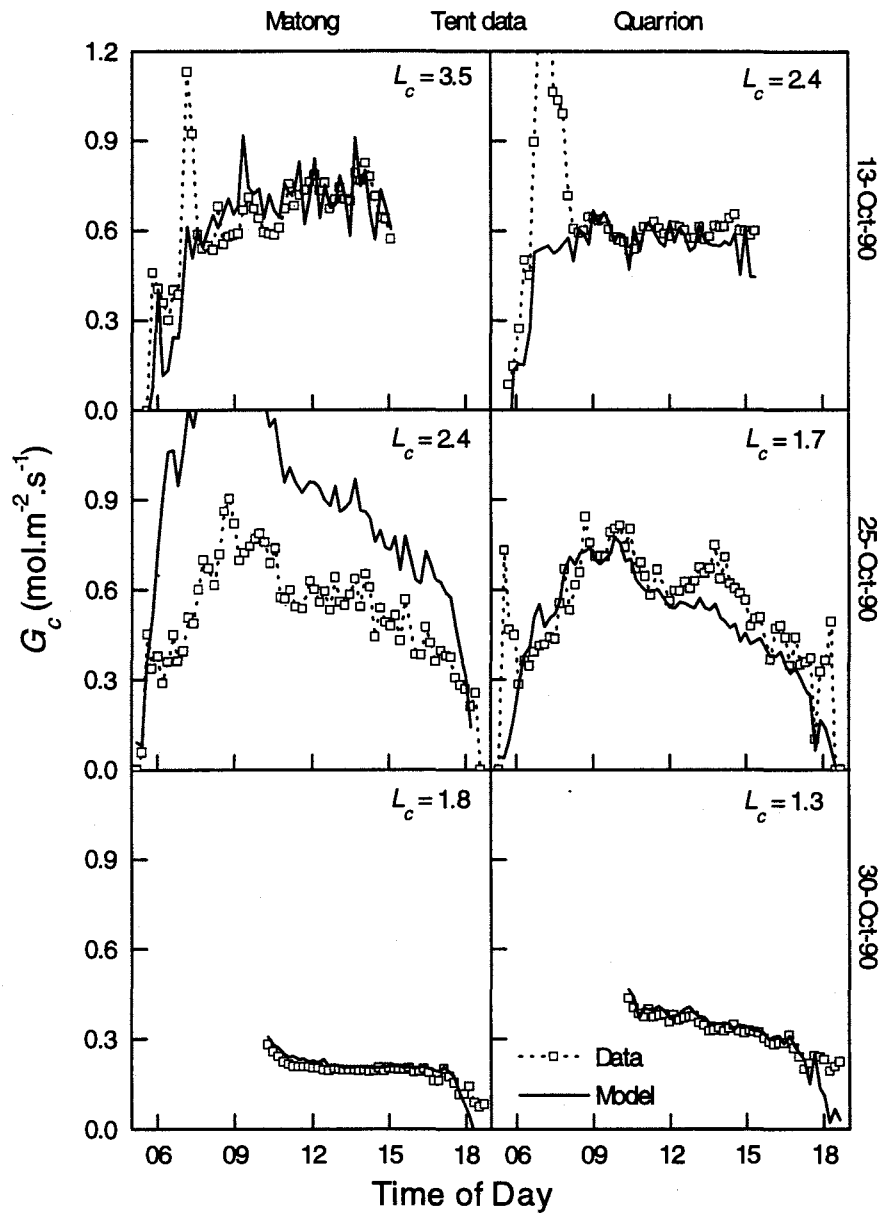
Figure 5.5 Model predictions of canopy conductance (G_c) with coefficients derived from leaf data (Model, ——), compared with canopy conductance (Data, —□) determined from tent measurements of canopy transpiration from two canopies of wheat cultivars Matong (left panels) and Quarrion (right panels). Three days' data are presented: 13-Oct-90 (top), 25-Oct-90 (middle) and 30-Oct-90 (bottom). Also shown are the canopy leaf area indices, L_c.
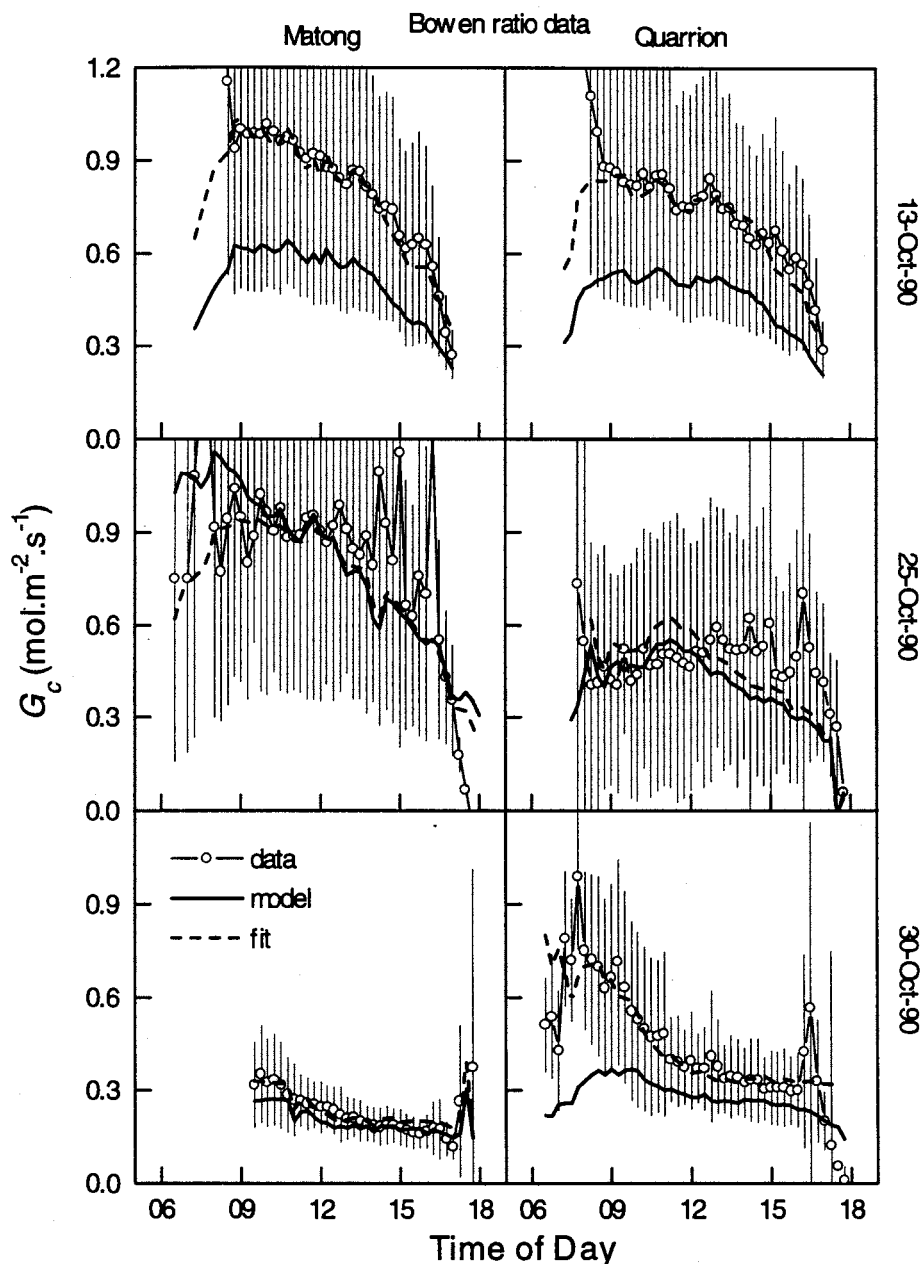
Figure 5.6 Comparison of canopy conductance (G_{cPM}) calculated from the Bowen ratio measurements of canopy transpiration using the inverted Penman-Monteith equation (eq. 5.5; data, —o—) with predictions of canopy conductance (G_{cBB}), using coefficients derived from leaf data (model, ——), and the fitted model (fit, - - -) for two canopies of wheat cultivars Matong (left panels) and Quarrion (right panels). Three days data are presented: 13-Oct-90 (top), 25-Oct-90 (middle) and 30-Oct-90 (bottom). Error bars on G_{cPM} were calculated from estimated uncertainty in the measurements (± 0.01 °C of wet and dry bulb temperatures, ± 5% of available energy and ± 20% of g_{aH}).

The model underestimated canopy conductance on most days, but did reflect the general diurnal trend. Model predictions were within the estimated uncertainty of the canopy conductance derived from the Penman-Monteith equation. On the 30-Oct, when the uncertainty of G_{cPM} was smaller, model predictions were better, but were very sensitive to the value of g_{aH}. Fitting the model to the canopy data showed that the model was able to describe the diurnal changes of canopy conductance (dashed lines in figure 5.6), but that in using the leaf coefficients the exact magnitude of the canopy conductance was not well predicted.

5.4.5. Canopy Transpiration

5.4.5.1. Tent Data

Canopy transpiration was predicted from modelled canopy conductance with coefficients from leaf data (Table 5.1), g_{aH} and D_l using eq. 5.8 (figure 5.7). There was excellent agreement between the model and data of transpiration on all days, except for the Matong canopy on 25-Oct, which as previously noted could be attributed to the poor fit of the leaf model on that day. Both the magnitude and the diurnal pattern of transpiration were reproduced by the model.

5.4.5.2. Bowen Ratio Data

Transpiration was modelled with the Penman-Monteith equation (eq. 5.5), using modelled canopy conductance (G_{cBB}) with coefficients from leaf data (Table 5.1) and g_{aH}. Modelled canopy transpiration was underestimated on days when the modelled canopy conductance was underestimated (ie. 13-Oct for both crops and 30-Oct for Quarrion, figure 5.6) and similar when conductance was more accurately predicted in comparison with the transpiration measured by the Bowen ratio system (figure 5.8). As stated earlier, transpiration from smooth canopies, such as in this study, is not very sensitive to canopy conductance, so that good agreement between the model and measurements were expected.

The error bars in figure 5.8 indicate a confidence range for the Bowen ratio measurements of transpiration based on an estimated uncertainty of ± 5% of available energy, ± 0.01 °C for wet and dry bulb temperatures.
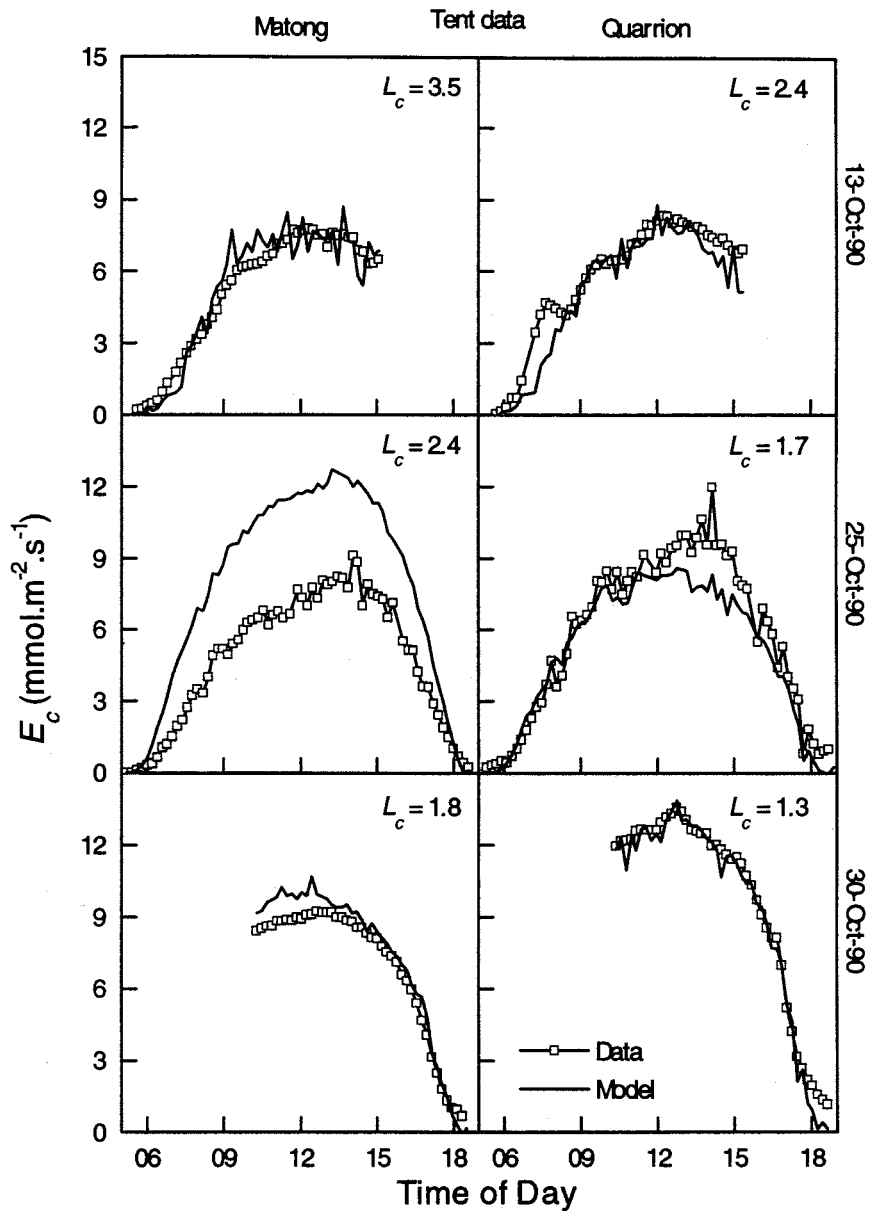
Figure 5.7 Comparison of canopy transpiration (E_c) measured with the tents (—□) and modelled transpiration (eq. 5.8, ——) calculated using the Leuning modified Ball-Berry model of stomatal conductance with coefficients derived from leaf data. Data are presented for three days: 13-Oct-90, 25-Oct-90 and 30-Oct-90 (top, middle and bottom panels respectively) and for the Matong and Quarrion canopies (left and right panels respectively).
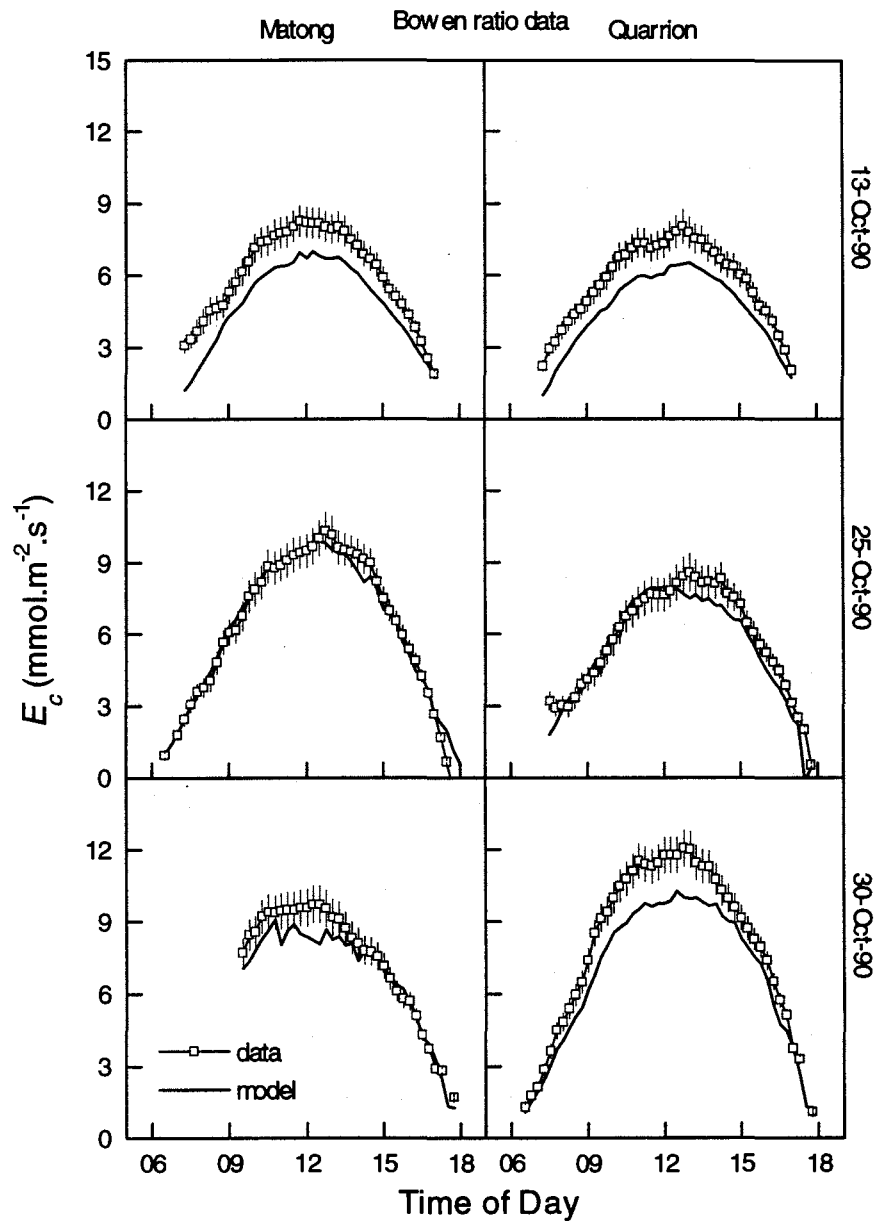
Figure 5.8 Comparison of transpiration (E_c) measured with the Bowen ratio system (–□–) and modelled canopy transpiration (eq. 5.9, ——) calculated using the Leuning modified Ball-Berry model of stomatal conductance with coefficients derived from leaf data. Error bars on E_c were calculated from estimated uncertainty in the Bowen ratio measurements (± 0.01°C of wet and dry bulb temperatures, ± 5% error available energy).

Coefficients were also obtained from fitting the model to all the leaf data combined (Table 5.1). Using these combined leaf coefficients improved the fit of the model on the 13-Oct and 25-Oct, but the estimates were worse for the 30-Oct since the extreme temperatures and low soil water content had a significant effect on the response of stomata to the environment (data not shown).

5.4.6.   Equilibrium Evaporation

The evaporation rate was close to the equilibrium evaporation rate in the morning of most days, typified by the data of 25-Oct, but was greater than the equilibrium evaporation rate when D_l was high, ie. in the afternoons and on very hot days (35°C) such as the 30-Oct (figure 5.9). The leaf-to-air vapour concentration difference (D_l) was greater than the vapour concentration deficit (D_r) until mid-afternoon when a negative sensible heat flux (H) reversed this ranking (figure 5.9).

The decoupling coefficient (Ω) averaged 0.7 on most days (figure 5.9), decreasing with increasing wind speed (data not shown). Increased coupling between the canopy surface and the atmosphere was observed on days of higher D_l (ie. 30-Oct), since stomatal conductance was reduced leading to smaller Ω. The close match between measured transpiration and the equilibrium evaporation was not because $r_{aH} \gg r_c$ ie. the surface was not decoupled from the atmosphere.
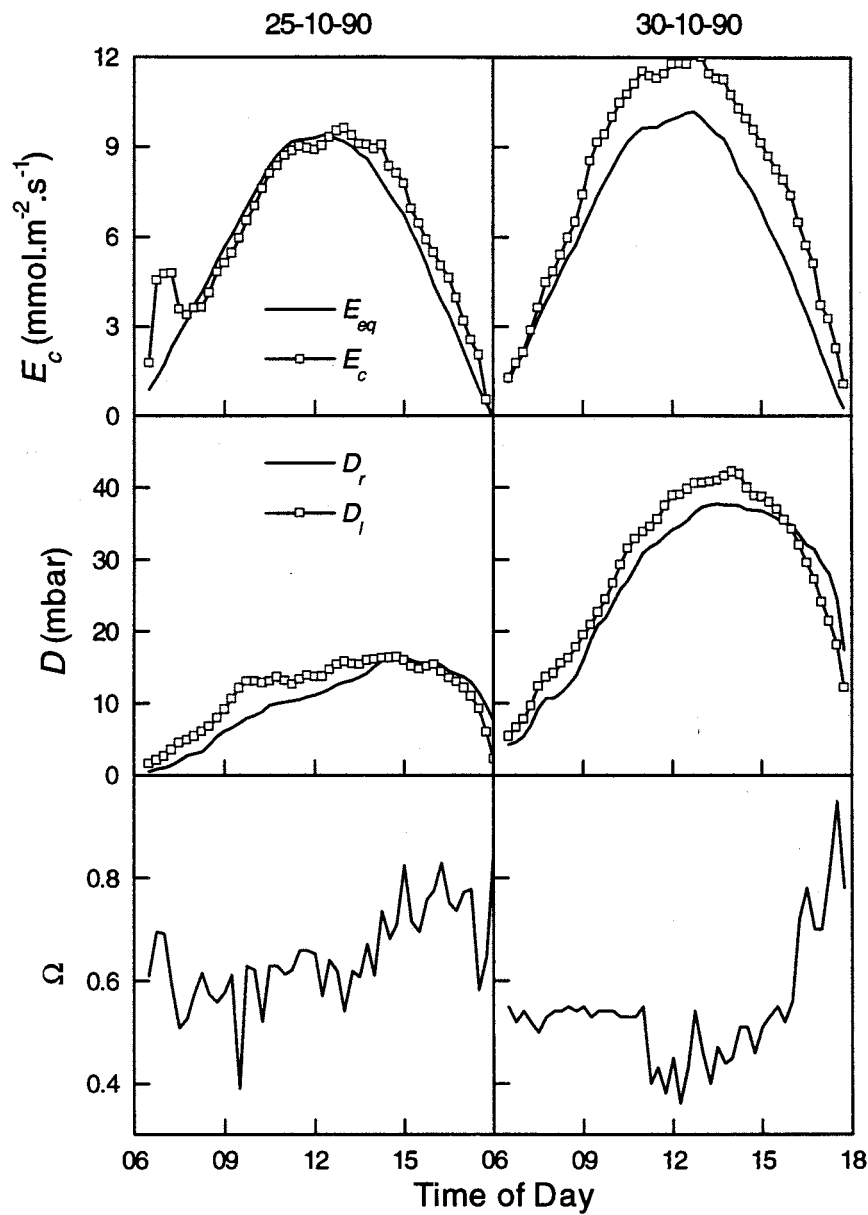
Figure 5.9 Comparison of the measured canopy transpiration rate (E_c, ——) with the equilibrium transpiration rate (E_{eq} —□—) for a typical day, 25-Oct (left panels), and an atypical, hot day, 30-Oct (right panels). Also shown are the vapour concentration deficit (D_r ——) and the leaf to air vapour concentration difference (D_l —□—). The decoupling coefficient (Ω) was lower on the hot day with higher D_r, indicating that the canopy was more closely coupled (Ω) to the atmosphere on that day (bottom panels).

5.5. Discussion

Canopy Conductance

These results demonstrate that scaling stomatal conductance models is a valid approach to modelling canopy conductance. The BBL stomatal model was successfully used in a big-leaf representation of a canopy. Both the magnitude and the responsiveness of canopy conductance to the environment were reproduced by the model. The model gave realistic predictions across a range of canopy leaf area indices (3.5 to 1.3 $m^2.m^{-2}$) and in both well-watered and water-stressed conditions.

Simpler scaling techniques, such as multiplying leaf conductance by the leaf area index, which do not consider the response of conductance to environmental variables, are not satisfactory and require empirical canopy shelter factors to get acceptable results (Rochette et al., 1991). Stomatal models that are only based on environmental variables (Jarvis, 1976), are not able to reproduce the variation of canopy conductance and in particular poorly describe the response of canopy conductance to low soil moisture (Kim & Verma, 1991b).

Use of observed photosynthesis as a variable in stomatal models was a significant improvement over models that do not (Chapter Four) and this benefit extends to modelling of canopy conductance. The model used in this chapter implicitly accounts for the within-canopy profiles of light and leaf nitrogen by using the correlation between conductance and photosynthesis and so facilitated the scaling of conductance from leaves to canopies. However, it should be remembered that photosynthesis in this model is not a truly independent variable, in that it must be either measured (as in this study) or estimated by use of a model of canopy photosynthesis (subsequent chapters). It remains to be seen if models are able to predict canopy photosynthesis with sufficient reliability to be combined with this model of canopy conductance.

The only other study that had measurements at both the leaf and canopy scales was similarly successful in scaling conductance using photosynthesis as a variable (Kim & Verma, 1991a). They concluded that soil evaporation was the main source of the discrepancy between modelled canopy conductance and the inferred surface conductance from the Penman-Monteith equation. The good agreement between model and data, in

this work, can be partly attributed to inclusion of estimates of soil evaporation, since g_{cPM} is very sensitive to errors in the measured evaporation.

Parameterisation of Canopy Conductance Models

Use of coefficients derived from leaf data in the model gave very good predictions of canopy conductance in the tents (figure 5.5). However, an infinite canopy aerodynamic conductance was assumed. Realistically a finite value would be more appropriate, which would result in the model underestimating canopy conductance and transpiration, as was observed in the comparison of the model with the Bowen ratio data (figures 5.6 & 5.8).

The canopy model worked best when the leaf conductance model explained a high proportion of the variance in the measured leaf conductance (r^2) (*eg.* 30-Oct). Little variation in stomatal conductance and D_l on the 25-Oct resulted in a poor estimate of the leaf coefficients. On days such as these, some other sampling strategy is required that will cover a greater range of conductance and so improve the estimate of the model coefficients. However, the diurnal variation of conductance was sufficient on most days to give a good estimate of the coefficients.

When the model was fitted to the data of canopy conductance (figure 5.6), the model accounted for much of the variation in conductance (figure 5.4). It was apparent that the coefficients obtained from fitting the model to the canopy data were different to those derived from the leaf data, although k increased on 30/31-Oct at both scales. Relating variation of the coefficients to other parameters (such as soil water content) will increase the utility of this model, although this was not possible with the present data.

Scaling Penman-Monteith from Leaves to Canopy

Despite the inevitable inclusion of some aerodynamic factors in the Penman-Monteith derived surface conductance (Finnigan & Raupach, 1987) there was good agreement in this study between g_{cPM} and the modelled canopy conductance. This is probably due to the consideration of soil evaporation as well as the evaluation of the aerodynamic resistance to sensible heat or water vapour transfer, instead of the resistance to momentum transfer (Thom, 1972; Garratt & Hicks, 1973; Verma, 1989).

This raises the issue of redefining the canopy aerodynamic resistance so that the surface conductance is a truly physiological variable, the parallel sum of conductances of all the individual leaves in the canopy. To a biologist this makes good sense, since the

leaf conductances are well defined, tangible and now predictable, whereas the extension of atmospheric transfer processes to the canopy surface has many uncertainties.

Aerodynamic resistances are based on K-theory, which breaks down in close proximity to the surface (Brutsaert, 1982) so that counter gradient fluxes can occur (Denmead & Bradley, 1985). In addition, consideration of the atmospheric stability, which affects the turbulent transfer, is no simple task using the Monin-Obukhov theory. The nature of turbulent transfer processes in the atmosphere, requires time averaging of rapidly fluctuating variables, so that aerodynamic resistances do not exist for any instant, but are defined as time averages. Since all these factors add considerable uncertainty to aerodynamic resistance data, r_{aH} would be a better variable to accumulate the unavoidable non-linearities that occur when scaling the Penman-Monteith equation from leaves to canopies (Finnigan & Raupach, 1987). McNaughton (1994) pointed out that choice of a canopy averaging scheme depends on the use of the bulk values and outlined an alternative canopy averaging scheme that allows the canopy conductance to be used for both water and CO_2 fluxes. Despite these problems in use of aerodynamic resistances and the discrepancies between the definitions of the bulk canopy resistances, there was good agreement between the model and the measurements as predicted by Raupach (1995). These difficulties in scaling the Penman-Monteith equation are unavoidable. However, use of Lagrangian models instead may overcome these problems, though the data requirements for them are at present still prohibitive for general use (Raupach et al., 1992).

Canopy Transpiration

There was good agreement between the Penman-Monteith predictions and the measurements, which reconfirms the Penman-Monteith equation as the model of choice for this type of study. Unfortunately good agreement does not corroborate the canopy conductance model, because the surface was quite uncoupled from the atmosphere ($\Omega = 0.7$). It is reassuring that there was an equally good agreement between the model and measurements of transpiration (figure 5.8) on a day when the decoupling coefficient was at its lowest (30-Oct).

Better agreement of the model with the tent measurements than with the Bowen ratio data, can be attributed to the use of an evaporation model that uses measured surface temperature to determine D_l (eq. 5.8). The Penman-Monteith equation (eq. 5.9) eliminates surface temperature but results in greater sensitivity of the model to g_{aH}.

5.6. Conclusions

The Leuning modified Ball-Berry stomatal model was applicable for use in a big-leaf representation of canopy conductance. Use of measured photosynthesis as a parameter in the model implicitly incorporated the effects of variation in light, temperature, soil water availability and leaf area. The response of canopy conductance to D_l and CO_2 concentration were incorporated in the model explicitly.

The model accounted for much of the variation in canopy conductance when it was fitted to the data. Use of leaf scale coefficients in the model gave predictions of canopy conductance that were in close agreement with the surface conductance inferred from the Penman-Monteith equation, despite the inherent sensitivity of such inferred conductances. Good agreement was also observed with the canopy conductance calculated from the tent measurements of evaporation.

Transpiration predicted from the modelled canopy conductance was in good agreement with measurements.

Surface temperature measurements need to be used with care to infer aerodynamic resistance to sensible heat flux, since the assumption of a negligible soil component is not always valid.

5.7. Appendix: Stability corrections for aerodynamic resistance calculations

The scheme described here to calculate the aerodynamic resistances is based on the work of many researchers. The specific equations are mostly from Verma (1989), while their general form was best presented by Brutsaert (1982). The theoretical context of this work comes from reading Brutsaert (1982), Thom (1975) and Arya (1988).

5.7.1. Theoretical context

The surface sub-layer of the planetary boundary layer is characterised as a fully turbulent region where the vertical fluxes do not change appreciably from their value at the surface. Within the surface sub-layer, turbulence is generated by frictional drag of the wind on the ground and buoyancy forces from surface heating. The force exerted on the surface by the air is called the surface shearing stress, τ. This force is transmitted as a vertical flux of horizontal momentum, apparent as a vertical profile of wind speed (Brutsaert, 1982).

Exact quantified solutions of fluxes or profiles of entities in turbulent motion are not possible, because there are too many unknown variables for the number of defining equations. The complexity of turbulent flow is described simply by use of the mean, called a first order moment, the variance (standard deviation squared), called a second order moment, and the covariance of one variable with another. Problems of turbulence are solved by closure, whereby variables (*ie.* the variance or covariance) are assumed constant at some point (Arya, 1988).

A common approach, in micrometeorology, has been to use first-order closure, where the second order moments are defined by a parameter (K), which is assumed to stay constant within the surface sub-layer (Stull, 1988). This closure technique is called the gradient-transport or K-theory, since it implies that, similar to molecular diffusion, turbulent fluxes occur down gradients of the entity being considered,

$$\tau = \rho K_m (\partial \bar{u}/\partial z) \tag{5.16}$$

where ρ is the density of moist air and $K_m = u_* k(z{-}d)$, is the turbulent diffusivity of momentum. The friction velocity, u_*, is a scaling velocity and is defined as

$$u_* \equiv (\tau/\rho)^{\frac{1}{2}} , \tag{5.17}$$

and can be obtained from the slope of a plot of $\ln(z)$ versus u in neutral conditions or from a direct measurement of the turbulence, as $\sqrt{u'w'}$, using sonic anemometers.

When atmospheric conditions are such that buoyancy forces are negligible (*ie.* neutral stability), the variation of wind velocity with height is accurately described by a logarithmic function,

$$\bar{u}(z) = \frac{u_*}{k} \ln\left(\frac{z - d}{z_{oM}} \right) \tag{5.18}$$

where k is von Karman's constant (0.41), d is the zero plane displacement and z_{oM} is the roughness length of the surface for momentum. The adjustments d and z_{oM} are included to represent the apparent surface where the momentum of wind would be absorbed if these profiles continued to the surface. Close to the surface, below a point about 1.5 - 3.5 times the height of the roughness elements, the viscosity of the air and the structure of individual roughness elements affect these profiles (Brutsaert, 1982).

When the fluxes of sensible and latent heat cause a stratification of air density that is greater than the adiabatic lapse rate, then buoyancy forces affect the profiles, so that they are no longer logarithmic (*ie.* non-neutral stability). Since non-neutral conditions are far more usual than neutral conditions, theories have been developed to account for these deviations from the logarithmic profiles. The two main measures of the atmospheric stability are the Richardson number and the Monin-Obukhov length (L), which are related.

5.7.2. Monin-Obukhov similarity theory

The Monin-Obukhov length (L_{MO}) is a measure of atmospheric stability and is defined as the ratio of buoyancy to mechanical forces and can be considered as the height at which the production of turbulence by the forces are equal,

$$L_{MO} = \frac{-u_*^3 \rho C_p T_a}{kgH} , \tag{5.19}$$

where ρ is the density of moist air (kg.m^{-3}), g is the acceleration due to gravity (9.81 m.s^{-2}), H is the sensible heat flux (W.m^{-2}), T_a is the absolute air temperature (K), and C_p is the specific heat of air (1012 J.g^{-1}.K^{-1}). The ratio of the reference height to the Monin-Obukhov length (ζ, zeta),

$$\zeta = \frac{z-d}{L_{MO}},$$

(5.20)

is a measure of the atmospheric stability; $\zeta < 0$ unstable, $\zeta > 0$ stable, $\zeta = 0$ neutral. It is used to generate correction factors (ϕ, phi) for the deviations from the non-neutral profile,

$$\frac{\partial u}{\partial z} = \frac{u_*}{k(z-d)} \cdot \phi_M(\zeta).$$

(5.21)

On the basis of experimental evidence the functions of ϕ for momentum are (Dyer & Hicks, 1970)

$$\phi_M = \begin{cases} (1-15\zeta)^{-\frac{1}{4}}, & \zeta < 0 \\ 1+5\zeta, & \zeta \geq 0 \end{cases}.$$

(5.22)

Stability correction functions for profiles of temperature were found to be related to those of momentum, $\phi_H = \phi_M^2$. Integration of these gradient profiles yields profiles of wind velocity and temperature,

$$\bar{u} = \int_{d+z_o}^{z} \frac{\partial u}{\partial z} \partial z = \frac{u_*}{k}\left[\ln\left(\frac{z-d_o}{z_{oM}}\right) - \Psi_M(\zeta)\right],$$

(5.23)

$$\bar{T_s} - \bar{T_z} = \frac{H}{ku_*\rho C_p}\left[\ln\left(\frac{z-d}{z_{oH}}\right) - \Psi_H(\zeta)\right].$$

(5.24)

Strictly potential temperature should be used in place of air temperature, where potential temperature is air temperature adjusted for isothermal pressure effects of height, given by the dry adiabatic lapse rate (0.01 K.m^{-1}), the theoretical decrease in temperature with air

expansion at decreasing pressure with altitude. The stability integrals (Ψ, psi) are given by the functions (Paulson, 1970)

$$\Psi_H = \Psi_M = -5\zeta \,, \qquad\qquad\qquad\qquad \zeta > 0 \qquad\qquad (5.25)$$

$$\Psi_M(\zeta) = 2\ln\left(\frac{1+x}{2}\right) + \ln\left(\frac{1+x^2}{2}\right) - 2\arctan(x) + \frac{\pi}{2}, \quad \zeta < 0 \qquad (5.26)$$

$$\Psi_H(\zeta) = 2\ln\left(\frac{1+x^2}{2}\right), \qquad\qquad\qquad \zeta < 0 \qquad\qquad (5.27)$$

where x is defined as

$$x = \phi_M^{-1} = \left(1 - 15\zeta\right)^{\frac{1}{4}}. \qquad\qquad\qquad\qquad (5.28)$$

5.7.3. Aerodynamic resistances

Linking the atmospheric turbulent fluxes with the physiology of a vegetated surface is best achieved by expressing the flux equations in a resistance form. Analogous with Ohm's law, a flux is equal to the gradient divided by the resistance. Within the surface sub-layer (but above the surface) there is an assumed similarity of the turbulent transfer processes for momentum, heat and water vapour so that the diffusivities (and resistances) are assumed equal for all pressures. These resistances can be extended to apply to fluxes between the surface (where $z = z_o + d$) and the reference height ($z = r$) so that the resistance to momentum transfer (r_{aM}) is defined as

$$r_{aM} = \frac{u}{C_a u_*^2}, \qquad\qquad\qquad\qquad\qquad (5.29)$$

where C_a is the molar concentration of air (ρ/M_a) to convert the resistance to molar units. This expression can be combined with the momentum profile equation (eq. 5.23), to eliminate u, so that

$$r_{aM} = \frac{1}{C_a k u_*} \left[\ln\left(\frac{z-d}{z_{oM}} \right) - \Psi_M(\zeta) \right].$$

(5.30)

Similarly the aerodynamic resistance to heat transfer (r_{aH}) between the surface and the reference height is

$$r_{aH} = C_p \frac{T_s - T_r}{H}.$$

(5.31)

However, there is considerable difficulty in obtaining appropriate values for the surface temperature, T_s. By using the flux profile expression for turbulent heat transfer (eq. 5.24) to eliminate the surface temperature an alternative expression is obtained,

$$r_{aH} = \frac{1}{C_a k u_*} \left[\ln\left(\frac{z-d}{z_{oH}} \right) - \Psi_H(\zeta) \right].$$

(5.32)

Combining this expression with the momentum flux-profile equation (eq. 5.23) to eliminate z-d, gives

$$r_{aH} = \frac{u}{C_a u_*^2} + \frac{1}{C_a k u_*} \left[\ln\left(\frac{z_{oM}}{z_{oH}} \right) + \Psi_M(\zeta) - \Psi_H(\zeta) \right].$$

(5.33)

It is apparent that compared with the definition of r_{aM} there is an additional resistance to heat transfer (r_b) so that

$$r_{aH} = r_{aM} + r_b.$$

(5.34)

This 'excess' or 'quasi-laminar layer' resistance is due to enhanced transfer of momentum at the surface by additional bluff body forces, which have no analogy in the transfer of heat or water vapour (Thom, 1972).

Experimental evidence suggests that $z_{oM}/z_{oH} = 7$ (Garratt & Hicks, 1973), so that r_b is a similar magnitude to r_{aM} up to a reference height 1 m above the apparent surface. Ignoring it leads to significant underestimates of r_{aH} (Verma, 1989). The similarity of transport processes for heat, water vapour and CO_2 allows identical resistances to be used (Brutsaert, 1982).

173

CHAPTER SIX:

MODELS OF CANOPY PHOTOSYNTHESIS

Chapter Contents

Summary

Multi-layer models of canopy photosynthesis can provide predictions that closely match observations. Their complexity can be prohibitive for use in models of larger processes such as crop growth or global carbon cycling. Simplified models that consider only two classes of leaves, sunlit and shaded leaves, have previously been shown to be adequate, but they do not readily incorporate within-canopy profiles of leaf properties.

Within-canopy profiles of leaf nitrogen have been cited as evidence for optimisation of canopy resources to maximise canopy photosynthesis. Recently, it has been suggested that an optimal distribution of leaf nitrogen allows simple big leaf models of photosynthesis to be used. These simple big leaf models require an empirical curvature factor to overcome the non-linear response of leaf photosynthesis to light, when applied to the canopy, which can create difficulties when the models are used for predictions with new combinations of variables.

In this chapter sunfleck penetration and random leaf orientation in canopies, factors which are often ignored, are shown to significantly affect the optimal distribution of leaf nitrogen. When these factors are considered the optimal distribution has a greater accumulation of leaf nitrogen in the upper leaves of the canopy, compared to the optimal distribution if these factors are ignored.

A new model of canopy photosynthesis is presented that treats the sunlit and shaded leaves as separate components. While similar to previously developed models, it is different in that it utilises the within-canopy profiles of leaf properties to develop a relatively simple analytical solution to the integration of the sunlit and shaded components of canopy photosynthesis. Use of the sun/shade model gives more accurate predictions of canopy photosynthesis than a simple big leaf model.

The new sunlit/shade model is shown to be as good as a multi-layer model of canopy photosynthesis, without the use of empirical curvature factors. When the simple big leaf model is fitted to predictions of canopy photosynthesis from the multi-layer model, it is shown that this curvature factor is not constant, but varies strongly with canopy leaf area index and to a lesser extent total canopy nitrogen. Canopy photosynthesis, predicted by the big leaf model, was overestimated by 25% at a canopy leaf area index of four, when the model was tuned for a leaf area of two, while the sun/shade model had no such error.

6.1. Introduction

Scaling gas exchange from leaves to paddocks was examined as part of a larger project to assess water-use efficiency in the field (Condon & Richards, 1993). Comparison of the water-use efficiency of two crops with genetically different stomatal conductances, was complicated by differences in leaf area index and different rates of soil evaporation. These differences also confounded an evaluation of the scaling of water-use efficiency from measurements alone (Chapter Three). Models of canopy gas exchange provide a theoretical framework for more thorough analysis and interpretation of the scaling of physiological processes. Use of a canopy model for analysis of such experiments requires that it be process based, physically realistic, yet be sufficiently simple to be effectively parameterised. Such models also fit the requirements of assessing the effects of climate change on vegetation.

Models of canopy photosynthesis must consider the heterogeneous light environment in canopies and the non-linear response of photosynthesis to light as demonstrated by many authors (Sinclair *et al.*, 1976; Norman, 1980; Smolander, 1984). Recognition that light attenuation through canopies can be described by Beer's law (Monsi & Saeki, 1953) led to several models of light penetration and absorption through canopies (Warren Wilson, 1960; de Wit, 1965; Cowan, 1968a; Ross & Nilson, 1967; Ross, 1975; 1981; Goudriaan, 1977). It is now generally accepted that penetration of light through canopies must separately consider beam and diffuse light, due to their different attenuation in canopies, as well as visible and near infra-red wavelengths due to differential absorptance by leaves (Goudriaan, 1977).

These models of light penetration became the basis for several comprehensive models of canopy photosynthesis (de Wit, 1965; Duncan *et al.*, 1967; Lemon *et al.*, 1971; Norman, 1979), which are currently used in crop models (Whisler *et al.*, 1986). They divide the canopy into multiple layers with many different leaf-angle classes, for which the absorbed light is used to determine leaf photosynthesis. Numerical integration of photosynthesis from each leaf-class gives canopy photosynthesis. The flexibility of multi-layer models allows within-canopy profiles of both environmental and physiological variables to be incorporated. While these models have been used for many applications, their complexity and the number of calculations involved with their multi-leaf-class description of canopies is a drawback for their inclusion in models of global carbon cycling (Sellers *et al.*, 1992).

Multi-layer models have been successfully simplified by considering only two classes of leaves; sunlit and shaded (Sinclair *et al.*, 1976; Norman, 1980). This simplification is effective because light in the canopy is essentially binomially distributed in either sunflecks or shade, so that the non-linear response of photosynthesis to absorbed light can be averaged in each of these classes with little error. Further simplification to models with only a single leaf layer introduces large errors and are inadequate for most purposes (Sinclair *et al.*, 1976; Norman, 1980; Boote & Loomis, 1991).

Another approach to the simplification of canopy photosynthesis models is to derive analytical solutions (Acock *et al.*, 1978; Johnson & Thornley, 1984) and so avoid numerical integration. However, analytical solutions can only be derived from specific equations (rectangular hyperbole) for the response of photosynthesis to light, which do not fit measurements as well as the preferred equations (non-rectangular hyperbole). Predictions of canopy photosynthesis from analytical models are not as close to measured rates as those from the sun/shade type models (Boote & Loomis, 1991).

Within-canopy profiles of leaf nitrogen (or photosynthetic capacity) have been shown to be significantly non-uniform in canopies of a diverse range of species (Spiertz & Ellen, 1978, wheat; DeJong & Doyle, 1985, peach; Hirose & Werger, 1987a, Solidago altissima; Pons *et al.*, 1989, Lysimachia vulgaris; Schieving *et al.*, 1992, Carex acutiformis; Sadras *et al.*, 1993, sunflower; Anten *et al.*, 1995, rice, soybean, sorghum & amaranthus). Profiles of leaf properties can be incorporated into multi-layer models of canopy photosynthesis and have a significant effect (Meister *et al.*, 1987). They are also accommodated by canopy models with analytical solutions (Acock *et al.*, 1978), but are not easily incorporated into the sun/shade models of canopy photosynthesis, except by empirical adjustments (Boote & Loomis, 1991).

Profiles of leaf properties have led to the hypothesis that leaves adapt or acclimate to their light environment such that a plants nitrogen resources may be distributed to maximise daily canopy photosynthesis (Field, 1983; Hirose & Werger, 1987a). An optimal distribution of leaf nitrogen is when any re-allocation of nitrogen would decrease daily photosynthesis. It has been further suggested that the optimal distribution of nitrogen occurs when the nitrogen is distributed in proportion to the profile of absorbed light in the canopy. The appropriate profile of absorbed light is the time average over the previous several days to a week, the time over which leaves are able to adapt. Several canopy models have been used to demonstrate that canopy photosynthesis is maximised

179

when leaf nitrogen is distributed in proportion to the profile of absorbed light (Hirose & Werger, 1987a; Wu, 1993; Badeck, 1995; Sands, 1995). However, contrary to the earlier demonstration that separate treatment of sunlit and shaded leaves is essential in canopy models (Sinclair *et al.*, 1976; Norman, 1980), many of the models used to examine optimal distributions of nitrogen have ignored the penetration of sunflecks and made the assumption of 100% diffuse light. While all diffuse light may be a reasonable assumption for some of the canopies examined where cloudy conditions predominate, it seems unlikely to be the case in canopies exposed to sunny conditions and is not a reasonable assumption for models that attempt to generalise the original hypothesis to all canopies.

The concept of an optimal distribution of leaf nitrogen has also been used as the basis for a new generation of big leaf models of canopy photosynthesis (Sellers *et al.*, 1992; Amthor, 1994). It was demonstrated by Farquhar (1989) that the equation describing whole leaf photosynthesis has the same form as for individual chloroplasts across a leaf, provided that the distribution of chloroplast photosynthetic capacity is in proportion to the profile of absorbed light and that the shape of the light response is identical in all layers, which he further stated was analogous with leaves in a canopy. If the distribution of photosynthetic capacity between leaves is in proportion to the profile of absorbed light then the equation describing leaf photosynthesis will also represent canopy photosynthesis (Sellers *et al.*, 1992).

The models of both Sellers *et al.* (1992) and Amthor (1994) also seem to contradict the accepted practice in modelling canopy photosynthesis that, at a minimum, separation into sunlit and shade leaves is essential to give accurate predictions. The analogy of leaves in a canopy with chloroplasts in a leaf breaks down because of differences in the nature of light distribution in each system. In a leaf, light is scattered in all directions by the first layer of cells, although its extinction through the leaf is still described by Beer's law. In a canopy while the time-averaged profile of absorbed irradiance is exponential (*ie*, described by Beer's law), the instantaneous profile of absorbed irradiance is not. Leaves in sunflecks deep in the canopy have much higher absorbed irradiance than the Beer's law would predict. Additionally, irradiance in canopies is dominated by direct beam light (often 80 - 90 %), so that leaf angle is critical in determining the amount of absorbed irradiance (Lambert's law). Leaves at the top of the canopy that are parallel to the direction of the beam only absorb diffuse irradiance. Instantaneous profiles of

absorbed irradiance in canopies do not follow Beer's law because of both sunfleck penetration and leaf angles.

The big-leaf models of Sellers *et al.* and Amthor overcome these limitations by using an empirical coefficient to increase the curvature of the light response of canopy photosynthesis. This reduces the overestimation of photosynthesis that would have occurred from using the averaged profile of absorbed light with no curvature factor. What implications does this have? Perhaps, very little. Big leaf models have been shown to accurately describe canopy photosynthesis (Amthor *et al.*, 1994). The problem with using this type of correction is that the empirical curvature coefficient may not be constant with different conditions, thus reducing the accuracy of predictions for new conditions such as canopies with different leaf area indices.

The big-leaf model based on the relationship between the profiles of absorbed light and leaf nitrogen is a powerful means to reduce the complexity of models of canopy photosynthesis. This new approach needs to be reconciled with evidence from earlier work that leaves of sunlit and shaded leaves must be treated separately (Sinclair *et al.*, 1976; Norman, 1980). It is desirable to combine these two approaches, so that the simplifications possible from the optimal distribution of photosynthetic resources can be used with the accuracy of canopy models which treat sunlit and shade leaves separately.

In this chapter I present such a model, that analytically integrates the photosynthetic capacity and absorbed light of the sunlit and shaded leaves separately. This new sunlit and shaded big leaf model is compared with a multi-layer model and with a simple big leaf model with empirical curvature coefficients. The effect of sunfleck penetration through canopies and leaf-angles is considered with respect to the optimal distribution of canopy nitrogen and compared with the assumptions of 100 % diffuse light. I examine the hypothesis that the new sun/shade model gives predictions of canopy photosynthesis as good as a multi-layer model, and is significantly better than the big-leaf models of Sellers and Amthor.

6.2. Model

6.2.1. Leaf Photosynthesis

The model of Farquhar *et al.* (1980) was used to describe leaf photosynthesis. This model describes photosynthesis as being limited by either the kinetics of the reactions catalysed by the enzyme ribulose-1,5-bisphosphate carboxylase/oxygenase (Rubisco), or by the regeneration of the substrate ribulose-1,5-bisphosphate (RuBP) which is driven by the electron transport reactions of the thylakoids.

The Rubisco limited rate of photosynthesis (A_V) is given by the equation:

$$A_V = V_l \frac{p_i - \Gamma_*}{p_i + K'} \tag{6.1}$$

where p_i is the intercellular CO_2 partial pressure, Γ_* is the CO_2 compensation point in the absence of mitochondrial respiration, V_l is the catalytic capacity of Rubisco per unit leaf area, K' is the effective Michaelis-Menten constant of carboxylation:

$$K' = K_c(1 + O/K_o) \tag{6.2}$$

K_c and K_o are Rubisco Michaelis-Menten constants for CO_2 and oxygen, respectively, and O is the O_2 partial pressure.

Farquhar *et al.* (1980) described leaf photosynthesis in terms of the CO_2 and O_2 partial pressures in the chloroplasts. The partial pressures in the chloroplasts and the intercellular air spaces were assumed equal, since, in the absence of measurements, internal resistances to diffusion were assumed to be zero. Recently, carbon isotope discrimination techniques have allowed estimates of the internal resistances (Evans *et al.*, 1986; von Caemmerer & Evans, 1991; Lloyd *et al.*, 1992; Evans *et al.*, 1994; Loreto *et al.*, 1992). The techniques are subject to several assumptions and the estimates are variable, although they do show a general correlation of increasing internal conductance with rate of photosynthesis, which seems to be related to surface area of chloroplasts exposed to intercellular air spaces (Evans *et al.*, 1994). This suggests that for a particular species a simple internal conductance porportional to photosynthetic capacity may be sufficient to account for this phenomenon. A finite internal resistance lowers the

partial pressures in the chloroplasts and thus affects the value of the Rubisco parameters K_c, K_o and Γ_* that are determined from gas exchange measurements. It is important to use the parameter values appropriate to the assumptions of internal conductance.

I examined the effect of including an internal conductance ($g_i = 0.5$ mol.m^{-2}.s^{-1} at $V_l =$ 100 μmol.m^{-2}.s^{-1}) and found that it had very little effect ($< 1\%$) on the diurnal course of canopy photosynthesis and inclusion of this phenomenon in a simple model of canopy photosynthesis is not warranted. I have assumed an infinite internal wall conductance to CO_2 diffusion and the appropriate values of the parameters are in Table 6.1.

RuBP regeneration limited rate of photosynthesis, A_J, is given by the equation:

$$A_J = J \frac{p_i - \Gamma_*}{4(p_i + 2\Gamma_*)} \tag{6.3}$$

where J is the electron transport rate, as indicated by production of NADPH, which can be empirically related to PAR (0.4-0.7μm) irradiance usefully absorbed by Photosystem II (PSII) by a non-rectangular hyperbola (Farquhar & Wong, 1984):

$$\theta_l J^2 - (I_{le} + J_m)J + I_{le} \cdot J_m = 0 \tag{6.4}$$

where θ_l is a curvature factor which determines how quickly the transition is made from the region of maximum quantum yield to the light saturated rate. The maximum electron transport rate (J_m) is a property of the amount and nature of the thylakoid membranes that varies with growth conditions; low nitrogen nutrition or low light in the growth environment results in low values of J_m (Evans & Farquhar, 1991). I_{le} is the effective absorbed PAR by PSII per unit leaf area and is related to absorbed irradiance per unit leaf area by the equation

$$I_{le} = I_l(1 - f)/2 \tag{6.5}$$

where f is a correction factor (~0.15) for the actual quantum yield in sunlight compared to the maximum which occurs with light of 0.6 μm. The factor 2 relates to the requirement of absorption of photons by both PSI and PSII to drive an electron from H_2O to $NADP^+$. The reasons for the observed quantum yield being lower than the theoretical maximum (8 quanta absorbed per 4 electrons transferred) are unclear. Evans

(1987) suggested that it may be due the spectral imbalance of sunlight with respect to the absorption characteristics of Photosystems I and II (PSI & PSII).

The actual rate of photosynthesis is determined as the minimum of these rates (providing $p_i > \Gamma_*$).

$$A_l = \min\{A_J, A_V\} - R_l \tag{6.6}$$

R_l is the non-photorespiratory respiration that continues in the light. Recent modifications to the model have included an additional limitation to photosynthesis associated with the capacity for export or utilization of the products of photosynthesis (Collatz et al., 1991). I have ignored this effect for the sake of simplicity as it is unlikely to be significant under most conditions.

It has been suggested that the transition from electron transport to Rubisco limited photosynthesis is not abrupt, but more gradual, with a range of conditions under which co-limitation occurs (Kirschbaum & Farquhar, 1984; Collatz et al., 1991). However, I believe this makes little difference to leaf photosynthesis in the field and the aggregate canopy photosynthesis, since only a small fraction of leaves are near the light saturation point at any moment. Consequently I have used the model in its simplest form ignoring this modification.

6.2.1.1. Respiration

Leaf respiration that continues in the light (R_l) is assumed to be a fixed proportion of Rubisco capacity. This is equivalent to assuming a fixed CO_2 compensation point, Γ, which is more tangible than a ratio. In this case I assumed a value of 44 µbar at 25°C, which is a reaonable value for wheat (Watanabe et al., 1994) and using the equation;

$$\frac{R_l}{V_l} = \frac{\Gamma - \Gamma_*}{\Gamma + K'}, \tag{6.7}$$

gives a value of $R_l = 0.0089V_l$. This ratio is lower than the value used by Collatz et al., (1991, 0.015) and Farquhar et al., (1980, 0.011), though in fact probably makes very little difference.

6.2.1.2. Effect of Temperature

All metabolic reactions of photosynthesis are affected by temperature. A variety of functions have been used to describe rate responses; the most popular being the Q_{10} and Arrhenius functions.

Biologists have often used the Q_{10} function (eq. 6.8) to describe temperature response phenomena; mostly for its simplicity. The Q_{10} value is simply the relative increase in a rate over a 10°C temperature range. It is specified at a particular temperature (T), as the Q_{10} itself generally changes with temperature. The Q_{10} allows easy comparison between studies, but its variation with temperature tends to limit its use over a wide temperature range.

$$k_T = k_{25} Q_{10}^{(T-25)/10} \tag{6.8}$$

In the Arrhenius function (eq. 6.9), preferred by biochemists to describe the effect of temperature on the rate of enzyme catalysed reactions, the activation energy (E_a) represents the kinetic energy of substrates required for the reaction to proceed. It is less affected by temperature, and it fits rates well over a wide range of temperatures.

$$k_T = k_{25} \exp\left(\frac{E_a(T-25)}{R \cdot 298.15 \cdot (T+273.15)} \right) \tag{6.9}$$

where R is the universal gas constant (8.314 J.mol^{-1}.K^{-1}).

However, many reactions of photosynthesis are reversible and a different activation energy is required for the reverse reaction. For equilibrium or net reactions, the apparent activation energy is not constant, but varies with the ratio of forward to reverse reactions. Also the activity of membrane bound enzymes varies as the fluidity of membrane lipids changes with temperature. For both these reasons and other factors, many reactions do not appear to have a constant activation energy. It usually increases at lower temperatures (eg.; Badger & Collatz, 1977).

Despite these limitations the Arrhenius function is a better descriptor of temperature response than the Q_{10} function and it still allows simple comparison of rate responses between studies. Use of empirical polynomial functions would avoid the falsely implied mechanistic basis of the Arrhenius function, but the coefficients do not allow easy comparison between studies.

In this work I have used the Arrhenius function; the activation energies of the relevant parameters are presented in Table 6.1 and their responses to temperature are plotted in figure 6.1.

Table 6.1 Photosynthesis parameters at 25°C and their activation energies, E (kJ.mol^{-1}). The Rubisco parameters K_c, K_o and Γ_* are defined assuming an infinite internal wall conductance to CO_2 diffusion.

Parameter	Value	E_a
K_c (μbar)	404[a]	59.4[b]
K_o (mbar)	248[a]	36.0[b]
V_l (μmol.m^{-2}.s^{-1})	100	64.8[b]
J_m (μmol.m^{-2}.s^{-1})	$2.1V_l^e$	37.0[c]
R_l (μmol.m^{-2}.s^{-1})	$0.0089V_l$	66.4[c]
Γ_* (μbar)	36.9[a]	27.0[d]

[a] von Caemmerer *et al.* (1994); [b] Badger and Collatz (1977); [c] Farquhar *et al.* (1980); [d] Jordan and Ogren (1984); [e] Watanabe *et al.* (1994)

This model of leaf photosynthesis defines Γ_* as a function of the Michaelis-Menten constants and the ratio of the maximal rates of oxygenation to carboxylation by Rubisco (Farquhar *et al.*, 1980, their eq. 38). Thus assuming a constant ratio of oxygenation to carboxylation, the temperature response of Γ_* is mathematically defined by the response of each of the components. However experimentally it is more accurate to measure Γ_* and its temperature response directly *in vivo* than its components. Thus I have used the temperature response of Jordan and Ogren (1984), which was very similar to that of Brooks and Farquhar (1985) but over a wider temperature range, and the more recent absolute values of Γ_* from von Caemmerer *et al.* (1994).

$$\Gamma_* = 36.9 + 1.88(T - 25) + 0.036(T - 25)^2 \qquad (6.10)$$
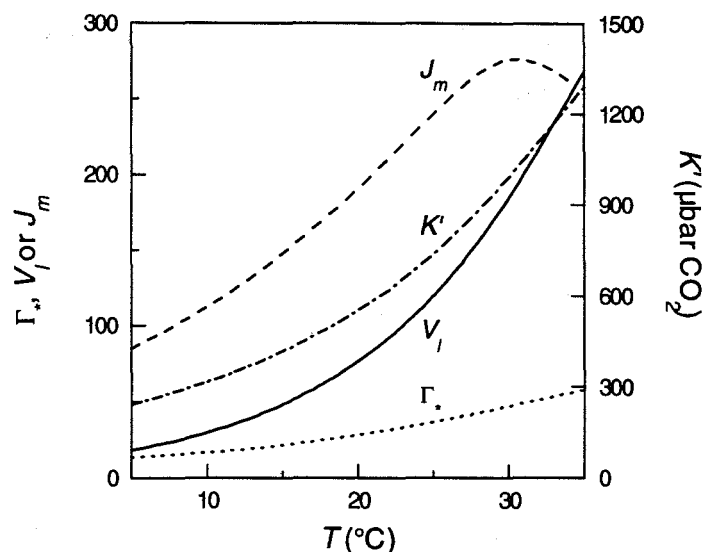
Figure 6.1 Effect of temperature on leaf photosynthesis parameters: V_i (μmol.m^{-2}.s^{-1}), J_m (μmol.m^{-2}.s^{-1}), Γ_* (μbar CO_2) and K' (eq. 6.2, μbar CO_2) modelled using activation energies in Table 6.1.

Maximum electron transport capacity, J_m, increases with temperature until a maximum is reached and then declines rapidly. Farquhar *et al.* (1980) modelled this phenomenon with the function

$$J_{m_T} = J_{m_{25}} \cdot \exp\left[\frac{(T/_{298} - 1)E_a}{RT}\right] \cdot \frac{\left(1 + \exp\left[\frac{S \cdot 298 - H}{R \cdot 298}\right]\right)}{\left(1 + \exp\left[\frac{ST - H}{RT}\right]\right)}, \tag{6.11}$$

where E_a is the activation energy of J_m and S and H are parameters to define the deactivation at high temperatures. This expression was based on data from isolated chloroplasts that had been growing at 25 °C. Harley *et al.* (1992) obtained parameter values for the response of photosynthesis to temperature in cotton. The functions they obtained were not statistically different to those originally used by Farquhar *et al.* (1980), so the latter functions and parameters values were retained. However, many plants, including wheat, acclimate to the growth temperature regime so that the temperature dependence of membrane bound processes such as electron transport, adapt to the

growth temperature (Björkman *et al.*, 1980; Sayed *et al.*, 1989). Expressions to describe temperature acclimation may need to include this phenomenon, although they have been ignored here.

6.2.1.3. Ratio of Rubisco to Electron Transport

It has been suggested that leaves tend to optimize their photosynthetic enzymes such that the transition from Rubisco to RuBP regeneration limited photosynthesis occurs at conditions often experienced by the leaves, so that neither Rubisco nor electron transport capacity is greatly in excess of that required for the growth conditions (von Caemmerer & Farquhar, 1981; Evans, 1986; Chen *et al.*, 1993). While there is some evidence to suggest that plants grown in controlled environments do distribute their resources in an optimal manner (von Caemmerer & Farquhar, 1981; Evans, 1986), it is more difficult to demonstrate in field grown plants; especially considering the variability of light and temperature and the uncertainty of 'normal' conditions. The partitioning between electron transport and Rubisco, must therefore be sub-optimal most of the time, since the optimal ratio will change during the day and between days.

Despite the preceding limitations to an optimal distribution, the ratio of $J_m:V_l$ varies little across a wide range of species (Wullschleger, 1993). In wheat the ratio is highly conserved across a wide range of conditions (Evans, 1983; Makino *et al.*, 1992; Watanabe *et al.*, 1994), although the ratio does vary with temperature in proportion to the ratio of the temperature sensitivities of the components. I have assumed a fixed ratio of $J_m:V_l = 2.1$ at 25 °C.

This ratio of $J_m:V_l$ affects the conditions under which photosynthesis is RuBP or Rubisco limited. At or below ambient CO_2 concentrations (< 350 ppm) and high light (> ~1200 μmol quanta.m^{-2}.s^{-1}) leaves will be Rubisco limited. While at low light (< ~500 μmol quanta.m^{-2}.s^{-1}) and ambient or greater [CO_2] (> 350 ppm) leaves will be RuBP regeneration limited. At some intermediate irradiance (between 500-1200 μmol quanta.m^{-2}.s^{-1}) the limitation will change from Rubisco to RuBP regeneration limited. This irradiance is known as the light saturation point of leaf photosynthesis (I_{lsat}), since there is no further increase in photosynthesis with increasing light. It can be calculated by combining eqs. 6.1-6.5 and rearranging to yield the expression:

$$I_{lsat} = V_l \frac{2}{(1-f)} \cdot \frac{4(p_i + 2\Gamma_*)(4\theta_l(p_i + 2\Gamma_*) - J_m/V_l(p_i + K'))}{(p_i + K')(4(p_i + 2\Gamma_*) - J_m/V_l(p_i + K'))}. \qquad (6.12)$$

Several of the parameters in the calculation of the light saturation point of photosynthesis are affected by temperature. Providing the ratio of J_m/V_l remains constant (at 25 °C), the light saturation point is a linear function of Rubisco capacity and the slope increases with increasing p_i and with temperature (figure 6.2). This relationship of decreasing light saturation point with decreasing Rubisco capacity becomes significant when photosynthesis of leaves is scaled to canopy photosynthesis, as explained in a later section.
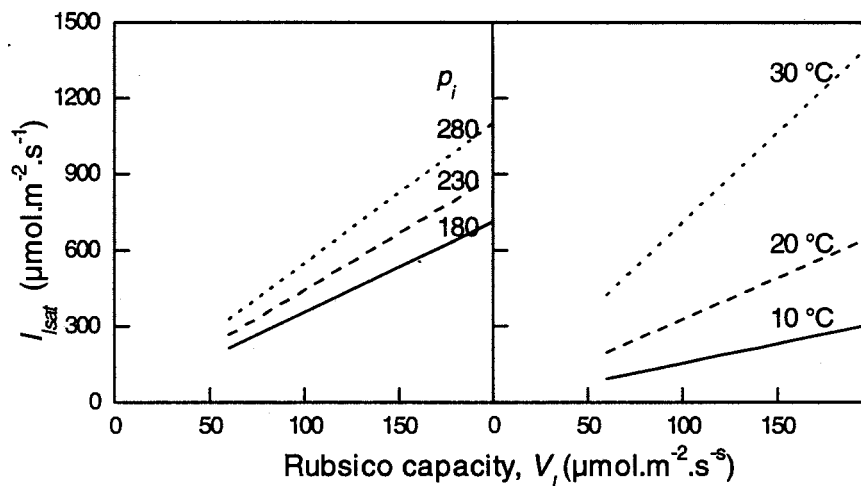
Figure 6.2 Light saturation point of leaf photosynthesis (I_{lsat}) (eq. 6.12), under conditions experienced in a canopy, where p_i is assumed constant while photosynthetic Rubisco capacity and irradiance decrease with depth in the canopy. The ratio of electron transport to Rubisco (J_m/V_l) is assumed constant. Three constant values of p_i are shown (left panel) 180 (solid line), 230 (dashed line) and 280 μbar (dotted line) and three temperatures (right panel) 10 (solid line), 20 (dashed line) and 30 °C (dotted line).

6.2.2. Stomatal Conductance and Intercellular CO_2

The Farquhar *et al.*, (1980) model of leaf photosynthesis has intercellular CO_2 concentration (c_i) as a variable, which is affected by both the supply of CO_2 by diffusion through the leaf boundary layer and stomata and by the rate of uptake by CO_2 fixation. The photosynthesis model must be coupled with a model of stomatal conductance to predict photosynthesis. I have used the Ball-Berry model (Ball *et al.*, 1987) as modified by Leuning (1995), that was evaluated in Chapter Four. Intercellular CO_2 concentration (c_i) was calculated using the equations for gas exchange presented by von Caemmerer & Farquhar (1981). The expressions for photosynthesis, conductance and diffusion of CO_2 were solved iteratively.

6.2.3. Light penetration in canopies

6.2.3.1. Canopy Structure

Canopy structure is the spatial arrangement of canopy elements (leaves and stems). It is determined by the canopy leaf area, orientation, and vertical and horizontal (clumping) distributions. I have assumed a horizontally homogeneous leaf distribution. Position in the canopy is defined by the downward cumulative leaf area, thus avoiding the need to specify the vertical leaf area distribution. Canopy leaf area is known from direct measurements. Leaf orientation is described following the work of Ross (1975; 1981), as discussed below.

One only has to look at a real plant canopy to appreciate that a mathematical description of its structure can be very complex. Consequently many assumptions are made in this modelling; further details are in the comprehensive treatment of Ross (1981). In this description I give the general form of the most pertinent equations and the specific forms appropriate to the explicit assumptions that I have made.

The spatial arrangement of leaves is described by the distribution function of leaf area orientation $g(\alpha_l, \phi_l)$ (Ross, 1975). This function defines the probability of leaf area being oriented with an inclination (α_l) to the horizontal and an azimuth orientation (ϕ_l):

$$\frac{1}{2\pi} \int_0^{2\pi} \int_0^{\pi/2} g(\alpha_l, \phi_l) \sin \alpha_l \, d\alpha_l d\phi_l \equiv 1. \tag{6.13}$$

The $\sin\alpha_l$ arises from the ratio of the circumference of circles ($2\pi r$) at different positions on a sphere, where their position is defined by α_l and $\sin\alpha_l$ is the radius of such circles. If leaves display no azimuth preference, as is the case with a wheat canopy, then ϕ_l is eliminated so that $g(\alpha_l, \phi_l) = g(\alpha_l)$ and eq. 6.13 may be simplified:

$$\int_0^{\pi/2} g(\alpha_l)\sin\alpha_l \, d\alpha_l \equiv 1. \tag{6.14}$$

Leaf inclination distributions range from the simplest, which are horizontal or vertical leaf angle distributions, to any number of complex possibilities in between. In the special case of uniform or spherical leaf angle distribution, all leaf orientations are equally probable and $g(\alpha_l, \phi_l) = 1$. By simple geometry and integration around the horizon of 2π, the distribution of leaf area as a function of angle is given by $g(\alpha_l) = \sin\alpha_l$.

Leaf angle is used to calculate absorbed beam irradiance per unit leaf area, by Lambert's cosine law, as $I_b\cos\alpha_l$. Absorbed irradiance is in turn used to calculate photosynthesis. In a multi-layer model, canopy photosynthesis is obtained by numerical integration of the leaf photosynthesis equations from all leaves. Thus, to apply Lambert's law, the canopy is divided into a number of discrete leaf-angle classes (depending on the detail required). The fraction of leaf area in each class (f_l) is obtained from the integral of the leaf area distribution function, $g(\alpha_l)$, which in the case of a uniform leaf-angle distribution is

$$f_l(\alpha_l) = \int_{\alpha_{l1}}^{\alpha_{l2}} g(\alpha_l)\,d\alpha_l = \int_{\alpha_{l1}}^{\alpha_{l2}} \sin\alpha_l\,d\alpha_l = \left[-\cos\alpha_l\right]_{\alpha_{l1}}^{\alpha_{l2}}. \tag{6.15}$$

A mean cosine of leaf-angle ($\overline{\cos\alpha_l}$) for each class is determined, rather than the cosine of the mean leaf-angle ($\cos\overline{\alpha_l}$) as has been used elsewhere (Norman, 1980). For each leaf-angle class the mean cosine of leaf-angle is determined as;

$$\overline{\cos\alpha_l} = \int_{\alpha_{l1}}^{\alpha_{l2}} g(\alpha_l)\cos\alpha_l\,d\alpha_l \bigg/ f_l = \tfrac{1}{2}\left[\sin^2\alpha_l\right]_{\alpha_{l1}}^{\alpha_{l2}} \bigg/ f_l \tag{6.16}$$

Calculated mean leaf inclinations for divisions of 1 and 5 leaf-angle classes are given in Table 6.2. For example, in a five leaf-angle classification of a uniform leaf-angle distribution, each class covers an interval of $18°$. The first class from $0-18°$ has a mean cosine of 0.976 and contains 4.9% of the leaf area, the second interval has a mean cosine

of 0.880 and contains 14.2% of the leaf area, and so on. Leaf angles nearest horizontal have most leaves, and conversely those nearest vertical have the least.

Table 6.2 Mean cosine of leaf-angle $(\overline{\cos\alpha_l})$ and distribution of leaf area (f_l) for a canopy of uniform leaf-angle distribution divided into 1 or 5 leaf-angle classes of equal leaf-angle divisions.

No. of leaf-angle classes	Interval range α_{l1} - α_{l2}		$\overline{\cos\alpha_l}$	f_l
1	0	90	0.500	1.000
5	0	18	0.976	0.049
	18	36	0.880	0.142
	36	54	0.698	0.221
	54	72	0.448	0.279
	72	90	0.155	0.309

6.2.3.2. Light Distribution

Irradiance at different levels in a canopy is determined principally by light penetration into the canopy. Attenuation of light by the canopy is affected by position of the sun, proportion of diffuse light, leaf area, orientation and their optical properties of reflectance and transmission. Solar elevation is calculated from the geometry of planetary rotation and fraction of diffuse light is modelled by a simple atmosphere attenuation model (Campbell, 1977). Light penetration was first modelled by Beer's law (which was first described by Bouguer, but is commonly known as Beer's law or the Beer-Lambert law (Iqbal, 1983)) by Monsi and Saeki (1953) and elaborated by many others, best summarised in the work of Goudriaan (1977). Light profiles are converted to light absorbed per unit leaf area at the appropriate leaf angles according to Lambert's cosine law, to drive photosynthesis, as detailed below.

Solar Geometry

The position of the sun in the sky is described by two parameters; elevation in the vertical and azimuth in the horizontal. Solar elevation (β) is a function of day of the year (t_d), latitude (λ) and time of day (t) and is geometrically defined by the equation (Jones, 1992):

$$\sin \beta = \sin \lambda \sin \delta + \cos \lambda \cos \delta \cos h \qquad (6.17)$$

where h is the hour angle of the sun and is given by $\pi(t - t_o)/12$, t is the time in hours and t_o is the time of solar noon at a particular location. Solar declination (δ, radians) is determined by tilt and rotation of earth and is a function of the day of the year, beginning with 1 on 1 January.

$$\delta = -23.4 \frac{\pi}{180} \cos\left[2\pi(t_d + 10)/365\right]. \qquad (6.18)$$

Azimuth of the sun (ϕ_s) is defined as the angle from south (for the southern hemisphere) where it is zero with east positive and west negative and is given by the expression (Iqbal, 1983):

$$\sin \phi_s = (\sin \beta \sin \lambda - \sin \delta)/\cos \beta \cos \lambda. \qquad (6.19)$$

Solar noon is calculated from the longitude and the ephemeris of the sun given by the equation of time (E_t), which accounts for the variation in period of rotation of earth. According to Iqbal (1983) this is given by

$$E_t = 229.18(0.000075 + 0.001868 \cos \Gamma_d - 0.032077 \sin \Gamma_d \\ -0.014615 \cos 2\Gamma_d - 0.04089 \sin 2\Gamma_d) \qquad (6.20)$$

where the factor 229.18 converts radians to minutes (time) and Γ_d is the day angle (radians) and is calculated as

$$\Gamma_d = 2\pi(t_d - 1)/365. \qquad (6.21)$$

The Equation of time combined with the longitude correction determines the time of solar noon as:

$$t_o = \left(4(L_s - L_e) + E_t\right)/60,$$ (6.22)

where L_s and L_e are the standard and local longitudes. The longitude correction is based on 4 minutes for every degree difference between the local and standard meridians. It is positive if the local meridian is east of the standard and negative west of the standard meridian. All international standard meridians are multiples of 15° east or west of Greenwich, England. For example, at Wagga Wagga (L_e = 147° 20.5' E and L_s = 150° E) the longitude correction is -10.63 minutes.

Fraction of diffuse light

Light is attenuated by scattering from gas molecules, water vapour and dust in the atmosphere, so that both the quantity and quality of light is changed at the earth's surface. The extent of the attenuation depends on the concentration of absorbers and the path length through the atmosphere. This process is described by a simple model for the attenuation of short-wave radiation (Campbell, 1977) that has been modified to describe attenuation of PAR:

$$I_b = a^m I_e \sin \beta,$$ (6.23)

where I_b is beam PAR. I_e is the extra-terrestrial quantum flux (2413 μmol quanta.m^{-2}.s^{-1}, calculated from the energy distribution of the solar 'constant' - 1367 W.m^{-2} with a 3.3 % seasonal variation as the mean distance between the sun and earth changes (Iqbal, 1983)). a is an empirical atmospheric transmittance coefficient that varies from 0.9 for very clear sky to 0.6 for hazy conditions and m is the optical air mass, which is defined as the ratio of the mass of atmosphere traversed per unit cross-sectional area of the solar beam to that traversed for a site at sea level if the sun was directly overhead. The value of m therefore decreases with altitude and increasing solar elevation and by ignoring the curvature of the earth's atmosphere, can be described by the expression

$$m = \left(P/P_o\right)/\sin \beta,$$ (6.24)

where P is atmospheric pressure and P_o is atmospheric pressure at sea level.

If scattering were solely responsible for attenuation of light in the atmosphere, then 50% of attenuated radiation would be forward scattered as diffuse light to the surface

and the remainder scattered back out to space. However, light absorption occurs at particular wavelengths characteristic of each absorber, so that less than 50% reaches the earth surface. Observations have ranged from 40 - 45 % of attenuated light that reaches the surface as diffuse light (Weiss & Norman, 1985). A value of 42.6 % was found to give a best fit to the available data. This can be expressed by the equation;

$$I_d = f_a(1 - a^m)I_e \sin \beta,$$

(6.25)

where I_d is diffuse PAR light intensity at the earth's surface and f_a is the proportion of attenuated PAR scattered forward to the earth's surface.

An expression for the diffuse fraction (f_o) of total light (beam plus diffuse) can be obtained by combining eqs. 6.23 & 6.25:

$$f_o = \frac{1 - a^m}{1 + a^m(1/f_a - 1)}.$$

(6.26)

Although this model was developed for the attenuation of short wave radiation which has slightly different scattering and absorption compared with PAR, I have assumed that the process is similar. These differences result in slightly different atmospheric transmission values based on PAR values compared to those based on short wave radiation.

Penetration in a canopy

A simple model of beam penetration is described below. It is extended to include penetration of diffuse light and scattering of beam and diffuse light by leaves. The model is then used to determine the fraction of sunlit leaves and the irradiance of sunlit and shaded fractions. Finally the absorption of light by leaves as distinct from their irradiance is described.

The distribution function of leaf orientation (g) was introduced earlier to describe canopy structure. When describing radiation penetration the leaf orientation function is combined with light direction and is called the $G(\alpha, \phi)$ function (Ross & Nilson, 1967). As explained by Ross (1975), it characterises the dependence of the effective leaf area to radiation penetration on both the light direction (α, ϕ) and on leaf orientation (α_l, ϕ_l). It is defined as the projection of a unit foliage area in the direction (α, ϕ):

$$G(\alpha,\phi) = \frac{1}{2\pi}\int_0^{2\pi}d\phi\int_0^{\pi/2} g(\alpha_l,\phi_l)|\cos nn_l|\sin\alpha\,d\alpha, \tag{6.27}$$

where n is the unit vector of light direction (α, ϕ), n_l is the unit vector of leaf blade orientation (α_l, ϕ_l), $\sin\alpha$ arises from resolving equal units of direction into elevation and azimuth and $\cos nn_l$ is the cosine of the angle of incidence of light on the leaf blade;

$$\cos nn_l = \cos\alpha\cos\alpha_l + \sin\alpha\sin\alpha_l\cos(\phi - \phi_l). \tag{6.28}$$

The G function may also be interpreted as the ratio of mean projected area of leaves on a plane normal to the sun's rays, to the actual leaf area.

Attenuation of light in a canopy is modelled using Beer's law, as originally applied to canopies by Monsi and Saeki (1953) and subsequently developed by Ross (1975; 1981) and Goudriaan (1977). If the canopy is divided into a finite number of thin layers of equal leaf area, sufficiently thin so there is no mutual shading within each independent layer, then the probability of a light beam being transmitted (τ_b) or not intercepted past a downward cumulative leaf area (L) is described by an exponential function;

$$\tau_b(L) = \exp\left(-G(\alpha,\phi)L/\sin\beta\right) \tag{6.29}$$

$G(\alpha, \phi)/\sin\beta$ is known as the extinction coefficient (k_b). τ_b is also the fraction of leaf area at depth L in sunflecks, so that near the top of the canopy the probability of beam transmission is close to one, and most of the leaves are sunlit. Distribution of leaf angles in a wheat canopy is approximately uniform (Ross, 1975), in which case G is independent of beam direction and $G = \frac{1}{2}$ and $k_b = 0.5/\sin\beta$. It is apparent that the extinction coefficient is dependent on the solar elevation, light penetrating deeper into the canopy at high solar elevations.

Direct Light

The transmission function (τ_b) is used to calculate the *spatially averaged* beam irradiance $I_b(L)$ relative to the beam irradiance at the top of the canopy $I_b(0)$;

$$I_b(L) = I_b(0)\exp(-k_bL). \qquad (\text{/m}^2\text{ gnd}) \tag{6.30}$$

This equation does not give the sunfleck light intensity. The beam intensity in the sunflecks is equal to that at the top of the canopy, but with a reduced leaf area in sunflecks.

Diffuse Light

Diffuse light from any point in the sky penetrates through a canopy with the same transmission coefficient as for beam light from that direction. Thus diffuse light transmission through a canopy is calculated by integrating the product of radiance of the sky (N_d) from direction n and the beam transmission (τ_b) of that elevation (α) over the whole sky;

$$\tau_d(L) = \frac{1}{I_d(0)} \int_{2\pi} N_d(L,n)\tau_b(L,\alpha)\sin\alpha\cos\alpha\, d\alpha\, d\phi, \tag{6.31}$$

where $N_d(L,n)$ is the radiance of the sky defined as the photon flux per unit solid angle in direction $n(\alpha, \phi)$ per unit area of sky at depth L in the canopy and $I_d(0)$ is the downward diffuse irradiance measured horizontally at the top of the canopy.

$$I_d(0) = \int_{2\pi} N_d(0,n)\sin\alpha\cos\alpha\, d\alpha\, d\phi \tag{6.32}$$

Diffuse sky radiance varies greatly, being affected by solar elevation, atmospheric transmission, cloud type and cover. The variability is so great that there is no simple method of modelling or describing the spatial source distribution of radiance except by direct measurements which are difficult to make. Clear sky radiance typically has high circumsolar radiance, low radiance at approx. 90° to the sun, increasing radiance near the horizon and varies with solar elevation (Gates, 1980; Iqbal, 1983). Typical completely overcast sky has a 3 fold increase in radiance from the horizon to the zenith. This has been defined by many authors as the standard overcast sky (SOC). Another simplification, often used, is to assume that radiance distribution is uniform over the entire sky or isotropic and is known as the uniform overcast sky (UOC). By integrating this distribution around the azimuth from 0 to 2π, the relative contribution of diffuse radiance as a function of elevation is given by

$$\frac{dI_d(0,\alpha)}{I_d(0)} = 2\sin\alpha\cos\alpha\, d\alpha. \tag{6.33}$$

197

This assumption simplifies the penetration integral so that it can be more easily solved (Cowan, 1968a; Ross, 1975);

$$\tau_d(L) = 2\int_0^{\frac{\pi}{2}} \exp(-k_b L)\sin\alpha\cos\alpha\ d\alpha$$
$$= (1 - L/2)\exp(-L/2) - (L/2)^2 E_i(-L/2)$$

(6.34)

where $E_i(x)$ is the exponential integral (Jahnke & Emde, 1945). Thus the diffuse light irradiance at depth L is given by the expression;

$$I_d(L) = I_d(0)\tau_d(L)$$

(6.35)

where $I_d(0)$ is the diffuse light intensity at the top of the canopy.
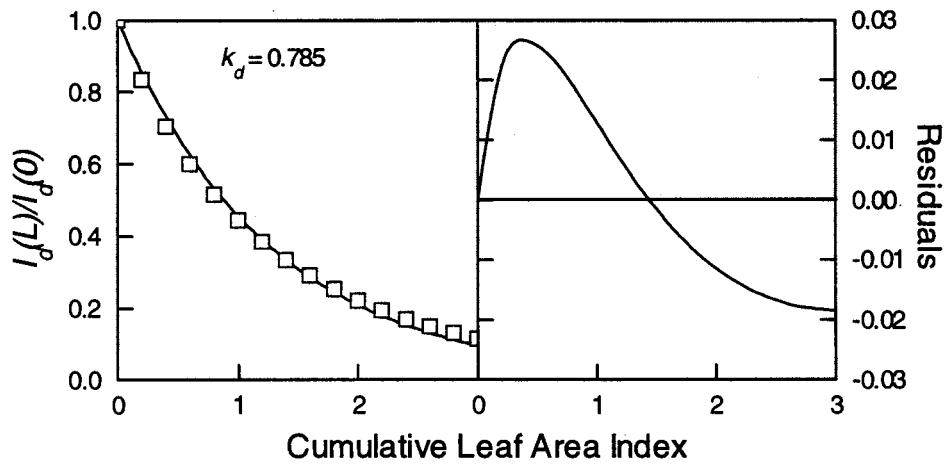
Figure 6.3 Left: Diffuse light penetration into a canopy from a uniformly radiant sky calculated according to Cowan (1968a) (eq. 6.34) and an exponential approximation. Right: Residuals from the exponential fit.

Solutions to eq. 6.34 are not easily calculated, so, following Goudriaan (1977), I approximated the diffuse penetration function with an exponential function, using a least squares fit (figure 6.3) to obtain a value for the diffuse extinction coefficient (k_d).

$$\tau_d(L) = \exp(-k_d L)$$

(6.36)

With a uniform sky radiance and $L_c = 3$ the best fit value of k_d is 0.785, which is lower than the value obtained by Goudriaan (1977, 0.805) due to his use of a greater leaf area. The maximum error of the exponential approximation is 2.7% overestimation at L = 0.5, where most leaves are sunlit anyway, while the 1.9% underestimate at L = 3.0 is acceptable for photosynthesis modelling. Use of this approximation greatly simplifies subsequent calculations.

Numerical integration of actual clear sky radiance penetrating a canopy with uniform leaf angle distribution suggests that UOC radiance overestimates the penetration of diffuse light in a canopy (Ross, 1981). Exponential approximations (error < 4%) to this penetration show a linear decrease in the extinction with solar elevation up to approx. 60° (fig. 6.4). The extinction coefficient obtained with UOC corresponds with the clear sky diffuse extinction when solar elevation is 60 - 70° above the horizon.
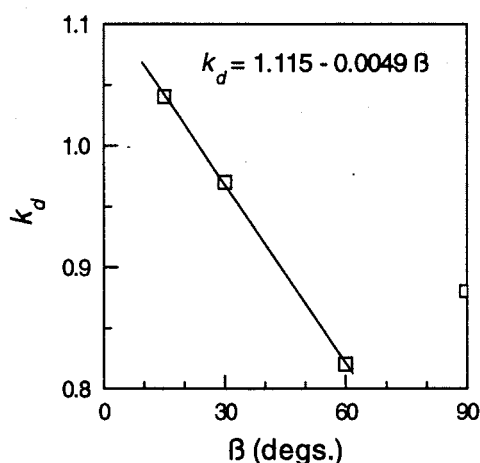
Figure 6.4. Extinction coefficients calculated for clear sky diffuse radiance penetrating a canopy with uniform leaf angle distribution. Clear sky radiation penetration data are from Ross (1981).

Down the canopy diffuse light from near the horizon will attenuate more quickly than that from the zenith. Opposing this is greater sky radiance from near the horizon compared with the zenith. I have ignored these effects and assumed that diffuse light is uniform in all directions at all depths in the canopy.

199

Scattered Light

In a real plant canopy leaves do not absorb all the intercepted light, a proportion being reflected or transmitted, scattering light in all directions. The scattered light is re-intercepted by adjacent leaves and either absorbed or rescattered. This multiple scattering increases canopy absorption beyond the absorption of individual leaves. These effects are modelled by an approximation of scattered light fluxes (Goudriaan, 1977). However to use this model correctly it is necessary to explain some detail of a more complex radiation transfer model.

Following Cowan (1968a) and Goudriaan (1977), I have assumed that the leaf reflection (ρ_l) and transmission (τ_l) coefficients are equal and their sum is defined as the scattering coefficient (σ). In a canopy of $L_c > 3.0$ reflection from the soil can be ignored. Error introduced with these assumptions is negligible for a canopy with spherical leaf angle distribution and facilitates an algebraic solution (Goudriaan, 1977). Detailed canopy light models (Goudriaan, 1977; Norman, 1979) calculate separate downward and upward light fluxes between thin layers $(L_l = 0.1)$ of canopy. A layer transmission coefficient $(\tau = \exp[-kL_l])$ is used to calculate the primary fluxes in adjacent layers. The flux of scattered light is calculated from light intercepted by each layer and the scattering coefficient; half directed upwards and half downwards. Several iterations of calculating fluxes in all layers of the canopy converge to a final solution of upward and downward fluxes. When the canopy leaf area is greater than 2.0 the upward light flux from soil reflection can be ignored (Goudriaan, 1977).

This model is simplified, for canopies of large leaf area, by defining an extinction coefficient of the net light flux $(I_{down} - I_{up})$. The effective extinction coefficient (k') for the net downward light flux is related to the extinction coefficient with no scattering (called the black leaf extinction coefficient) (k) by the equation (Goudriaan, 1977)

$$k' = k(1-\sigma)^{\frac{1}{2}}.$$

(6.37)

The net beam light flux including scattering (I'_b) is given by the equation

$$I'_b(L) = I_b(0)(1 - \rho_{cb})\exp(-k'_b L),$$

(6.38)

where $\rho_{cb}(\beta)$ is the canopy reflection coefficient for beam light as a function of solar elevation. It accounts for the upward light flux that is lost as canopy reflectance and is determined empirically by the equation (Goudriaan, 1977)

$$\rho_{cb}(\beta) = 1 - \exp\left(-2\rho_h k_b / (1 + k_b)\right),$$ (6.39)

and ρ_h is the canopy reflection coefficient assuming horizontal leaves and is independent of solar elevation and is given by

$$\rho_h = \frac{1 - (1 - \sigma)^{\frac{1}{2}}}{1 + (1 - \sigma)^{\frac{1}{2}}}.$$ (6.40)

Numerical integration of sky light (UOC) penetration with scattering by leaves (I'_d) showed that the total diffuse light extinction coefficient (k'_d) is affected by the same factor as beam light (eq. 6.37) (Goudriaan, 1977):

$$I'_d(L) = I_d(0)(1 - \rho_{cd}) \exp(-k'_d L),$$ (6.41)

where ρ_{cd} is the canopy reflection coefficient for diffuse light and is calculated by numerical integration of the product of sky radiance and $\rho_{cb}(\alpha)$ for that direction by the equation

$$\rho_{cd} = \frac{1}{I_d(0)} \int_0^{\frac{\pi}{2}} N_d(\alpha) \rho_{cb}(\alpha) d\alpha.$$ (6.42)

In the case of a uniform leaf angle distribution and $\sigma = 0.15$ the value of eq. 6.42 was calculated with UOC as $\rho_{cd} = 0.036$ (lower than the value obtained by Goudriaan (1977 0.) since he assumed $\sigma = 0.20$).

In contrast to this model, Norman (1982) calculated scattered light fluxes using an extinction coefficient of $k(1-\sigma)$. It differs from the correct expression, presented by Goudriaan (1977), by the exponent of ½, which arises from consideration of multiple scattering.

Total Irradiance

So far direct, diffuse and scattered irradiance have been calculated as separate components. Plants, however, do not make these distinctions. Total irradiance including scattering (I') is calculated as the sum of beam light with scattering plus diffuse light with scattering.

$$I'(L) = I_b'(L) + I_d'(L)$$
$$= I_b(0)(1 - \rho_{cb}) \exp(-k_b'L) + I_d(0)(1 - \rho_{cd}) \exp(-k_d'L) \tag{6.43}$$

Sunlit and shaded leaves

The fraction of leaves in sunflecks, f_{Sun}, is derived from the beam penetration function,

$$f_{sun}(L) = \tau_b = \exp(-k_b L). \tag{6.44}$$

The fraction of leaves in shade is $1 - f_{Sun}$.

Irradiance of sunlit (I_{Sun}) and shade (I_{Sh}) leaves is calculated separately by assuming that diffuse, scattered diffuse and scattered beam light impinges on all leaves, while sunlit leaves in addition receive direct beam light.

$$I_{sh}(L) = I_d'(L) + I_{bs}(L) \tag{6.45}$$

The net scattered beam light (I_{bs}) is calculated as the difference between the beam flux (I_b) and the beam flux with scattering (I'_b).

$$I_{bs}(L) = I_b'(L) - I_b(L)$$
$$= I_b(0)\big((1 - \rho_{cb}) \exp(-k_b'L) - \exp(-k_b L)\big) \tag{6.46}$$

Irradiance of leaves in sunflecks is the beam intensity, which is constant through the canopy, plus the total diffuse light.

$$I_{sun}(L) = I_b(0) + I_{sh}(L) \tag{6.47}$$

Sunfleck irradiance is dominated by beam intensity so there is only a small reduction in sunfleck light intensity with depth (see figure 6.5), although there is a reduction in the fraction of leaves in each layer in sunflecks.
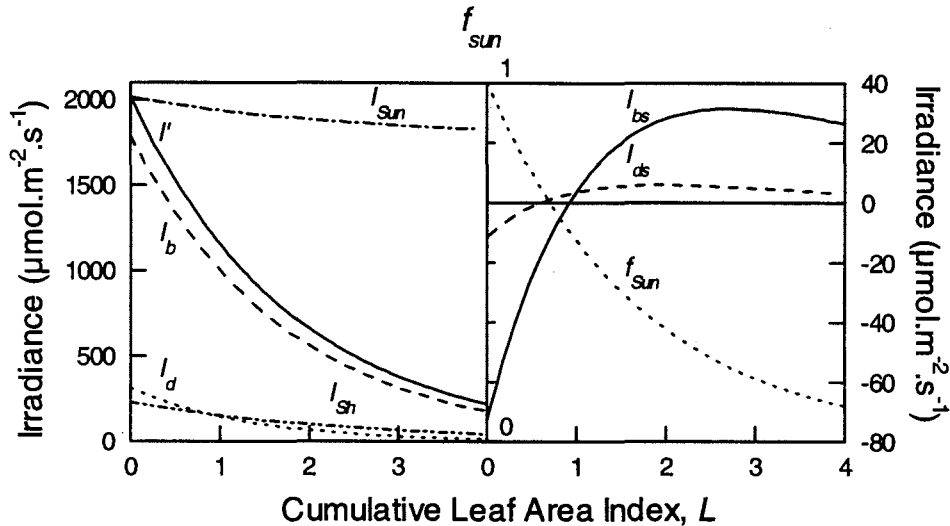
Figure 6.5. Modelled light penetration through a canopy. Irradiance above the canopy was 2100 (μmol quanta.m^{-2}.s^{-1}), with 15% as diffuse light and a solar elevation of 60°. *Left:* Fluxes are; beam (I_b, eq. 6.30), diffuse (I_d, eq. 6.35), total irradiance including scattering (I', eq. 6.43), irradiance in shaded (I_{Sh}, eq. 6.45) and in sunfleck (I_{Sun}, eq. 6.47) positions. *Right:* Net downward scattered fluxes of beam (I_{bs}, eq. 6.46) and diffuse (I_{ds}, eq. 6.35 - eq. 6.41) light and the fraction of canopy that is sunlit (f_{Sun}, eq. 6.44). The negative fluxes of scattered light at the top of the canopy are the upward fluxes which appear as canopy reflection. Note these irradiances are as would be measured on a horizontal plane, they are not irradiances at the angle of leaves, nor absorbed irradiance (as explained later).

Absorbed Light

At this stage I have described beam, diffuse and scattered irradiance. Total irradiance at any depth in a canopy is the sum of these components. However there are many other factors in addition to irradiance that affect the amount of light absorbed. Light absorbed per unit leaf area is additionally affected by leaf interception, leaf angle, leaf absorption and multiple scattering. Calculation of absorbed light requires attention to these factors as outlined below.

Absorption of all light fluxes per unit leaf area is determined as the change in irradiance with depth, which mathematically is the first differential. The effect of leaf absorption depends on whether scattering is included in the flux or whether it is treated separately. If a flux does not include scattering, then absorbed light is further reduced by the absorptivity of the leaves $(1-\sigma)$. Alternatively if the flux is a net flux where canopy reflectance and scattering are already included then absorbed light is calculated simply as the differential.

Considering only direct beam light, the average beam light absorbed per unit leaf area (I_{lb}) is calculated by the first differential of eq. 6.30 by the leaf absorptivity.

$$
\begin{aligned}
I_{lb}(L) &= -\partial I_b(L)/\partial L(1-\sigma) \\
&= k_b I_b(0)\exp(-k_b L)(1-\sigma) \\
&= k_b I_b(L)(1-\sigma)
\end{aligned} \tag{6.48}
$$

Thus, absorbed beam irradiance averaged over an entire layer at any position is the product of irradiance at that depth, the extinction coefficient and the leaf absorptivity. In contrast the expression for the beam light with scattering absorbed per unit leaf area does not include the leaf absorptivity (from eq. 6.38):

$$
\begin{aligned}
I'_{lb}(L) &= k'_b I'_b(L) \\
&= k'_b I_b(0)(1-\rho_{cb})\exp(-k'_b L)
\end{aligned} \tag{6.49}
$$

Absorbed diffuse light per unit leaf area (I_{ld}) is also calculated as the differential (of eq. 6.35),

$$
I_{ld}(L) = k_d I_d(0)\exp(-k_d L)(1-\sigma), \tag{6.50}
$$

or including the scattered diffuse light (I'_{ld}), the differential of eq. 6.41,

$$
\begin{aligned}
I'_{ld}(L) &= k'_d I'_d(L) \\
&= k'_d I_d(0)(1-\rho_{cd})\exp(-k'_d L)
\end{aligned} \tag{6.51}
$$

Absorbed total irradiance including scattering (I'_l) is calculated as the sum of absorbed beam with scattering (eq. 6.49) and absorbed diffuse with scattering (eq. 6.51).

$$I'_l = I'_{lb}(L) + I'_{ld}(L) \qquad (6.52)$$

Sunlit and shaded leaves

Separation of light absorption into sunlit and shade leaves is calculated as the differential of the respective irradiances. Thus light absorbed by shade leaves per unit leaf area (I_{lSh}) is calculated as the sum of diffuse absorbed and scattered beam absorbed.

$$I_{lSh}(L) = I'_{ld}(L) + I_{lbs}(L) \qquad (6.53)$$

Absorbed scattered beam light is calculated as the difference between absorbed beam (eq. 6.48) and absorbed beam with scattering (eq. 6.49) rather than the differential of eq. 6.46, since this would not allow for scattered light generated by intercepted beam light that is not absorbed.

$$
\begin{aligned}
I_{lbs}(L) &= I'_{lb}(L) - I_{lb}(L) \\
&= I_b(0)\big(k'_b(1-\rho_{cb})\exp(-k'_b L) - k_b(1-\sigma)\exp(-k_b L)\big)
\end{aligned}
\qquad (6.54)
$$

For the sake of completeness, the absorbed scattered diffuse light was calculated as the difference between the absorbed diffuse light profile (eq. 6.50) and the absorbed diffuse with scattering light profile (eq. 6.51),

$$
\begin{aligned}
I_{lds}(L) &= I'_{ld}(L) - I_{ld}(L) \\
&= I_d(0)\big(k'_d(1-\rho_{cd})\exp(-k'_d L) - k_d(1-\sigma)\exp(-k_d L)\big)
\end{aligned}
\qquad (6.55)
$$

Irradiance absorbed by sunlit leaves is calculated as absorbed beam plus absorbed diffuse and absorbed scattered beam. However while diffuse and scattered irradiance are assumed to be isotropic, beam light is unidirectional and thus the angle of incidence on leaves must be considered.

There are two methods of calculating light intensity, when considering leaf angles, that at first appearances are quite different. Light intensity at the angle of individual leaves depends on the cosine of the angle of incidence of beam light with the leaf surface according to Lambert's law, while the light absorbed per unit leaf area is the differential of irradiance with depth. These apparently different approaches are related since the differential of irradiance with depth is determined by the attenuation of light which is a

function of the distribution of leaf angles. Thus leaf angles affect the differential of irradiance and they affect intensity calculated according to Lambert's law. It follows that Lambert's law determines intensity at any leaf angle, while the absorbed irradiance calculated from the differential applies only to leaves at the average cosine of leaf angles.

In a canopy with a uniform leaf orientation there is a range of leaf angles. Light intensity on leaves perpendicular to the sun's rays will have maximum intensity, while leaves parallel to the sun's rays will have the lowest illumination from only diffuse and scattered light (figure 6.6).
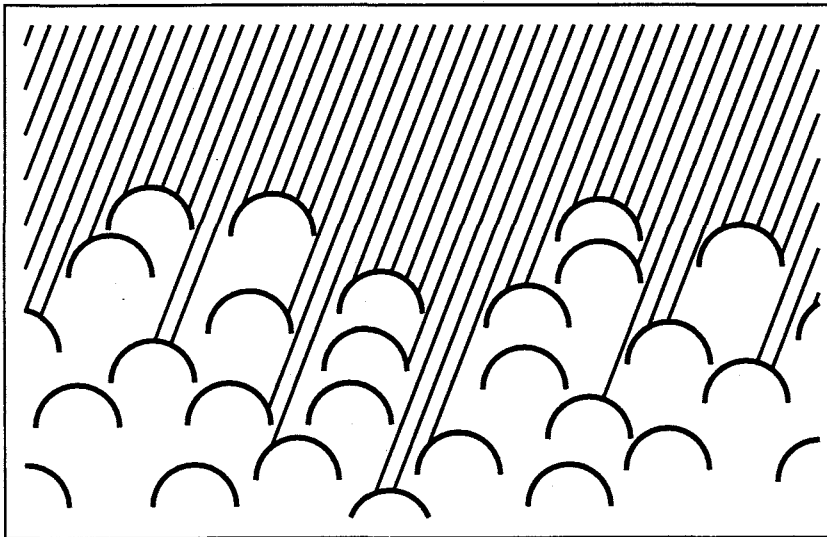
Figure 6.6 Light penetration through a canopy of uniform leaf-angle distribution, which is represented by hemisperical arrays of leaves. Direct beam light is predominantly intercepted by leaves at the top of the canopy, but some sunflecks penetrate even to the lowest leaves. The irradiance of the leaves depends on the angle at which the beam strikes the leaf surface. Leaves perpendicular to the beam absorb the greatest amount of light, and those parrallel the least.

Since with a uniform leaf-angle distribution all orientations are equally probable, the distribution of beam-leaf incidence angles is independent of solar position and the distribution is identical to that of the leaf angles. Beam intensity on a plane perpendicular to the beam direction is calculated by dividing beam intensity on a horizontal plane by the sine of solar elevation ($I_b(0)/\sin\beta$). The absorbed beam irradiance in sunflecks (I_{lbSun}) at

the mean leaf angle is given by the product of the beam intensity and the cosine of the leaf angle and is independent of depth. By definition beam irradiance of shade leaves is zero.

$$I_{lbSun}(\beta) = (1-\sigma)I_b(0)\overline{\cos\alpha_l}/\sin\beta \qquad (6.56)$$

This equation is related to eq. 6.48 by recalling that the average cosine of leaf angles of a uniform leaf orientation is 0.5 (Table 6.2), and that $k_b = 0.5/\sin\beta$. Total absorbed light on sunlit leaves (I_{lSun}) is the sum of absorbed beam plus absorbed total diffuse light.

$$I_{lSun}(L,\beta) = (1-\sigma)I_b(0)\overline{\cos\alpha_l}/\sin\beta + I_{lSh}(L) \qquad (6.57)$$

This equation is used to calculate the light absorbed at various leaf angles of sunlit leaves. An example of the absorbed light profiles for the mean cosine of leaf angle is shown in figure 6.7

The calculation of absorbed light for the sun/shade model could be simplified by the equations presented by Norman (1982), at least in simple homogeneous canopies. The
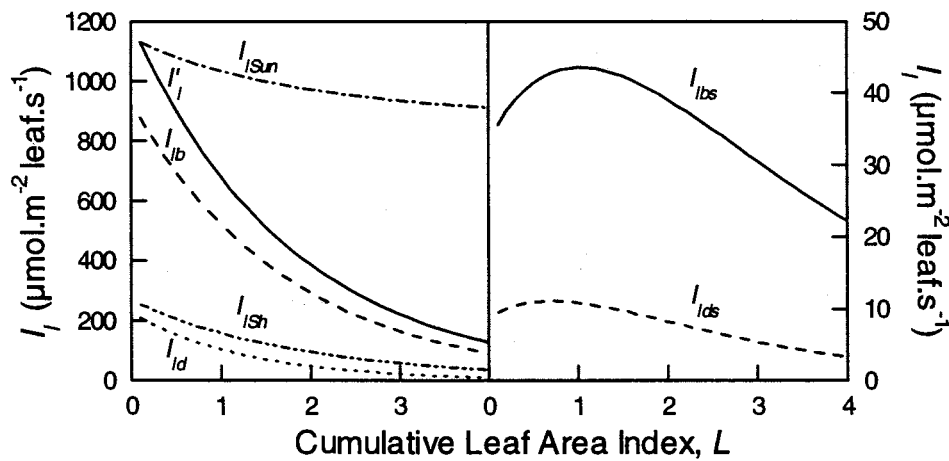
Figure 6.7 Modelled light absorption though a canopy; net absorbed including scattered light (I'_l, eq. 6.52), beam absorbed (I_{lb}, eq. 6.48), diffuse absorbed (I_{ld}, eq. 6.50), net absorbed by sunlit leaves (I_{lSun}, eq. 6.57), net absorbed by shade leaves (I_{lSh}, eq. 6.53), scattered beam absorbed (I_{lbs}, eq. 6.54) and scattered diffuse absorbed (I_{lds}, eq. 6.55). Conditions above the canopy as in figure 6.5 and assuming a uniform leaf angle distribution.

equations used here were retained to allow comparison with a multi-layer model, without additional uncertainly introduced by the approximations of Norman's simpler equations. The more complex equations also allow internal checks within the model to reduce the chance of errors. For example, light absorbed by a canopy can erroneously be greater than incident light (table 5 of Norman, 1980). These equations also ensure that calculations are for absorbed light, not just incident light, which in the case of diffuse light is often overlooked.

6.2.4. Distribution of leaf nitrogen in canopies

Distribution of leaf nitrogen, N_l, between leaves in the canopy was modelled as exponentially decreasing with depth in the canopy (Hirose & Werger, 1987a). Leaf nitrogen was converted to Rubisco capacity, V_l, assuming a linear relationship between N_l and V_l.

The model of Hirose and Werger (1987a) describes leaf nitrogen distribution, $N_l(L)$, in the canopy relative to a nominal nitrogen at the top of the canopy, N_o, according to the equation

$$N_l = N_o \exp\left(-k_n L/L_c\right) \tag{6.58}$$

where k_n is the coefficient of leaf nitrogen allocation. Describing the distribution as a function of the relative position in the canopy (L/L_c) indirectly defines the maximum and minimum leaf nitrogen contents and removes the direct effect of canopy leaf area on the distribution.

A linear relationship between V_l and N_l was assumed (Evans, 1983; Field & Mooney, 1986) with a residual leaf nitrogen content of $N_l = 25$ mmol.m^{-2} (ie. ~ 0.5% N, when $V_l = 0$):

$$V_l = \chi_n\left(N_l - 25\right), \tag{6.59}$$

where χ_n, is the ratio of measured Rubisco capacity to leaf N. χ_n was calculated from values of V_l (from leaf photosynthetic measurements) and from measurements of N_l.

These exponential functions imply a continuous decline in leaf photosynthetic capacity. However leaves of wheat plants do not exist at a continuum of depths, nor of

photosynthetic capacities, but rather at discrete intervals. I have assumed that all flag leaves at the top of the canopy have similar photosynthetic capacity and that the next leaf, or penultimate, has substantially lower photosynthetic capacity. This model of leaf nitrogen distribution was applied to discrete leaf layers by calculating the mean leaf nitrogen of a cohort of leaves and similarly a mean photosynthetic capacity of the layer.

6.2.5. Canopy Photosynthesis

In a uniform crop, such as wheat, it is assumed that the canopy is horizontally homogeneous, and that only vertical variation need be considered. The main source of variation in the physical environment is the light intensity. Since the response of photosynthesis to light is non-linear (eqs. 6.3 & 6.4) the method of spatial integration can introduce errors (Smolander, 1984). The requirement for accuracy at this level of detail needs to be weighed against the complexity of the model and the concomitant increase in the number of calculations required (Norman, 1980).

To overcome the non-linear response of leaf photosynthesis to irradiance, integration of canopy photosynthesis, by summation of leaf photosynthesis, requires the division of a canopy into many leaf categories based on their absorbed irradiance. As outlined in the introduction, the parallel profiles of leaf photosynthetic capacity and absorbed irradiance offer an alternative approach to canopy integration; scaling by use of a big leaf model. Three canopy models were compared, that differed in the number of layers used to represent the canopy; a simple big leaf model, a sun/shade model and a multi-layer model.

The simplest is a big leaf model, which assumes that the canopy can be represented by a single big leaf. This assumption is valid when the vertical profile of photosynthetic capacity is optimally distributed to maximise photosynthesis, which in turn means that it is distributed in proportion to the absorbed light profile (Farquhar, 1989). While the distribution of photosynthetic capacity can be optimal at *an instant* in time, it can not be optimal for all times, since the leaf photosynthetic capacity can not be reallocated between leaves on the time scale of light variation in a canopy. Light distribution varies in a canopy as leaves flutter, with clouds and as the light penetration changes with the traverse of the sun across the sky on its diurnal and seasonal course. Extending the concept of optimal distribution of photosynthetic capacity to maximising daily photosynthesis, implies that photosynthetic capacity be distributed in proportion to the

profile of daily absorbed light, which is the summation of light absorbed by each layer of a canopy over the whole day. If the distribution of photosynthetic capacity follows that of the daily absorbed light, then the big leaf model may work, at least to the extent that the instantaneous light profile is similar to that of the daily absorbed light.

The penetration of beam light, its' variation through the day and the range of leaf angles in a canopy of uniform leaf angle distribution, all affect the ability of the big leaf model to simulate the diurnal changes in canopy photosynthesis. These canopy features are explicitly incorporated by dividing the canopy into sunlit and shaded fractions and modelling each fraction separately with a big leaf model. This is the second canopy model tested, the sun/shade model. It is more complex than the simple big leaf model, but its' more detailed treatment of the light profiles overcomes some of the errors associated with the simplifying assumptions of a big leaf model.

The most complex method, the multi-layer model, integrates the non-linear light response of leaf photosynthesis by treating the canopy as many layers with many leaf-angle classes. Photosynthesis is calculated for each of these categories and then summed to obtain canopy photosynthesis. Details of these canopy models are presented in the following sections.

6.2.5.1. Multi-Layer Integration

This method of calculating canopy photosynthesis was based on the CUPID model (Norman, 1982). The canopy was split into multiple layers ($L_t = 0.1$). Each layer was separated into sunlit and shaded fractions (eq. 6.44) and the sunlit fraction divided into 5 leaf angle classes (eq. 6.15). Absorbed irradiance for each leaf class was calculated for shaded (eq. 6.53) and sunlit (eq. 6.57) fractions separately. Leaf nitrogen was calculated for leaves of each layer (eq. 6.58) and converted to photosynthetic capacity (eq. 6.59). Leaf photosynthesis is calculated for each leaf class (eqs. 6.1-6.6) less leaf respiration calculated from the Rubisco capacity (eq. 6.7). Canopy photosynthesis is calculated by the summation of the product of leaf photosynthesis by the leaf area in each class.

6.2.5.2. Big-Leaf Model

In contrast to the multi-layered model, a big leaf model integrates the input profiles and calculates a single photosynthetic rate as though the canopy were a single big leaf. Canopy absorbed irradiance, nitrogen, photosynthetic capacity and leaf respiration were

calculated for the entire canopy by integration as outlined below. The leaf photosynthesis model (eqs. 6.1-6.6) was then applied to the canopy as though it were a single big leaf.

Canopy Light Absorption

The irradiance absorbed by the canopy (per m^2 ground) was determined by integrating I'_l (eq. 6.52) over the entire canopy leaf area (L_c = m^2 leaf/m^2 gnd).

$$I_{lc} = \int_0^{L_c} I'_l dL$$
$$= I_b(0)(1-\rho_{cb})(1-\exp(-k'_b L_c)) + I_d(0)(1-\rho_{cd})(1-\exp(-k'_d L_c))$$

(6.60)

Canopy nitrogen and photosynthetic capacity

Total canopy nitrogen, N_c, was calculated by integration of the leaf nitrogen profile (eq. 6.58) over the entire canopy.

$$N_c = \int_0^{L_c} N_l dL$$
$$= N_o(1-\exp(-k_n))/(k_n/L_c)$$

(6.61)

Canopy photosynthetic capacity, V_c, was calculated as the integral of leaf photosynthetic capacity over the entire canopy.

$$V_c = \int_0^{L_c} V_l dL = \chi_n \int_0^{L_c} N_l - 25 dL$$
$$= L_c \chi_n (N_o(1-\exp(-k_n))/k_n - 25)$$

(6.62)

Leaf respiration of the canopy, R_{lc}, was calculated by integration of leaf respiration,

$$R_{lc} = \int_0^{L_c} R_l dL$$
$$= R_l/V_l \cdot V_c$$

(6.63)

where R_l/V_l is the ratio of leaf respiration to leaf Rubisco capacity (eq. 6.7).

An alternative approach to photosynthesis modelling is to allow co-limitation of photosynthesis by both electron transport and Rubisco (Kirschbaum & Farquhar, 1984;

Collatz *et al.*, 1991), which can be applied to canopies (Sellers *et al.*, 1992; Wang & Jarvis, 1993; Amthor, 1994). Mathematically this is achieved by a non-rectangular hyperbola,

$$\theta_c A_c^2 + (A_J + A_V)A_c + A_J A_V = 0,$$
(6.64)

where A_c is determined as the smaller root of the solution. The degree of co-limitation and thus the curvature of the photosynthesis light response is determined by the value of θ_c.

6.2.5.3. Sun/Shade Model

This final canopy integration method splits the big leaf model into sunlit and shaded fractions. Since this fraction changes during the day with solar elevation (eq. 6.44), so too the light absorption and the photosynthetic capacity of sunlit and shaded leaf fractions change. Photosynthetic capacity of individual leaves do not change during the day, but the division between the sunlit and shaded portions of the canopy does. Calculation of light absorption and photosynthetic capacity of the separate sunlit and shaded fractions is outlined in the following sections.

Canopy Light Absorption of Sunlit and Shaded Fractions

Irradiance absorbed by the sunlit leaf fraction of the canopy (I_{lcSun}) is calculated as an integral of absorbed irradiance (eq. 6.57) and the sunlit leaf area fraction (eq. 6.44). This irradiance is absorbed by only the sunlit part of the canopy. The sunlit leaf area index of the canopy is

$$L_{Sun} = \int_0^{L_c} f_{Sun}(L)dL = \left(1 - \exp(-k_b L_c)\right)/k_b,$$
(6.65)

while the shaded leaf area index of the canopy is $L_{Sh} = L_c - L_{Sun}$.

Irradiance absorbed by the separate sunlit and shade fractions of the canopy is defined such that the total light absorbed (I_{lc}) is the sum of the two parts,

$$I_{lc} = I_{lcSun} + I_{lcSh}.$$
(6.66)

The total irradiance absorbed by the canopy and the components absorbed by the sunlit and shaded fractions are all expressed on a ground area basis (μmol quanta.m^{-2} ground.s^{-1}). The irradiance absorbed by the sunlit fraction of the canopy is given as the sum of diffuse light, scattered beam and direct beam components

$$
\begin{aligned}
I_{lcSun} &= \int_0^{L_c} I_{lSun}(L) f_{Sun}(L) dL \\
&= \int_0^{L_c} I'_{ld}(L) f_{sun}(L) dL + \int_0^{L_c} I_{lbs}(L) f_{sun}(L) dL + \int_0^{L_c} I_{lb}(L) f_{sun}(L) dL
\end{aligned}
\tag{6.67a}
$$

which are,

$$
\int_0^{L_c} I'_{ld}(L) f_{sun}(L) dL = I_d(0)(1 - \rho_{cd})\left(1 - \exp\left(-(k'_d + k_b)L_c\right)\right) k'_d / (k'_d + k_b),
\tag{6.67b}
$$

$$
\int_0^{L_c} I_{lbs}(L) f_{sun}(L) dL = I_b(0)\begin{bmatrix}(1-\rho_{cb})\left(1 - \exp\left(-(k'_b + k_b)L_c\right)\right) k'_b / (k'_b + k_b) \\ -(1-\sigma)\left(1 - \exp(-2k_b L_c)\right)/2\end{bmatrix},
\tag{6.67c}
$$

$$
\int_0^{L_c} I_{lb}(L) f_{sun}(L) dL = I_b(0)(1-\sigma)\left(1 - \exp(-k_b L_c)\right).
\tag{6.67d}
$$

Irradiance absorbed by the shaded leaf area of the canopy is an integral of absorbed irradiance in the shade (eq. 6.53) and the shaded leaf area fraction. Alternatively it can be calculated as the difference between total canopy absorption (eq. 6.60) and the sunlit leaf area absorption (eq. 6.67).

$$
\begin{aligned}
I_{lcSh} &= \int_0^{L_c} I_{lSh}(L)(1 - f_{Sun}(L)) dL \\
&= I'_{lc} - I_{lcSun} \\
&= \int_0^{L_c} I'_{ld}(L)(1 - f_{Sun}(L)) dL + \int_0^{L_c} I_{lbs}(L)(1 - f_{Sun}(L)) dL
\end{aligned}
\tag{6.68a}
$$

The last line expresses the irradiance absorbed by the shaded leaf area as the sum of diffuse irradiance absorbed by shaded leaves and scattered beam irradiance absorbed by shaded leaves, which are

$$\int_0^{L_c} I'_{ld}(L)(1 - f_{Sun}(L))dL = I_d(0)(1 - \rho_{cd}) \left[\begin{array}{c} 1 - \exp(-k'_d L_c) \\ -(1 - \exp(-(k'_d + k_b)L_c))k'_d / (k'_d + k_b) \end{array} \right], \quad (6.68b)$$

$$\int_0^{L_c} I_{lbs}(L)(1 - f_{Sun}(L))dL = I_b(0) \left[\begin{array}{c} (1 - \rho_{cb}) \left(\begin{array}{c} 1 - \exp(-k'_b L_c) \\ -(1 - \exp(-(k'_b + k_b)L_c))k'_b / (k'_b + k_b) \end{array} \right) \\ -(1 - \sigma)(1 - \exp(-k_b L_c) - (1 - \exp(-2k_b L_c))/2) \end{array} \right]. \quad (6.68c)$$

An example of canopy absorption of irradiance and its separation into sunlit and shaded fractions is presented in figure 6.8.
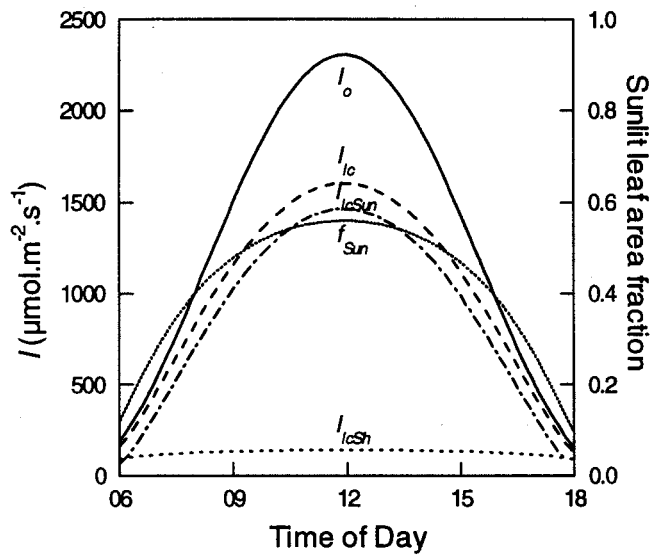
Figure 6.8 Modelled irradiance and absorption (per unit ground area) by a canopy of leaf area = 2.4. I_o, total irradiance above canopy; I_{lc}, irradiance absorbed by entire canopy ; I_{lcSh}, irradiance absorbed by shaded leaf fraction of canopy; I_{lcSun}, irradiance absorbed by sunlit leaf fraction of canopy; f_{Sun}, sunlit leaf area fraction.

Photosynthetic Capacity of sunlit and shaded leaf fractions.

Photosynthetic capacity of the sunlit leaf fraction of the canopy, V_{cSun}, is calculated by an integral of the leaf photosynthetic capacity (eq. 6.59) and the sunlit leaf area fraction (eq. 6.44).

$$V_{cSun} = \int_0^{L_c} V_l(L) f_{Sun}(L) dL$$

$$= \chi_n \left(\frac{N_o \left(1 - \exp(-k_n - k_b L_c)\right) / (k_n / L_c + k_b)}{-25 \left(1 - \exp(-k_b L_c)\right) / k_b} \right) \tag{6.69}$$

Photosynthetic capacity of the shaded leaf fraction of the canopy, V_{cSh}, is calculated by an integral of the leaf photosynthetic capacity (eq. 6.59) and the shaded leaf area fraction (eq. 6.44). As with the calculation of absorbed light the photosynthetic capacity of the shade leaf fraction can be calculated as the difference between canopy photosynthetic capacity and the shade fraction photosynthetic capacity.

$$V_{cSh} = \int_0^{L_c} V_l(L) f_{Sh}(L) dL$$

$$= V_c - V_{cSun} \tag{6.70a}$$

$$V_{cSh} = \chi_n \left\{ N_o \left[\frac{(1 - \exp(-k_n)) / k_n / L_c}{-(1 - \exp(-k_n - k_b L_c)) / (k_n / L_c + k_b)} \right] -25 \left(L_c - (1 - \exp(-k_b L_c)) / k_b \right) \right\} \tag{6.70b}$$

An example of the distribution of photosynthetic capacity between sunlit and shaded leaf fractions of the canopy is shown in figure 6.9.

Canopy photosynthesis was obtained by adding the photosynthetic contribution from the two components, minus the leaf respiration of the canopy (R_{lc}),

$$A_c = A_{cSun} + A_{cSh} - R_{lc} . \tag{6.71}$$
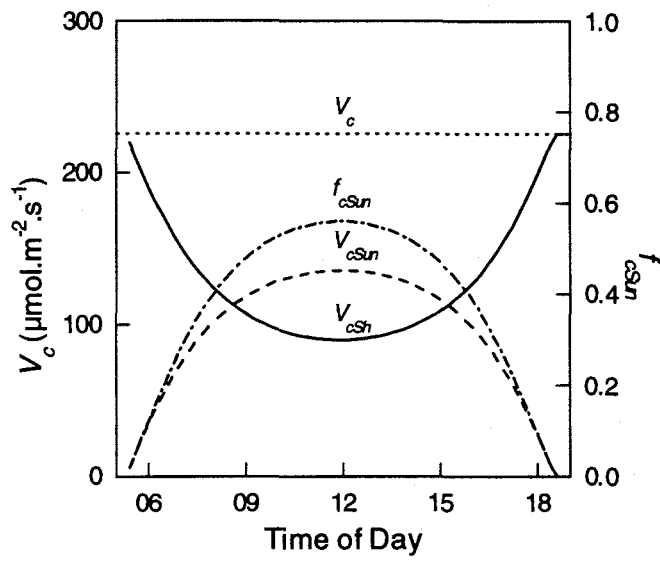
Figure 6.9 Photosynthetic capacity of the entire canopy, V_c, (eq. 6.62) and separated into sunlit, V_{cSun}, (eq. 6.69) and shaded, V_{cSh}, (eq. 6.70) leaf fractions. The fraction of the canopy that is sunlit, f_{cSun}, is also shown.

6.3. Results & Discussion

6.3.1. Distribution of Leaf Nitrogen and Absorbed Light

Model parameters were obtained from measurements in a canopy of wheat (Table 6.3). Values for other parameters were assumed and are given in the List of Symbols. Measurements of PAR were used in the multi-layer model to generate the predicted distribution of absorbed light in relation to the distribution of leaf nitrogen in the canopy (figure 6.10). Nine leaf-angle classes were used analagous to the angles given for five classes in Table 6.2. An instantaneous profile of absorbed light was calculated by averaging the absorbed light of all leaves (sunlit and shaded) in a layer at midday (maximum solar elevation was 68° above the horizon). Integration of all such distributions for all times during the day gave the daily profile of absorbed irradiance.

Table 6.3 Parameter values for the multi-layer model obtained from measurements in a wheat crop at Wagga Wagga, NSW, four days after anthesis.

Parameter	Value
Date	25-Oct
latitude	-35° 3.5' S
a	0.75
L_c	2.4
V_l	100
N_l	120
N_o	136
k_n	0.54

The basis for the big leaf models of canopy photosynthesis (Sellers *et al.*, 1992; Amthor, 1994) is that leaf nitrogen should be distributed in a canopy in proportion to the time-averaged profile of absorbed light. It can be seen in figure 6.10 that this wheat canopy does indeed have a distribution of leaf nitrogen that is approximately in proportion to the profile of daily absorbed light. If leaf nitrogen were exactly distributed in proportion to the absorbed light, the modelled distribution would be a straight line diagonally across the figure. In addition, an instantaneous profile of absorbed light is

also shown in figure 6.10. This too has a distribution that is nearly in proportion to the profile of leaf nitrogen, giving confidence to the basis of the big leaf models.
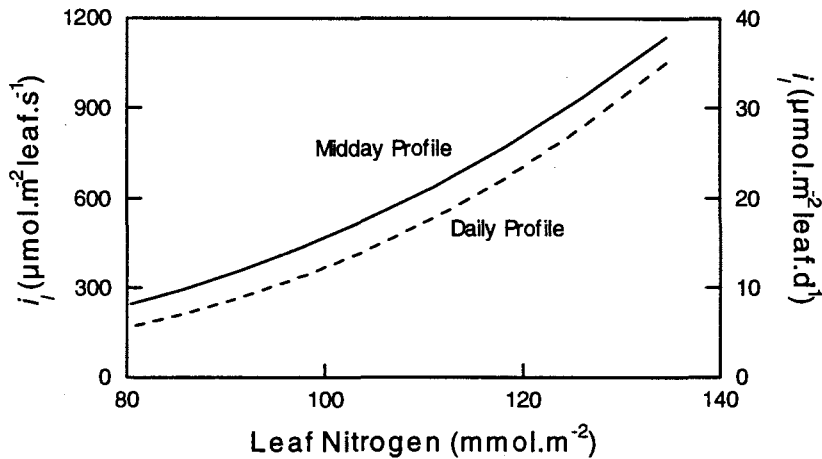
Figure 6.10 Modelled distribution of the midday average (of sunlit and shaded leaves) (——, μmol quanta.m^{-2} leaf.s^{-1}) and daily average (- - -, (mol quanta.m^{-2} leaf.d^{-1}) absorbed irradiance by leaves in a homogenous canopy, of uniform leaf angle (α) distribution, as a function of leaf nitrogen (N) content (mmol.m^{-2} leaf).

With the parameters for the multi-layer model set as above, an instantaneous distribution of absorbed light in relation to leaf nitrogen was predicted for the sunlit and shaded leaves separately (figure 6.11). The distribution presented was calculated for midday, other times gave similar distributions but at lower levels of absorbed light. The vertical (or z) axis indicates the distribution or proportion of leaves at each level of absorbed light for the sunlit and shaded leaf fractions separately. A uniform leaf angle distribution was assumed, so that the probability of a leaf being at an angle between α and $\alpha + d\alpha$ is $\Pr(\alpha, \alpha + d\alpha) = \sin\alpha\, d\alpha$. This leaf angle distribution function together with the fraction of sunlit leaf area (eq. 6.44) generated the curved surface and is shown as the proportion of sunlit leaves on the left-hand vertical or z axis. Each layer of the canopy, as indicated by leaf nitrogen content, has a range of absorbed light for the sunlit leaves at different leaf angles, which were calculated from eq. 6.57. Leaves near perpendicular to the sun beam direction had the highest absorbed light (2040-1830 μmol.m^{-2}.s^{-1}), but were only a small proportion of the sunlit leaves. Leaves parallel to the beam direction absorbed only diffuse light (430-220 μmol.m^{-2}.s^{-1}) and were a high

proportion of the sunlit leaves. At any particular leaf angle absorbed light decreased slightly with depth in the canopy due to the attenuation of diffuse and scattered light. At layers deeper in the canopy, indicated by lower leaf nitrogen, the proportion of sunlit leaves at each light level decreased. The proportion of each layer shaded increased with depth in the canopy, shown as the vertical plane at the rear of figure 6.11 and the right-hand or z axis.

In contrast to the distribution of *average* absorbed light (figure 6.10), when the distribution of absorbed light for the sunlit and shaded fractions of the canopy are shown
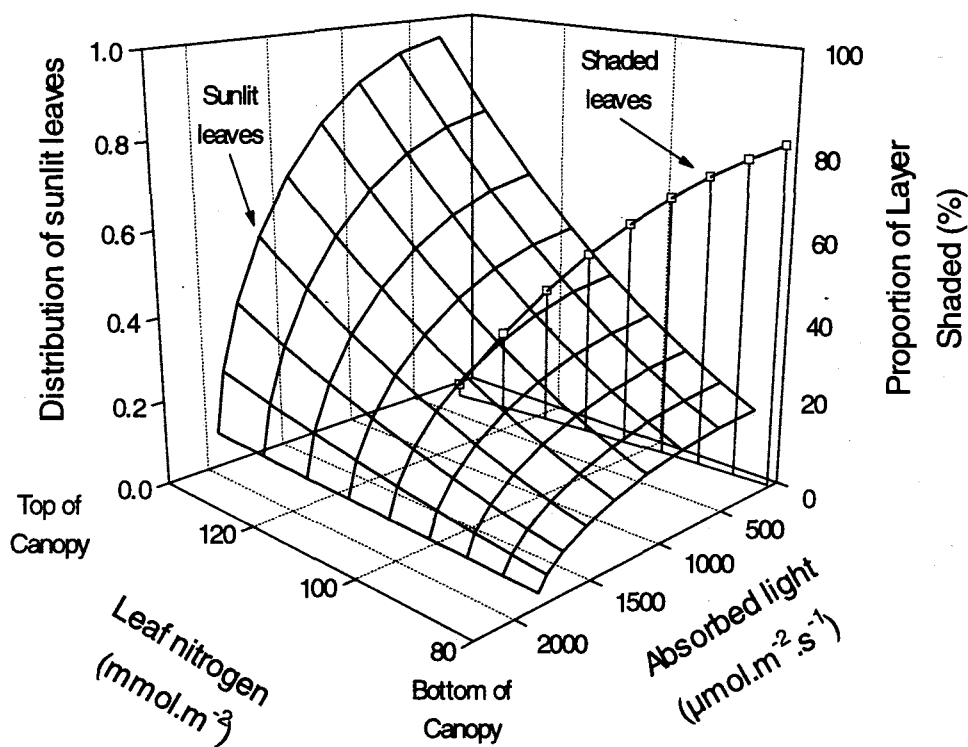
Figure 6.11 Model predictions of the instantaneous distribution of light absorbed by sunlit and shaded leaves (μmol quanta.m^{-2} leaf.s^{-1}) in relation to the leaf nitrogen distribution. Profiles were generated as in figure 6.10. The vertical axis on the left is the probability distribution of sunlit leaves with respect to the light absorption defined by the leaf angle (Lamberts cosine law), and is Pr(α, α + dα)/dα = sinα. The distribution of sunlit leaves is represented by the 3 dimensional surface (left vertical axis). The distribution of shade leaves was assumed independent of leaf angle and is represented by the vertical plane at the lowest absorbed light levels (–□–, right vertical axis).

separately (figure 6.11), its relationship with the distribution of leaf nitrogen is very different. No longer is the instantaneous distribution of absorbed light in proportion to the distribution of leaf nitrogen (*ie.* a diagonal line). When the sunlit and shaded leaves were averaged the distribution of leaf nitrogen was approximately in proportion to the instantaneous distribution of absorbed light (figure 6.10). In contrast, the profile of leaf nitrogen and the distribution of absorbed light for the sunlit and shaded leaves of the canopy show no resemblance of being related to each other (*ie.* no diagonal line across figure 6.11, cf. figure 6.10).

Inspection of the *average* light profiles (figure 6.10), suggests that leaf nitrogen is approximately distributed in proportion to profiles of both daily and the instantaneous absorbed light, which is a requirement for the simplification in the big leaf models. However, if the distribution of absorbed light of sunlit and shade leaves is used, then it is apparent that the distribution of leaf nitrogen is not in proportion to the profile of absorbed light (figure 6.11) and that the basis for the big leaf models is not valid.

This conflict arises because the *time averaged* distribution of absorbed light in canopy is quite different to the *instantaneous* distribution of absorbed light, when sunfleck penetration and the effect of leaf angles are considered in calculating the absorbed light profiles. As stated in the introduction many canopy modellers have recognised the importance of treating sunlit and shaded leaves separately (Sinclair *et al.*, 1976; Norman, 1980). The analysis presented here has applied that principle to the profiles of absorbed light and leaf nitrogen required by the new generation of big leaf models (Sellers *et al.*, 1992; Amthor, 1994). If average profiles of light are used, contradicting the dictum of keeping sunlit and shaded leaves separate, then the profile of absorbed light is in proportion to the profile of leaf nitrogen. A big leaf model working from this assumption will then have errors associated with averaging the light profiles, which have been shown to be large (Sinclair *et al.*, 1976; Norman, 1980). In fact the models of Sellers *et al.*, (1992) and Amthor (1994) hide these errors by using a curvature factor in the response of canopy photosynthesis to absorbed light. I will demonstrate the effect of this curvature factor in a later section.

6.3.2. Optimal Distribution of Leaf Nitrogen

Profiles of *average* absorbed irradiance are also used in several models that examine the optimal distribution of leaf nitrogen to maximise canopy photosynthesis (Hirose &

Werger, 1987a; Wu, 1993; Badeck, 1995; Sands, 1995). This greatly simplifies the analysis, but unless the canopies are grown under continuous diffuse light, the profile of average irradiance is not a realistic representation of canopies receiving direct beam light, that will have sunflecks penetrating to all levels of the canopy and (assuming a uniform leaf angle distribution) a range of leaf angles with different amounts of absorbed irradiance at all levels in the canopy.

I parameterised the multi-layer model as described above, but with canopy layers of L = 0.5 and five leaf-angle classes (to speed the optimisation) and examined the distribution of leaf nitrogen required to maximise the daily integral of canopy photosynthesis. Total canopy photosynthetic Rubisco capacity was kept constant at 225 $\mu mol.m^{-2}.s^{-1}$ (ground area basis), but reallocated between different layers. Two approaches were taken regarding assumptions about using absorbed light to calculate leaf photosynthesis. First, the light was averaged from all leaves of a layer to calculate the average rate of photosynthesis. Second, absorbed light for each of the five leaf-angle classes of sunlit leaves and the shaded leaves was calculated separately and converted to leaf photosynthesis. The average profile of absorbed light was identical in both cases. The optimum distribution of leaf photosynthetic capacity was determined for each case by calculating the sensitivity of photosynthesis of each layer to an additional unit of photosynthetic capacity, dA/dV. Units of photosynthetic capacity were manually moved from layers with low values of dA/dV to layers with high values of dA/dV, until all layers had equal values of dA/dV, which is the condition of maximum canopy photosynthesis (Field, 1983). This manual redistribution of photosynthetic capacity avoided any assumptions about the shape of the optimal distribution of leaf photosynthetic capacity in the canopy. The final optimal distributions together with the actual measured distribution are shown in figure 6.12.

The actual profile (measured in the field and described by parameters in Table 6.3) was significantly different from a uniform distribution of leaf photosynthetic capacity. Both optimal distributions had steeper profiles of leaf photosynthetic capacity than the actual measured profile, with more capacity at the top and less capacity lower in the canopy. The optimal distribution obtained with calculations based on separate sunlit and shaded leaves was steeper than when the light was averaged.

Daily canopy photosynthesis for the optimal distribution increased by 9 % when sunlit and shaded leaves were calculated separately compared to that obtained with the

actual distribution, but only by 5 % when average light was used. Daily canopy photosynthesis with the actual distribution of leaf photosynthetic capacity increased by 19 % with the assumption of averaged light compared to that obtained with separate sun and shade components. Clearly, assumptions about averaging of light in a canopy affect conclusions as to the optimal distribution of leaf photosynthetic capacity.
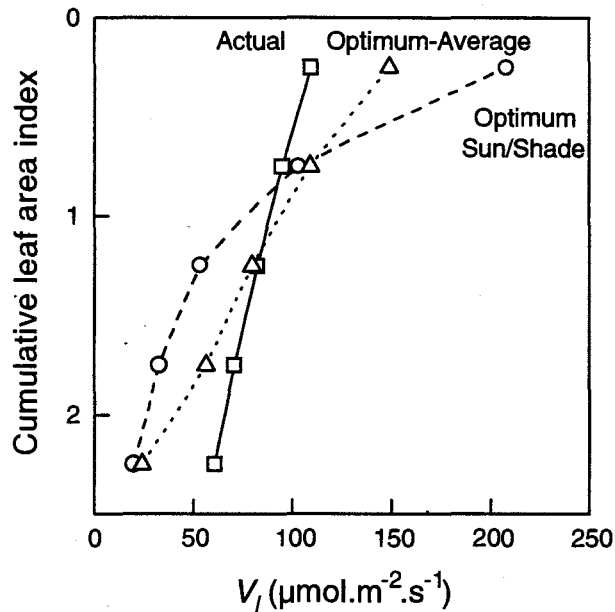
Figure 6.12 Modelled distributions of leaf photosynthetic capacity, based on measurements in a wheat canopy (Actual, —□—), the optimum using average absorbed light for each layer (optimum - average, ···△···) and the optimum with calculations for sunlit and shaded leaves separately (optimum sun/shade, - - o - -).

The amount of photosynthetic capacity at the top of the canopy was perhaps unrealistically high for the distribution based on sunlit and shaded leaves. A curved relationship between leaf photosynthetic capacity and leaf nitrogen may have been more appropriate as this would have prevented such high values of leaf photosynthetic capacity from being predicted in the optimal solution. However, a different relationship between leaf photosynthetic capacity and leaf nitrogen would not significantly alter the comparison as it would affect both optimal solutions.

6.3.3. Comparison of Canopy Photosynthesis Models

Predictions from several multi-layer models have been compared with field measurements of canopy photosynthesis and were capable of adequately reproducing diurnal trends (Lemon *et al.*, 1971; Caldwell *et al.*, 1986; Norman & Polley, 1989; Grant, 1992a). On this basis multi-layer models have been used as a baseline for comparing simplified canopy integration schemes (Norman, 1980; 1993; Goudriaan, 1986; Baldocchi, 1993; Johnson *et al.*, 1989; Reynolds *et al.*, 1992; Sinclair *et al.*, 1976). While comparisons of models with field data are unequivocally the ultimate test, comparisons between models allow structural differences to be tested without the compounding effects of parameter uncertainties.

The predicted response of canopy photosynthesis to absorbed light was compared for the multi-layer, sun/shade and big leaf canopy models (figure 6.13). The simulations were conducted with environmental variables set at constant values of: $T_a = 20$ °C, $e_a = 1.0$ kPa, $c_a = 33$ Pa and $g_a = 100$ mol.m^{-2}.s^{-1} (*ie.* zero aerodynamic resistance). The diurnal variation of incident light was taken from measurements at Wagga, on the 25-Oct. Simulations for the big leaf model were made with the canopy curvature factor set as, $\theta_c = 1.0$, and by adjusting θ_c to obtain the best fit with the multi-layer model ($\theta_c =$
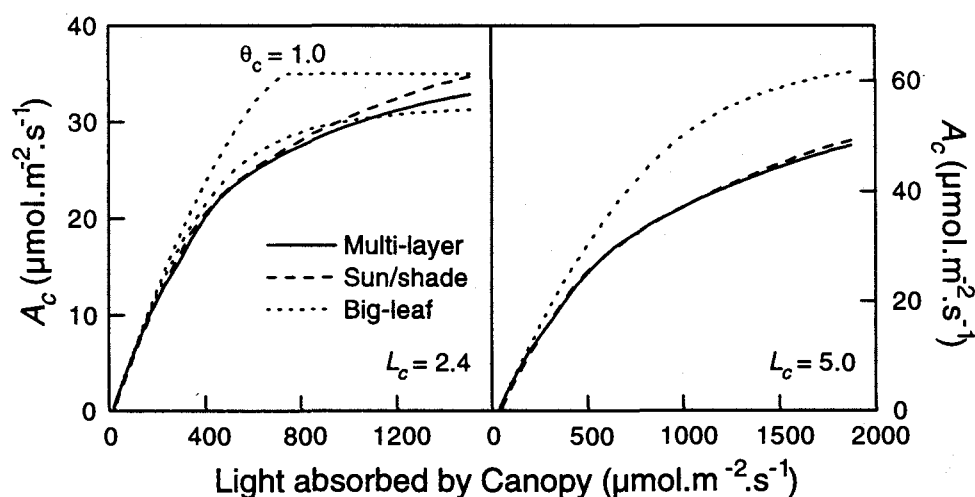
Figure 6.13 Comparison of simulated response of canopy photosynthesis to absorbed light for the multi-layer (——), sun/shade (- - -) and big leaf (·····) models with a leaf area index of 2.4 (left panel) and 5.0 (right panel). Simulations from the big leaf model are shown with $\theta_c = 1.0$ and 0.94, obtained by fitting. $\theta_c = 0.94$ was used for the simulations at high leaf area index.

0.94). The simulations at high leaf area index were made with the same value of θ_c = 0.94. Simulations by the multi-layer model were used as the standard for evaluation of the big leaf model and the sun/shade model.

Simulated response of canopy photosynthesis to absorbed light was quite unrealistic from the big leaf model with θ_c = 1.0. Adjustment of θ_c improved the simulation by the big leaf model, but the shape of the response to absorbed light still did not match that predicted by the multi-layer model. Simulations from the sun/shade model slightly overestimated canopy photosynthesis at high light compared to the multi-layer model, but otherwise accurately reproduced the response of canopy photosynthesis to absorbed light.

At high leaf area index, canopy photosynthesis, as simulated by the multi-layer model, showed less tendency to reach light saturation than at low leaf index. The sun/shade model again accurately reproduced the response of canopy photosynthesis to absorbed light. With θ_c = 0.94, the big leaf model significantly overestimated canopy photosynthesis, particularly at high light. Better simulations by the big leaf model were obtained by again adjusting the curvature factor.

The magnitude of the error in the Big-Leaf model predictions of gross canopy photosynthesis were estimated by calculating the daily gross photosynthesis over a range of canopy leaf areas and leaf photosynthetic capacities (figure 6.14). The predictions of the Big-Leaf model were 25% greater than the multi-layer model at a leaf area of 4 and 50% greater at a leaf area of 6. The errors of the Big Leaf model when leaf photosynthetic capacity was changed were smaller, but still significant, overestimating by 10% when V_l = 150 $\mu mol.m^{-2}.s^{-1}$. There was no effect of CO_2 concentration on the performance of the big leaf model (data not shown).

Selection of a value of θ_c in the big leaf model is difficult *a priori*, but easier *a posteriori*. I fitted the big leaf model by adjusting the value of θ_c such that the big leaf model predictions matched the multi-layer model predictions by minimising the sum of residuals squared. The value of θ_c, required to give the best fit, varied with leaf area index and leaf nitrogen content, but not with atmospheric CO_2 concentration (figure 6.15). At low leaf area index θ_c approached 1.0 and decreased as the canopy leaf area index increased. θ_c approached 1.0 at both low and high leaf nitrogen content and reached a minimum of 0.905 at a leaf nitrogen content of 130 $mmol.m^{-2}$.
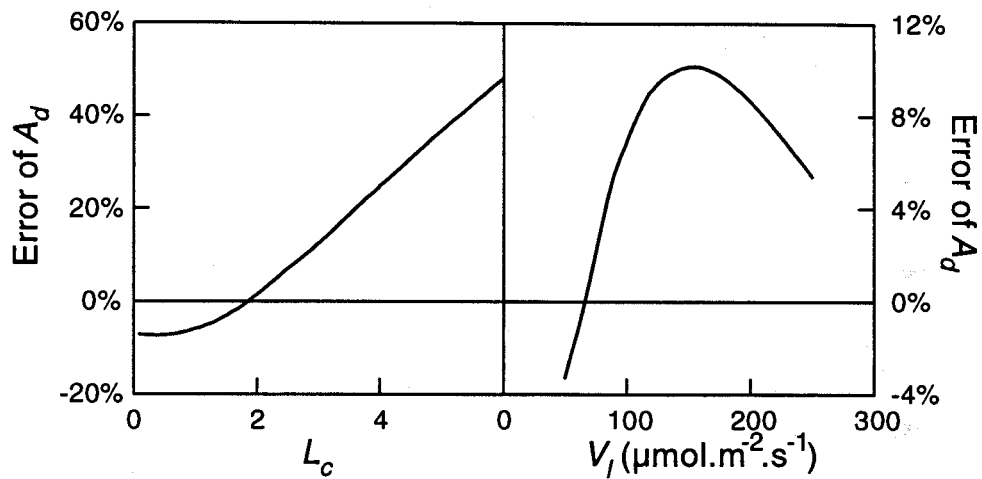
Figure 6.14 Error in the Big-Leaf model prediction of daily gross photosynthesis compared with the multi-layer model predictions with changing canopy leaf area (L_c) and leaf photosynthetic capacity (V_l). Model simulations were made using diurnal environmental data from 25-Oct with coefficients obtained for the Matong crop; $L_c = 2.41$, $V_l = 93$ $\mu mol.m^{-2}.s^{-1}$ and a fitted $\theta_c = 0.94$.
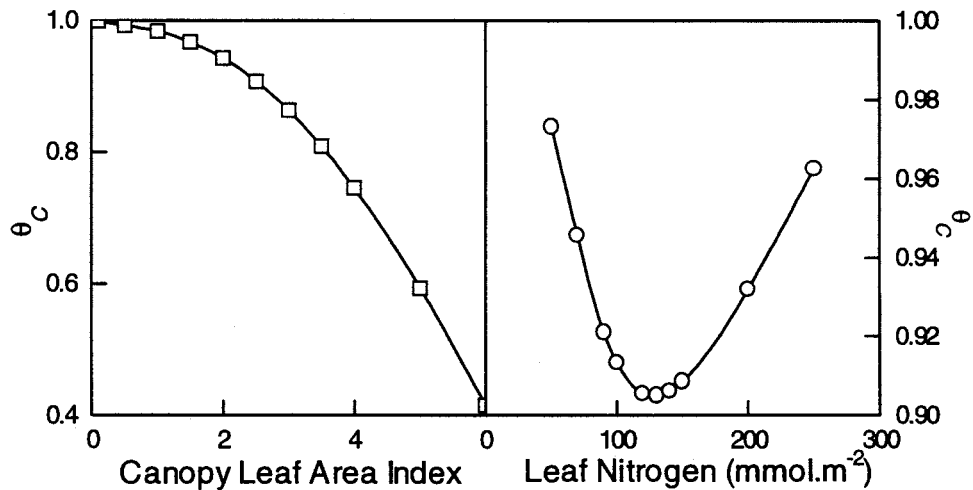
Figure 6.15 Variation of the parameter of canopy photosynthesis co-limitation, θ_c, with canopy leaf area and leaf nitrogen content of leaves at the top of the canopy. Values were obtained from fitting the big leaf model predictions to those of the multi-layer model and minimising the squared sum of residuals.

Use of co-limitation of photosynthesis in canopy photosynthesis models is attractive since it allows the use of simple big leaf models. Unfortunately the value of θ_c is not constant and varies with the leaf nitrogen content as well as the canopy leaf area. In contrast, the predictions from the sunlit/shade big leaf model match those of the multi-layer model without the use of an empirical fitting parameter.

Measured diurnal courses of environmental variables were used to predict gross canopy photosynthesis for the same wheat canopy as described previously for the 25-Oct. Predictions from the sun/shade model closely matched both the multi-layer model, as shown in the previous simulations, and also matched gross canopy photosynthesis (measured net canopy CO_2 flux plus respiration) (figure 6.16). The electron transport- and Rubisco-limited rates of canopy photosynthesis are shown for the sunlit and shaded fractions of the canopy as predicted by the sun/shade model. In the sun/shade model the rate of photosynthesis for the sunlit and shaded fractions of the canopy are calculated as the minimum of either the electron transport limited or Rubisco limited rates. It is
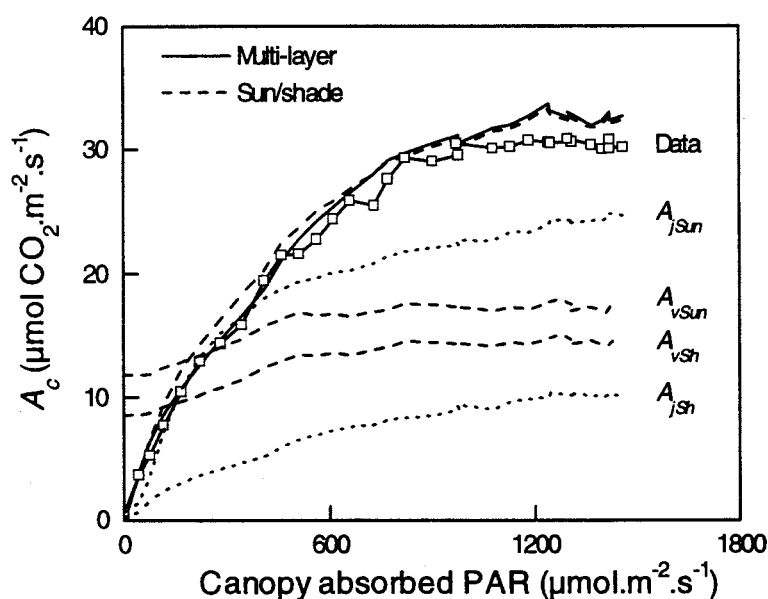
Figure 6.16 Light response of gross canopy photosynthesis (A_c) measured with the tent (—□—) compared with predictions from the sun/shade model (- - -) and multi-layer (——) model of canopy photosynthesis. Modelled electron-transport (A_j, - - -) and rubisco-limited (A_v, ·····) rates of photosynthesis are shown for the sunlit and shaded fractions of the canopy. Data are of a wheat canopy of cultivar Matong on 25-Oct measured by the tent.

apparent in figure 6.16 that the shaded fraction of the canopy is always electron transport limited (*ie.* $A_{jSh} < A_{vSh}$) and that the sunlit leaves are usually Rubisco-limited ($A_{vSun} < A_{jSun}$), except when the absorbed light is very low. The fraction of leaves in the sunlit fraction increased from 0% at low light to 56% at the maximum solar elevation.

The light response of the sunlit/shade model deviated from the multi-layer model only at intermediate light levels (200-400 μmol PAR absorbed $.m^{-2}.s^{-1}$) and the deviation was consistently observed with other data sets not shown. The discrepancy between the sunlit/shade model and the multi-layer model occurred near the point at which the sunlit fraction changed from electron transport limited to Rubisco limited photosynthesis. At this light intensity representation of photosynthesis by the sunlit fraction as limited either by electron transport or by Rubisco involves a simple averaging of a continuum of light intensities caused by a range of leaf angles. As light intensity increases the proportion of leaves in the sunlit leaf fraction that are not Rubisco limited decreases and so this simplification improves until the associated errors are not detectable. These errors have the same cause as those associated with the simplifications in the big leaf model representation of canopy photosynthesis, but are have much less impact on the accuracy of the sun/shade model than the big leaf model.

6.4. Further Discussion & Conclusions

Models of Canopy Photosynthesis

The sun/shade model of canopy photosynthesis presented in this chapter gave predictions of canopy photosynthesis that closely matched simulations from a multi-layer model, but with far fewer calculations. The model was robust over a range of canopy leaf area and environmental variables. Differences between predictions of the sun/shade model, the multi-layer model and flux measurements were well within the errors of any canopy flux measurement technique and within the accuracy of parameter determination given the stochastic nature of leaf photosynthetic capacity and other parameters. The simplicity of the sun/shade model should make it attractive for incorporation into models of crop growth, global carbon cycling and of other higher level processes.

A big leaf model, similar to those proposed by Sellers (1992) and Amthor (1994), was found to be less accurate than the sun/shade model. Approximations, implicit in the big leaf model, were found to cause distortions in the modelled response of canopy photosynthesis to light compared with the multi-layer model. Fitting the curvature factor in the big leaf model did not correct all the discrepancies. The value of the curvature factor required to reproduce the response of canopy photosynthesis to light, as modelled by the multi-layer model, was found to vary with canopy leaf area index, and to a lesser extent, with leaf nitrogen content. Errors associated with using a fixed value of the curvature factor (for $L_c = 2$) were 25% of daily gross canopy photosynthesis at a leaf area of 4 and even greater at higher leaf areas. These errors are unacceptably large, particularly when canopy leaf area is varying, such as in crop growth models or models that predict the response of vegetation to climate change.

Optimal Distribution of Leaf Nitrogen

Models that use average light in canopy layers to determine the optimal distribution of photosynthetic capacity to maximise canopy photosynthesis are flawed in their often implicit assumptions that the time-averaged light profile is identical to the instantaneous profiles of absorbed light. Leaf nitrogen is, indeed, often distributed such that it follows the profile of time averaged absorbed light, but it does not mean that it also resembles the instantaneous profile of absorbed. The flawed logic results in misleading conclusions about the optimal distribution of leaf nitrogen to maximise canopy photosynthesis.

CHAPTER SEVEN:

SCALING UP PHOTOSYNTHESIS

Chapter Contents

Summary

Understanding the dynamics of CO_2 fluxes from canopies is a vital component of assessing water-use efficiency and carbon cycling of natural ecosystems. Scaling photosynthesis from leaves to canopies allows knowledge from the leaf scale to be applied at the canopy scale and is facilitated by use of mechanistic models of photosynthesis. The objective of this chapter is to test a simple two-layered model of canopy photosynthesis applied to sunlit and shaded leaves, that is a scaled version of a biochemically based model of leaf photosynthesis, with field data.

Canopy fluxes were measured with ventilated chambers and Bowen ratio systems over large paddocks of wheat with two cultivars of contrasting water-use efficiency. Concurrent measurements of leaf gas exchange were used to determine the leaf photosynthetic capacity. Photosynthetic capacity of the canopy was estimated from the canopy model.

Diurnal decline in photosynthetic capacity, and recovery overnight, was observed at both the leaf and canopy scales. This was attributed to increasing water stress during the day, because a regression based on cumulative evaporation was able to explain much (r^2 = 0.87) of the diurnal variation of photosynthetic capacity of leaves and the canopy. Sun/shade model predictions reproduced the diurnal response of canopy photosynthesis to absorbed light, although the model was not accurate in predicting the absolute flux due to the high variability of leaf data between days which was used to parameterise the canopy model. Canopy and soil respiration was typically 20 to 30% of daily gross canopy photosynthesis, but rose to 50% on days with air temperature over 30°C.

The sun/shade model of canopy photosynthesis allowed incorporation of within-canopy profiles of photosynthetic capacity and accurately reproduced the response of canopy photosynthesis to absorbed light without the use of any empirical factors. This model was simpler than a multi-layered model and avoided the assumptions required in big-leaf models of canopy photosynthesis. These features make this model of canopy photosynthesis suitable for assessing the effect of plant physiological traits on canopy water-use efficiency and the dynamics of carbon cycling in natural ecosystems.

7.1. Introduction

Greater crop yields through improved water-use efficiency (WUE) have come closer to being realised through the development of carbon isotope discrimination (Δ) as a tool to quickly assess large numbers of breeding lines (Hall *et al.*, 1994). However, the relationship between Δ and WUE has not been consistent between experiments in pots and field trials (Condon *et al.*, 1990). Effective use of Δ requires an improved understanding of the scaling up of physiological processes from leaves to canopies. Scaling up physiological processes is also receiving attention, from an ecological perspective, to improve the understanding of carbon and water dynamics of vegetation and their response to climate change (Carlson, 1991; Ehleringer & Field, 1993; Jarvis, 1995).

Mathematical models are an integral part of scaling physiological processes as they synthesise the non-linear biological responses to the environment and facilitate analysis of fluxes in unregulated field conditions. If models are based on a mechanistic representation of physical processes then the value of parameters can be examined in a biological context, an attribute which empirical models do not have. Models that can be applied at adjacent spatial scales in the same form (scaling models) allow insight gained from one level to be applied at the next higher level (Norman, 1993). Although there are considerable benefits in using scaling models, it is not always possible to find scaling models of processes with matching parameters; each case must be examined independently (Raupach, 1995). Like all models, scaling models must be evaluated against experimental data and found to adequately describe the processes, with realistic parameters values. Validated scaling models can be used to make predictions of canopy fluxes, using leaf level data. Understanding the variation of parameters at leaf and canopy scales can lead to better predictions of canopy fluxes.

A model of stomatal conductance (Ball *et al.*, 1987; Leuning, 1990; Collatz *et al.*, 1991; Leuning, 1995) that is based on the correlation of stomatal conductance with photosynthesis (Wong *et al.*, 1979) was verified at the leaf (Chapter Four) and canopy scales (Chapter Five). A biochemically based model of leaf photosynthesis (Farquhar *et al.*, 1980) is now widely accepted and has been tested in controlled environment experiments (Farquhar & von Caemmerer, 1982; Harley *et al.*, 1992), but less often with field data. These leaf-scale models have been incorporated into multi-layer models of canopy photosynthesis and transpiration (Reynolds *et al.*, 1992; McMurtrie *et al.*, 1992;

Leuning *et al.*, 1995), but their validity for use in scaling from leaves to canopies, with both *in situ* leaf measurements and canopy flux data, has been demonstrated in only a few cases (Baldocchi & Harley, 1995).

Simple big-leaf models of canopy photosynthesis, based on the distribution of photosynthetic capacity in proportion to the distribution of absorbed light offer easier parameterisation (Sellers *et al.*, 1992; Amthor, 1994). However, single-layer models of canopy photosynthesis have been shown to be inaccurate due to averaging of the non-linear response of leaf photosynthesis to absorbed light (Sinclair *et al.*, 1976; Norman, 1980). These inaccuracies were also shown to exist in big-leaf models due to the mistaken assumption that the instantaneous and time-averaged profiles of absorbed irradiance in canopies are similar (Chapter Six). Models that treat the canopy as two-layers, sunlit and shaded leaves, overcome the flaws of big-leaf models (Sinclair *et al.*, 1976; Norman, 1980), but have not included spatial variation of leaf photosynthetic capacity in the canopy (Boote & Loomis, 1991). In Chapter Six I presented a sun/shade model of canopy photosynthesis that incorporates variation of leaf photosynthetic capacity in the canopy and uses the preferred, Farquhar *et al.*, model of leaf photosynthesis.

A field experiment was conducted to examine the scaling-up of photosynthesis and water-use efficiency from leaves to canopies. Two cultivars of wheat, Matong and Quarrion, chosen for their contrasting water-use efficiency, due primarily to differences in stomatal conductance, were grown in large adjacent paddocks. Concurrent measurements of gas exchange of leaves were used to parameterise the model of leaf photosynthesis. Canopy flux measurements were used to test the scaling up of photosynthesis by the sun/shade canopy model.

The main objectives of this chapter are to compare photosynthetic model parameters at leaf and canopy scales and to test the sun/shade model of canopy photosynthesis against field data. The measured responses of canopy and soil respiration to temperature were extrapolated to allow comparison of model predictions of gross canopy photosynthesis with net canopy CO_2 flux data. The distribution of photosynthetic capacity in relation to the distribution of absorbed light in the canopies, is examined.

7.2. Model

Details of the sun/shade model of canopy photosynthesis were presented in the previous chapter (Six). The essential equations of the model are used to calculate 1) the sunlit proportion of the canopy leaf area, 2) the light absorbed by the sunlit and shaded portions of the canopy, 3) the photosynthetic capacity of the sunlit and shaded portions of the canopy, and 4) photosynthesis with the model of Farquhar *et al.*, (1980). All photosynthetic parameters were adjusted for temperature as indicated in the previous chapter.

7.2.1. Photosynthetic Capacity of Leaves

Photosynthetic Rubisco capacity of leaves (V_l) was determined from light saturated rates of photosynthesis and a rearrangement of the Farquhar *et al.*, (1980) model of leaf photosynthesis,

$$V_l = A_l \frac{(p_i + K')(\Gamma + K')}{(p_i - \Gamma)(\Gamma_* + K')},$$
(7.1)

where the variables were defined in the previous chapter. Use of Γ, the CO_2 compensation point, in the above equation allows for leaf respiration in the light (R_d) to vary in proportion to V_l.

Farquhar *et al.* (1980), described the electron transport potential (J_m) as increasing with temperature up to 30°C and then decreasing with further increases in temperature. At high temperatures, photosynthesis may be limited by RuBP regeneration rather than Rubisco despite high levels of absorbed light (2000 $\mu mol.m^{-2}.s^{-1}$) (Farquhar *et al.*, 1980). Electron transport (J) was calculated from a rearrangement of the model of leaf photosynthesis,

$$J = (A_l + R_d) \frac{4(p_i + 2\Gamma_*)}{p_i - \Gamma_*},$$
(7.2)

where R_d was calculated as $0.0089V_l$ from eq. 7.1. J_m was calculated from the electron transport light response curve (Farquhar & Wong, 1984) as

$$J_m = \frac{J(I_{le} - \theta J)}{I_{le} - J}$$

(7.3)

and I_{le} is PAR usefully absorbed by Photosystem II per unit leaf area as given in the previous chapter $(I_f(1-f)/2)$. J_m was converted to photosynthetic Rubisco capacity assuming a fixed ratio of 2.1 for $J_m:V_l$ at 25 °C (Makino *et al.*, 1992; Wullschleger, 1993). At other temperatures the ratio varies with the sensitivities of J_m and V_l to temperature.

The Farquhar *et al.* (1980) model expresses leaf photosynthesis as the minimum of the Rubisco and RuBP limited rates of photosynthesis. When this model is rearranged for interpretation of data, as expressed above, the true photosynthetic capacity of leaves is determined from the maximum of the Rubisco and RuBP regeneration limited rates of photosynthesis. In practice V_l was calculated from measurements of leaf photosynthesis using eq. 7.1, J_m was calculated from eqs. 7.2 & 7.3, both were adjusted to equivalent values at 25 °C using their temperature dependencies (Chapter Six), J_m was converted to units of Rubisco capacity, by the ratio of 2.1, and the apparent photosynthetic capacity taken as the maximum capacity from either the Rubisco or electron transport limited rates.

7.2.2. Photosynthetic Capacity of Canopies

The photosynthetic capacity of canopies was assessed using the sun/shade model of canopy photosynthesis. A uniform (spherical) leaf angle distribution was assumed, so that the fraction of the canopy that is sunlit (f_{sun}) is dependent only on leaf area and solar elevation (β), which was calculated using equations presented in the previous chapter. Photosynthesis of the shaded portion of the canopy (A_{cSh}) was assumed to be light limited (RuBP regeneration limited), as indicated by the sun/shade model (previous chapter). Photosynthesis at low levels of absorbed light is relatively insensitive to photosynthetic capacity (Mooney *et al.*, 1981; Field, 1983; Pons *et al.*, 1989; Schieving *et al.*, 1992; Sadras *et al.*, 1993), allowing A_{cSh} to be determined from the equations of absorbed light and an approximate estimate of photosynthetic capacity of the shaded portion of the canopy (V_{cSh}).

Photosynthesis of the sunlit portion of the canopy is Rubisco limited (light saturated) for most of the day (previous chapter). As with the leaf data, canopy photosynthetic

capacity of the sunlit portion (V_{cSun}) was calculated from a rearrangement of the photosynthesis model (eq. 7.1), by substituting for A_l with $A_{cSun} = A_c - A_{cSh}$ and using the Ball-Berry/Leuning stomatal model (Chapter Five) to determine conductance of the sunlit portion of the canopy and hence estimate p_i. Total canopy photosynthetic capacity (V_c) was calculated from V_{cSun} and used to determine a better estimate of V_{cSh}. Further iterations of the calculations with the new estimate of V_{cSh} changed the value of V_c marginally.

7.2.3. Daily absorbed light profile

Big-leaf models implicitly assume that leaf photosynthetic capacity or leaf nitrogen is distributed in the canopy in proportion to the time-averaged (daily) absorbed irradiance. The daily irradiance absorbed at each level in the canopy, $I_{lday(L)}$, was calculated by integration of the instantaneous absorbed irradiance from sunrise to sunset with a multi-layer model (Chapter Six),

$$I_{lday}(L) = \int_{t_{sunrise}}^{t_{sunset}} I_l(L)dt \qquad (7.4)$$

There is no simple analytical solution to this integral, so it was calculated numerically. The profile of daily absorbed irradiance varies through the year (figure 7.1). Solutions to the distribution of daily absorbed light were simplified by assuming an exponential extinction of net irradiance (*ie.* adjusted for canopy reflection and including the scattered components). If k_i is the extinction coefficient of daily irradiance in the canopy, then the absorbed light profile is defined relative to the daily irradiance at the top of the canopy, $I_{day}(0)$, by the equation,
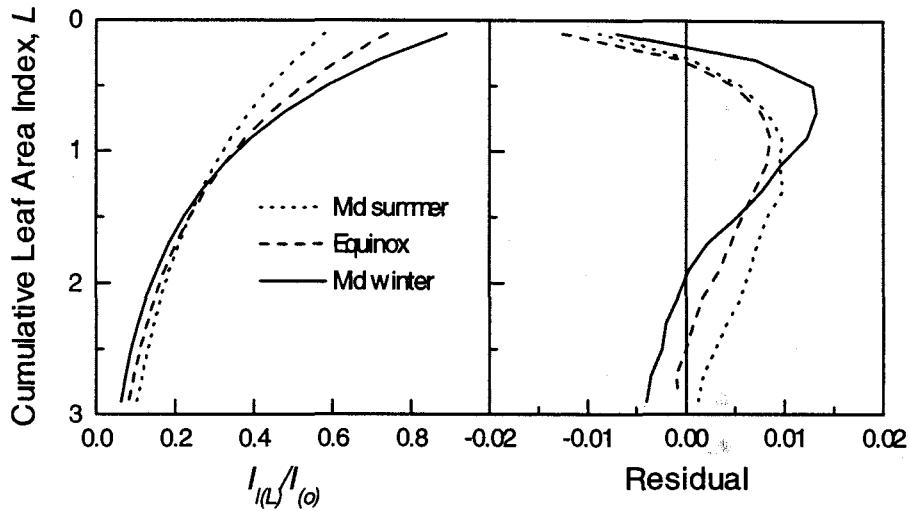
Figure 7.1 *Left:* Numerical solutions of the daily integral of absorbed light, $I_{I(L)}$, relative to incident light at the top of the canopy, $I(o)$, (eq. 7.4). *Right:* Residuals, relative to $I(o)$, from fitting the exponential approximation (eq. 7.5) to the distribution of daily absorbed light with values of the extinction coefficient calculated from eq. 7.6.

$$I_{Iday}(L) = k_i I_{day}(0)(1 - \rho_c)\exp(-k_i L)$$ (7.5)

where $I_{day}(0)$ is the daily irradiance incident at the of the canopy, calculated as the integral from sunrise to sunset of $I(0)$. This equation gives approximations with deviations of less than 2% of incident light at the top of the canopy, compared to the numerical solutions of the daily absorbed light profile (figure 7.1).

The extinction coefficient, k_i, varies through the year with the maximum solar elevation of each day, calculated from latitude (λ) and solar declination (δ) as $\pi/2-|\delta-\lambda|$ (figure 7.2). When k_i is plotted against the sine of the maximum daily solar elevation, $\sin\beta_{max}$, (figure 7.3) it is apparent that most of the variation can be accounted for by the equation (cf. definition of $k_b = 0.5/\sin\beta$)

$$k_i = 0.598/(\sin\beta_{max})^{0.747}.$$ (7.6)
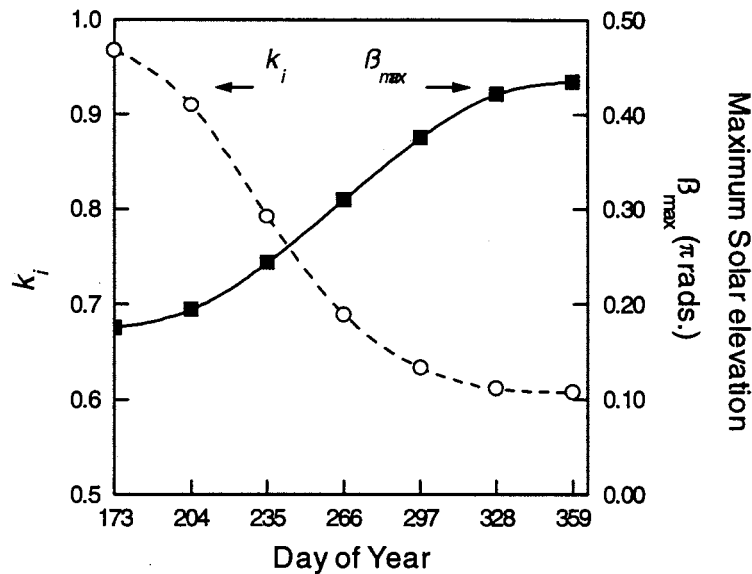
Figure 7.2 Extinction coefficient of daily absorbed irradiance, k_i (open symbols), and maximum daily solar elevation, β_{max} (solid symbols), for days from winter solstice (173) to summer solstice (359) for the latitude 35°3.5' S of Wagga Wagga.

Given that leaves exist at discrete intervals, it was necessary to calculate light absorbed by a layer of leaves for comparisons of absorbed light with leaf photosynthetic capacity. The light absorbed by a layer of leaves depends on their area, which was determined by direct measurements of leaf dimensions and the number of heads of wheat per m² (Table 7.1). The daily absorbed light of a layer relative to available light at the top of the canopy was calculated as the integral of eq. 7.5,

$$\overline{I_{lday}(L_{l_1})} \Big/ \Big(I_{day(0)}(1 - \rho_c)\Big) = \int_{L_{l_0}}^{L_{l_1}} k_i \exp(-k_i L_l) dL \Big/ \Big(L_{l_1} - L_{l_0}\Big)$$

$$= \Big[\exp(-k_i L_{l_1}) - \exp(-k_i L_{l_0})\Big] \Big/ \Big(L_{l_1} - L_{l_0}\Big)$$

(7.7)
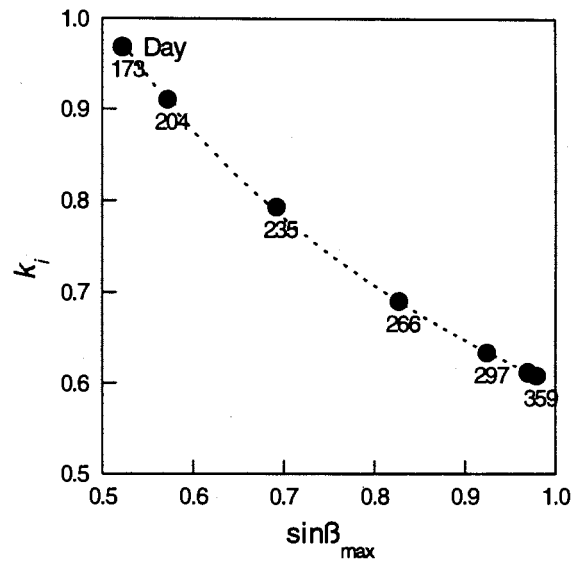
Figure 7.3 Daily light absorption extinction coefficient, k_i, plotted against sine of maximum solar elevation for various days of the year for Wagga Wagga.

7.3. Experimental Methods

Field experiments were conducted as part of a larger project to assess the scaling of water-use efficiency (WUE) from small plots to paddocks. Details were given in Chapter Two. A brief outline is reiterated here.

Two cultivars of wheat, Matong and Quarrion, were grown in large (5 ha) adjacent plots. Photosynthesis was measured on individual leaves, sections of canopy and the whole paddock on several days prior to anthesis, near anthesis and post anthesis. Data from 1990 were used to test the sun/shade model of canopy photosynthesis outlined in the preceding section.

Leaf nitrogen distribution in the canopy was determined from samples of leaves (flag and penultimate) from both canopies on two days (25 and 30 October). The samples were dried, finely ground and analysed by elemental analysis (Carlo Erba 1108). The same samples were analysed for the ratio of $^{13}C:^{12}C$ in a stable isotope ratio mass spectrometer (VG, Isomass).

Soil CO_2 flux measurements were made using a small portable chamber attached to the Li-Cor 6200 (see chapter 3 for more details). Data were collected on several days coinciding with other flux measurements.

Soil respiration is a temperature dependent process. Soil temperature ($T_{s,z,t}$) was not measured, but was estimated from a simple model based on heat diffusion in soil (Campbell, 1977). Diurnal soil temperature variation has an increasing phase lag and a decreasing amplitude compared to air temperature with depth in the soil,

$$T_{s,z,t} = \overline{T}_{s,0} + \exp(-z/D)\left(T_{s,0,t-z/(2\pi D)} - \overline{T}_{s,0}\right),$$ (7.8)

where $\overline{T}_{s,0}$ is the average surface temperature (over 24 hours), z is the depth in the soil (0.05 m), D ($= (2\kappa/\omega)^{1/2}$) is the damping depth, κ is the thermal diffusivity of the soil (8×10^{-7} $m^2.s^{-1}$) (Baver et al., 1972), ω is the angular frequency of temperature oscillation ($2\pi/\tau$ s^{-1}), τ is the period of oscillation (86400 s), $z/(2\pi D)$ is the time lag of temperature variation in the soil compared to the surface and $T_{s,0,t-z/(2\pi D)}$ is the surface temperature at that time. Surface temperature was not measured, but was assumed equal to air temperature since radiation penetration through the canopy to the soil was 10-30 % of total radiation.

The measured canopy CO_2 flux included respiration from stems, heads, roots and soil. Estimated respiration was added to the measured CO_2 flux to calculate gross canopy photosynthesis, thus allowing direct comparison with modelled canopy photosynthesis. Canopy respiration was estimated from CO_2 flux measurements at night. Data from several nights were analysed to obtain a temperature response function, which was used to extrapolate the respiration measurements to daytime with higher temperatures.

As with the tent CO_2 flux measurements, canopy respiration was added to the Bowen ratio CO_2 fluxes to allow direct comparison with the modelled gross canopy photosynthesis. Small gradients at night prevented CO_2 flux measurements at night with the Bowen ratio system, so estimates of canopy respiration from the tent were used. However, chamber over-pressure is known to suppress soil CO_2 fluxes (Kanemasu et al., 1974). The extent of soil CO_2 flux suppression in the tent was assessed by using an additional fan to suck air as well as blowing, removing the over pressure, and by only sucking air. It was estimated that soil CO_2 fluxes were reduced by 80% in the tent. Thus in addition to the tent measured canopy respiration an additional 80% of the independently measured soil flux was added to the Bowen ratio CO_2 flux data to obtain gross canopy photosynthesis.

7.4. Results

7.4.1. Canopy nitrogen and leaf area distribution

Leaf nitrogen distribution in the canopy was determined on two days shortly after anthesis (25 and 30 October) (Table 7.1). Flag leaves were larger (26%), had higher (37%) nitrogen content and lower (15%) specific leaf area (SLA) than penultimate leaves in both canopies. Leaves of the Matong canopy were larger (43%), had lower nitrogen content (9%) and similar SLA to those of Quarrion.

Table 7.1 Leaf size, specific leaf area (SLA) and leaf nitrogen (N_l) of wheat cultivars Matong and Quarrion on 25 and 30 October. The number of heads per m^2 was determined from the final harvest and assumed equal to the number of stems. Sample size: n = 8 on 25-Oct and n = 11 on 30-Oct. Standard errors in parenthesis. Samples for elemental N analysis were two leaves combined.

Cultivar	No. of Heads	Date	Leaf	Area $(cm^2.leaf^{-1})$	SLA $(cm^2.g^{-1})$	N_l $(mmol.m^{-2})$
Matong	270	25-Oct	flag	45 (2.7)	181 (5.6)	119 (5.1)
			penultimate	40 (3.3)	214 (8.5)	91 (3.4)
		30-Oct	flag	43 (2.3)	187 (6.2)	115 (10.9)
			penultimate	28 (2.4)	211 (6.7)	88 (10.7)
Quarrion	342	25-Oct	flag	33 (2.9)	187 (4.5)	130 (7.2)
			penultimate	31 (2.8)	226 (10.2)	89 (5.5)
		30-Oct	flag	26 (2.0)	179 (4.6)	137 (3.4)
			penultimate	20 (1.6)	212 (7.3)	96 (4.7)

Over the five days between measurements there was a greater reduction in the green leaf area of penultimate leaves (49%) than flag leaves (13%) and little change in SLA or nitrogen content per unit leaf area. Leaf area of both canopies decreased by 26% over this period. Flag leaves as a proportion of the total canopy increased from 53% to 60% in Matong, and from 51% to 57% in Quarrion.

These data were used to parameterise the model of leaf nitrogen distribution (Hirose & Werger, 1987a) for the two canopies (figure 7.4). A single value of N_o and k_n for each crop was fitted to data on both days. The profiles of leaf nitrogen were steeper in

Quarrion than Matong as indicated by a higher nitrogen distribution coefficient, k_n, and a higher value of N_o. Narrower leaves, resulting in less leaf area in the flag leaf layer, and a lower leaf area index in Quarrion, compared to Matong, contributed to the steeper distribution of leaf nitrogen, as the nitrogen contents of the penultimate leaves of both crops were similar.
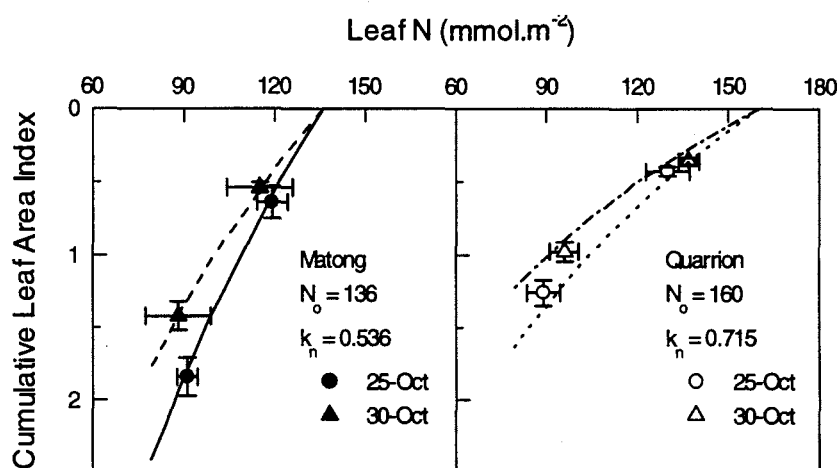
Figure 7.4 Distribution of leaf nitrogen for wheat canopies of cultivars Matong (solid symbols) and Quarrion (open symbols) measured on 25-Oct (circles) and 30-Oct (triangles). Lines are the exponential N distribution model (Hirose & Werger, 1987a), with the parameters as indicated. The data points represent the average leaf nitrogen of flag and penultimate leaves. Standard errors are shown as error bars.

Leaf nitrogen was converted to leaf photosynthetic capacity assuming a linear relationship (see Chapter Six) and the distribution of V_l in the canopies was plotted against the modelled distribution of daily absorbed light (figure 7.5). Profiles of relative daily absorbed light and relative leaf photosynthetic capacity were plotted, to account for the changes in the absolute canopy photosynthetic capacity and total absorbed light due to changes in canopy leaf area and solar position.

Profiles of photosynthetic capacity in the Matong canopy were not as steep as the profiles of daily absorbed light, whereas the profiles of photosynthetic capacity and light in the Quarrion canopy were closely matched. The relative distribution of photosynthetic capacity became steeper in both canopies as the crops matured, which suggests that the

distribution of photosynthetic may have deviated even further from the relative distribution of daily absorbed light earlier in the season, although no measurements in this canopy were available. Analysis of data from other wheat canopies (van Herwaarden, 1995) shows that as wheat crops mature leaf nitrogen (mmol.m^{-2}) is removed from all leaves uniformly, so that as leaf area of the canopy decreases the relative distribution profile becomes steeper and more closely matched to the relative profile of daily absorbed light.
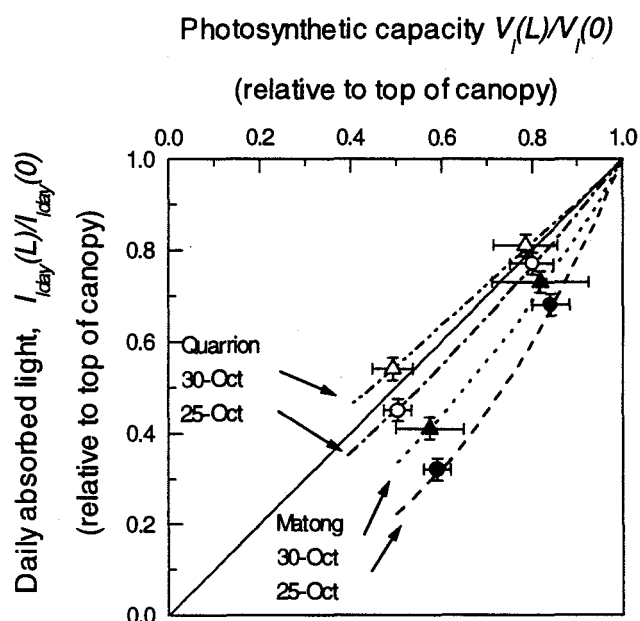
Figure 7.5 Relative leaf nitrogen distribution plotted against the relative distribution of daily absorbed light. Also shown is the 1:1 line of a match in the distribution of leaf photosynthetic capacity and daily absorbed light. Error bars are standard errors.

7.4.2. Soil Respiration

Measured soil respiration (R_s) was characterised by high spatial variability (coefficient of variation = 0.3) (figure 7.6). The increase in R_s appeared to be related to soil temperature (T_s), since it reached a maximum later than air temperature. However, an Arrhenius plot of $\ln(R_s)$ against $1/RT_{s,0.05}$ showed no significant variation in R_s due to

T_s. Many observations of R_s have been shown to vary *between* days with T_s (Lloyd & Taylor, 1994). Measurement techniques have limited resolution of diurnal trends (Schlesinger, 1977), although eddy correlation measurements show that R_s does respond to diurnal variation of T_s (Baldocchi *et al.*, 1986). From another study of soil respiration under wheat crops (unpublished data) I determined that R_s responds to temperature with an activation energy of 53 kJ.mol^{-1}. Since most measurements of R_s were made between 10:00 and 16:00, there was little variation in T_s within a day. Measurements at other times (night) may have increased the temperature range and allowed a temperature response to be observed.
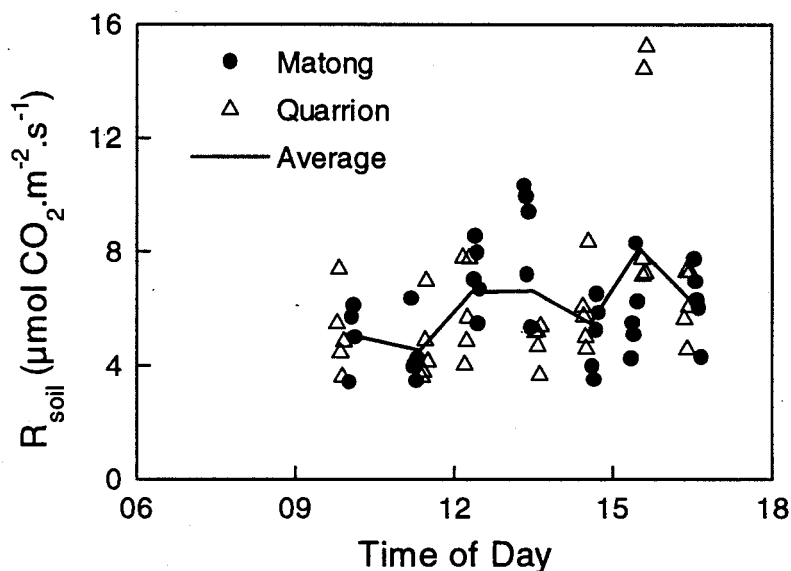
Figure 7.6 Soil respiration measured beneath the Matong (o) and Quarrion (Δ) canopies, with a chamber attached to a Li-Cor 6200 collected on 25-Oct and the combined average.

Variation in soil respiration between days was explained by variation in relative soil water content (W). The temperature component of variation in R_s was removed by calculating soil respiration at 10°C ($R_{s(10)}$), using the assumed temperature response. A linear regression of the natural log of $R_{s(10)}$ with the natural log of W accounted for 61% of the variation (standard errors of coefficients shown in parentheses),

245

$$\ln R_{s(10)} = 1.50(\text{0.08}) + 1.77(\text{0.10}) \ln W,$$ (7.9)

where $R_{s(10)}$ is in $\mu mol.m^{-2}.s^{-1}$ and W is a fraction. Since data for W were available only on a fortnightly basis, the regression could not account for any diurnal variation. Soil respiration was extrapolated from the measured soil respiration (Table 7.2) or the regression with available soil water content (eq. 7.9) when measurements were not available and the assumed temperature response.

Table 7.2 Average soil respiration adjusted to 10°C, $R_{s(10)}$ ($\mu mol\ CO_2.m^{-2}.s^{-1}$).

Date	Matong	Quarrion
05-Sep	7.05	5.32
18-Oct	1.17	1.09
24-Oct	2.60	3.45
25-Oct	2.54	2.61
30-Oct	0.69	0.71
31-Oct	0.53	0.52
01-Nov	0.92	1.21

7.4.3. Canopy Respiration

As light levels decreased at sunset, the canopy CO_2 flux became negative (*ie.* respiration dominated), reaching its most negative just after complete darkness. The CO_2 flux approached zero through the night as the temperature dropped, reaching a minimum before sunrise just prior to the minimum temperature. As light levels increased at sunrise the CO_2 flux increased and became positive. Low wind speeds during the night allowed $[CO_2]$ in the canopy to increase to 500 ppm. Large changes in $[CO_2]$ in each puff of wind, made flux measurements based on a differential IRGA very variable on some nights.
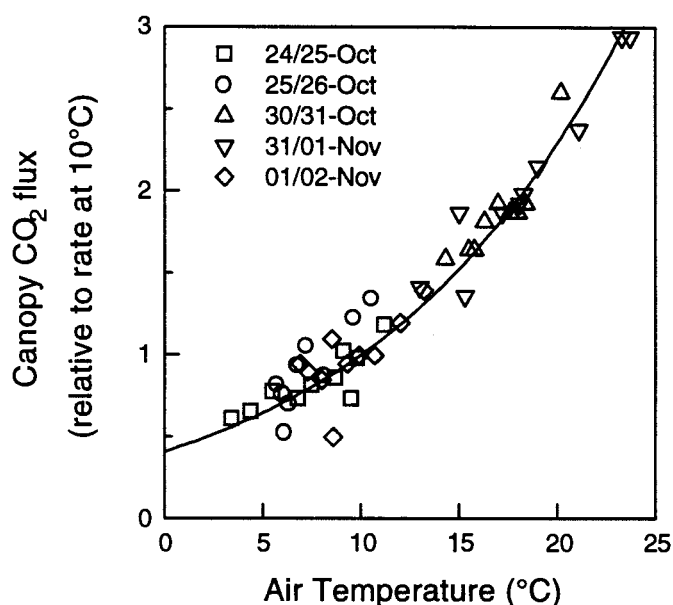
Figure 7.7 Hourly averages of night CO_2 fluxes (relative to the rate at 10°C) from the Matong wheat canopy of five separate nights that were used to determine the temperature response of canopy respiration. Data were obtained with a ventilated chamber. The line is the function that was fitted on an Arrhenius plot, with an activation energy of 57.1 (se = 2.7) kJ.mol^{-1}.

Canopy (including the unsuppressed soil component) respiration (R_c) was estimated from tent CO_2 fluxes at night. Data from five nights were used on an Arrhenius plot of the temperature response (figure 7.7). The data were fitted concurrently so that data from each night were allowed a separate intercept and a common slope. An activation

Table 7.3 Canopy respiration rate, including the unsuppressed soil respiration, adjusted to 10 °C, $R_{c(10)}$.

Date	Matong	Quarrion
12-13/10	2.27	2.14
17-18/10	2.82	2.34
24-25/10	2.45	1.81
25-26/10	1.71	2.27
30-31/10	1.77	2.10
31/10-1/11	1.77	2.26
1-2/11	2.01	1.46

energy of 57.1 kJ.mol^{-1} was calculated from the slope, which was very close to 58 kJ.mol^{-1} reported by Baldocchi (1994b) in a wheat crop. Canopy respiration rate at 10°, $R_{c(10)}$, was calculated from Arrhenius plots on all nights using the fitted activation energy for both canopies (Table 7.3).

Brooks & Farquhar (1985) and Kirschbaum & Farquhar (1987) observed decreases in respiration of leaves in light compared with dark respiration, but Azcón-Bieto & Osmond (1983) did not, although reviews by Graham (1980) and Krömer (1995) give several reasons why the decrease could occur. The magnitude and existence of the effect remains elusive, but nevertheless I have assumed that canopy respiration during the day was 85% of the rate at night, since leaves were only 10% of crop biomass (see Chapter Three) and the specific respiration rate of leaves is three times greater than that of spikes and four times greater than that of stems (McCullough & Hunt, 1993). Modelled canopy respiration (figure 7.8) was considerably greater during the day than at night since air temperatures were higher.
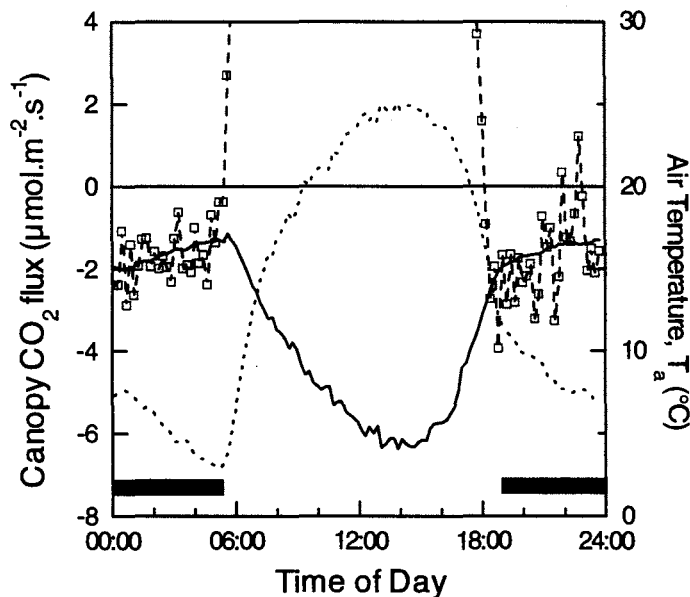
Figure 7.8 Modelled canopy respiration (——) extrapolated from measurements of canopy CO_2 flux at night (- - □ --) and the air temperature (·····). Data are the CO_2 flux measurements of the Matong canopy on the 25-Oct. Solid bars at the bottom indicate night.

7.4.4.   Leaf photosynthetic capacity

Measurements of leaf photosynthesis (A_l) were made on ten separate days in 1990. Data of photosynthetic Rubisco capacity of leaves (V_l) on a day just after anthesis and the following week are presented in figure 7.9.

A_l declined during the day, despite an increase in intercellular CO_2 partial pressure (p_i), so that calculated V_l declined during the day, even after adjusting for the effects of
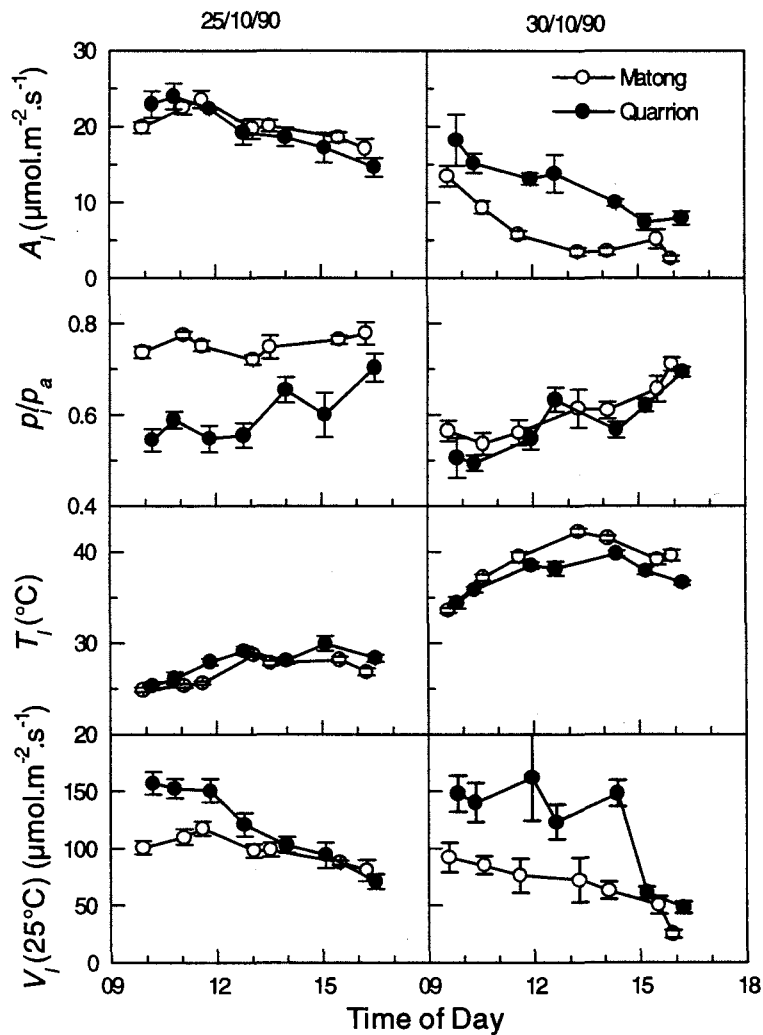
Figure 7.9 Leaf photosynthesis (A_l), ratio of intercellular to atmospheric CO_2 partial pressures (p_i/p_a), leaf temperature (T_l) and photosynthetic (Rubisco) capacity adjusted to 25°C (V_l) of flag leaves in canopies of Matong (–o–) and Quarrion (–●–) on 25-Oct (left) and 30-Oct (right). Standard errors are shown as error bars. Each point is the mean of measurements on 5 leaves.

temperature. The decline in V_l and A_l during each day became more pronounced as the season progressed.

High temperatures on 30-October reduced the modelled rate of electron transport so that apparent photosynthetic capacity of the leaves was calculated from the maximum of the RuBP-regeneration limited rate and the Rubisco limited rate of photosynthesis and converted to units of Rubisco capacity assuming a constant ratio of $J_m{:}V_m = 2.1$ (at 25 °C) (figure 7.10), as previously explained. Photosynthetic capacity was calculated from the RuBP regeneration equations (eqs. 7.2 & 7.3), yielding results which were greater than the photosynthetic capacities calculated from the Rubisco equation (eq. 7.1) for all measurements after 10:30, when leaf temperature rose above 36°C in both Matong and Quarrion.
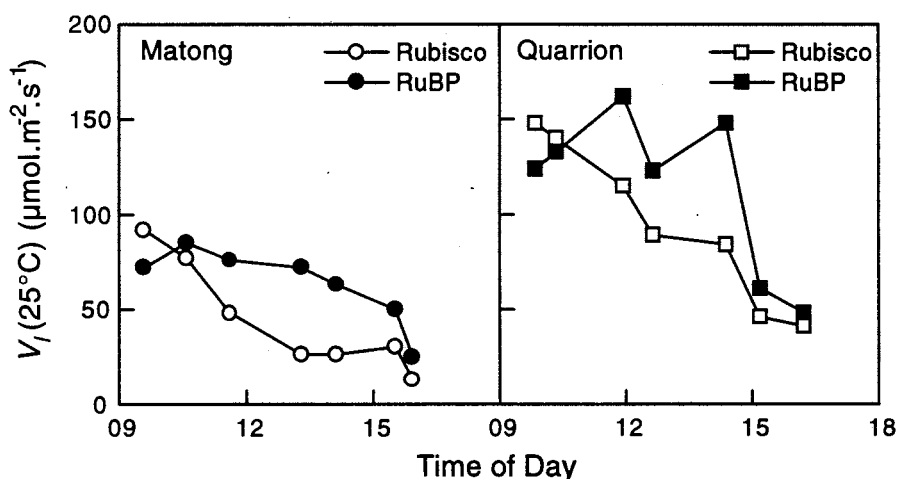
Figure 7.10 Photosynthetic Rubisco capacity of flag leaves of Matong (left panel) and Quarrion (right panel), calculated assuming Rubisco limited photosynthesis (Rubisco, open symbols) or RuBP regeneration limited photosynthesis (RuBP, solid symbols) on 30 October.

The diurnal decline in apparent photosynthetic capacity was less severe when the effect of high temperature on RuBP regeneration limited photosynthesis was considered, compared to the decline in the apparent photosynthetic capacity derived from the Rubisco equation only. On other days temperatures were not so high so apparent

photosynthetic capacity was calculated from only the equations describing Rubisco limited photosynthesis.

Mean V_l for all days are plotted in figure 7.11. There were significant changes in V_l on successive days that did not follow the estimated decline in leaf nitrogen content, but were associated with variation in temperature, relative soil water content and senescence of the canopies (figure 7.12). V_l was similar in both canopies prior to anthesis, but was higher in Quarrion than Matong post-anthesis (figure 7.11). V_l of leaves in both canopies declined as the season progressed, the decline being more rapid in the Matong canopy than Quarrion.
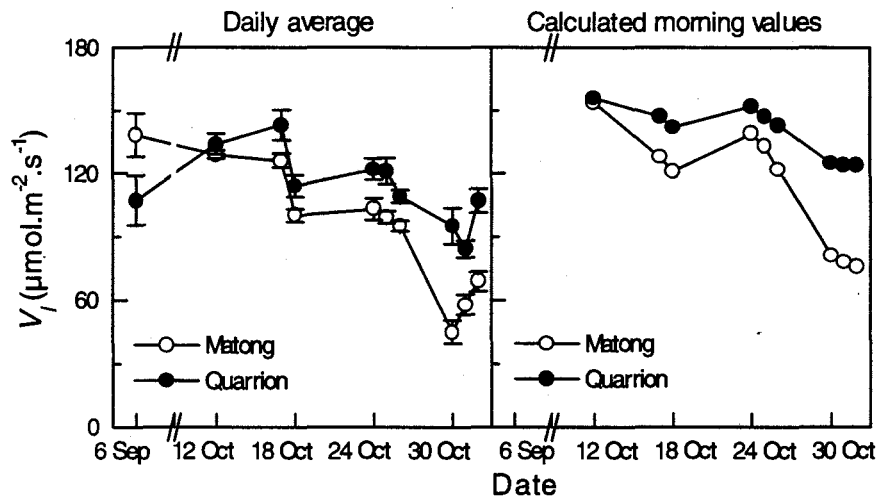
Figure 7.11 *Left panel:* Average apparent Rubisco capacity (V_l) of fully sunlit flag leaves in canopies of Matong (—o—) and Quarrion (—●—) on ten days near anthesis. *Right panel:* Rubisco capacity of flag leaves calculated by a regression with relative soil water availability, leaf temperature and accumulated canopy evaporation at 10:00 (eq. 7.10). Standard errors are shown as error bars.

The recovery of apparent photosynthetic capacity each morning (figure 7.9) suggests that the decline in apparent photosynthetic capacity during each day was not associated with changes in Rubisco capacity but rather some temporary down regulation of photosynthesis. Gunasekera and Berkowitz (1993) found no effect of water stress on Rubisco activity but suggested that some step in RuBP regeneration may have been limiting (other than temperature effects). If this phenomenon were due to water stress,

then the measured leaves, which were perpendicular to the beam direction at the top of the canopy, were probably more stressed than other leaves. Thus these leaf measurements may not be representative of the diurnal changes of leaf photosynthetic capacity of the entire canopy.
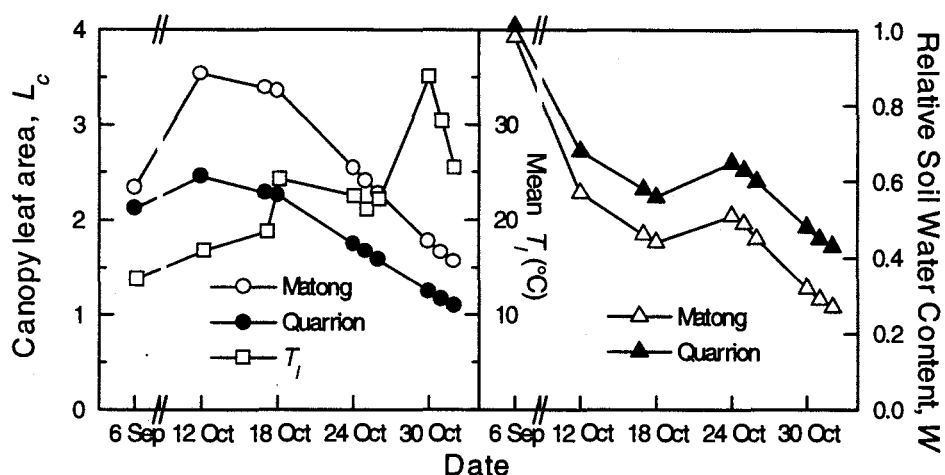
Figure 7.12 Canopy leaf area (L_c), left panel (circles), average leaf temperature (T_l) (squares) and relative soil water availability (W), right panel (triangles), for canopies of Matong (open symbols) and Quarrion (filled symbols) during the period of leaf photosynthesis measurements.

The changes in photosynthetic Rubisco capacity may have been caused by declining leaf water potential, but it was not measured. Instead the relative soil water content (W) and the daily accumulated evaporation from the canopy (ΣE_c) were used as indicators of plant water status. A multiple linear regression of V_l, with cultivar as a factor, accounted for much of the variation (Table 7.4),

$$V_l(25°) = a + bW + cT_l\Sigma E_c \qquad (7.10)$$

where a, b and c are the regression intercept and coefficients. Separate values of a and b were determined for each cultivar and a common coefficient c for both cultivars. Relative soil water content accounted for variation in V_l between days, while ΣE_c accounted for the decline in V_l during the day, with greater sensitivity on hotter days.

The maximum values of apparent photosynthetic capacity, observed each morning are a more appropriate parameter for determining canopy photosynthetic capacity. Since morning measurements were not taken on all days the regression (eq. 7.10) was used to estimate leaf photosynthetic capacity at mid-morning (10:00). Estimated mid-morning values of leaf photosynthetic capacity were less variable than the earliest measurements on each day (at different times) and showed a decline consistent with canopy maturity and senescence (figure 7.11).

Table 7.4 Coefficients of the regression analysis of variation in Rubisco photosynthetic capacity of leaves ($V_{j(25)}$, $\mu mol.m^{-2}.s^{-1}$) in Matong and Quarrion; a, constant, b, coefficient of relative soil water availability (W) and c, coefficient of leaf temperature (T_l, °C) and accumulated canopy evaporation (ΣE_c, $mol.day^{-1}$) interaction. Standard errors of coefficients in parenthesis.

Crop	a	b	c	r^2
Matong	30 (8)	243 (19)		
			-0.0087 (0.0006)	0.87
Quarrion	107 (14)	89 (29)		

7.4.5. Canopy Photosynthetic Capacity

Canopy photosynthetic capacity (V_c) was calculated using the sun/shade model as previously described. V_c was greater in Quarrion than Matong and decreased during the day (figure 7.13), as was also observed at the leaf scale (figure 7.9). The decrease in V_c during the day was not as marked as at the leaf scale. Changes in V_c before 9:00 and after 15:00 are probably not realistic because the calculations to determine the fraction of sunlit leaf area are not accurate at low solar elevations (Goudriaan, 1977) and the assumption of Rubisco limited photosynthesis is not valid. The regression used to describe the diurnal variation in leaf photosynthetic capacity (eq. 7.10) also described the decrease of V_c during the day, although the coefficient was lower $(c = 0.0035)$ (data not shown).
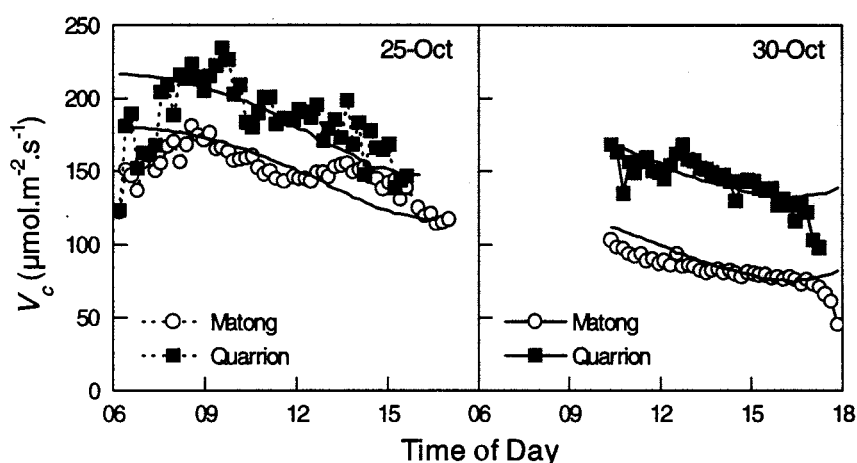
Figure 7.13 Photosynthetic Rubisco capacity of the Matong (o) and Quarrion (■) canopies on 25-Oct and 30-Oct (left and right panels), derived from CO_2 flux data, measured with the tents, and the sun/shade model of canopy photosynthesis. Also shown as lines are the modelled canopy photosynthetic capacities predicted by the regression derived from leaf data (c = -0.0087) (eq. 7.10).

7.4.6. Comparison of Model with Data

7.4.6.1. Instantaneous Photosynthesis

Predictions of canopy photosynthesis by the sun/shade model, using photosynthetic capacity derived from the leaf measurements and the regression (eq. 7.10), were compared with tent measured CO_2 fluxes on nine days and with the Bowen ratio flux
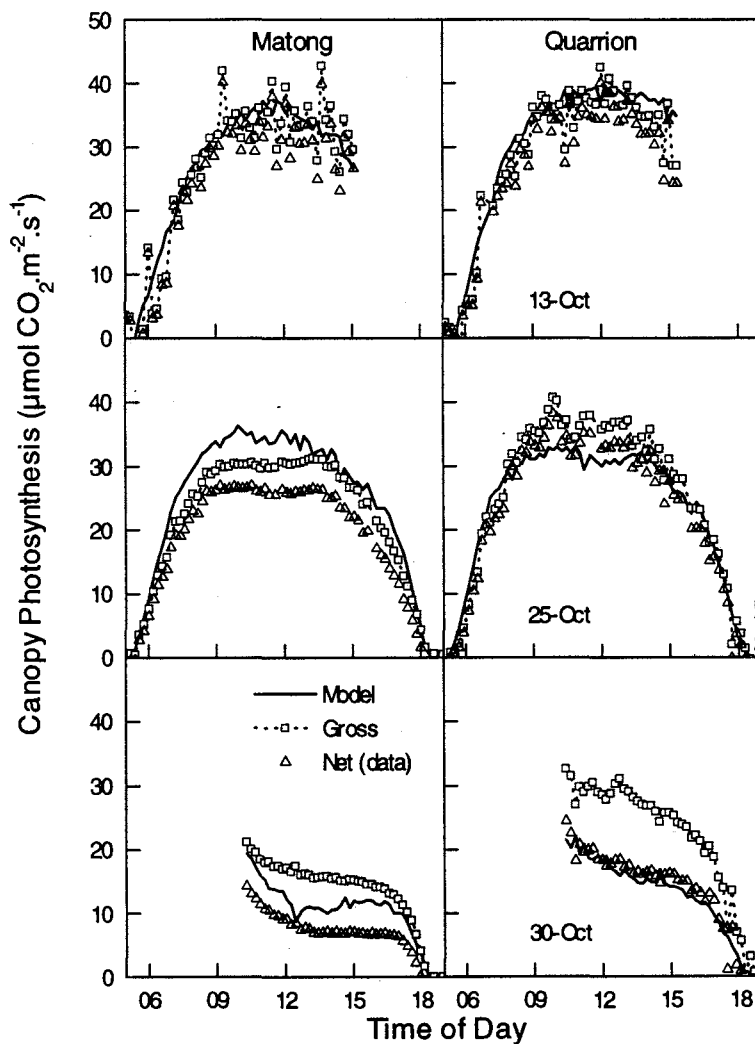
Figure 7.14 Comparison of modelled canopy photosynthesis (——) with gross canopy photosynthesis (··□··) calculated from measured net CO_2 fluxes by the tents (Δ) on 13-Oct (top), 25-Oct (middle) and 30-Oct (bottom) for canopies of Matong (left) and Quarrion (right). Model parameters were derived from leaf photosynthesis data measured concurrently with the canopy data.

data on twelve days. Data from three days are shown representing periods prior to anthesis (13-Oct), near anthesis (25-Oct) and post anthesis (30-Oct) (figures 7.14 & 7.15). These measurements covered a range of temperatures (mean daily T_a = 15-35°C) and canopy leaf areas (L_c = 3.5 - 1.0).

On 13-Oct temperature was low (mean daily T_a = 15°C) and the calculated canopy and soil respiration was a small component of net canopy CO_2 flux so that gross canopy photosynthesis was only slightly greater than the measured CO_2 flux. In contrast, on 30-Oct high temperatures (mean daily T_a = 35°C) resulted in much larger calculated rates of canopy and soil respiration, so that the estimated gross canopy photosynthesis was much
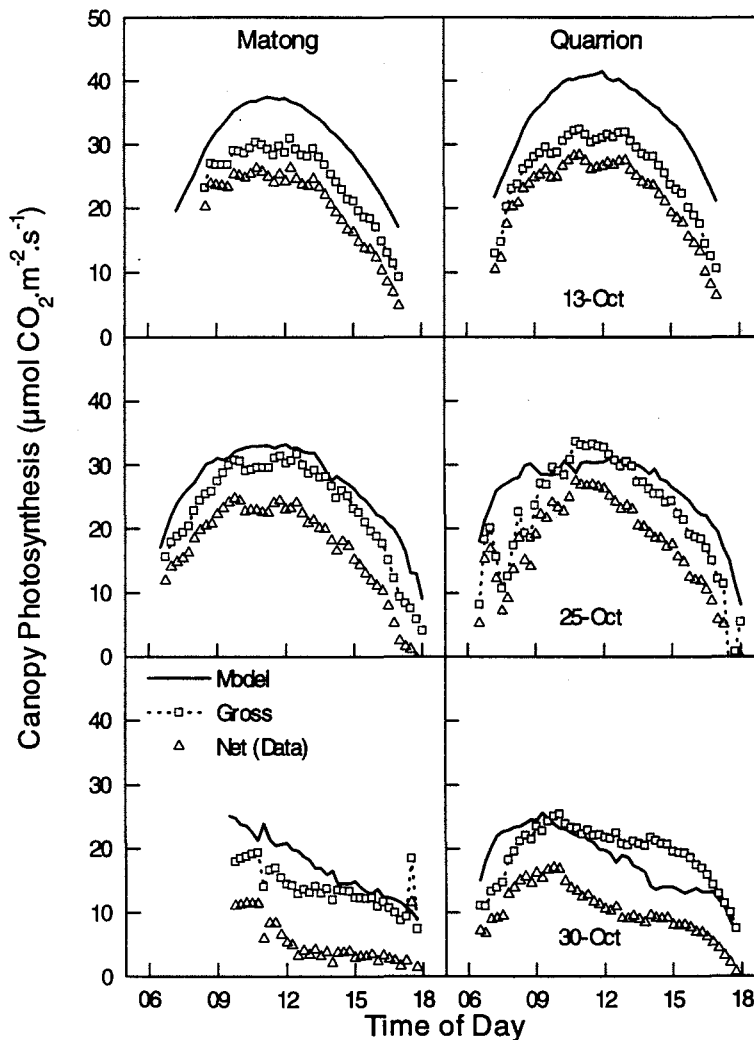
Figure 7.15 As in figure 7.14, but comparing the model of canopy photosynthesis with Bowen ratio data of canopy CO_2 fluxes.

greater than the measured net canopy CO_2 flux. Respiration was calculated by extrapolation of night CO_2 flux measurements, which covered the temperature range from 5-25°C (figure 7.8). Extrapolation of the response of respiration to temperature beyond this range, up to 35°C, may not be valid, possibly over-estimating respiration.

In Matong, model predictions closely matched gross canopy photosynthesis on 25-Oct and 30-Oct for both tent and Bowen ratio data. On 13-Oct the model matched the tent data but not the Bowen ratio data, which were lower than the model predicted. Different flux data from the tent and Bowen ratio systems were not consistently observed, in Matong (Chapter Three), so one system may have been in error. On the 13-Oct the canopy leaf area index was near its maximum (3.5 $m^2.m^{-2}$), suggesting that the higher rate measured by the tent and predicted by the model was the real rate of canopy photosynthesis.

The tent data of Quarrion were shown to be systematically higher than the fluxes measured by the Bowen ratio system, as the tent was in part of the paddock that had denser leaf area than the average of the patchy crop (Chapter Three). Model predictions of canopy photosynthesis for Quarrion matched the Bowen ratio flux measurements on 25-Oct and 30-Oct, but overestimated the CO_2 fluxes on 13-Oct.

7.4.6.2. Daily Photosynthesis

Daily rates of canopy photosynthesis predicted from the sun/shade model and the measured canopy photosynthesis were compared for all days of measurements (figure 7.16). Similar comparisons could be made with midday fluxes, since photosynthesis at these times is the major component of the daily total. However, comparisons with the daily total removes the short term fluctuations due to temperature and light variations and provides an indication of overall model fit.

Model predictions for the Matong canopy were greater than measurements for days pre-anthesis and near anthesis. Post-anthesis predictions were closer to the measurements. Model predictions for Quarrion were lower than the tent measurements for all days, and higher than the Bowen ratio data. Model predictions of canopy photosynthesis in the tents were different to predictions for comparison with Bowen ratio data, since the tents had more diffuse light, were warmer and had different turbulence.

257
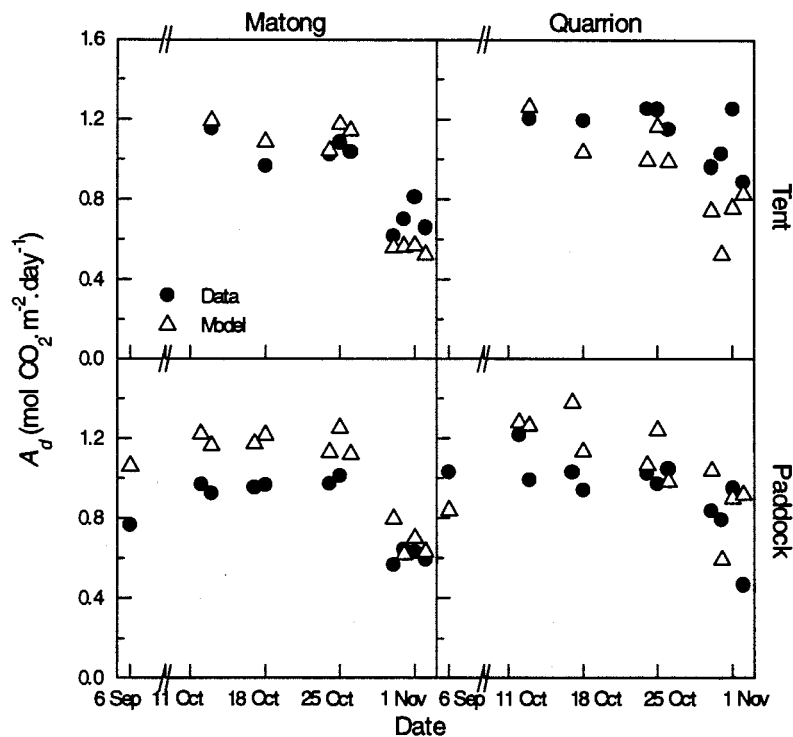
Figure 7.16   Daily gross canopy photosynthesis integrated from flux measurements (●) and model predictions (△) of all days of measurements. Tent measurements (top panels) and Bowen ratio (bottom panels). Cultivar Matong (left panels) and Quarrion (right panels). Model predictions were based on morning leaf photosynthetic capacity values.

Photosynthesis of stems and the developing spikes may have made an increasing contribution to canopy photosynthesis, which was not measured separately nor included in the models.

Canopy respiration increased as the crop matured, which could also be attributed to increasing temperature. The ratio of net daytime canopy photosynthesis to gross canopy photosynthesis decreased as the season progressed (figure 7.17).
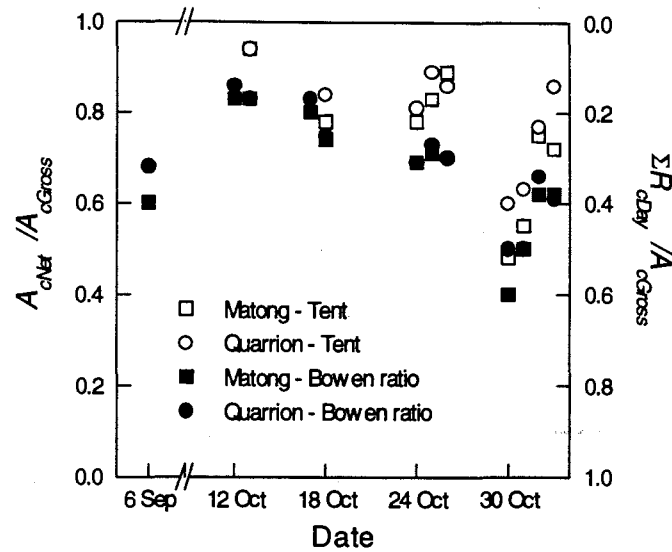
Figure 7.17 Ratio of net daytime canopy photosynthesis to gross canopy photosynthesis (A_{cNet}/A_{cGross}) of Matong (squares) and Quarrion (circles), measured with the tent (open symbols) or a Bowen ratio system (solid symbols). Total daytime canopy respiration as a fraction of gross photosynthesis ($\Sigma R_{cDay}/A_{cGross}$) is shown on the right axis. Note this canopy respiration is daytime only, it does not include respiration during the night.

7.4.7. Sensitivity analysis

Sensitivity of the sun/shade model was assessed by changing each parameter by 10% and calculating the response of predicted daily gross canopy photosynthesis, expressed as a relative response (($\Delta A_c/A_c)/(\Delta x/x)$). The sensitivities to an increase or decrease of the parameters were similar so they are expressed as the average (Table 7.5). Sensitivities were assessed for two days data, 25-Oct and 30-Oct. The latter had lower canopy leaf area and higher temperatures.

At temperatures near 25°C, on 25-Oct, the most influential parameters were those directly measured, particularly V_l, L_c and p_i. The first two determine canopy photosynthetic capacity, which together with p_i determine the rate of canopy photosynthesis. Changes in canopy respiration and its activation energy had less effect on canopy photosynthesis. These parameters were more influential on hot days (30-Oct) when respiration was a greater proportion of gross photosynthesis. Leaf nitrogen (N_l)

259

and electron transport capacity (J_m) had little effect on canopy photosynthesis, because the former is only used to model the distribution of photosynthetic capacity in the canopy, while the latter only affects photosynthesis of shaded leaves, which have previously been shown to be relatively insensitive to photosynthetic capacity (Field, 1983; Sadras *et al.*, 1993).

Table 7.5 Sensitivity, $(\Delta A_c/A_c)/(\Delta x/x)$, of the sun/shade model of gross canopy photosynthesis to each parameter. Data for the model were from the Matong canopy on 25-Oct (Mean day $T_a = 22°C$) and 30-Oct ($T_a = 35°C$). The parameters are separated into those that were directly measured (left columns) and those that were estimated from the best values in the literature (right columns).

Measured Parameters	Sensitivity 25-Oct	Sensitivity 30-Oct	Estimated Parameters	Sensitivity
L_c	0.68	0.99	Γ_*	-0.33
p_i	0.68	1.16	k_n	-0.18
V_l	0.55	0.49	E_V	-0.16
R_c	-0.27	-1.10	k_b	-0.11
E_{Rc}	-0.26	-2.16	θ	0.11
J_m	0.08	-	$E_{K'}$	0.07
N_l	0.02	-	k_d	0.04
			ω	0.04

The model of canopy photosynthesis was less sensitive to parameters estimated from published values. The most influential of these was Γ_*, which is related to the Michaelis-Menten constants of Rubisco (Farquhar *et al.*, 1980, their eq. 38). The parameter describing the distribution of nitrogen in the canopy, k_n, was not very influential as previously described (Hirose & Werger, 1987a). The activation energies of Rubisco parameters, E_V, E_{Ko} and E_{Kc} had a small effect on daily canopy photosynthesis, despite a large diurnal temperature change. This highlights the dominance of photosynthesis during the middle of the day when temperature variations were small compared to the relatively low photosynthetic rates that occurred during the hours of rapid temperature change at either end of the day. The canopy light extinction coefficients, k_b and k_d, and the coefficient of light scattering by leaves, ω, were the least influential.

Temperature had a large effect on the sensitivity of the model (Table 7.5). On the second day analysed (30-Oct), the respiration parameters R_c and E_{Rc} had much greater effect on modelled canopy photosynthesis. This day was characterised by high temperatures and high respiration rates with an estimated 50% of gross photosynthesis respired during the day. The influence of L_c, V_l and p_i was enhanced at higher temperatures.

For each of the parameters an uncertainty of their values was estimated (Table 7.6). In the case of measured parameters the uncertainty was based on the standard error of the measurements. Uncertainties for the estimated parameters was calculated from the typical range of values observed in the literature, which was assumed to be a ±95% confidence interval, and thus approximately twice the standard error. The uncertainty was combined with the model sensitivity to the parameters (Table 7.5) to obtain an estimate of the potential error in gross canopy photosynthesis (ΔA_{Cgross}) (Table 7.6). Adding only those error estimates that are greater than 1%, provides a combined uncertainty of ±20% of gross canopy photosynthesis. While this is probably an upper estimate, it provides an indication of the overall confidence in the model predictions and suggests which parameters are likely sources of error.

Table 7.6 Uncertainty estimate of parameters and their effect on modelled gross canopy photosynthesis when combined with the model sensitivity. Model sensitivity estimates were from the 25-Oct (Table 7.5). The uncertainty estimates were based on standard errors in the case of measured parameters and on an estimate of the range of typical values for the case of the estimated parameters.

Measured Parameter	Uncertainty %	ΔA_{Cgross} %	Estimated Parameter	Uncertainty %	ΔA_{Cgross} %
L_c	10	6.8	Γ_*	5	1.7
p_i	1.5	1.0	k_n	10	1.5
V_l	5.7	3.1	E_V	5	0.8
R_c	12.6	-3.4	k_b	10	1.1
E_{Rc}	4.7	-1.2	θ	7	0.8
J_m	8.2	0.6	$E_{K'}$	5	0.4
N_l	5.4	0.1	k_d	10	0.4
			ω	13	0.5

7.5. Discussion

7.5.1. Variation of photosynthetic capacity

Interpretation of photosynthesis measurements in this experiment was aided by use of the Farquhar *et al.* model of leaf photosynthesis which allowed separation of the stomatal and non-stomatal effects on photosynthesis. The decline in photosynthesis during the day was interpreted as a decrease in photosynthetic capacity at both the leaf and canopy scale as p_i did not decline (figures 7.9 & 7.13). A regression equation explained the decline in photosynthetic capacity as a function of cumulative evaporation, which is presumably a surrogate for declining leaf or soil water status, which have previously been associated with decreasing photosynthesis in wheat (Johnson *et al.*, 1974; Martin & Ruiz-Torres, 1992; Morgan *et al.*, 1993).

The mechanistic basis for the decline in photosynthetic capacity is not known. Water stress possibly inhibits electron transport in isolated chloroplasts (Boyer & Bowen, 1970; Keck & Boyer, 1974), although Kaiser (1987) and Graan & Boyer (1990) showed that high CO_2 concentrations can remove such inhibition. The decline in Rubisco activity under water stress is insufficient to explain the decrease of photosynthesis of leaves (Gimenez *et al.*, 1992; Gunasekera & Berkowitz, 1993). One difficulty in determining the mechanism of water stress effects on photosynthesis is the tight coordination between the Rubisco, RuBP regeneration components of the photosynthetic apparatus, so that each component regulates its activity to match the other. Thus, where I have expressed the decline in photosynthetic capacity as a decrease in Rubisco capacity the actual mechanism of the decline may be caused by reduced electron transport or reduced activation of Rubisco.

The response of photosynthesis to water stress is not included in the Farquhar *et al.* model of leaf photosynthesis, nor any other mechanistic model. This is a serious limitation to the use of Farquhar *et al.* model for analysis of field data or the prediction of photosynthesis in water-limited conditions, which are relevant to any study of water-use efficiency or the carbon dynamics of many ecosystems of the globe. Empirical relationships describing the decline in photosynthetic capacity in response to water potential have been used in models of leaf and canopy photosynthesis, although the sensitivity of the response varies (Grant, 1992b; Grant, 1992a).

Alternative explanations for the decline in apparent photosynthetic capacity during the day are triose phosphate limitations to photosynthesis (Sharkey, 1985) or heterogeneous stomatal opening (Terashima *et al.*, 1988). Depletion of available phosphates for photosynthesis has been suggested as an explanation for decreased photosynthesis with low sink strength (Herold, 1980), at high CO_2 (Sharkey, 1985) or low temperature (Sage & Sharkey, 1987), but seem highly unlikely during grain filling of wheat at the warm temperatures encountered in this experiment. Patchy gas exchange across leaves has been observed in a diverse range of plants in artificial conditions, but not in wheat and only to a limited extent in field conditions (Terashima, 1992). Additionally, Cheeseman (1991) showed the effect of variable stomatal opening on calculations of photosynthesis to have been minimal with the extent of patchiness observed in most experiments, although what happens under water stress is not clear. Thus, these phenomena of triose phosphate limitations to photosynthesis and patchy gas exchange are possible alternative explanations for the observed diurnal decline in apparent photosynthetic capacity, but it is unlikely that they were significant. New approaches using fluorescence imaging of patchy leaves may indicate to what extent photoinhibition is contributing to this phenomenon.

7.5.2. Comparison of model with canopy flux data

The observed diurnal variation of gross canopy photosynthesis was predicted by the sun/shade canopy model, although the model was not accurate in predicting the absolute flux (figures 7.14 & 7.15). This is not a reflection of structural flaws in the model, but rather indicates the difficulty of parameterising canopy photosynthetic capacity from stochastic leaf-scale data. The comparison of these model predictions with canopy data reflect the difficulty of scaling photosynthesis from leaves to canopies. Differences between the model predictions and the measured fluxes were of a similar magnitude to the differences between the tent and Bowen ratio flux measurements.

The sun/shade model of canopy photosynthesis described here, implicitly assumes profiles of leaf photosynthetic capacity, which have been shown to affect canopy photosynthesis (Field, 1983; Hirose & Werger, 1987a; Reynolds *et al.*, 1992). As such, this model overcomes a limitation of previous sun/shade models of canopy photosynthesis (Boote & Loomis, 1991). Separate treatment of the sun and shaded leaves avoids the problem that single-layer models have with averaging the non-linear

response of photosynthesis to absorbed light (Norman, 1980; Johnson *et al.*, 1989; Reynolds *et al.*, 1992).

Big-leaf models of canopy photosynthesis have been proposed (Sellers *et al.*, 1992; Amthor, 1994). They are based on the assumption of an optimal distribution of photosynthetic capacity within the canopy in relation to the distribution of absorbed light. In this study, the distribution of photosynthetic capacity did follow the distribution of daily absorbed light (figure 7.5) as has been observed in many other canopies (Hirose & Werger, 1987a; Anten *et al.*, 1995). However, this does not validate the big-leaf models, despite its presentation as a scaled-up mechanistically-based model. I showed in the previous chapter (Six) that big-leaf models are based on the incorrect assumption of the similarity of the instantaneous and time-averaged profiles of absorbed light in canopies. Use of inappropriate scaling models, that do not accurately represent the processes, can be very misleading as their scaling basis can lead to a false sense of validity. For example, Lloyd *et al.*, (1995) fitted a big-leaf model to canopy flux data, and proceeded with a mechanistic interpretation of canopy photosynthesis in terms of electron transport-limited and Rubisco-limited photosynthesis, when the parameters fitted at the canopy scale did not correspond with their leaf scale equivalents. Their model did not explain much of the variation in photosynthesis, showing light saturation that was not observed in the data. The variation in canopy photosynthesis that was explained by their model was a result of the use of a non-rectangular hyperbola for the light response of canopy photosynthesis, which has no mechanistic basis in terms of the biochemistry of photosynthesis. Errors involved with averaging of light over sunlit and shaded leaves for use in the non-linear response of photosynthesis to light are large (Sinclair *et al.*, 1976; Norman, 1980; Smolander, 1984). The sun/shade model of canopy photosynthesis evaluated here overcomes these problems of big-leaf models and has the advantages of allowing within-canopy profiles of leaf photosynthetic capacity and the use of a biochemically based model of photosynthesis.

If the data in figure 7.14 & 7.15 were plotted as modelled versus measured, then the correlation coefficient is 0.80, and suggest that the model works well across a range of canopy leaf areas and environmental conditions. Presentation of model predictions and data in this manner tends to mask the light saturation of canopy photosynthesis and curvature predicted by some models that measurements of CO_2 fluxes do not sustain (Baldocchi, 1989; 1992; 1993; Lloyd *et al.*, 1995).

7.5.2.1. Model predictions of Daily Photosynthesis

Comparisons of measured and modelled canopy photosynthesis were made with daily integrated gross photosynthesis (figure 7.16). The measured daily gross photosynthesis was remarkably constant while the canopy leaf area was sufficient to intercept most of the light (ie. until 30-Oct), which reinforces canopy light interception as the main determinant of canopy photosynthesis (Monteith, 1977; Barnes et al., 1990). The sun/shade model predictions varied more than the canopy fluxes, due to uncertainty and variance in the leaf photosynthesis, leaf nitrogen, canopy leaf area and canopy respiration measurements (figure 7.11 & Table 7.5).

The apparent decline in leaf photosynthetic capacity as the crop matured (figure 7.11) is in contrast to the approximately constant rate of measured daily canopy photosynthesis. Harley & Tenhunen (1991) also found significant seasonal variation in apparent leaf photosynthetic capacity of Quercus coccifera in response to water stress. One possible explanation is that the measured leaves in this study were not representative of all leaves in the canopy. It seems likely that the most exposed leaves at the top of the canopy, which were also those measured, were more subject to water stress than the rest of the leaves in the canopy. Dwyer and Stewart (1986) and Pattey et al. (1991) observed greater effect of water stress on more exposed leaves in corn fields and concluded that extensive sampling is necessary to extrapolate leaf measurements to the canopy scale, particularly with water stress conditions.

7.6. Conclusions

Diurnal variation of apparent photosynthetic capacity at both the leaf and canopy scale complicated application of the sun/shade model to this data set. The mechanistic Farquhar *et al.*, model of leaf photosynthesis does not include the effect of water stress. A simple regression model could describe the variation of photosynthetic capacity, but a mechanistically based, or more universal, model of this phenomena would be preferable.

Predictions from the sun/shade model of canopy photosynthesis mimicked the diurnal variation of measured canopy gross photosynthesis, accurately reproducing the canopy response to absorbed light (figures 7.14 & 7.15), but not the absolute canopy CO_2 flux, due to the difficulty of parameterising the model from leaf scale measurements. Despite the variability of leaf photosynthetic capacity, predicted daily canopy photosynthesis followed the day-to-day variation of measured daily gross canopy photosynthesis.

The major sources of uncertainty were leaf photosynthetic capacity, canopy leaf area measurements and estimates of canopy respiration from night-time CO_2 flux measurements. At high temperatures (>30°C) the temperature response of canopy respiration became an important factor, rising to 50% of the daily gross canopy photosynthesis. In future, estimates of canopy respiration during the day could be made by covering the tent with aluminium sheeting to block light and heat. Although there are uncertainties with this technique, such as post-illumination burst of respiration, it would at least provide some estimate of canopy respiration.

The sun/shade canopy model overcame the problems of big-leaf models, allowed incorporation of within-canopy profiles of photosynthetic capacity and was a reasonable predictor of canopy photosynthesis. The sun/shade canopy model presented here is a truly scaled version of the Farquhar *et al.* model of leaf photosynthesis. It is based on well understood leaf physiological processes that have measurable parameters, with known biological significance and requires no fitting at the canopy scale. The numerical simplicity of this canopy model will facilitate its incorporation into models to assess the effect of plant physiological traits on water-use efficiency or models of global carbon cycling.

7.7.   Appendix: Atmospheric attenuation of PAR

Data of diffuse light were not collected, but were estimated using the model of atmospheric attenuation of PAR (eq. 6.26). The atmospheric transmission coefficient (a), was estimated from the model of light scattering by the tent and an incidental measure of diffuse light in the tent. PAR was measured continuously inside the tents, which were constructed of an aluminium frame and plastic walls. As the sun traversed the sky, there were two occasions each day, at approx. 07:15 and 16:45, when the frame cast a shadow on the light sensor (figure 7.18). The diffuse light measured by the sensors on these occasions was used to calculate an atmospheric transmission coefficient as outlined below.

The ratio of measured irradiance to the extrapolated unhindered irradiance was used as a measure of the fraction of diffuse light in the tent (f_t) at the point of maximum shading. The fraction of diffuse light outside the tent (f_o) was calculated from f_t by use of a rearrangement of the model of light scattering by the tent (eq. 3.11);

$$f_o = f_w(1 - f_t)(1 - 1/\tau_t) + f_t,$$ (7.11)

where τ_t is the transmission coefficient of the side panel of the tent (eq. 3.10) and f_w is the fraction of light intercepted by the tent walls scattered into the tent (eq. 3.6). This value of f_o was then used to determine a by rearranging the model of atmospheric attenuation of light (eq. 6.26):

$$a = \left[\frac{1 - f_o}{1 + f_o(1/f_a - 1)} \right]^{1/m}.$$ (7.12)

where f_a is the proportion of forward scattering to the earth's surface by atmospheric attenuation of PAR and m is the optical air mass and is defined as the ratio of the mass of atmosphere traversed per unit cross-sectional area of solar beam to that traversed for a site at sea level if the sun were directly overhead (Campbell, 1977).
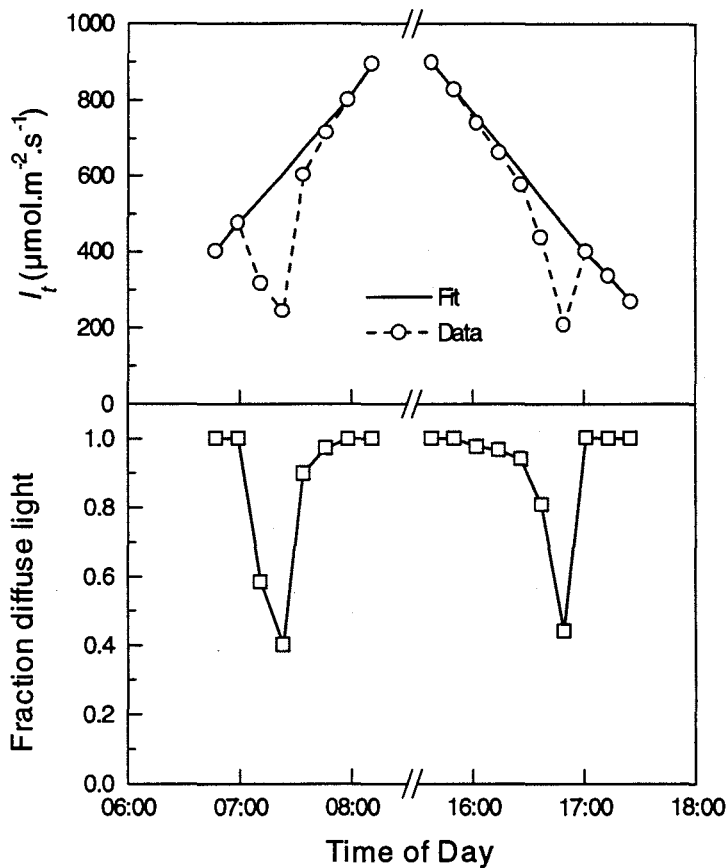
Figure 7.18 Light intensity in the tent, measured with a PAR sensor, as affected by shadows, that was used to determine fraction of diffuse light and to calculate the atmospheric transmission coefficient using eq. 7.12.

Values for a calculated for each day of measurements are given in Table 7.7. An example of the shading is shown in figure 7.18 for 25-Oct. Between the hours of 07:00 and 08:00 and again between 16:00 and 17:00, the irradiance measured by the PAR sensor dropped below the typical diurnal sinusoidal light curve. These times corresponded with a shadow cast on the sensor by the frame of the chamber. As the shadow moved across the sensor the apparent irradiance dropped as the sensor moves into penumbral shadow and reached a minimum in umbral shadow. Apparent irradiance increased as the sensor moved out through the penumbra and returned to the diurnal sinusoidal trace. At the minimum irradiance only diffuse light reached the sensor. The unshaded irradiance over this period was determined by extrapolating from the diurnal irradiance trace, allowing a calculation of the ratio of apparent to unhindered irradiance.

The minimum value of this ratio was used as a point measurement of f_t, which was adjusted for scattering of light by the tent and converted to f_o using eq. 7.11 and then converted to a using eq. 7.12 (Table 7.7).

Table 7.7 Atmospheric transmission coefficients calculated from shadows cast on the light sensor inside the tents.

Date	Matong		Quarrion	
	AM	PM	AM	PM
12/10		0.67		0.74
13/10	0.73		0.78	
17/10		0.66		0.73
18/10	0.72	0.75	0.75	0.74
24/10	0.71	0.68	0.72	0.71
25/10	0.75	0.72	0.73	0.70
26/10	0.77		0.75	
30/10		0.62		0.62
01/11	0.66	0.61	0.72	0.64

Atmospheric transmission coefficient (a)

Calculated values of a were different between morning and afternoon. This could be attributed to several factors. Most importantly the data may not have coincided with the point of maximum shading, so that the calculated diffuse light may have included a proportion of penumbral light. This would have led to an over-estimation of f_t and low values of a. Differences between sensors, due to different calibrations or different cosine responses, were probably small. Differences have existed between each tent due to unknown different amounts of dust on the walls with different scattering properties. The observed decrease in a through the day was expected as the humid planetary boundary layer increased in depth with increasing atmospheric attenuation. Data from days with high cirrus cloud (30-Oct to 01-Nov) show lower values of a as expected (Gates, 1980). Despite these limitations, values for a were adequate to use in the model of atmospheric attenuation to extrapolate estimates of f_o over the entire day, given that solar elevation was the major source of variation of f_o.

CHAPTER EIGHT:

COMBINED MODELS OF PHOTOSYNTHESIS,

CONDUCTANCE AND TRANSPIRATION

Chapter Contents

Summary

A combination equation model, for use with a two-layer canopy model that treats sunlit and shaded fractions of the canopy separately, is presented to determine transpiration and leaf temperatures of a canopy. It was combined with a Sun/Shade canopy model of gross canopy photosynthesis and a stomatal conductance model.

A comparison with a multi-layer canopy model demonstrated that the Sun/Shade canopy model, accurately partitioned the available energy between sensible and latent heat and between the sunlit and shaded fractions of the canopy. A simple single layer big leaf model overestimated canopy photosynthesis, particularly mid-morning and mid-afternoon, due to the averaging of the non-linear light response of photosynthesis.

Model predictions from the Sun/Shade canopy model, with three different parameterisation schemes, were compared with ten days data of canopy fluxes over a range of air temperatures and canopy leaf areas. When parameters were derived from the canopy data, the model reproduced canopy photosynthesis, stomatal conductance, sensible heat flux and transpiration very well (r = 0.92, 0.95, 0.86, 0.95 respectively). With parameters derived from leaf measurements, obtained concurrently with the canopy data, the model still performed well but with more scatter (r = 0.90, 0.64, 0.80, 0.84 respectively). Ignoring the daily variation of parameter values, to mimic *a priori* choice of parameters, introduced significant bias in the stomatal conductance predictions, but no more variability in the flux measurements (r = 0.91, 0.83, 0.73, 0.83 respectively).

The separate treatment of the sunlit and shaded fractions of the canopy in this model, allowed very good predictions of diurnal variation of photosynthesis and water use; as good as a multi-layer model but with far fewer calculations. It provided a significant improvement over single-layer big leaf models, and can be used with more confidence to explore canopy responses to changed environments as may occur with increasing atmospheric CO_2 concentrations.

The response of transpiration efficiency (ratio of gross canopy photosynthesis to canopy transpiration) to reduced stomatal conductance was predicted, by the sun/shade canopy model, to diminish at the canopy scale compared to the leaf scale, but the response to altered photosynthetic capacity was similar at the leaf and canopy scales. The modelled effect of canopy leaf area on direct soil evaporation had a large impact on water-use efficiency (ratio of net canopy CO_2 flux to total canopy evaporation).

8.1. Introduction

Scaling physiological process from leaves to canopies is important to understanding how plants with physiological traits that confer improved water-use efficiency (ratio of photosynthesis to evaporation) at the leaf scale, can benefit crops at the canopy scale. Recently, it has also been investigated from the perspective of understanding vegetation response to climate change (Ehleringer & Field, 1993; Jarvis, 1995). An essential part of scaling physiological processes are mathematical models. Mechanistic models of leaf scale processes that can be scaled to describe canopy processes are particularly powerful, because knowledge from the leaf scale can provide insight into the behaviour of the canopy scale processes (Norman, 1993). To be useful, models must be realistic, accurate and sufficiently simple to be parameterised; attributes, which are often incompatible (Raupach & Finnigan, 1988).

Earlier work showed that a simple Big Leaf model was unlikely to able to adequately reproduce the diurnal change of canopy photosynthesis (Chapter Five). This was found to be due to the highly non-linear response of photosynthesis to absorbed light. An alternative canopy model which treats sunlit and shaded fractions of the canopy separately was developed (the Sun/Shade canopy model), which overcame these problems and reproduced canopy data well (Chapter Six). This model still retained the advantage of being much simpler than a multi-layer model, although these also reproduced canopy data well.

Several models of stomatal conductance were compared with a set of leaf data (Chapter Four). Those that utilised the relationship between stomatal conductance and photosynthesis (Cowan, 1977; Ball et al., 1987; Leuning, 1995) were found to be better able to explain the data than those that only used environmental variables. These stomatal models were also found to adequately describe canopy conductance and transpiration (Chapter Five), although the value of the parameters were different at each spatial scale.

Having treated the photosynthesis and water use aspects of canopy physiology separately in these preceding chapters, it remains to combine them and validate their predictions against canopy scale data. The linkages between photosynthesis and water use through the intercellular CO_2 concentration and the energy balance need to be included. Since the radiation load on the sunlit and shaded leaves is very different, a leaf

energy balance for each fraction of the canopy needs to be used. Division of the combination equation for evaporation, and energy balance, between two sections of a canopy was demonstrated in sparse canopies, where the soil and foliage were treated separately (Shuttleworth & Wallace, 1985; Shuttleworth & Gurney, 1990). Such a scheme could be modified for use on the separate sunlit and shaded fractions of a canopy.

This chapter presents the Sunlit/Shade combination equation to combine the photosynthesis and evaporation models. It compares the Sun/Shade canopy model with a multi-layer model and with the simple Big Leaf model. Predictions from the Sun/Shade canopy model are then compared with ten days of data from a wheat canopy, with a range of air temperatures and canopy leaf area. The chapter then goes on to show model predictions of canopy responses to high CO_2 and changes of canopy leaf area. The Sun/Shade canopy model is used to compare the response of transpiration efficiency (ratio of gross canopy photosynthesis to canopy transpiration) to changes in stomatal conductance or photosynthetic capacity at both the leaf and canopy scales.

8.2. Methods

In combining the photosynthesis and water use models a leaf energy balance needs to be included since changes in stomatal conductance affect the partitioning of available energy between latent and sensible heat. Additionally, the radiation balance includes long-wave radiation which is affected by surface temperature. These effects are incorporated as describe below.

8.2.1. Leaf energy balance

Changes in surface temperature change the long-wave radiation ($\varepsilon_l\sigma T_l^4$) from the surface and affect the energy balance which in turn affects the available energy (Q) for evaporation. The feedback between surface temperature and evaporation rate can be incorporated into the combination equation by use of the isothermal net radiation concept,

$$
\begin{aligned}
Q &= I_{PAR} + I_{NIR} + L_d - L_u \\
&\cong Q_o - g_r C_p \Delta T
\end{aligned}
\tag{8.1}
$$

where I_{PAR} and I_{NIR} are the net absorbed PAR and NIR radiation, L_d and L_u are the long-wave radiation from the sky and the canopy respectively and Q_o is the isothermal net radiation (the available energy if leaf temperature were equal to air temperature, T_a),

$$
Q_o = I_{PAR} + I_{NIR} + L_d - \varepsilon_l \sigma T_a^4,
\tag{8.2}
$$

and g_r is a radiative conductance ($4\sigma\varepsilon_l T^3/C_p$), σ is the Stefan-Boltzmann constant, ε_l is the thermal emissivity of the leaf, T is air temperature, C_p is the isobaric specific heat of air, ΔT is the temperature difference between the leaf and air outside the boundary layer ($T_l - T_a$) and the last term of eq. 8.1 accounts for the additional radiation exchange as a result of the difference between leaf and air temperatures. Note exchange of thermal radiation is assumed to be significant from only one side of the canopy, the upper surface exposed to the sky.

Introducing this concept into the combination equation results in the expression for evaporation rate (E_l) (Cowan cited in; Jones, 1976) (see appendix for details),

$$E_l = \frac{\varepsilon r^*_{bH} Q_o / L + D}{r_s + r_b + \varepsilon r^*_{bH}} .$$

(8.3)

where ε is the rate of increase in the latent heat content of saturated air with increase in sensible heat content, L is the latent heat of vaporisation of water, D is the water vapour concentration deficit of the air outside the boundary layer, r_s is the stomatal resistance, r_b is the boundary layer resistance and r^*_{bH} is the combined resistance to sensible and radiative heat transfer in parallel $(1/(1/r_{bH} + g_r))$.

Related equations can also be derived for the surface temperature and sensible heat flux (H) (see appendix for details),

$$\Delta T = \frac{r^*_{bH}(Q_o(r_s + r_b) - LD)}{C_p(r_s + r_b + \varepsilon r^*_{bH})} .$$

(8.4)

$$H = C_p \Delta T / r_{bH}$$

(8.5)

7.2.2.4.3. Leaf boundary layer resistances

Conductance to sensible heat transfer across a leaf boundary layer under forced convection (g_{bHw}) is given as (Jones, 1992)

$$g_{bHw} = 1/r_b = 0.01(u/w_l)^{\frac{1}{2}} P/(RT_k)$$

(8.6)

where the conductance is the reciprocal of the resistance (r_b), u is the wind speed, w_l is the dimension of the leaf in the direction of the wind (typically 0.02 m for wheat leaves, in this study) and the empirical coefficient has a value of 0.01.

7.2.2.4.4. Boundary layer conductance in free convection

At low wind speeds leaf temperature can increase so that free convection is a significant factor that needs to be considered in calculating leaf boundary layer conductances. Monteith (1973) showed that for free convection the leaf boundary layer conductance is

$$g_{bHf} = 0.5 D_H \, G_r^{1/4} / w_l \cdot P/(RT_k)$$ (8.7)

in which D_H is the molecular diffusivity for heat and the Grashof number (G_r) is

$$G_r = 1.6 \times 10^8 |T_l - T_a| w_l^3$$ (8.8)

where T_l and T_a are leaf and air temperatures respectively.

Total boundary layer conductance to heat is obtained by adding the forced and free convection components in parallel,

$$g_{bH} = g_{bHw} + g_{bHf} .$$ (8.9)

Boundary layer conductance to transfer of other entities (water vapour and CO_2) differs to that for heat. In forced convection the conversion from heat is in proportion to the ratio of diffusivities to the power 2/3, while in free convection the 3/4 power is appropriate (Bird et al., 1960) cited in (Finnigan & Raupach, 1987),

$$g_{bi} = g_{bHw} (D_H / D_i)^{2/3} + g_{bHf} (D_H / D_i)^{3/4} .$$ (8.10)

8.2.2. Combination equations for Sun/Shade canopy model

Applying the combination equation to separate sunlit and shaded fractions of the canopy, to determine evaporation and leaf temperature, is more complicated than with a big leaf model, because not all resistances apply to all fluxes. Shuttleworth and Wallace (1985) presented an evaporation model that could be applied to sparse canopies with evaporation from the soil as well as the foliage. I have adapted their model to be used for separate sunlit and shaded layers within the canopy.

8.2.2.1. Resistance framework

The canopy is considered to have two classes of leaves; sunlit and shaded, with different radiation, stomatal conductance and leaf temperatures. Resistance to transfer of water vapour, heat and CO_2 in the two-layer system is given in figure 8.1.
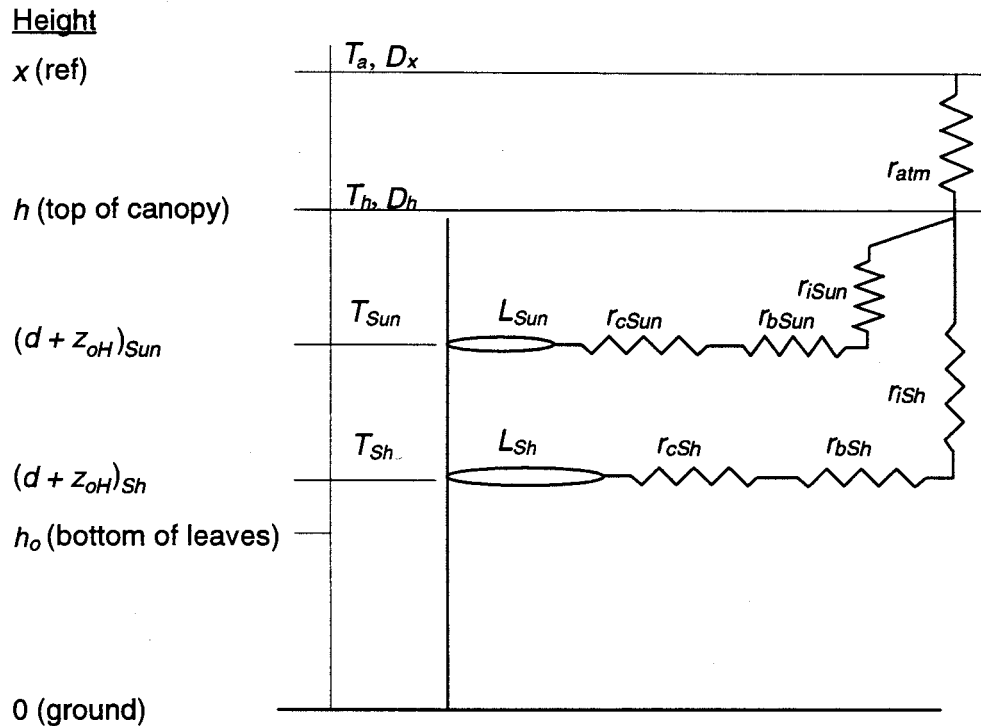
Figure 8.1 Schematic diagram of resistances (r), temperatures (T) and water vapour deficit (D) for a 2-layer model of canopy evaporation. Subscripts refer to values associated with: Sun - sunlit fraction of canopy, Sh - shaded fraction of canopy, c - canopy stomatal, b - leaf boundary layer, i - within canopy and atm - atmospheric.

Resistances to transport in the turbulent boundary layer above and within the canopy are assumed to be equal for heat, water vapour and CO_2, yet different in leaf boundary layers (which are assumed to be effectively laminar (Finnigan & Raupach, 1987)) in proportion to the ratio of molecular diffusivities to the $^2/_3$ power (Bird et al., 1960). Individual leaves have a stomatal and boundary layer conductance, which are assumed to act in parallel with other leaves in the canopy. (The impact of alternative assumptions for leaf to canopy scaling of stomatal conductance, such as those suggested by McNaughton (1994) and Raupach (1995) are discussed later.) Within-canopy transport is described by K-theory, which despite being invalid in some situations (Denmead & Bradley, 1985) has been shown to given acceptable results (Dolman & Wallace, 1991; Van den Hurk & McNaughton, 1995). The transport coefficient, K, is integrated to the top of the canopy to give a within-canopy resistance to transfer. Resistance to transfer

from the top of the canopy to the reference height is given by integration of an assumed log profile of wind speed, ignoring stability corrections (which were insignificant in the situations studied here, see figure 5.2).

Use of the Penman-Monteith equation in a two-layer system requires definition of a water vapour deficit, D (mol/mol), at the point at which the two layers have a common path of transport, in this case the top of the canopy, h. Water vapour deficit at the top of the canopy, D_h, is calculated from the water vapour deficit at the reference height, D_x, the above-canopy aerodynamic resistance, r_{atm}, and the total evaporation rate, E, such that,

$$\begin{aligned} D_h &= D_x - (\varepsilon + 1)r_{atm}\left(E - E_q\right) \\ &= D_x - (\varepsilon + 1)r_{atm}E + \varepsilon r_{atm}Q/L \end{aligned} \tag{8.11}$$

where $E_q = \varepsilon Q/(L(\varepsilon+1))$, is the equilibrium evaporation rate (which is the rate of evaporation that occurs if the overlying atmosphere is in full adjustment with the underlying surface).

Utilizing the isothermal net radiation form of the combination equation (Jones, 1976), expressions can be written for the latent heat flux from the sunlit leaf portion of the canopy,

$$LE_{Sun} = \left(\varepsilon r^*_{aSun}Q_{oSun} + LD_h\right)/\left(r_{cSun} + r_{aSun} + \varepsilon r^*_{aSun}\right), \tag{8.12}$$

and the shaded leaf portion of the canopy,

$$LE_{Sh} = \left(\varepsilon r^*_{aSh}Q_{oSh} + LD_h\right)/\left(r_{cSh} + r_{aSh} + \varepsilon r^*_{aSh}\right). \tag{8.13}$$

where r_{cSun} and r_{cSh} are the canopy stomatal resistances for the sunlit and shaded portions of the canopy, r_{aSun} and r_{aSh} are the leaf-boundary layer and within-canopy resistances to sensible heat transfer in series $(r_b + r_i)$ for the sunlit and shaded portions of the canopy, and r^*_{aSun} and r^*_{aSh} are the combined leaf-boundary layer and within-canopy resistances with the additional parallel conductance of radiative heat transfer for the sunlit and shaded portions of the canopy,

$$r_{aSun}^* = \frac{1}{1/(r_{bSun} + r_{iSun}) + g_{rSun}},$$

(8.14)

$$r_{aSh}^* = \frac{1}{1/(r_{bSh} + r_{iSh}) + g_{rSh}}.$$

(8.15)

Q_o is the isothermal available energy and g_r is the associated radiative conductance for the sunlit and shaded fractions of the canopy as explained in the Appendix.

8.2.2.2. Two-layer evaporation

A simple expression for D_h using isothermal radiation, can not be obtained. Instead, iteration with the solution for surface temperature is used to determine Q in eq. 8.11. Substitution of D_h (eq. 8.11) into the expressions for LE_{Sun} and LE_{Sh} (eqs. 8.12 & 8.13) leads to

$$LE_{Sun} = \left(\varepsilon r_{aSun}^* Q_{oSun} + L(D_x - E(\varepsilon + 1)r_{atm}) + \varepsilon r_{atm} Q\right) / \left(r_{cSun} + r_{aSun} + \varepsilon r_{aSun}^*\right),$$

(8.16)

$$LE_{Sh} = \left(\varepsilon r_{aSh}^* Q_{oSh} + L(D_x - E(\varepsilon + 1)r_{atm}) + \varepsilon r_{atm} Q\right) / \left(r_{cSh} + r_{aSh} + \varepsilon r_{aSh}^*\right).$$

(8.17)

Total evaporation is given by $LE = LE_{Sun} + LE_{Sh}$. Collecting terms of LE and simplifying with the definitions; $R_{Sun} = r_{cSun} + r_{aSun} + \varepsilon r_{aSun}^*$, $R_{Sh} = r_{cSh} + r_{aSh} + \varepsilon r_{aSh}^*$ and $R_a = (\varepsilon + 1)r_{atm}$ leads to the evaporation model for two layers (see Appendix), which can be written so that both components converge to a Penman-Monteith type equation when either R_{Sun} or R_{Sh} are infinite,

$$LE = C_{Sun}P_{Sun} + C_{Sh}P_{Sh},$$

(8.18)

where the terms are given as

$$C_{Sun} = R_{Sh}(R_{Sun} + R_a) / \left(R_{Sun}R_{Sh} + R_a(R_{Sun} + R_{Sh})\right),$$

(8.19)

$$C_{Sh} = R_{Sun}(R_{Sh} + R_a) / \left(R_{Sun}R_{Sh} + R_a(R_{Sun} + R_{Sh})\right),$$

(8.20)

$$P_{Sun} = \left(\varepsilon r^*_{aSun} Q_{oSun} + LD_x + \varepsilon r_{atm} Q\right) / \left(r_{cSun} + r_{aSun} + \varepsilon r^*_{aSun} + (\varepsilon + 1) r_{atm}\right), \tag{8.21}$$

$$P_{Sh} = \left(\varepsilon r^*_{aSh} Q_{oSh} + LD_x + \varepsilon r_{atm} Q\right) / \left(r_{cSh} + r_{aSh} + \varepsilon r^*_{aSh} + (\varepsilon + 1) r_{atm}\right). \tag{8.22}$$

8.2.2.3. Two-layer surface temperature

As with the evaporation calculations, surface temperature calculations require determination of the temperature at the top of the canopy, T_h. Beginning with the sensible heat flux, H, between h and x,

$$H = C_p \left(T_h - T_x\right) / r_{atm} \tag{8.23}$$

and introducing the energy balance, $Q = LE + H$, and isothermal radiation results in

$$Q_o - g_r C_p \left(T_h - T_x\right) - LE = C_p \left(T_h - T_x\right) / r_{atm} \tag{8.24}$$

Rearrangement results in the expression for T_h,

$$T_h = T_x + r^*_{atm} \left(Q_o - LE\right) / C_p, \tag{8.25}$$

where r^*_{atm} is the combined atmospheric resistance to sensible and radiative heat transfer in parallel ($1/(1/r_{atm} + g_r)$). The same equation can be rewritten for the temperatures of the sunlit fraction of the canopy,

$$T_{Sun} = T_h + r^*_{aSun} \left(Q_{oSun} - LE_{Sun}\right) / C_p, \tag{8.26}$$

and of the shaded fraction of the canopy,

$$T_{Sh} = T_h + r^*_{aSh} \left(Q_{oSh} - LE_{Sh}\right) / C_p. \tag{8.27}$$

8.2.2.4. Calculation of boundary layer resistances

7.2.2.4.1. Above canopy resistance

The atmospheric resistance to turbulent transport from the top of the canopy to the reference height, r_{atm}, is calculated assuming a log profile of wind speed (u_z),

$$u_z = \frac{u_*}{k} \ln\left(\frac{z-d}{z_{oM}}\right) \tag{8.28}$$

where u_* is the friction velocity, k is von Karman's constant (0.41), z is the height above the ground, d is the zero plane displacement in the canopy and z_{oM} is the surface roughness of the canopy for momentum transfer. An expression for u_* is obtained by rearrangement of eq. 8.28,

$$u_* = u_x k \left/ \ln\left(\frac{x-d}{z_{oM}}\right) \right. \tag{8.29}$$

where u_x is wind speed at the reference height, x.

Diffusivity for momentum transfer, K_M, is assumed as

$$K_M = k u_*(z-d), \text{ for } z > h. \tag{8.30}$$

Integration of the momentum flux over the height interval from h to x leads to the definition of the aerodynamic resistance to momentum, which combined with the above definitions gives,

$$r_{atm} = r_a(h,x) = \frac{RT_k}{P} \int_h^x \frac{dz}{K_M} = \frac{RT_k}{Pk^2 u_x} \ln\left(\frac{x-d}{z_{oM}}\right) \ln\left(\frac{x-d}{h-d}\right). \tag{8.31}$$

The term RT_k/P converts to molar units, where R is the universal gas constant (8.314 J.K^{-1}.mol^{-1}), T_k is the absolute air temperature and P is atmospheric pressure (Pa).

7.2.2.4.2.   Within canopy resistances

Below the top of the canopy the transfer coefficient is assumed to follow an exponential profile as a function of height in the canopy,

$$K_M = K_h \exp\left(-n(1 - z/h)\right), \text{ for } z < h \tag{8.32}$$

where n is a constant $(= 2.5)$ and K_h is obtained by combining eqs. 8.31 & 8.32,

$$K_h = ku_*(h - d) = k^2 u_x (h - d) \Big/ \ln\left(\frac{x - d}{z_{oM}}\right). \tag{8.33}$$

(However Thom, (1971) found that K is almost constant within the canopy, as the drag coefficient of individual elements increases at slower wind speeds deeper in the canopy. This alternative scheme was also used to evaluate the model.)

As described earlier, the resistance to transfer over a height interval is given as

$$
\begin{aligned}
r_i = r_a(z_1, z_2) &= \frac{RT_k}{P} \int_{z_1}^{z_2} \frac{dz}{K_M} = \frac{RT_k}{PK_h} \int_{z_1}^{z_2} \exp\left(n(1 - z/h)\right) dz \\
&= \frac{RT_k}{P} \frac{\ln\left((x - d)/z_{0m}\right)}{k^2 u_x (h - d)} \frac{h}{n} \left(\exp\left(n(1 - z_2/h)\right) - \exp\left(n(1 - z_1/h)\right)\right)
\end{aligned}
\tag{8.34}
$$

The fraction of leaves at any depth in the canopy that is sunlit, f_{Sun}, is given by the penetration of direct beam light in the canopy, $\exp(-k_b L)$. The total fraction of the canopy that is sunlit, f_{cSun}, is given as the integral of f_{Sun} over the whole canopy leaf area,

$$f_{cSun} = \int_0^{L_c} f_{Sun} dL \Big/ L_c = \int_0^{L_c} \exp\left(-k_b L\right) dL \Big/ L_c = \left(1 - \exp\left(-k_b L_c\right)\right) / \left(k_b L_c\right). \tag{8.35}$$

In compliment to the sunlit fraction is the fraction of canopy that is shaded, $f_{cSh} = 1 - f_{cSun}$.

Within canopy resistance for the sunlit and shaded fractions of the canopy are calculated by assuming that they are at different levels, $(d + z_o)_{Sun}$ and $(d + z_o)_{Sh}$ respectively, which are calculated assuming that for the whole canopy $d = 0.63h$ and $z_o = 0.13h$ (Monteith, 1973) and

$$d + z_o = 0.63h + 0.13h = 0.76h. \tag{8.36}$$

The mean sink height of the sunlit canopy fraction $(d + z_o)_{Sun}$ and shaded canopy fraction $(d + z_o)_{Sh}$ are given as

$$(d + z_o)_{Sun} = h(1 - 0.24 f_{cSun}),$$ (8.37)

$$(d + z_o)_{Sh} = h_o + f_{cSh}(0.76h - h_o),$$ (8.38)

where h_o is the mean height of the lowest leaves in the canopy. These definitions result in $(d + z_o)_{Sun}$ varying from $0.76h$, if all the canopy were sunlit $(f_{cSun} = 1.0)$, to h when f_{cSun} approaches zero. Conversely, $(d + z_o)_{Sh}$ varies from $0.76h$, if all the canopy were shaded $(f_{cSun} = 0.0)$, to h_o when f_{cSh} approaches zero.

7.2.2.4.5. Integrated canopy boundary layer conductance

Since the leaves act in parallel, the bulk leaf boundary layer conductance is obtained by integration over the canopy leaf area. This requires a wind profile within the canopy, which was earlier implicitly defined as a function of height in the canopy (eq. 8.32). However, to integrate over the canopy leaf area requires a wind profile defined on a cumulative leaf area basis. The inter-conversion between height and leaf area profiles of wind speed requires a profile of leaf area density. Assuming a typical leaf area density profile (Norman, 1979), the wind profile could be approximated by a simple expression

$$u_z = u_h \exp(-k_u L), \text{ for } z < h,$$ (8.39)

where k_u $(= 0.5)$ is the within-canopy wind extinction coefficient and u_h is the wind speed at the top of the canopy,

$$u_h = u_z \ln((h - d)/z_{oM})/\ln((x - d)/z_{oM}).$$ (8.40)

The bulk leaf boundary layer conductance (G_b) is obtained by combining the above expressions and integrating over the depth of the canopy,

$$1/R_b = G_b = \int_o^{L_c} g_{b(z)} dL = g_{b(h)} \int_o^{L_c} \exp(-0.5L)^{\frac{1}{2}} \cdot dL$$
$$= (u_h/w_l)^{\frac{1}{2}}/100 \cdot P/(RT_k)(1 - \exp(-0.25L))/0.25$$ (8.41)

The bulk leaf boundary layer conductance for the sunlit fraction (G_{bSun}) is obtained by integrating with the fraction of sunlit leaves, $f_{Sun} = \exp(-k_b L)$ over the canopy,

$$1/R_{bsun} = G_{bsun} = \int_o^{L_c} g_{b(z)} f_{sun} dL = g_{b(h)} \int_o^{L_c} \exp(-0.5L)^{\frac{1}{2}} \cdot \exp(-k_b L) \cdot dL$$
$$= (u_h/w_l)^{\frac{1}{2}} / 100 \cdot P/(RT_k)(1 - \exp(-(0.25 + k_b)L_c)) / (0.25 + k_b)$$

(8.42)

The bulk leaf boundary layer conductance for the shaded fraction of the canopy (G_{bSh}) is calculated as the difference between the bulk leaf boundary layer conductance and the sunlit fraction leaf boundary layer conductance; $G_{bSh} = G_b - G_{bSun}$.

8.2.3. Within-Canopy Profiles for the Multi-Layer Model

The Sun/Shade canopy model was evaluated by comparison with a multi-layer model. In addition to light penetration, leaf photosynthesis, stomatal conductance and leaf energy balance which were described previously, the sensible and latent heat fluxes and the CO_2 flux generate within-canopy profiles of T_a, c_a and water vapour concentration, w_a. These profiles are also affected by soil fluxes.

Soil evaporation (E_{soil}) was estimated as the equilibrium evaporation rate driven by the available energy at the soil surface (Q_{soil}) (Black *et al.*, 1970), which was calculated from the incident light, canopy absorption and the measured ground heat flux (G). Sensible heat flux from the soil (H_{soil}) was calculated as $Q_{soil} - LE_{soil}$. Soil and canopy respiration were estimated from measurements of CO_2 fluxes at night, with temperature corrections (Chapter Seven). No information of the source distribution of the respiration was available so respiration was assumed to occur entirely at the ground surface.

The resistance to within canopy transport between two levels was calculated from the transport coefficient K as described earlier (eq. 8.34). Profiles were generated by iteratively calculating fluxes and profiles. Initial estimates of the flux distributions were made assuming no canopy profiles. These were then used to generate profiles beginning from the top of the canopy and proceeding to the bottom. Flux calculations were repeated and new profiles generated until stable values were achieved. Use of a damping function resulted in stable solutions after approximately four iterations.

8.3. Results and Discussion

An analysis of the multi-layer model is presented in the first section, followed by an analysis of the Sun/Shade canopy model, which was compared with the Multi-Layer model. The Sun/Shade canopy model was then compared with canopy data using three different parameterisation schemes: parameters derived from canopy scale data (*ie*. fitting the model to the data); parameters for each day derived from leaf data; and single values of parameters derived from leaf data of all days combined (*ie*. typical for this vegetation, but without detailed day-to-day variations).

8.3.1. Multi-Layer Model

The multi-layer model was run assuming a uniform leaf-angle distribution divided into three leaf-angle classes ($\overline{\alpha} = 21°$, 47°, 76° from horizontal, see Chapter Six) in layers of 0.5 leaf area ($m^2.m^{-2}$) with data from 25-Oct-90 at 12:00 for the Matong cultivar of wheat. Model predictions for the three leaf-angle classes of sunlit leaves were averaged after weighting by their fractional leaf area (f_α = 0.13, 0.37, 0.50). Within-canopy profiles of leaf-scale variables (per unit leaf area) for sunlit leaves, shaded leaves and the average are shown in figures 8.2 & 8.3.

Available energy (Q) was nearly constant with depth in the canopy for both sunlit and shaded leaves, but the weighted average decreased because the fraction of sunlit leaves decreased with depth in the canopy. The profile of absorbed PAR (I_l) was steeper than the profile of Q, a reflection of more rapid attenuation of PAR than near infra-red wavelengths. Shaded leaves had a negative sensible heat flux, absorbing heat from the air, while sunlit leaves all had positive sensible heat fluxes. Sensible heat increased with depth, because stomatal conductance decreased and the leaf boundary layer conductances decreased with lower wind speeds deeper in the canopy. However, the weighted average of sensible heat flux for all leaves was nearly constant with depth.

Photosynthesis of the shaded leaves was only 5 $\mu mol.m^{-2}.s^{-1}$ lower than the sunlit leaves. This occurred despite the contrast in I_l, and is a reflection of the light saturation of the sunlit leaves. Lower Q on the shaded leaves resulted in lower T_l, and lower D which offset the lower photosynthesis so that the conductance of shaded leaves was only slightly lower (0.1 $mol.m^{-2}.s^{-1}$) than that of the sunlit leaves. This led to lower c_i (>20 $\mu mol.mol^{-1}$) in sunlit leaves compared with shaded leaves.
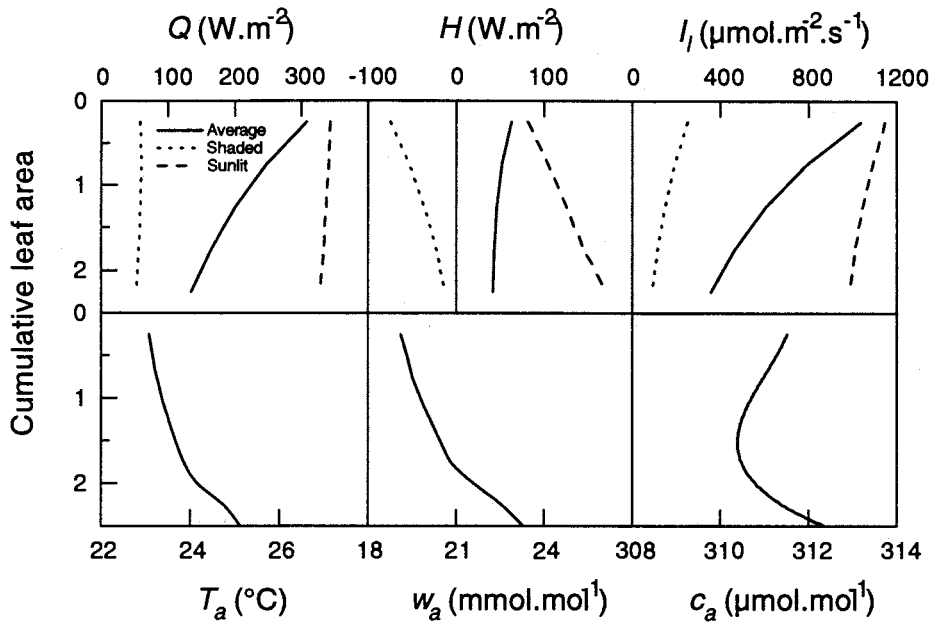
Figure 8.2 Within canopy profiles of available energy (Q), sensible heat flux (H), absorbed PAR (I_l), air temperature (T_a), water vapour concentration (w_a) and atmospheric CO_2 concentration (c_a). for sunlit (- - -), and shaded (·····) leaves and the average (——) (weighted by the sunlit leaf area fraction) as a function of cumulative leaf area. Fluxes are expressed per unit leaf area.
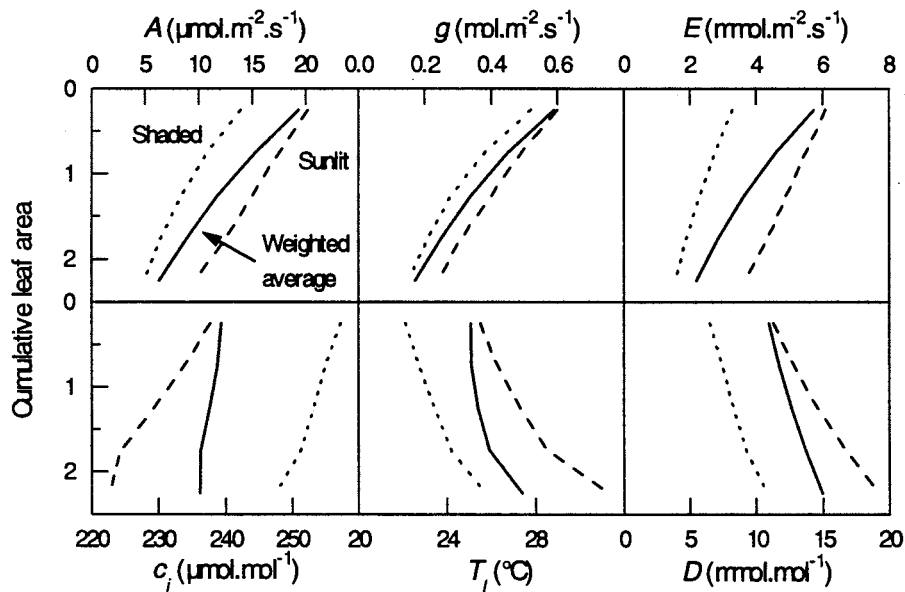
Figure 8.3 Within canopy profiles of leaf photosynthesis (A), leaf stomatal conductance (g), leaf evaporation (E), intercellular CO_2 concentration (c_i), leaf temperature (T_l) and leaf-to-air water vapour difference (D_l). for sunlit (- - -), and shaded (· ·) leaves and the average (——) (weighted by the sunlit leaf area fraction). Fluxes are per unit leaf area.

Both T_l and D increased steeply with depth for both sunlit and shaded leaves, while the weighted averages increased more gradually with depth. The decrease of c_i with depth was more rapid on the sunlit leaves than the shaded leaves, while the average was nearly constant with depth.

Both T_a and w_a increased with depth in the canopy in accordance with upward fluxes of latent and sensible heat from the leaves and soil, which were more apparent as a function of height (figure 8.4). The leaves of the canopy were only present between 0.5 to 0.8 m above the ground and the top of the canopy was at 1.0 m. The profile of c_a showed a decrease at the top of the canopy associated with the leaves and their photosynthetic sink for CO_2 and an increase in c_a beneath the lowest leaves associated with soil respiration acting as a CO_2 source. These modelled profiles of c_a and w_a resemble profiles measured in a similar wheat canopy at Wagga Wagga in the following year (Raupach et al., 1992; Denmead, 1995), although soil evaporation was much lower on that day because not rain had fallen for several days, resulting in shallower profiles of water vapour within the canopy.

Specifying cause and effect in this canopy model is complicated by the feedback loops generated by the leaf and canopy boundary layers and the interdependence of
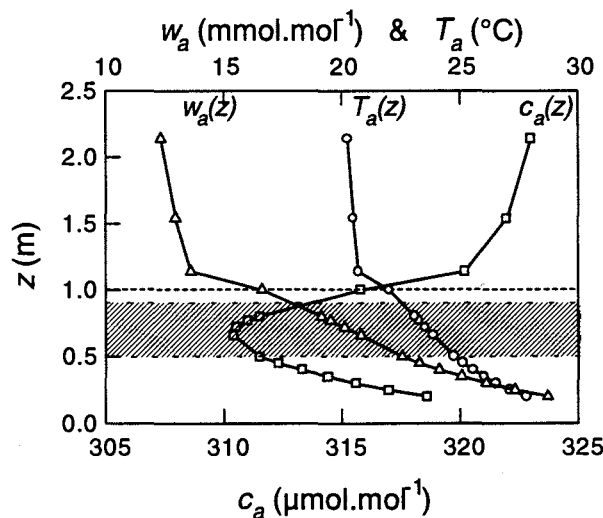
Figure 8.4 Multi-layer model predictions of within-canopy profiles of air temperature (T_a), water vapour concentration (w_a) and CO_2 concentration (c_a) with height (z). Models parameters as in figure 8.2. Dotted line indicates the top of the canopy. The shaded area represents the height of the leaves.

photosynthesis and conductance. Analysis of these loops and feedbacks is presented later. Use of K-theory to describe within-canopy transport has been shown to be deficient where gusts of wind or large scale eddies penetrate the canopy infrequently (Denmead & Bradley, 1985). Lagrangian modelling techniques developed by Raupach (1989) predict the concentration profiles as the sum of contributions from 'near-field' components, described by diffusion theory, and 'far-field' components, for which diffusion is inappropriate. Comparisons of predicted within-canopy profiles from K-theory and the Raupach model have shown that K-theory adequately describes the 'far-field' component which is much larger than the 'near-field' component and so reasonably approximates the profiles generated by the more physically correct model (Van den Hurk & McNaughton, 1995) and that errors from use of K-theory are minimal (Dolman & Wallace, 1991).

8.3.1.1. Effect of free convection

At low wind speeds leaf boundary layer conductance due to forced convection is very low. If such leaves also receive high radiation, their leaf temperature can increase dramatically so that free convection, driven by the heating of the air and its buoyancy,
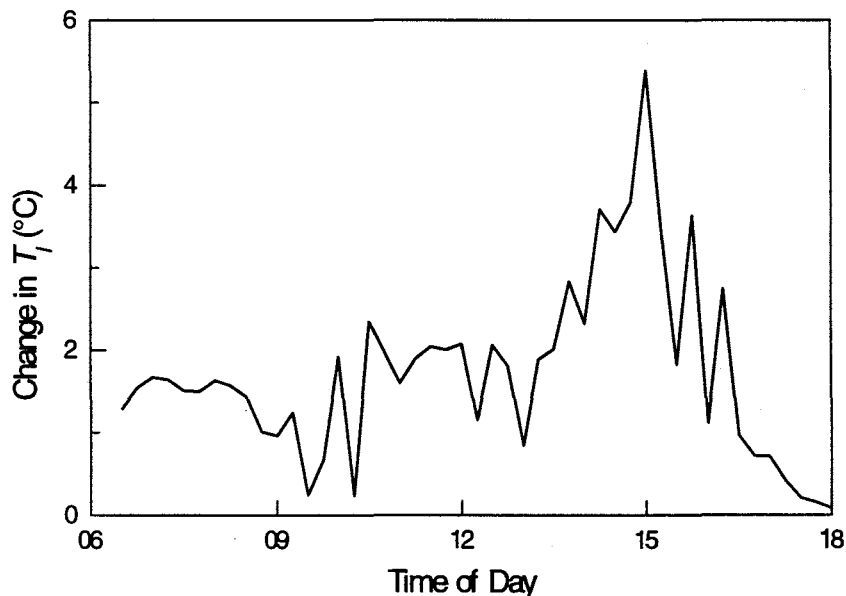
Figure 8.5 Effect of not including free convection in the leaf energy balance on leaf temperature (T_l). The effect is shown for sunlit leaves at a leaf angle nearly perpendicular (21°) to the solar beam at the bottom of the canopy for the Matong canopy on 25-Oct-90.

becomes significant. Free convection then prevents extreme leaf-to-air temperature differences from occurring. The effect is demonstrated in figure 8.5, where modelled leaf temperature was from 2 - 5 °C warmer if free convection was ignored in the leaf energy balance. The effect of free convection is greater for leaves deep in the canopy where wind speeds are slower and stomatal conductance is small (due to lower photosynthetic capacity); in particular those leaves that are sunlit receiving the highest radiation load.

8.3.1.2. Effect of temperature

On days with hot ambient air temperatures, it was apparent that the model overestimated stomatal closure, so that leaf temperature rose rapidly and canopy evaporation and photosynthesis were greatly reduced (figure 8.6). It appears that the stomatal model was too sensitive to D_l, predicting unrealistic midday stomatal closure. However, using any of the stomatal response functions to humidity (based on rh, D_l or $\sqrt{D_l}$) produced similar results. Only when the stomatal model was fitted to the canopy data for that day ($g = 0.01 + 0.474A/(c\text{-}\Gamma)(83+D_l)$, $r^2 = 0.88$) did the model have
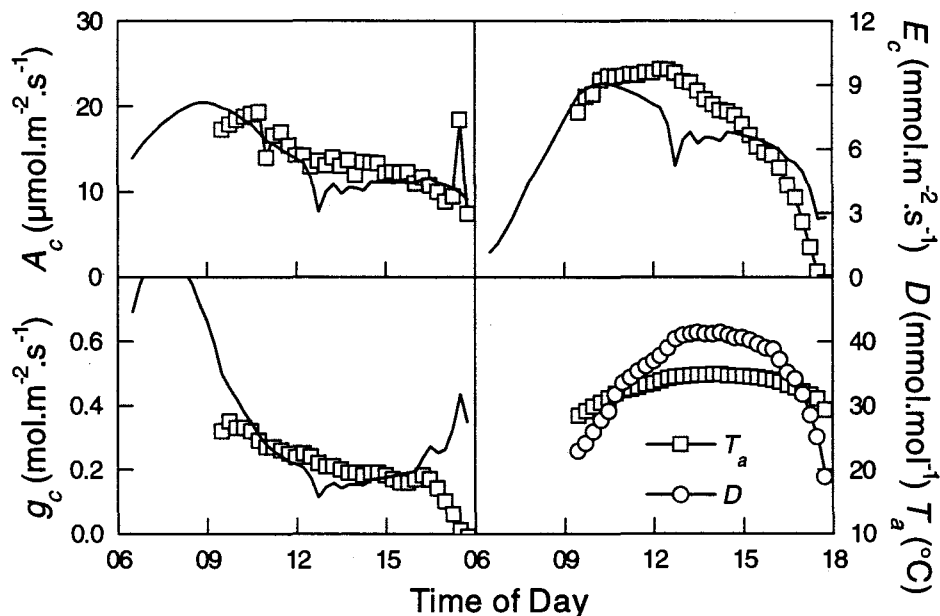
Figure 8.6 Fluxes measured by the Bowen ratio system (——□——) and model predictions (———) of gross canopy photosynthesis (A_c), conductance (G_c) and transpiration (E_c) for the Matong canopy on 30-Oct. Also shown are the measured ambient air temperature (T_a) and water vapour concentration deficit of the air (D) 0.6 m above the top of the canopy.

reasonable predictions. Yet, even using these fitted parameters the model became unstable when ambient air temperature was increased by only 2°C. This behaviour suggested that the model had some unrealistic temperature response, but which component was not readily apparent.

The behaviour of the model, at high temperatures, was explored by changing T_a with constant humidity and all other factors held constant at their midday values (*ie. I & u*). At high T_a (~ 34°C) and D_l modelled photosynthesis abruptly declined, stomata closed, c_i increased and leaf temperature rose (figure 8.7). The cause of this behaviour was not
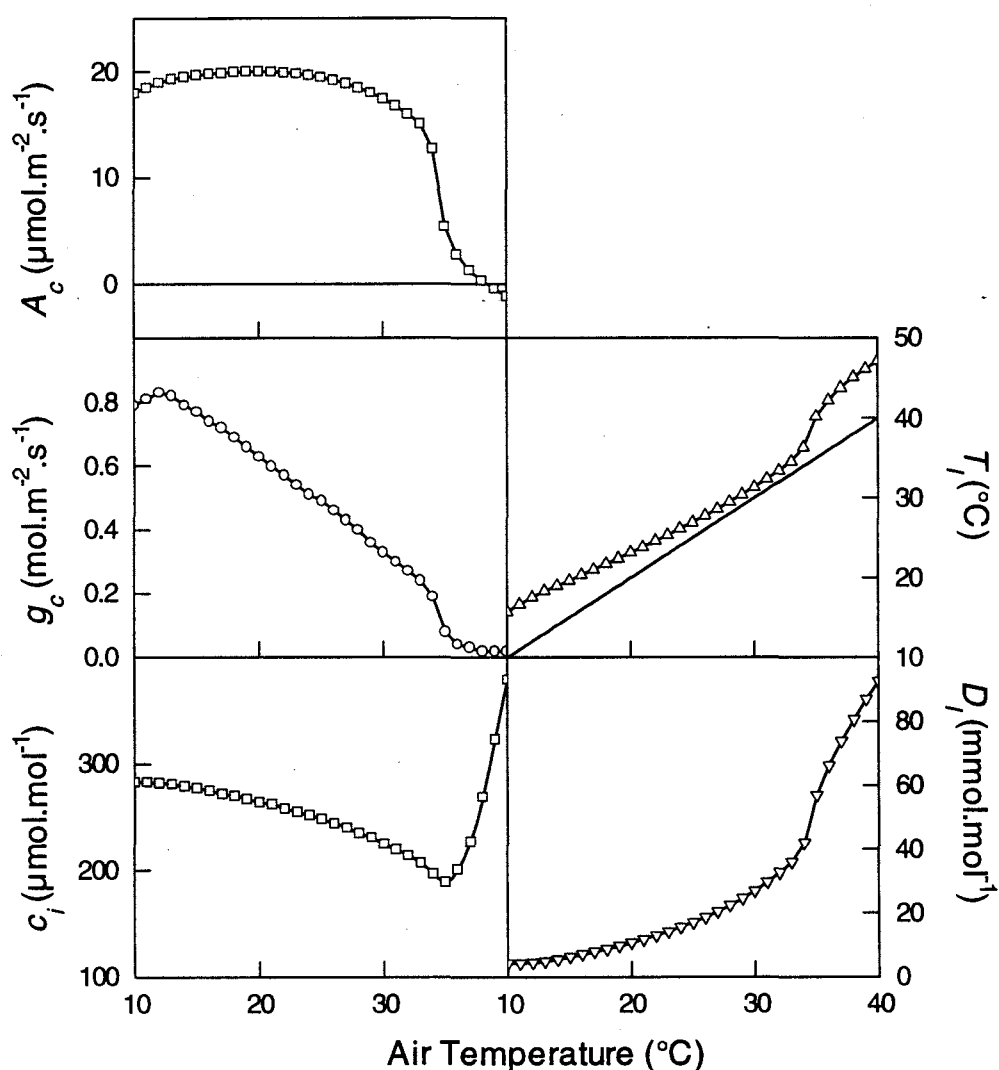
Figure 8.7 Modelled response of canopy photosynthesis, stomatal conductance and leaf temperature to air temperature.

292

readily apparent, due to the many interacting feedback loops in the model. These loops were analysed using control theory as described below.

8.3.1.3. Gain of the feedback loops involving photosynthesis, conductance and the leaf energy balance

The feedback loop through the leaf energy balance is outlined in figure 8.8. Leaf temperature affects photosynthesis and leaf-to-air water vapour deficit, which both determine stomatal conductance, which in turn partitions available energy between evaporation and sensible heat and so determines leaf temperature completing the loop. There are two additional loops involving the feedback from photosynthesis and stomatal conductance via p_i.
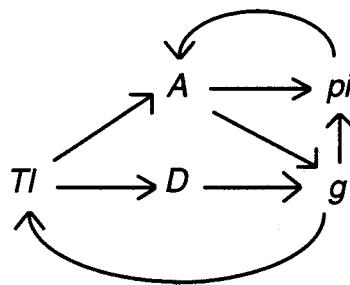
Figure 8.8 Feedback loops of the leaf energy balance, photosynthesis (A), stomatal conductance (g) and intercellular CO_2 partial pressure (p_i) as implemented in the canopy model.

Control theory was used in the analysis of the behaviour of these loops. It examines the effect of perturbations to the system through use of partial differentials, calculated with other factors remaining constant. The stability of feedback systems is assessed by the loop gain, which is the amplification of a perturbation to a variable through the loop. Gains greater than 1 lead to the system becoming unstable, while a gain of zero means that no feedback occurs and a gain less than -1 can result in unstable oscillations, depending on the time lags in the system. Stable systems have gains between -1 and +1.

The A-p_i loop gain (G_A) was calculated as

$$G_A = \left|\frac{\partial A}{\partial p_i}\right|_{T_l} \left|\frac{\partial p_i}{\partial A}\right|_g ,$$

(8.43)

and the A-g-p_i loop gain (G_g) was

$$G_g = \left|\frac{\partial p_i}{\partial g}\right|_A \left|\frac{\partial A}{\partial p_i}\right|_{T_l} \left|\frac{\partial g}{\partial A}\right|_D .$$

(8.44)

The A/D-g-T_l loop gain (G_T) was determined from the perturbation to A (dA) as

$$dA = \left|\frac{\partial A}{\partial T_l}\right|_{p_i} dT_l + \left|\frac{\partial A}{\partial p_i}\right|_{T_l} \left(\left|\frac{\partial p_i}{\partial A}\right|_g dA + \left|\frac{\partial p_i}{\partial g}\right|_A dg \right) ,$$

(8.45)

which was rearranged to

$$dA = \left(\left|\frac{\partial A}{\partial T_l}\right|_{p_i} dT_l + \left|\frac{\partial A}{\partial p_i}\right|_{T_l} \left|\frac{\partial p_i}{\partial g}\right|_A dg \right) \Big/ (1 - G_A) .$$

(8.46)

Similarly the perturbation to g (dg) was calculated as

$$dg = \left|\frac{\partial g}{\partial A}\right|_D dA + \left|\frac{\partial g}{\partial D}\right|_A dD .$$

(8.47)

Substitution for dA and rearranging lead to

$$dg = \left(\left|\frac{\partial g}{\partial A}\right|_D \left|\frac{\partial A}{\partial T_l}\right|_{p_i} dT_l + \left|\frac{\partial g}{\partial D}\right|_A dD(1 - G_A) \right) \Big/ (1 - G_A - G_g) .$$

(8.48)

Further substitution for dT_l and dD then lead to

$$G_T = \frac{\partial T_l}{\partial g} \left(\left|\frac{\partial A}{\partial T_l}\right|_{p_i} \left|\frac{\partial g}{\partial A}\right|_D + \frac{\partial D}{\partial T_l} \left|\frac{\partial g}{\partial D}\right|_A (1 - G_A) \right) \Big/ (1 - G_A - G_g) .$$

(8.49)

Evaluation of these equations as a function of temperature showed that none of the loop gains were greater than 1 (figure 8.9), meaning that system never became completely unstable. However, the abrupt decrease in A (figure 8.7) occurred at $T_a = 34$ °C, which also coincided with the maximum of G_T at $T_l = 39$ °C (figure 8.9). This maximum was *not* associated with the maximum G_g or minimum G_A, but the most negative value of $(\partial A/\partial T_l)_{p_i}$. This rapid decline in A in response to T_l was due to the modelled response of electron transport processes of photosynthesis to temperature.
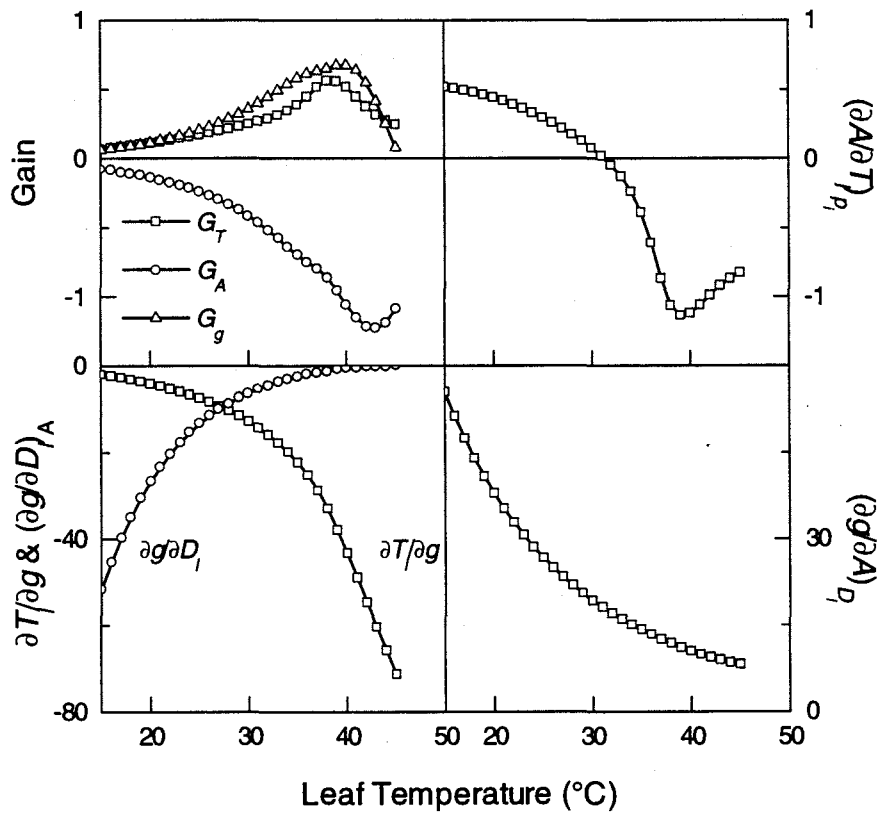
Figure 8.9 Loop gains and partial differentials for the leaf energy balance, photosynthesis and conductance feedback loops.

The leaf photosynthesis model (Farquhar *et al.*, 1980) used here defines photosynthesis as the minimum of the Rubisco limited rate or the electron transport limited rate. In this analysis the change between limiting rates was smoothed mathematically by use of a non-rectangular hyperbola,

$$\theta A^2 - (A_v + A_J)A + A_v A_J = 0,$$ (8.50)

where θ (=0.98) is the curvature factor. This overcame problems of calculating partial differentials of discontinuous functions.

While most of the leaves were light saturated and therefore had Rubisco limitations to their photosynthesis, when temperature increased the rate of electron transport declined to such an extent that they became electron transport limited. Electron transport was described in the model as having a temperature optimum of ~ 30 °C, above which it declined rapidly with further increases in temperature. The linkage between stomatal conductance and photosynthesis, used in this model, then caused the conductance to decrease rapidly, increasing leaf temperature, which combined with the high gain of this feedback loop, at T_l = 39 °C, caused the observed response of the model to temperature. Thus the loop involving feedback between the leaf energy balance, photosynthesis and conductance was causing the midday decrease in modelled photosynthesis and conductance. It was not a result of the choice of stomatal response function to humidity.

8.3.2. Sun/Shade Canopy Model

8.3.2.1. Resistances

Typical diurnal trends for the integrated leaf boundary layer (r_b), within-canopy (r_i) and above canopy aerodynamic (r_{atm}) resistances for the Sun/Shade canopy model are shown in figures 8.10A & 8.10B. r_{atm} was a small component of total aerodynamic resistance (R_a) in both fractions. For both sunlit and shaded leaves R_a was dominated by r_b, which was obtained by summing the individual leaf boundary layer resistances in parallel, so that as the proportion of leaves sunlit or shaded changed so did the partitioning of r_b between the leaf fractions (figure 8.10C). Hence r_{bSh} was low at both ends of the day when all leaves were shaded and r_{bSun} was high at the same time. r_i was a small component for the sunlit leaves, but a larger component for the shaded leaves at both ends of the day. Comparing the aerodynamic resistances with the stomatal resistance (R_c) it is clear that the physiological component is the dominant resistance (figures 8.10D & 8.10E).

Comparison of resistances for a big-leaf representation of the canopy show that the physiological and aerodynamic components were comparable (figure 8.10F). This occurred because stomatal resistances were added in parallel so that the canopy resistance was lower than the sun/shade components, whereas the big-leaf aerodynamic resistance was not directly comparable to the sun/shade resistances because it was calculated from assuming a single layer source at the notional canopy surface, $d + z_{oH}$, and a logarithmic wind profile.

The magnitudes of these resistances suggest that the scheme used to define the aerodynamic components is not very important. Canopy profiles of temperature, humidity or CO_2 concentration that develop will not greatly affect the model predictions, because the stomatal and leaf boundary layer resistances are larger than the within-canopy or above-canopy resistances. Thus while these resistances were based on K-theory to define the within canopy transport, any errors introduced by the invalidity of the use of K-theory are unlikely to have much impact. K-theory is also much simpler to use than the rigorous Lagrangian approach.
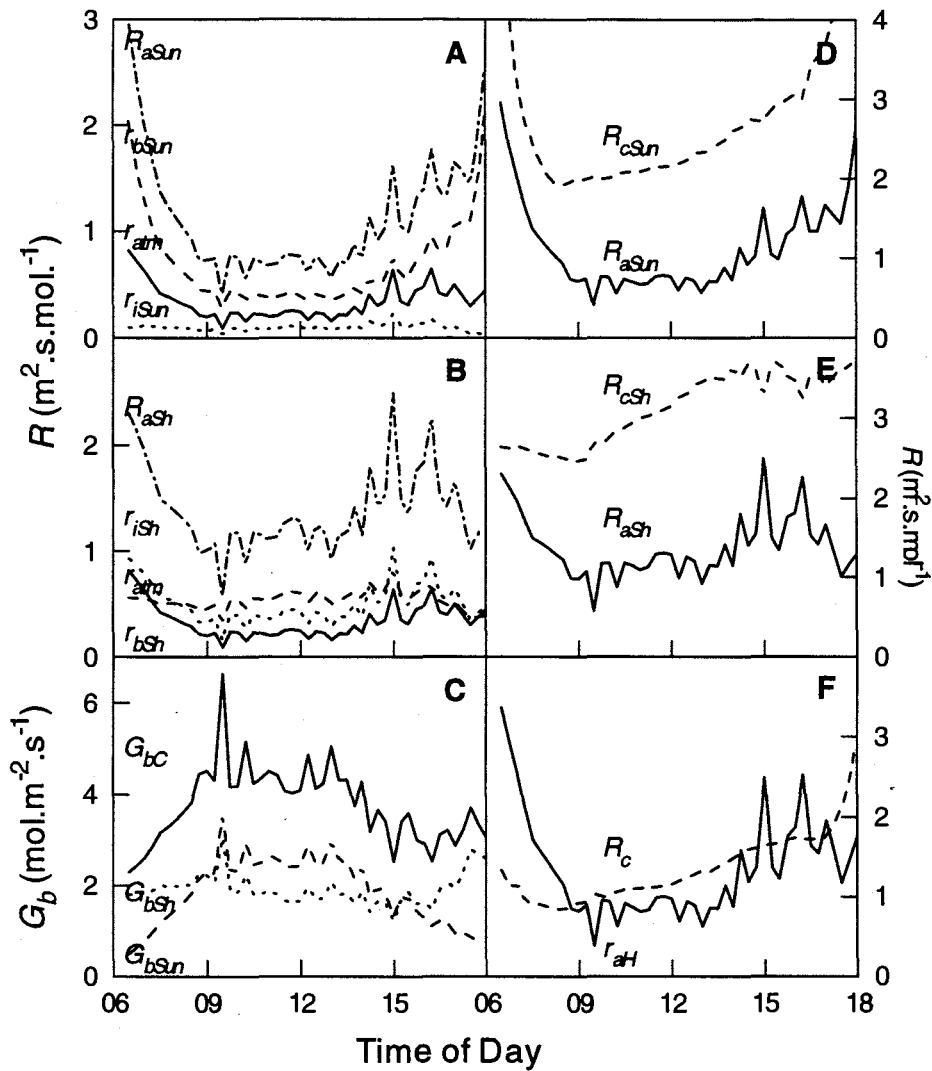
Figure 8.10 Components of the aerodynamic and physiological resistances and conductances in the Sun/Shade canopy model calculated for the 25-Oct. **A** and **B** aerodynamic components of resistances for the sunlit and shaded fractions of the canopy (R_a total, r_i within-canopy, r_{atm} above-canopy, r_b integrated leaf boundary layer resistances). **C** integrated leaf boundary conductances (G_{bC} total, G_{bSh} shaded fraction, G_{bSun} sunlit fraction). **D** and **E** stomatal and aerodynamic components of resistance for sunlit and shaded fractions respectively (R_c and R_a). **F** Total stomatal resistance (R_c) and total 'big leaf' aerodynamic resistance (r_{aH}).

8.3.2.2. Comparison with Multi-Layer model

The Sun/Shade canopy model was evaluated by comparison with the Multi-Layer model, assuming that the latter gives an accurate representation of canopy fluxes. Photosynthesis, conductance, transpiration and sensible heat flux from sunlit and shaded leaves in the Multi-Layer model were aggregated separately to facilitate comparison with the Sun/Shade canopy model (figure 8.11).

Overall the agreement between the two models was very good for all the fluxes and conductances. Small differences between the models were observed but they were within acceptable limits. These differences possibly arose because the Multi-Layer model generated within-canopy profiles of D_l.
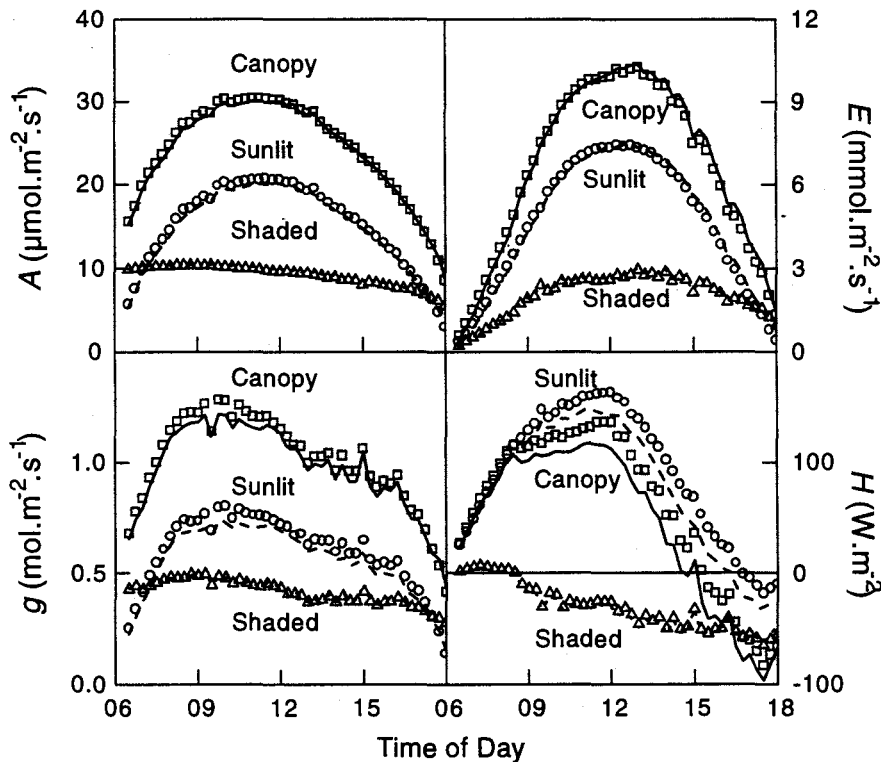
Figure 8.11 Comparison of photosynthesis (A), conductance (g), transpiration (E) and sensible heat flux (H) from the sunlit and shaded fractions of the canopy as predicted by the Sun/Shade canopy model (lines) and Multi-Layer canopy model (symbols). The lines are sometimes obscured when the predictions from both models coincide.

8.3.2.3. Comparison with Big-Leaf model

Predictions from the simpler Big-Leaf model were very close to those of the Sun/Shade canopy model, as the empirical curvature factor (θ_c = 0.94) of the Big-Leaf model was adjusted to give a good fit (figure 8.12). Predictions of photosynthesis from the Big-Leaf model were greater than the Sun/Shade canopy model at mid-morning and mid-afternoon, as expected from the analysis of these models in Chapter Six. As a result of the high photosynthesis, stomatal conductance was also overestimated by the simple Big Leaf model. However, the transpiration and sensible heat flux were not greatly affected, since they were not very sensitive to stomatal conductance with the conditions on this day. Differences between the models were greater when θ_c was not fitted.
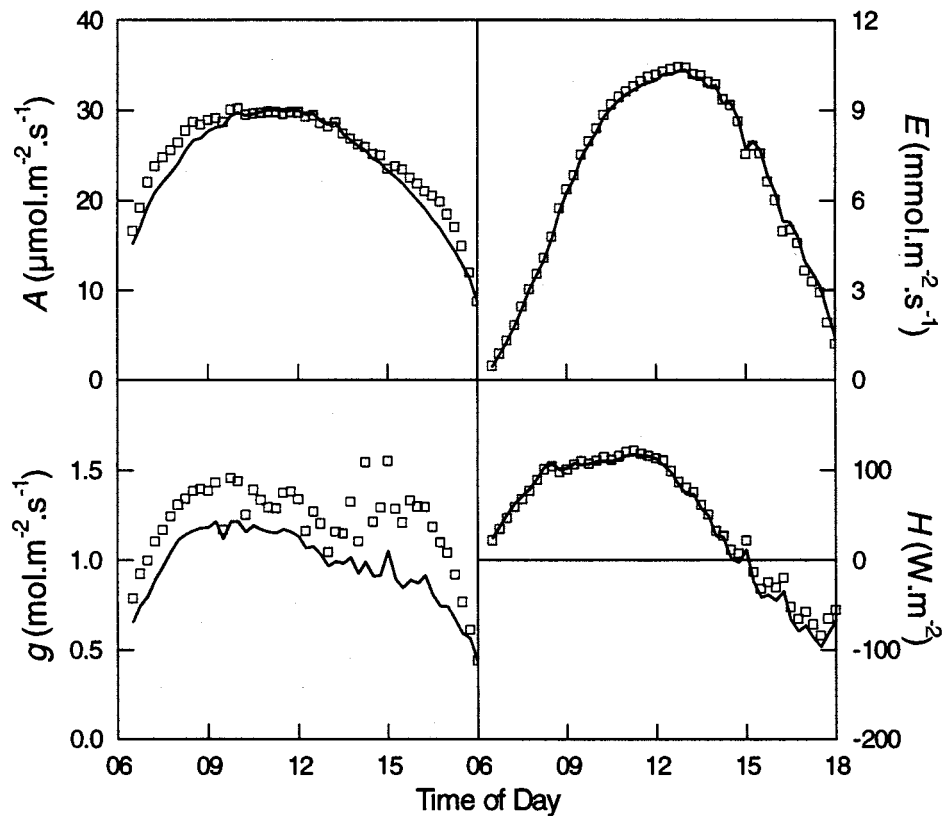
Figure 8.12 Comparison of photosynthesis (A), conductance (g), transpiration (E) and sensible heat flux (H) from the Big Leaf model (□) and the Sun/Shade canopy model (—).

8.3.3. Comparison with data

Evaluation of the Sun/Shade canopy model was conducted from three perspectives, with different sources of parameter values. Firstly, parameters were derived from the canopy scale data by fitting the model. This allowed the model structure and assumptions to be assessed. Secondly, parameter values were derived from leaf-scale measurements, allowing evaluation of the model's suitability for scaling from leaves to canopies. Finally, parameter values were selected *a priori*, for situations when the model is used for predictive purposes.

8.3.3.1. Parameters fitted to canopy data

Parameter values from fitting the model to canopy data were given in Chapter Five for conductance and Chapter Seven for photosynthetic capacity. Model predictions, using fitted parameters for each day, were compared with the canopy data (figure 8.13). Conductance data, selected from periods when the canopy was dry to avoid high conductances from evaporation of dew and a few other anomalous data points, and all photosynthesis, transpiration and sensible heat flux data from each day were plotted.

Available energy (Q) in the canopy model was determined by radiation reflection, interception and penetration components of the model. It matched the measured available energy (R_n - G) with an $r^2 = 0.92$ (data not shown). Since radiation was the main driving variable for the model, the reproduction of the available energy provides a base line for comparison of the other components of the model.

Overall, the model performed very well, accurately reproducing the canopy photosynthesis, transpiration, sensible heat flux and canopy conductance data. The observed scatter was due to random variations in the measurements, which were not reproduced by the model. The model showed no sign of curvature in the relationship between modelled and measured photosynthesis, thus supporting the validity of the model structure with sunlit and shaded leaves.

8.3.3.2. Parameters fitted to leaf data

In the second approach, for evaluating the model for scaling between spatial scales, parameters for the stomatal model and the photosynthetic capacity were obtained from

the leaf data for each day. Modelled canopy fluxes using leaf derived parameters are plotted against the canopy data in figure 8.14.
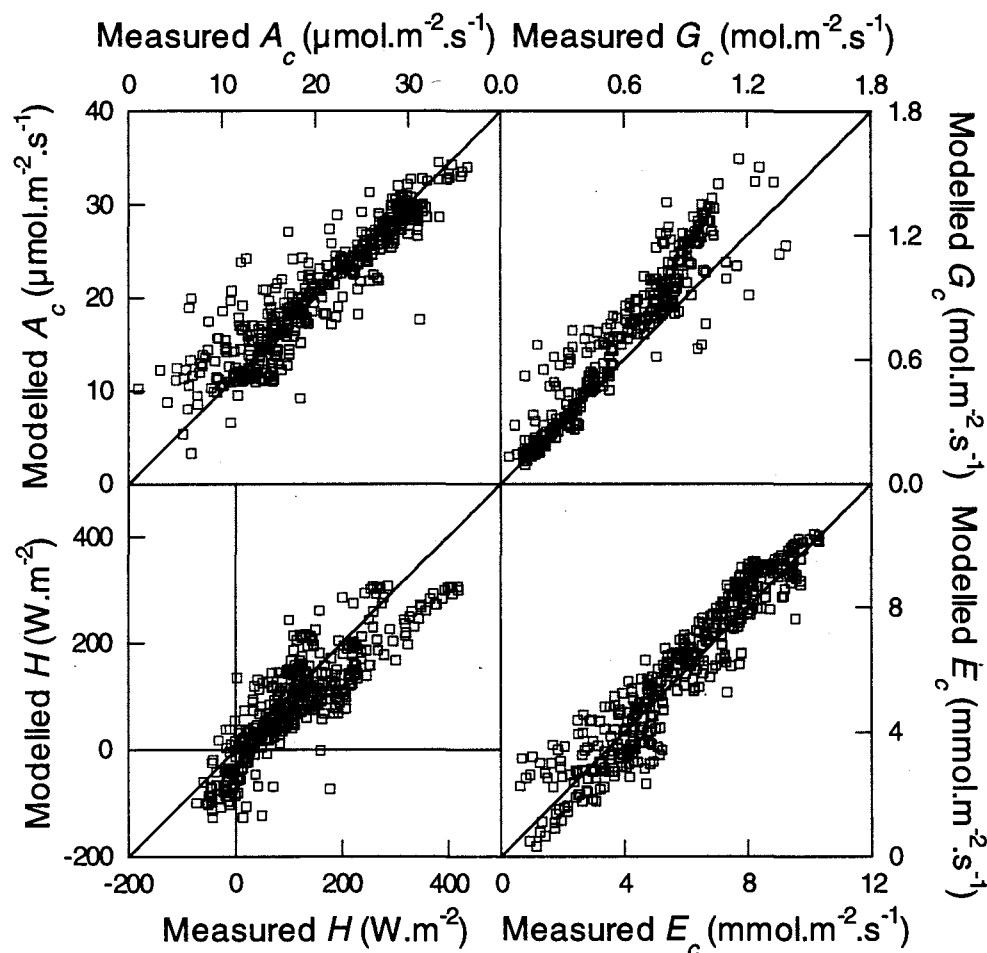
Figure 8.13 Comparison of model predictions and data, using parameters obtained from canopy scale measurements.

Stomatal conductance was much more variable when the leaf-scale parameters were used, than when the canopy-scale parameters were used in the model (cf. figure 8.13). This was probably due to the limited range of data that were available at the leaf scale, thus preventing a more accurate determination of the stomatal response to humidity, whereas at the canopy scale a greater range of D_l was available for fitting the model. Despite the increased variability of stomatal conductance, there was no systematic bias. Photosynthesis was overestimated by about 5 $\mu mol.m^{-2}.s^{-1}$ by the model using the leaf

scale parameters, with a little more scatter. As a result of the increased variability of stomatal conductance, the transpiration estimates were considerably more variable, but without any systematic bias. Similarly, the sensible heat flux had more scatter. Model predictions from any individual day were consistently offset from the data for the whole day; the magnitude of the offset depended on the particular parameter values of that day.
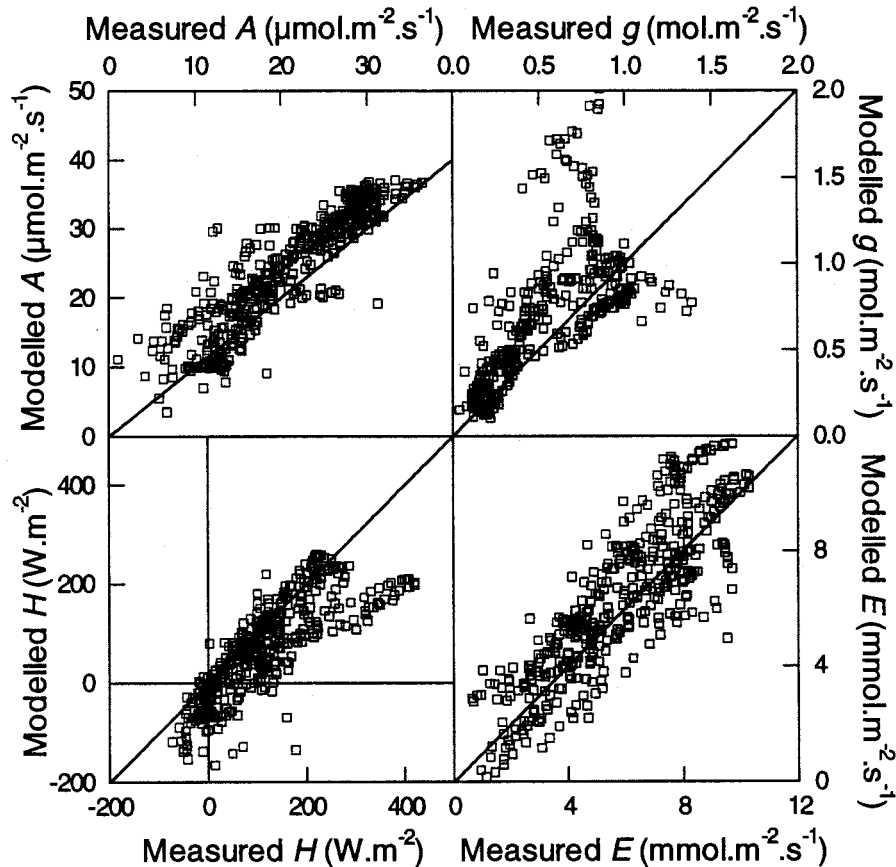
Figure 8.14 Comparison of model predictions with data, using parameters for each day obtained from leaf scale measurements.

8.3.3.3. Parameters from all data combined

All the leaf-scale data were pooled and used to fit the stomatal conductance model and determine the average leaf photosynthetic capacity. These parameters were then used in the model for predictive purposes, but did not vary between days. This is typical

of situations where the parameters describing gas exchange of different vegetation types would be assigned with no day-to-day variability of the parameters. A comparison of the model predictions, using this parameterisation scheme, with measurements is shown in figure 8.15.
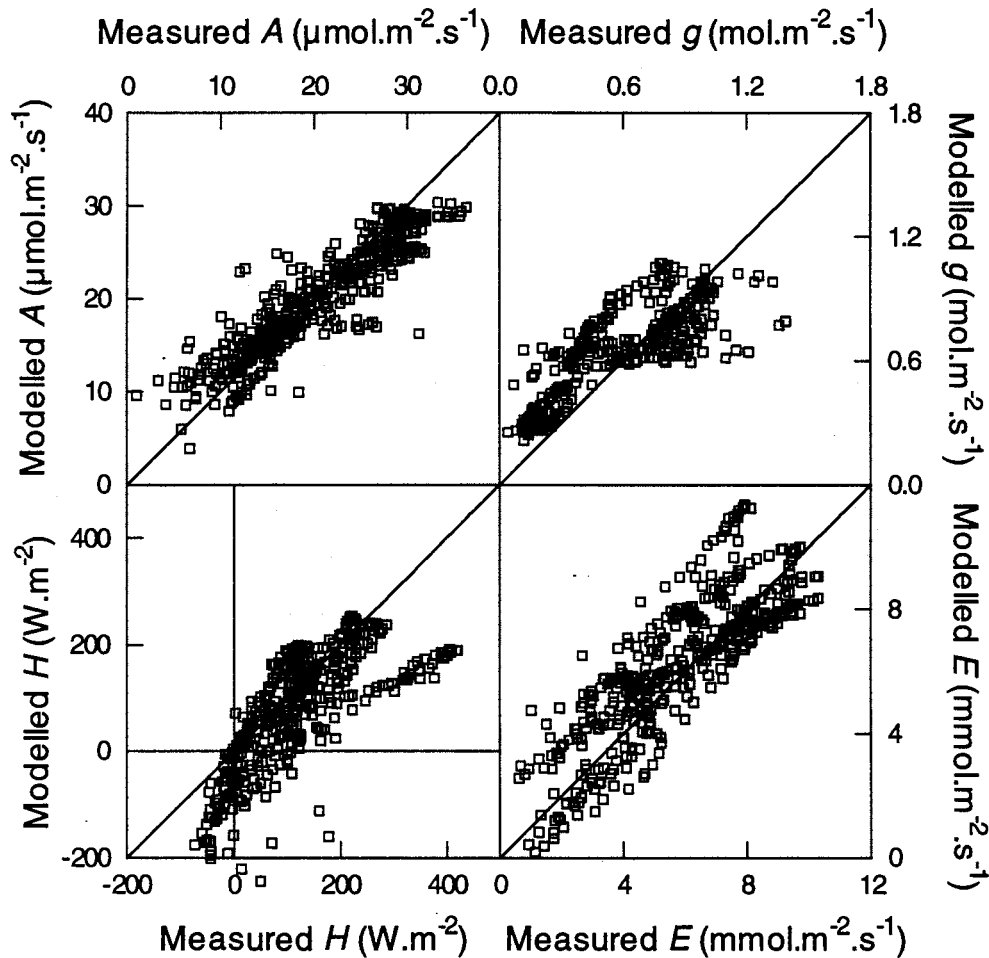
Figure 8.15 Comparison of model predictions with data, using parameters obtained from leaf scale data with all days data combined and assuming a single value for the leaf photosynthetic capacity.

Under this parameterisation scheme, canopy photosynthesis had more scatter than when parameters for each day were used and showed a tendency to underestimate high rates, but overestimate low rates. Stomatal conductance was not predicted very well,

particularly at high conductances. This suggests that the relationship between stomatal conductance and photosynthesis utilised in this model was changing in ways that were not accounted for by using a single relationship for all days. The cause of this variability was probably declining soil water content and encroaching drought. Despite the poor prediction of stomatal conductance, transpiration was still fairly well predicted, indicative of the insensitivity of transpiration to stomatal conductance for this canopy.

8.3.4. Canopy Responses to CO_2

The Sunlit/Shaded canopy model was used to predict canopy responses to altered atmospheric CO_2 concentrations through its effect on leaf photosynthesis and stomatal conductance (figure 8.16).   With all other parameters held constant, daily canopy transpiration decreased and gross photosynthesis increased with rising atmospheric CO_2 concentration.   The ratio of photosynthesis to transpiration (A_d/E_d), or transpiration efficiency, increased even more rapidly with rising CO_2. From 0.8 to 2 times measured CO_2 concentrations the response of A_d and E_d was nearly linear. The measured average CO_2 concentration was 328 $\mu mol.mol^{-1}$, which is lower than the atmospheric average due
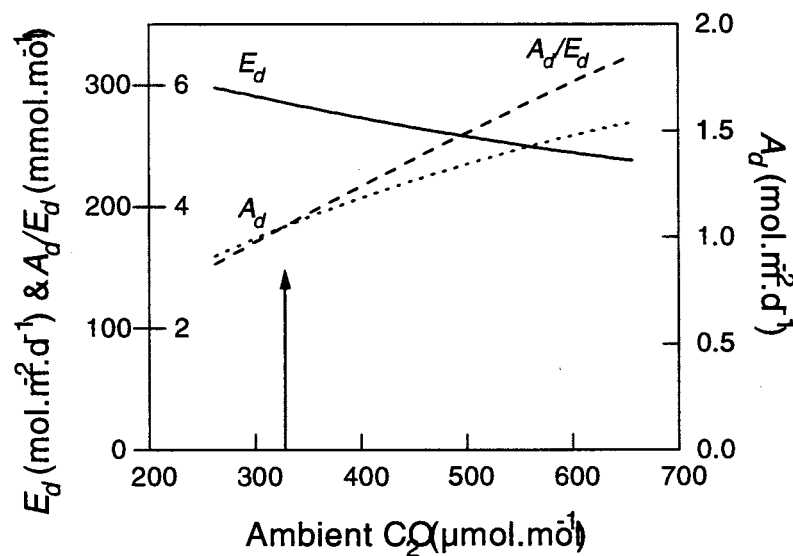
Figure 8.16 Effect of atmospheric CO_2 concentration on daily canopy fluxes of CO_2 and water vapour. Data were generated using the Sun/Shade canopy model using the atmospheric conditions of the 25-Oct (L_c = 2.41 $m^2.m^{-2}$). The arrow marks the measured CO_2 concentration at canopy height of the original data (c_a = 328 $\mu mol.mol^{-1}$).

to the draw-down caused by the uptake of CO_2 by the crop.

The interaction between CO_2 concentration and canopy leaf area was examined by predicting the effect of doubling CO_2 concentration on daily photosynthesis and evaporation over a range of canopy leaf areas (figure 8.17). Changing canopy leaf area affects the amount of radiation absorbed by the canopy and the penetration of radiation to the soil. In this simulation I assumed the soil was moist and that soil evaporation was at the equilibrium evaporation rate determined from the radiation penetration through the canopy. I further assumed canopy respiration to increase in proportion to canopy
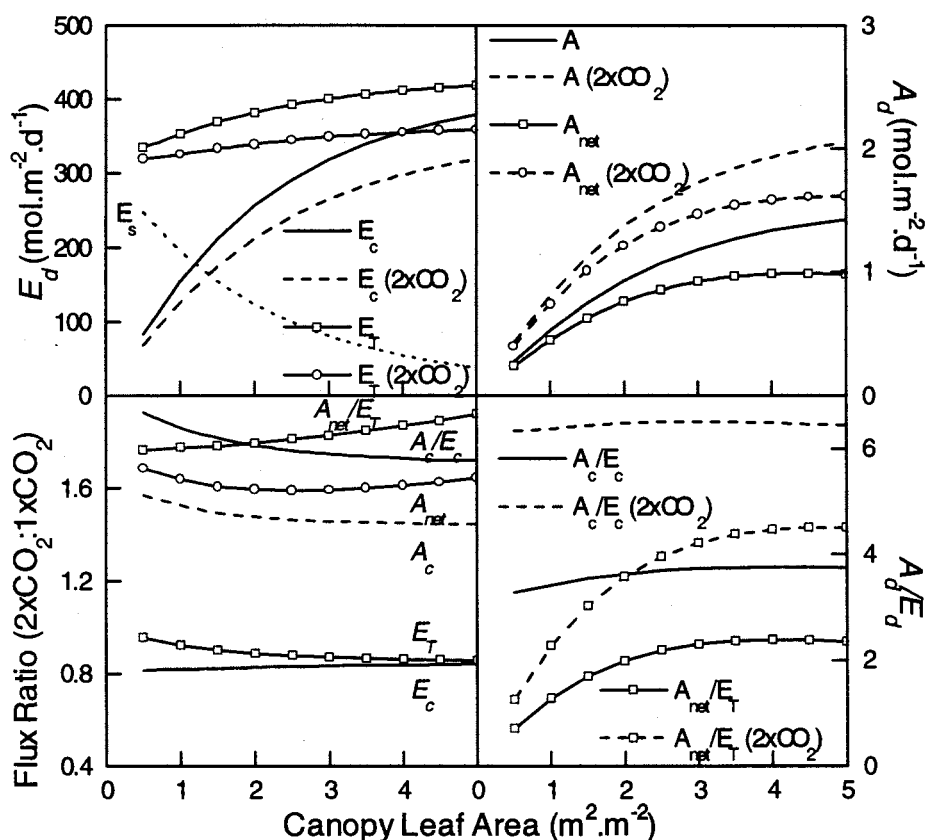
Figure 8.17 Comparison of the effect of 2 x CO_2 concentration (- - -) with ambient CO_2 levels (——) on canopy transpiration (E_c), total evaporation (E_T), gross canopy photosynthesis (A_c), net canopy CO_2 flux (A_{net}), transpiration efficiency (A_c/E_c) and water-use efficiency (A_{net}/E_T) over a range of canopy leaf areas; with (symbols) and without (lines only) soil fluxes. Also shown is the ratio of fluxes and efficiencies at 2 x CO_2: ambient CO_2. Soil evaporation (E_s) was unaffected by CO_2 concentration. Data for the simulation were from 25-Oct, with ambient CO_2 concentration of 328 μmol.mol^{-1}.

photosynthetic capacity. No effect of elevated CO_2 concentrations on canopy respiration were included as it is unclear what response, if any, may occur. Similarly, no acclimation of photosynthesis to elevated CO_2 was included in the model.

Total evaporation (E_T) decreased only slightly in canopies with low leaf area because of the increasing contribution of soil evaporation and even less at 2 × CO_2. Net canopy CO_2 flux (A_{net}) did not increase with leaf area greater than 4, due to canopy closure and increasing respiration with further leaf area. 2 × CO_2 caused canopy transpiration (E_c) to decrease by 20% at all leaf areas, while the effect on total evaporation (E_T) was only slightly less, particularly at low leaf area where the contribution of soil evaporation was not affected by CO_2 concentration. Gross canopy photosynthesis (A_c) was enhanced 1.46 times by 2 × CO_2, and net photosynthesis (A_{net}) by 1.6 times.

The effect of leaf area and 2 × CO_2 on water-use efficiency differed from the effect on transpiration efficiency. While transpiration efficiency (A_c/E_c) was relatively constant across the range of canopy leaf areas at both ambient and 2 × CO_2, water-use efficiency (A_{net}/E_T) increased dramatically as canopy leaf area increased up to a leaf area of 4, due to decreasing soil evaporation. The enhancement of transpiration efficiency by 2 × CO_2 approached 2 at low leaf area and decreased with increasing leaf area to 1.7, due to the diminishing response of A_c to CO_2 with increasing leaf area. In contrast water-use efficiency was enhanced by 2 × CO_2 by a factor of 1.7 at low leaf area and increased with increasing leaf area up 1.9 times, due to the increasing reduction of E_T at double CO_2 with increasing leaf area.

The enhancement of water-use efficiency by an average factor of 1.8 agrees with experiments of elevated CO_2 on gas exchange of cotton plants (Wong, 1979) where A/E was enhanced by 1.8 to 2 fold by a 1.94 times increase in CO_2 concentration, and on a eucalyptus forest canopy (Wong & Dunin, 1987) where A/E increased 2 fold with 2 × CO_2.

While this model does demonstrate the effect of CO_2 on canopy physiology and the partitioning of energy between latent and sensible heat, it does not include the full secondary effects of altered canopy leaf area or prevailing air conditions of temperature and humidity. Conditions at the reference height were assumed to be unaffected by the underlying surface. Canopy boundary layers only affected the air beneath the reference height and within the canopy. Decreased evaporation at high CO_2 concentrations due to reduced stomatal conductance may cause higher air temperature and lower air humidity

at the reference height, thus offsetting the effect of lower conductance on evaporation rate. However, total evaporation and transpiration was reduced by only 20% at $2 \times CO_2$ so that this feedback may not have a large impact. These effects could be included if their response to CO_2 concentration was known.

8.3.5. Scaling Transpiration Efficiency

Scaling of transpiration efficiency from leaves to canopies was examined with the sun/shade canopy model by calculating daily canopy transpiration (E_c), gross canopy photosynthesis (A_c) and their ratio (A_c/E_c) (figure 8.18). Stomatal conductance was varied by altering the coefficient (a_1) in the model of stomatal conductance, $g = g_o + a_1 A/((c + \Gamma)(k + D))$. The same coefficients and data as for the canopy were used to calculate daily leaf transpiration efficiency and the photosynthesis-weighted average leaf conductance of a horizontal leaf at the top of the canopy, which was used as the x-ordinate in figure 8.18.
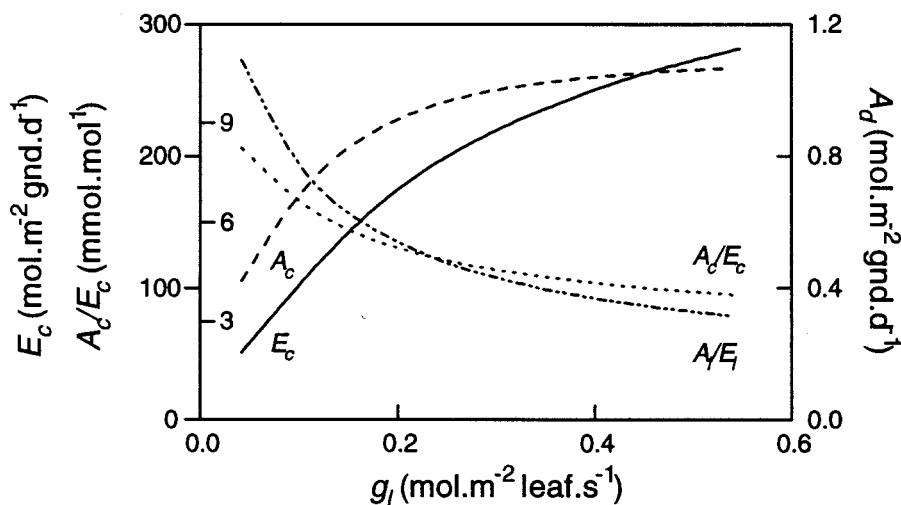
Figure 8.18   Modelled daily canopy transpiration (E_c), gross canopy photosynthesis (A_c) canopy transpiration efficiency (A_c/E_c) and leaf transpiration efficiency (A/E_l) with varying stomatal conductance (g_l) of a horizontal leaf at the top of the canopy. Diurnal variation of light, wind speed, air temperature, humidity and the coefficients for the model were obtained from the Bowen ratio flux data of Matong on 25-Oct, $k = 24.07$, $L_c = 2.41$ and $V_l = 93$. Stomatal conductance was calculated as the photosynthesis weighted average for the day. Averages for 10:00 - 14:00 were $T_a = 20°C$, $w_a = 12.6$ mmol.mol^{-1} and $g_{aH} = 1.18$.

Transpiration efficiency was more responsive to changing stomatal conductance at the leaf scale than at the canopy scale, which was expected due to the additional boundary layer conductance at the canopy scale. The difference in the response of transpiration efficiency between the leaf and canopy scale was not as large as might have been expected. On days with lower wind-speeds the boundary layer conductance would be reduced and the difference in transpiration efficiency at the leaf and canopy scale would be greater. On hotter days, with higher leaf-to-air water vapour concentration differences (eg. 30-Oct), transpiration efficiency was lower, but the response to varying conductance was still greater at the leaf than at the canopy scale.

The sun/shade canopy model was also used to simulate the variation of transpiration efficiency in response to varying leaf photosynthetic capacity (figure 8.19), which was similar at both the leaf and canopy scale as expected. The feedback effect of the canopy boundary layer was expected to have less effect when photosynthetic capacity was changed than when stomatal conductance was changed, because the canopy CO_2 fluxes are small in comparison to the atmospheric concentration ($A_c/c_a = 25/330$) causing only a small draw-down in CO_2 concentration, whereas the H_2O (and heat) fluxes are large ($E_T/w_a = 10/13$) causing significant increase in humidity (and temperature), which affect the concentration gradient and hence feedback on the fluxes.
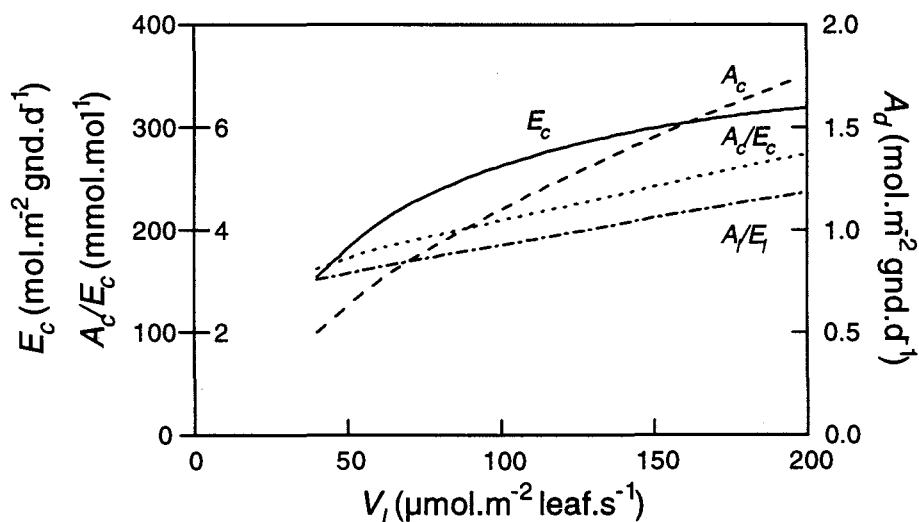
Figure 8.19 Modelled daily canopy transpiration (E_c), gross canopy photosynthesis (A_c) canopy transpiration efficiency (A_c/E_c) and leaf transpiration efficiency (A/E_l) with leaf photosynthetic capacity (V_l) of a horizontal leaf at the top of the canopy. Data and coefficients as in figure 8.18.

8.4. Further Discussion and Conclusions

8.4.1. Sun/Shade canopy model

The Sun/Shade canopy model presented here performed as well as a multi-layer model and accurately reproduced diurnal changes of canopy fluxes. It performed better than a single-layer Big-Leaf model, which overestimated canopy photosynthesis at intermediate light levels. Other attempts at using single-layer big leaf models to describe canopy photosynthesis have involved either fitting the model to data (Lloyd *et al.*, 1995) or have used empirical scaling coefficients to tune the model to the data (Johnson *et al.*, 1989; Amthor *et al.*, 1994). While both these approaches are valid when using the models to explain or reproduce data sets, they are of limited value if the models are to be used for predictive purposes, such as investigating the response of vegetation to climate change when canopy leaf area or nitrogen content may change (see Chapter Six). Under such altered environments the empirical coefficients and fitted parameters of Big-Leaf models change, but in what manner it is difficult to say *a priori*. The Sun/Shade canopy model has the advantage that it is based on leaf scale processes that have been integrated to the canopy scale without the use of scaling coefficients (other than canopy leaf area). The response of leaf gas exchange to light, humidity, temperature, CO_2 concentration, nutrition and leaf age can all be explained by the Farquhar *et al.* (1980) model of photosynthesis, which can confidently be used to scale these responses to the canopy level. These models do not, however, consider secondary effects of acclimation of photosynthesis to either altered CO_2 concentration (Sage, 1994) or temperature (Berry & Björkman, 1980), nor the response of respiration to elevated CO_2 (Amthor, 1991). When the nature and extent of acclimation become clearer these effects could also be included.

The choice of parameters for the model does affect its performance. Fitting the model to the data worked well, which is reassuring but not surprising. However the day-to-day variation of the parameters can not yet be completely explained (as discussed in Chapters Four, Five and Seven).

8.4.2.   Leaf temperature and free convection

Inclusion of the effects of free convection on leaf boundary layer conductance had a significant effect, reducing some leaf temperatures by up to 3 °C. These effects would be even greater in a canopy with leaves bigger than those of the canopy in this study (0.02 m). Omission of this phenomenon from canopy models could lead to significant errors.

It is apparent from the multi-layer model, which considered many leaf angle classes, that the temperature of leaves at the top of the canopy can vary by as much as 6 °C depending on their orientation to the sun and by as much as 10 °C for leaves at the bottom of the canopy. Despite this large variation in leaf temperature the Sun/Shade canopy model which aggregated the leaves into only two classes, was still able to reproduce canopy transpiration and sensible heat flux. This suggests that averaging over non-isothermal surfaces may not be a problem, and that this type of model could be used for averaging over patchwork landscapes with different energy balances (Raupach, 1995).

8.4.3.   Response of photosynthesis to temperature

Linking stomatal conductance to photosynthesis had many advantages in that responses to temperature, light, leaf nutrition and age were all accommodated. However, the modelled response of photosynthesis to high temperature caused unrealistically low stomatal conductances, with consequent extreme leaf temperatures. This phenomenon was not caused by the type of stomatal response to humidity. Further work needs to be done to explore the decline of photosynthesis at high temperatures and its relationship with stomatal conductance.

8.4.4.   Sensitivity of Transpiration Efficiency to Leaf Properties

It has been suggested that where improved transpiration efficiency at the leaf scale arises from reduced conductance rather than greater photosynthetic capacity that the benefit would be diminished at the canopy scale due to feedback effects of the canopy boundary layer (Farquhar et al., 1989b). This was confirmed by the model predictions presented in this chapter. Benefits to transpiration efficiency from greater photosynthetic capacity were predicted to be equally beneficial at the canopy scale as the leaf scale.

Although transpiration efficiency was nearly constant across a range of canopy leaf areas, water-use efficiency (including soil fluxes) increased dramatically up to canopy closure ($L_c = 4$). These effects of different leaf area on water-use efficiency were much greater than the benefits from reduced stomatal conductance or greater photosynthetic capacity. Thus any attempt to improve water-use efficiency of crops by altering leaf physiological traits needs to ensure that canopy leaf area is not adversely affected. Similarly, canopy responses to elevated atmospheric CO_2 are more sensitive to changes in canopy leaf area that may occur, than to the direct effects on physiology.

8.5. Appendices

8.5.1.   Derivation of the combination equation with isothermal net radiation.

The water vapour flux is given by

$$E = \frac{w_i - w_a}{r_s + r_b},$$ (8.51)

where w is the water vapour concentration (mol.mol^{-1}) of intercellular air spaces (w_i) and ambient air (w_a) outside the boundary layer of resistance r_b. r_s is the stomatal resistance. The sensible heat flux (H) is given by

$$H = C_p \Delta T / r_{bH}$$ (8.52)

where C_p is the molar heat capacity of air, r_{bH} is the boundary layer resistance to heat transfer and ΔT is the difference between leaf temperature and air temperature outside the boundary layer ($T_l - T_a$). Available energy (Q) can be expressed as

$$Q \cong Q_o - 4\sigma\varepsilon_l T^3 \Delta T$$ (8.53)

where Q_o is the isothermal radiation (available energy if leaf temperature were equal to air) and the last term accounts for the radiation exchange as a result of the difference between leaf and air temperatures. Introducing the concept of radiative conductance ($g_r = 4\sigma\varepsilon_l T^3 / C_p$), the above equation can be rewritten as

$$Q \cong Q_o - g_r C_p \Delta T$$ (8.54)

Rearranging eq. 8.5 to obtain ΔT and using the energy balance (Q = H + LE) results in

$$\Delta T = r_{bH} H / C_p = r_{bH}(Q - LE)/C_p,$$ (8.55)

which substituting for Q using eq. 8.54 results in

$$\Delta T = \frac{r_{bH}\left(Q_o - g_r C_p \Delta T - \lambda E\right)}{C_p} = \frac{Q_o - \lambda E}{C_p\left(g_{bH} + g_r\right)} = \frac{r_{bH}^*\left(Q_o - \lambda E\right)}{C_p}. \tag{8.56}$$

where g_{bH} is the boundary layer conductance to sensible heat transfer ($1/r_{bH}$) and r_{bH}^* is the combined resistance to sensible and radiative heat transfer in parallel ($1/(g_{bH} + g_r)$).

Using the approximation of $w_i \cong w_a' + (s/P)\Delta T$, where w' is the saturated vapour concentration and s is the change in saturated vapour pressure with temperature ($dw'P/dT$), the combination equation is derived from eq. 8.51, and combined with the expression for ΔT (eq. 8.56),

$$E = \frac{w_a' + (s/P)\Delta T - w_a}{r_s + r_b} = \frac{w_a' + (s/P)r_{bH}^*\left(Q_o - LE\right)/C_p - w_a}{r_s + r_b}. \tag{8.57}$$

Defining D as the vapour concentration deficit of air ($w_a' - w_a$) and ε as $sL/(C_p P)$, the above equation can be rearranged to give,

$$E = \frac{(\varepsilon/L)r_{bH}^*\left(Q_o - LE\right) + D}{r_s + r_b}. \tag{8.58}$$

Collecting terms of E, gives

$$E\left(r_s + r_b + \varepsilon r_{bH}^*\right) = (\varepsilon/L)r_{bH}^* Q_o - D, \tag{8.59}$$

which can be rearranged to

$$E = \frac{\varepsilon r_{bH}^* Q_o/L + D}{r_s + r_b + \varepsilon r_{bH}^*}. \tag{8.60}$$

8.5.2. Leaf temperature with isothermal radiation.

Combine expressions for ΔT (eq. 8.56) with the above isothermal combination equation,

$$\Delta T = \frac{r_{bH}^*}{C_p}\left(Q_o - L\frac{\varepsilon r_{bH}^* Q_o/L + D}{r_s + r_b + \varepsilon r_{bH}^*}\right),$$

(8.61)

which simplifies to

$$\Delta T = \frac{r_{bH}^*\left(Q_o(r_s + r_b) - LD\right)}{C_p\left(r_s + r_b + \varepsilon r_{bH}^*\right)}.$$

(8.62)

8.5.3. Derivation of a two layer evaporation model with molar units.

Adding eqs. 8.16 & 8.17, multiplying by the denominators gives

$$LE\left(r_{cSun} + r_{aSun} + \varepsilon r_{aSun}^*\right)\left(r_{cSh} + r_{aSh} + \varepsilon r_{aSh}^*\right)$$

$$= \left(\varepsilon r_{aSun}^* Q_{oSun} + L(D_x - E(\varepsilon + 1)r_{atm}) + \varepsilon r_{atm}Q\right)\left(r_{cSh} + r_{aSh} + \varepsilon r_{aSh}^*\right).$$

$$+ \left(\varepsilon r_{aSh}^* Q_{oSh} + L(D_x - E(\varepsilon + 1)r_{atm}) + \varepsilon r_{atm}Q\right)\left(r_{cSun} + r_{aSun} + \varepsilon r_{aSun}^*\right)$$

(8.63)

Collecting terms of LE and simplifying with the definitions; $R_{Sun} = r_{cSun} + r_{aSun} + \varepsilon r_{aSun}^*$, $R_{Sh} = r_{cSh} + r_{aSh} + \varepsilon r_{aSh}^*$ and $R_a = (\varepsilon + 1)r_{atm}$ gives

$$LE\left(R_{Sun}R_{Sh} + R_a(R_{Sun} + R_{Sh})\right)$$

$$= \left(\varepsilon r_{aSun}^* Q_{oSun} + LD_x + \varepsilon r_{atm}Q\right)R_{Sh} + \left(\varepsilon r_{aSh}^* Q_{oSh} + LD_x + \varepsilon r_{atm}Q\right)R_{Sun}$$

(8.64)

This equation can be rearranged so that both components of the RHS converge to a Penman-Monteith type equation when either R_{Sun} or R_{Sh} are infinite, so that

$$LE = C_{Sun}P_{Sun} + C_{Sh}P_{Sh},$$

(8.65)

where the terms are given as

$$C_{Sun} = R_{Sh}(R_{Sun} + R_a)/\left(R_{Sun}R_{Sh} + R_a(R_{Sun} + R_{Sh})\right),$$

(8.66)

$$C_{Sh} = R_{Sun}(R_{Sh} + R_a)/\left(R_{Sun}R_{Sh} + R_a(R_{Sun} + R_{Sh})\right),$$

(8.67)

$$P_{Sun} = \left(\varepsilon r^*_{aSun} Q_{oSun} + LD_x + \varepsilon r_{atm} Q\right) \Big/ \left(r_{cSun} + r_{aSun} + \varepsilon r^*_{aSun} + (\varepsilon + 1)r_{atm}\right),$$

(8.68)

$$P_{Sh} = \left(\varepsilon r^*_{aSh} Q_{oSh} + LD_x + \varepsilon r_{atm} Q\right) \Big/ \left(r_{cSh} + r_{aSh} + \varepsilon r^*_{aSh} + (\varepsilon + 1)r_{atm}\right).$$

(8.69)

8.5.4. Isothermal radiation in the Sun/Shade canopy model

The energy available (Q) for evaporation consists of several wavelength components that are differentially absorbed by canopies; photosynthetically active radiation (PAR, 0.4 - 0.7 μm), near infra-red (NIR, 0.7 - 3.0 μm) and long-wave (L, 3 - 100 μm). The reflection, transmission and absorption of PAR and NIR have been treated earlier and can be summarised as

$$Q = I_{PAR} + I_{NIR} + f_{cSky}(L_d - L_u),$$

(8.70)

where I_{PAR} and I_{NIR} are the net absorbed PAR and NIR radiation, L_d and L_u are the long-wave radiation from the sky and the canopy respectively and f_{cSky} is the fraction of long-wave radiation from the sky absorbed by the canopy. Canopy interception of long-wave radiation is calculated assuming an isothermal sky of uniform emittance, so that it is intercepted by the canopy in a similar manner to diffuse visible radiation, but assuming total absorption by the leaves. f_{cSky} is obtained by integrating the absorption profile of diffuse radiation over the whole canopy

$$f_{cSky} = \int_o^{L_c} k_d \exp(-k_d L) dL = \left(1 - \exp(-k_d L_c)\right),$$

(8.71)

where k_d (0.78) is the diffuse radiation extinction coefficient for a canopy of uniform leaf angle distribution and a uniform radiance from the sky.

Separating long-wave radiation absorption into sunlit and shaded leaf fractions of the canopy is achieved by integrating with the profile of leaf area in sunfleck given by the extinction of beam radiation, $\exp(-k_b L)$. k_b is the beam extinction coefficient which varies with solar elevation, β, such that $k_b = 0.5/\sin\beta$, for a canopy with uniform leaf-angle distribution. Long-wave radiation absorption by the sunlit fraction of the canopy is given as

$$f_{cSkySun} = \int_o^{L_c} k_d \exp(-k_d L) \exp(-k_b L) dL$$
$$= \left(1 - \exp(-(k_d + k_b)L_c)\right) k_d / (k_d + k_b)$$

(8.72)

Long-wave radiation absorption by the shaded fraction of the canopy is determined by difference, $f_{cSkySh} = f_{cSky} - f_{cSkySun}$. The long-wave radiation absorption is incorporated into the definition of isothermal radiation so that

$$Q_o = I_{PAR} + I_{NIR} + f_{cSky}\left(L_d - \varepsilon_l \sigma T_a^4\right),$$

(8.73)

and the radiative conductance is

$$g_r = f_{cSky} \, 4\varepsilon_l \sigma T_a^3 / C_p.$$

(8.74)

Similar expressions for isothermal radiation and radiative conductance of sunlit and shaded fractions of the canopy are used, where f_{cSky} is replaced by either $f_{cSkySun}$ or f_{cSkySh} respectively.

317

CHAPTER NINE:

ADVECTION BETWEEN CROPS WITH DIFFERENT

CONDUCTANCES

Chapter Contents

Summary

Advection is the variation of vertical fluxes with distance downwind from the interface between two surfaces with contrasting properties. At the interface of a change in surface properties air in the canopy boundary layer is modified by the new surface and takes some distance before a new equilibrium is reached. At the interface this process of re-equilibration is apparent as horizontal gradients of temperature, humidity, turbulence or fluxes depending on the change that has occurred.

Assessment of crop water use in small plots with contrasting evaporation rates is affected by advection as the plots are too small to allow complete equilibrium between the surface and the air. Canopy boundary layers affect the evaporation rate of crops, but it is unclear how large the effect of advection is on water use of small plots. Two varieties of wheat, with inherently contrasting conductances, were grown in extensive adjacent paddocks. This provided the opportunity to assess horizontal gradients of air temperature, humidity and surface radiative temperature with a set of sensors travelling across the interface between the crops. Additional measurements of wind speed allowed the resolution of the energy balance into latent and sensible heat fluxes along the transect.

On several days wind came over the canopy with high conductance across the interface and into the crop with low conductance, allowing analysis of advection across a transition from high to low conductance. Bowen ratio measurements of the fluxes in the centre of each extensive paddock showed the canopy with high conductance to have 10% greater latent heat flux than the canopy with low conductance. Transect measurements showed a 0.5°C increase in air temperature measured 0.25 m above canopy height, but no detectable increase in humidity. Surface radiative temperature increased 1.5°C and leaf-to-air vapour concentration difference increased 2 mmol.mol^{-1}. Sensible heat flux increased by 30% and latent heat flux decreased by 10% at the interface, but did not show significant change with distance downwind from the leading edge. Calculated canopy conductance and evaporation rate at the surface also showed a step change and indicated some readjustment in the first 10 m from the interface. Footprint corrections reconciled the variation of fluxes along the transect measured above the canopy and at the surface. Horizontal gradients of air and surface temperature indicated that advection was indeed occurring, but that it had minimal impact on the evaporation rate in this case.

9.1. Introduction

Productivity in dryland agriculture is limited by water supply (French & Schultz, 1984). Improvements in crops' efficiency of using the limited water resource has recently received much attention (Ehleringer *et al.*, 1993). However, it has long been recognised that interactions between the vegetation and the overlying atmosphere moderate the extent to which water use can be manipulated. Canopy boundary layers cause the air immediately adjacent to the crop surface to be modified by the energy balance of the crop; typically becoming warmer and more humid than the ambient air well above the crop. The effect of the canopy boundary layer is to reduce the sensitivity of evaporation to changes in stomatal conductance (Jarvis & McNaughton, 1986). Air in the boundary layer above an extensive area of uniform vegetation develop temperature, humidity and CO_2 fields which are in equilibrium with the surface exchange of heat, water vapour and CO_2 and are horizontally uniform.

Plant breeders regularly use small plots (2 x 5 m) to assess new selections of plant cultivars, due to the large number of lines to be assessed. If small plots have different rates of evaporation, due to either different water regimes, leaf area, or stomatal conductance, then the layer of air adjacent to the crop surface will not be fully adjusted to the evaporation rate of the underlying surface, thus limiting the validity of the results in terms of assessing water use that would occur in an extensive paddock. Knowledge of the magnitude of these effects and theories to predict them will allow the validity of small plot experiments to be assessed.

Changes in air humidity and temperature following a step change in surface characteristics are described by the development or modification of the canopy boundary layer and the evolutionary process is called advection. Several theories have been developed and numerical simulations used to describe advection, as recently reviewed by Itier *et al.*, (1994) and Garratt (1990). Experimental observations of advection are very limited and have usually been made at the interface of very contrasting land surfaces (Rider *et al.*, 1963 tarmac to grass; Millar, 1964 dry land to irrigated clover; Davenport & Hudson, 1967 dry fallow to irrigated barley; Lang *et al.*, 1974 dry land to wetland rice; Brunet *et al.*, 1994 dryland to irrigated barley). While experimental observations are consistent with models of advection, the models are not sufficiently proven for predictive purposes (Itier *et al.*, 1994).

Observations of advection between crops with less dramatic, but more realistic, differences in transpiration rates have not been made. These types of measurement are very demanding on instrument accuracy, as the vertical variation is much greater than the horizontal gradients associated with advection.

A large project was established to assess water-use efficiency of two cultivars of wheat, Matong and Quarrion, with contrasting water-use efficiencies due to their inherently different stomatal conductances. The cultivars were grown in adjacent paddocks, providing a continuous canopy, with a step change in stomatal properties. A system of moving sensors was built along a transect across the interface between the two crops, allowing direct measurement of the horizontal variation of air temperature and humidity and surface radiative temperature with the same set of sensors.

This chapter describes the measurements along the transect. They are used to test the hypothesis that extensive paddocks are required to make realistic assessment of plant attributes that affect water-use of crops. The hypothesis is tested by examining the advection across the interface of two wheat crops with contrasting stomatal properties and assessing its effect on canopy transpiration.

9.2. Methods

Details of the field site, agronomy and equipment used for the observations presented in this chapter were given in Chapter Two. A brief outline is given below.

Two cultivars of wheat, Matong and Quarrion, were grown in 1990 in adjacent 5 ha paddocks. Stomatal conductance of Quarrion was typically 40% lower than of Matong, which (together with differences in leaf area) resulted in slightly lower rates of evaporation and total water use over the season (Chapter Three).

A system of moving sensors, the 'monorail', was built across the interface between the two crops, 28.75 m into Quarrion and 30 m into Matong (figure 9.1).
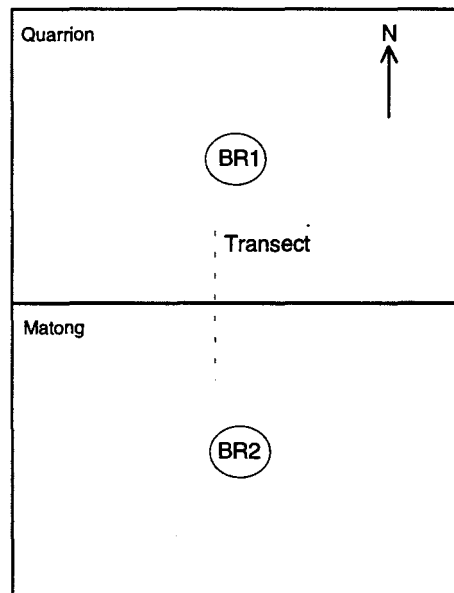
Figure 9.1 Layout of the wheat crops and the transect (not to scale).

The monorail had sensors for air temperature at 0.25 m and 0.50 m above the top of the crop and a humidity sensor at 0.25 m above the crop. Two surface radiative temperature sensors (30° view angle) were mounted at 0.77 m above crop height and pointed down at an angle of 45° due east and west. Data were recorded in both

directions every 1.68 m along the transect. A single transect required approximately 4 minutes for a single transect (0.23 m.s⁻¹) and a similar time in reverse.

Data were filtered post-collection to delete erroneous numbers, which occurred primarily in the data transmission via radio and RS-232 serial line. Data were further filtered by rejecting whole transects when net radiation varied more than 10% from the run average to avoid the effect of clouds and non-stationarity. Data were averaged over five metre intervals and over periods of one hour to provide sufficient points to detect the expected small horizontal variations.

9.2.1. Flux calculations

Wind speed was assumed to follow a log profile

$$u_{z_2} - u_{z_1} = \frac{u_*}{k} \ln\left(\frac{z_2 - d}{z_1 - d}\right),$$

(9.1)

where u_{z2} and u_{z1} are the wind speeds at heights z_2 and z_1, u_* is the friction velocity, d is the zero displacement plane in the canopy (the notional surface where wind speed is zero) and k is von Karman's constant. Wind speed measurements at 0.25 and 0.50 m above canopy height were used to calculate the friction velocity,

$$u_* = k(u_2 - u_1) \Big/ \ln\left(\frac{z_2 - d}{z_1 - d}\right).$$

(9.2)

The diffusivity of momentum (K_M) is assumed to be given as, $K_M = ku_*(z - d)$, so that the resistance to momentum transfer from heights z_2 to z_1 is

$$r_{aM} = \frac{RT_k}{P} \int_{z_1}^{z_2} \frac{dz}{K_M} = \frac{RT_k}{P} \frac{1}{ku_*} \ln\left(\frac{z_2 - d}{z_1 - d}\right),$$

(9.3)

where RT_k/P converts from resistance units of s.m⁻¹ to m²s.mol⁻¹, R is the universal gas constant, T_K is temperature in Kelvin and P is atmospheric pressure. I assumed that the diffusivities and resistances to transfer of momentum, heat and water vapour are equal $(K_M = K_H = K_V, r_{aM} = r_{aH} = r_{av})$ and that stability corrections were similar for both crops, but ignored as they are probably diminished close to the surface (Brutsaert, 1982).

Sensible heat flux (H) is the product of aerodynamic resistance (r_{aH}) calculated as above, and the measured difference in air temperature over the same height interval,

$$H = C_p \left(T_1 - T_2 \right) / r_{aM} , \qquad (9.4)$$

where C_p is the molar heat capacity of air. The energy balance was used to calculate the latent heat flux (LE)

$$LE = R_n - G - H , \qquad (9.5)$$

from ground heat flux (G), which was measured in the centre of each paddock and assumed to be constant for each crop along the transect, and net radiation (R_n) measured above the Matong crop, adjusted for the variation in emitted long-wave radiation (L_u) along the transect,

$$L_u = \varepsilon_c \sigma T_K^4 , \qquad (9.6)$$

where ε_c is the long wave emissivity of the crop (0.98), σ is the Stefan Boltzmann constant (5.67×10^{-8} W.m^{-2}.K^{-4}) and T_K is the surface temperature along the transect.

Strictly, the fluxes calculated from the temperature and wind profiles above a crop are only valid for equilibrium conditions, when the airstream is fully adjusted to the surface beneath. Following a change in surface properties the zone of modified air (blending height), Z_b/X, increases in proportional to $u_*/u(z)$ and the layer of air fully adjusted to the surface (internal boundary layer), Z_f/X, increases in proportion to $x(u_*/u(z))^2$ (Raupach & Finnigan, 1995). With the measured ratio of $u_*/u = 1/7$, the footprint for fluxes over the height interval of 0.25 - 0.50 m above the canopy was calculated to range from 2 - 25 m upwind. It follows that fluxes calculated from the temperature and wind speed profiles, will be fully representative of the upwind crop until approximately 2 m fetch into the downwind crop and that only at the extreme downwind end of the transect will the flux be representative of the downwind crop. In conditions of strong local advection fluxes calculated from profiles would be distorted by the non-equilibrium conditions. In the anticipated conditions of weak advection in this study, the errors may not be too large, although they will not truly reflect the actual fluxes. Despite these problems, fluxes have been calculated from the profiles and are compared with the surface fluxes.

Surface fluxes can be compared with fluxes calculated over the interval 0.25 - 0.50 m above canopy height, by using a weighted averaging scheme for the footprint area of that height. A footprint distribution, similar in shape to that calculated by Schuepp *et al.* (1990), was used to weight the surface fluxes (Table 9.1).

Table 9.1 Footprint weighting scheme to relate surface fluxes to fluxes measured over the interval of 0.25- 0.50 m above canopy height.

Distance upwind (m)	Weighting
0	0.00
-5	0.20
-10	0.40
-15	0.25
-20	0.10
-25	0.05
Total:	1.00

The downwind distance from the interface between the crops, or fetch (x), was calculated from the average wind direction $(\overline{\theta})$ and the location of each data point along the transect (l),

$$x = l / \cos\overline{\theta}, \qquad (9.7)$$

which was calculated for each data point by vector resolution of the wind speed (u) and direction over the preceding three minutes,

$$\overline{\theta} = \operatorname{atan}\left(\frac{\sum\limits_{t-3}^{t} u\sin\theta}{\sum\limits_{t-3}^{t} u\cos\theta} \right). \qquad (9.8)$$

Averaging periods were selected so that wind direction did not change significantly during each period. This resulted in the wind direction being a scaling factor to convert from location to fetch, but did not alter the spatial distribution of the data.

9.2.2. Canopy Conductance

Variation of canopy conductance (g_c) along the transect was modelled with the Leuning (1995) modified Ball-Berry model of stomatal conductance (Ball *et al.*, 1987), as applied to canopies (Chapter Five),

$$g_c = g_o L_c + a_1 \frac{A_c}{(c_a - \Gamma)(k + D_l)},$$ (9.9)

where g_o is intercept of the regression model representing non-stomatal conductance to water vapour transfer, L_c is canopy leaf area index, a_1 is the slope of the regression model, A_c is gross canopy photosynthesis (calculated from measurements as discussed in previous chapters), c_a is measured CO_2 concentration at the top of the canopy, Γ is the CO_2 compensation point of leaf photosynthesis calculated from an Arrhenius function of measured leaf temperature (activation energy of 38.8 kJ.mol^{-1}) and k is a fitted coefficient of the stomatal model. Values of the coefficients for the respective canopies were given in Chapter Five. In the calculations of canopy conductance, A_c and c_a were assumed to be constant for each canopy along the transect, although in fact a small feedback from conductance to photosynthesis does occur, which was ignored.

A second estimate of evaporation along the transect was calculated from g_c by the diffusion equation,

$$E_c = \frac{D_l}{(1/g_c + 1/g_{aH})},$$ (9.10)

where g_{aH} is the aerodynamic resistance to sensible heat transfer from the surface to 0.30 m above the canopy, calculated from measurements of u_* with corrections for the additional resistance to heat transfer compared to momentum and the effect of atmospheric stability, as discussed in Chapter Five.

9.3. Results

The time response of the sensors combined with their movement along the transect, could potentially create a lag in the data in relation to their position of measurement. Such a lag would appear as hysteresis in the data collected from north runs compared to south runs. Data were averaged separately for north and south runs for many data sets; an example from 18-Oct 13:00-14:00 is shown in figure 9.2. No hysteresis was detected
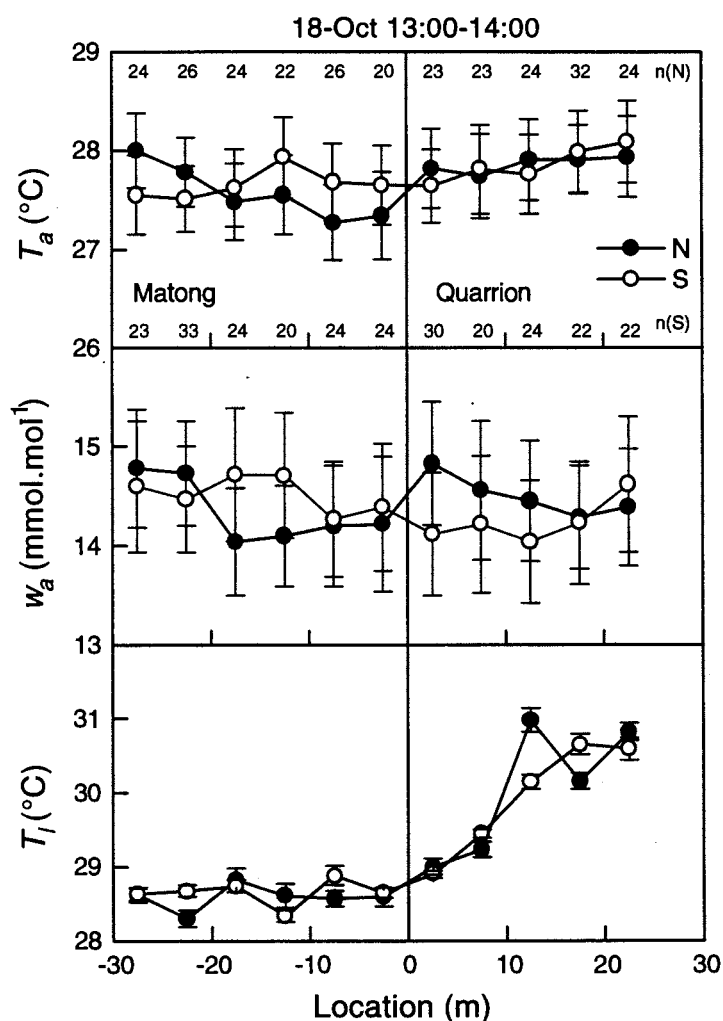
Figure 9.2 Spatial variation of air temperature (T_a), humidity (w_a) at 0.25 m above crop height and surface radiative temperature (T_l) with the sensors travelling north (N) and south (S). Standard errors are shown as error bars. The number of data points (n) at each location is shown separately for the North and South runs.

consistently in either air temperature, humidity or surface radiative temperature for different wind conditions. Different canopy densities (leaf area index) of the two crops may have resulted in different amounts of soil surface being seen by the infra-red sensors. The higher surface radiative temperatures of Quarrion may be partly attributed to its lower leaf area index (see Chapter Three) and higher soil surface temperatures as a result of greater radiation penetration to the soil.

Data were collected over many days in the weeks before and after anthesis, but not all with suitable wind speed and direction. Data from the 12-Oct and 24-Oct had southerly wind, and the 18-Oct and 30-Oct had northerly wind. Other days had very light winds, winds from the east or west, or patchy clouds.

9.3.1. Transition from High to Low Conductance

Data of 12-Oct, 9:00-10:00
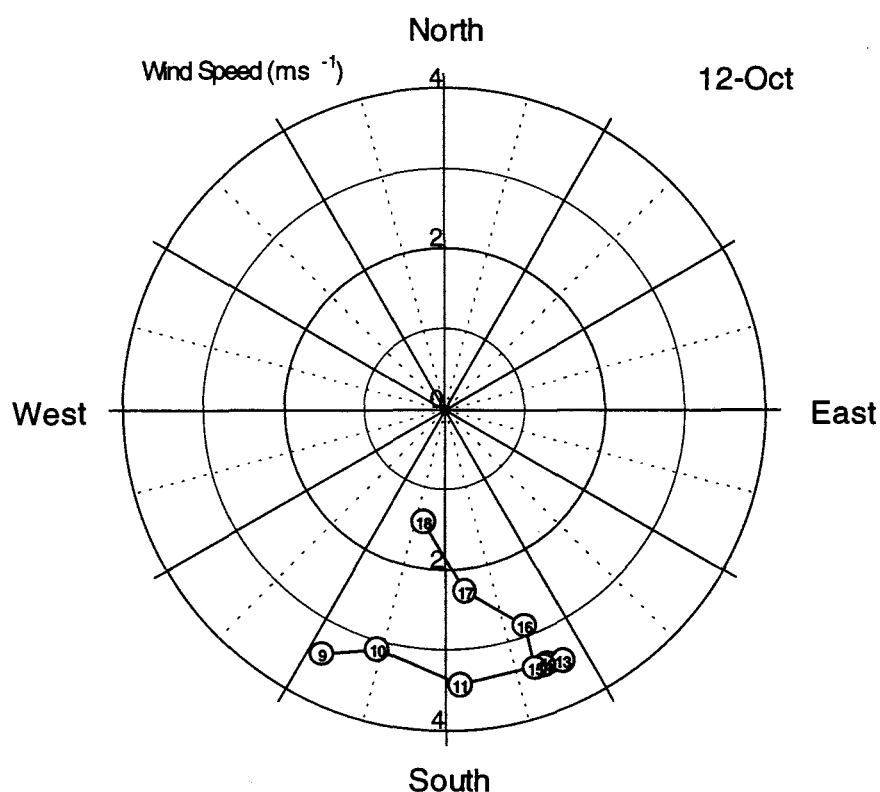
Figure 9.3 Diurnal variation of wind speed (0.5 m above crop height) and direction on the 12-Oct.

On 12-Oct the wind blew from the south coming over the Matong crop with higher conductance and then over the Quarrion crop, with low conductance. Variation of wind speed and direction is shown in figure 9.3.

The energy balance of the crops measured by the Bowen ratio system in the centre of each paddock was different, with Matong having a greater flux of latent heat and lower flux of sensible heat than the Quarrion crop (figure 9.4).

Figure 9.4 Available energy (R-G), sensible heat flux (H) and latent heat flux (LE) of the Matong (——) and Quarrion (- - -) crops on 12-Oct, measured with Bowen ratio systems.

Analysis of the net radiation (R_n) measured in conjunction with the monorail revealed that high cloud was present, causing large variation in R_n, that was not apparent in the fifteen minute averages of the Bowen ratio data (figure 9.5).
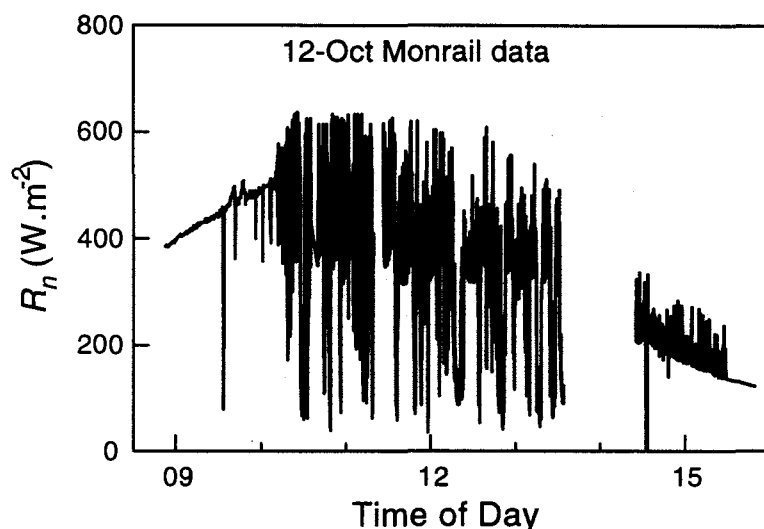
Figure 9.5 Diurnal variation of net radiation (R_n) measured at six second intervals in conjunction with the monorail data collection on 12-Oct.

Data from between 9:00 and 10:00 were suitable for analysis, after removing a few runs when clouds were present (figure 9.6). Air temperature (T_a) increased, as expected, as the air was influenced by the Quarrion crop with lower conductance. Air humidity (w_a) decreased over Quarrion, but it was no greater than the variation observed over Matong. There was a significant increase in surface temperature (T_l) over Quarrion compared to Matong, but again there was considerable spatial variation that was not associated with the interface between the crops. The net effect on the leaf-to-air vapour concentration difference ($D_l = w_s(T_l) - w_a$) was that it increased substantially over the Quarrion canopy.

Figure 9.6 Variation of air temperature (T_a), humidity (w_a), surface radiative temperature (T_l), leaf-to-air vapour concentration difference (D_l), calculated canopy conductance (G_c), canopy transpiration at the surface (E_c), canopy transpiration at 0.25-0.50m with footprint corrections (·····), sensible heat (H) and latent heat (LE) fluxes across the interface between crops with wind blowing from a canopy with high conductance (Matong) onto a canopy with lower conductance (Quarrion).

The sensible heat flux (H) calculated from the monorail data was 48% greater over Quarrion than Matong in accordance with the Bowen ratio measurements (figure 9.4). The latent heat flux was 10% lower over Quarrion than Matong, which agreed with the difference in evaporation estimated from canopy conductance. Evaporation, estimated from conductance, was lowest at the leading edge of Quarrion and thereafter increased slightly as D_l increased with further distance into Quarrion. Variation of surface temperature was largest of all the measured parameters, so that large gradients of D_l were calculated, which reduced G_c and caused the observed variation of evaporation. This phenomenon was not observed in the latent heat flux, due to the footprint area of the fluxes measured at 0.25 - 0.50 m above canopy height smearing the subtle changes that occurred at the interface. Using the footprint corrections (Table 9.1) the variation of surface transpiration flux was comparable to the variation of the latent heat flux above the canopy.
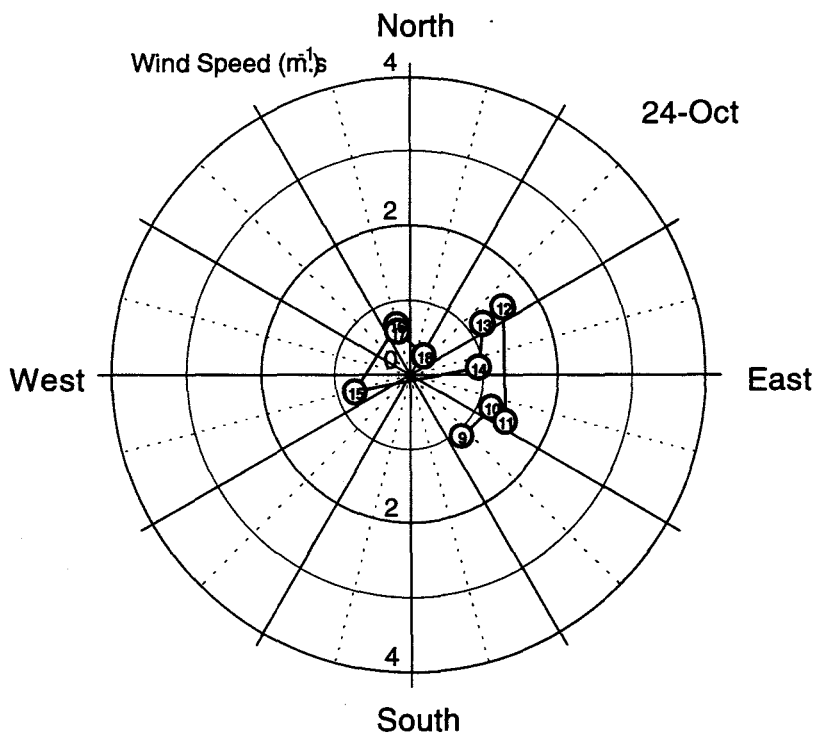
Figure 9.7 Diurnal variation of wind speed (0.5 m above crop height of 1.02 m) and direction on the 24-Oct.

On 24-Oct winds were very light and from all directions (figure 9.7). Only data from 9:00 - 10:00 were suitable for analysis of advection. Data from other times showed the contrast between the two crops, but the wind came along the interface confounding the analysis of advection.

The energy balance measured by the Bowen ratio system in the centre of each paddock showed high latent heat fluxes (figure 9.8), which were expected as 33 mm of
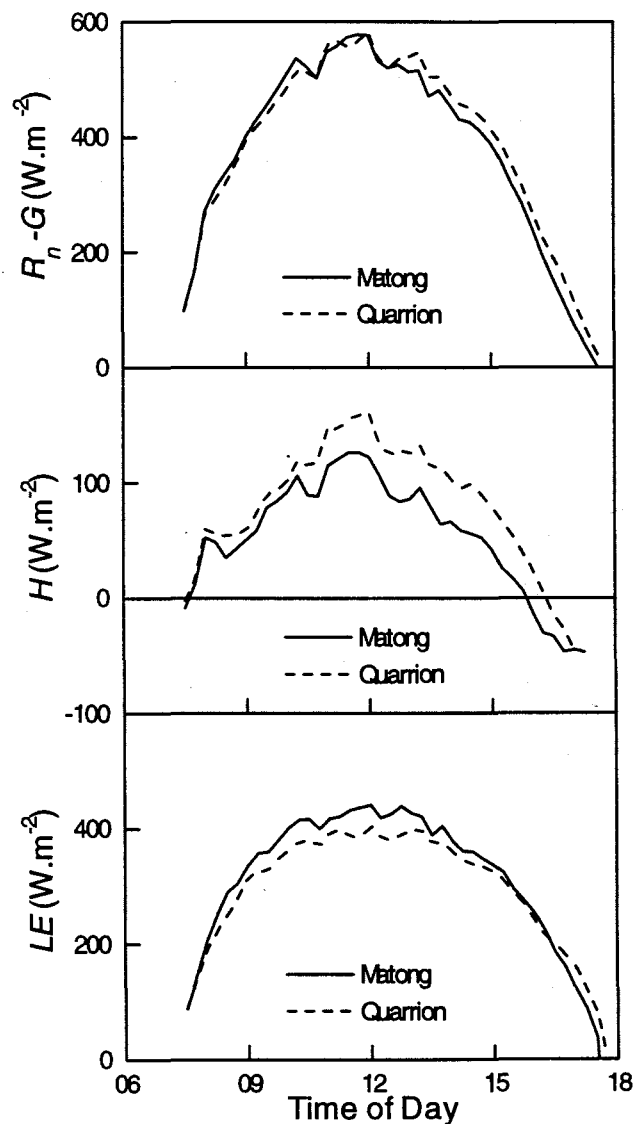

Figure 9.8 Available energy (*R-G*), sensible heat flux (*H*) and latent heat flux (*LE*) of the Matong (——) and Quarrion (- - -) crops on 24-Oct, measured with Bowen ratio systems.

rain fell two days earlier on 22-Oct. Part of this latent heat was presumably from substantial soil evaporation, which would have been greater for the Quarrion canopy than the Matong, as the former had less complete canopy closure (L_c = 1.75 & 2.55 respectively).

Net radiation measured with the monorail data showed that the sky was clear all day (data not shown). Air and leaf temperature increased and humidity decreased over Quarrion compared to Matong (figure 9.9), as expected from a southerly wind coming over the canopy with higher evaporation rate (Matong) and then across the canopy with a lower evaporation rate. Changes in T_a, w_a, T_l and D_l along the transect and have been fitted to a power function of fetch. Typically, the exponents ranged from 1/4 to 1/24, which are consistent with the range given by Itier *et al.* (1994) for the advection model of Philip (1959; 1987). No further attempt was made to fit this model or examine the parameters, other than to use the form of the equations to give the shape of the curves. Further analysis may reveal whether the fitted model coefficients are plausible under a range of conditions.

The sensible heat flux for this data set, calculated from the temperature and wind profiles, was only 25 % of the flux measured by the Bowen ratio systems. This large discrepancy was possibly due to the light wind (average 1.08 m.s^{-1} at 0.50 m above the
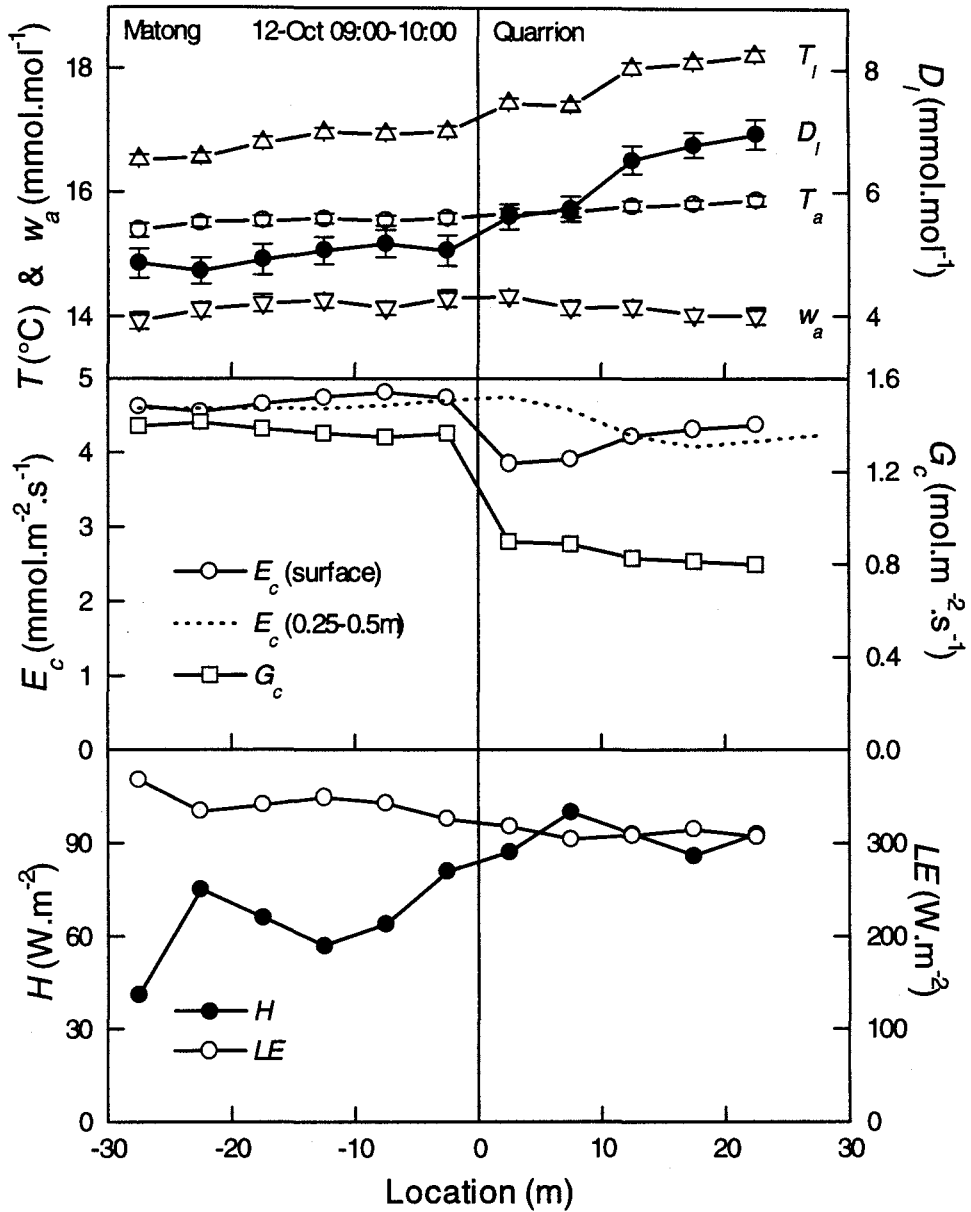

Figure 9.9 Variation of air temperature (T_a), humidity (w_a), surface radiative temperature (T_l) and leaf-to-air vapour concentration difference (D_l) across the interface between crops with wind blowing from a canopy with high conductance (Matong) onto a canopy with lower conductance (Quarrion).

top of the canopy), whereas greater wind speed in the previous data set (12-Oct 09:00-10:00) allowed the gradient approach to work reasonably well.

Data of 30-Oct, 11:00-12:00

Faster water use by the Matong crop, compared to Quarrion, led to greater soil water deficits in Matong and reversed the ranking of conductance of the two crops, so that Matong had lower conductance than Quarrion (Chapter Three). North-westerly wind in the morning of the 30-Oct (figure 9.10) was suitable for analysis of advection, with wind coming from a canopy of higher conductance across a canopy of lower conductance, but in the opposite direction to the previous data sets. This data set allowed the analysis of gradients across the transition from high to low conductance, in the opposite physical direction to the previous data sets for the 12-Oct and 24-Oct, so that it is possible to see if it was the location rather than advection that was causing the variation along the transect.
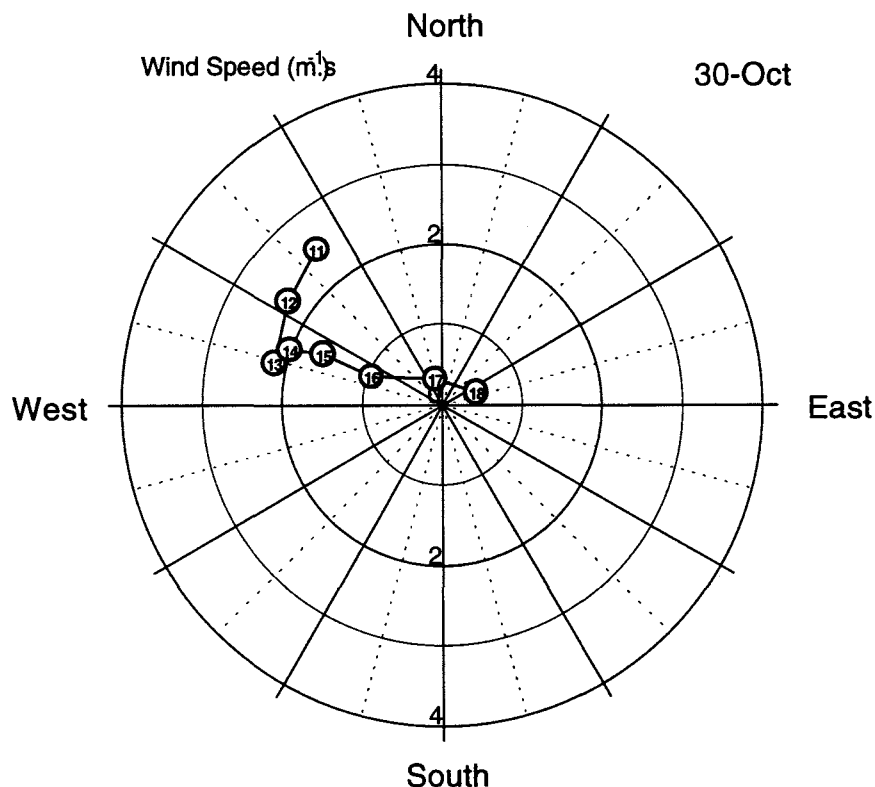
Figure 9.10 Diurnal variation of wind speed (0.5 m above crop height of 1.07 m) and direction on the 30-Oct.

The energy balance in the centre of each paddock on 30-Oct showed that the ranking of the two crops had reversed, with Quarrion having higher latent heat flux and lower sensible heat flux than Matong (figure 9.11).
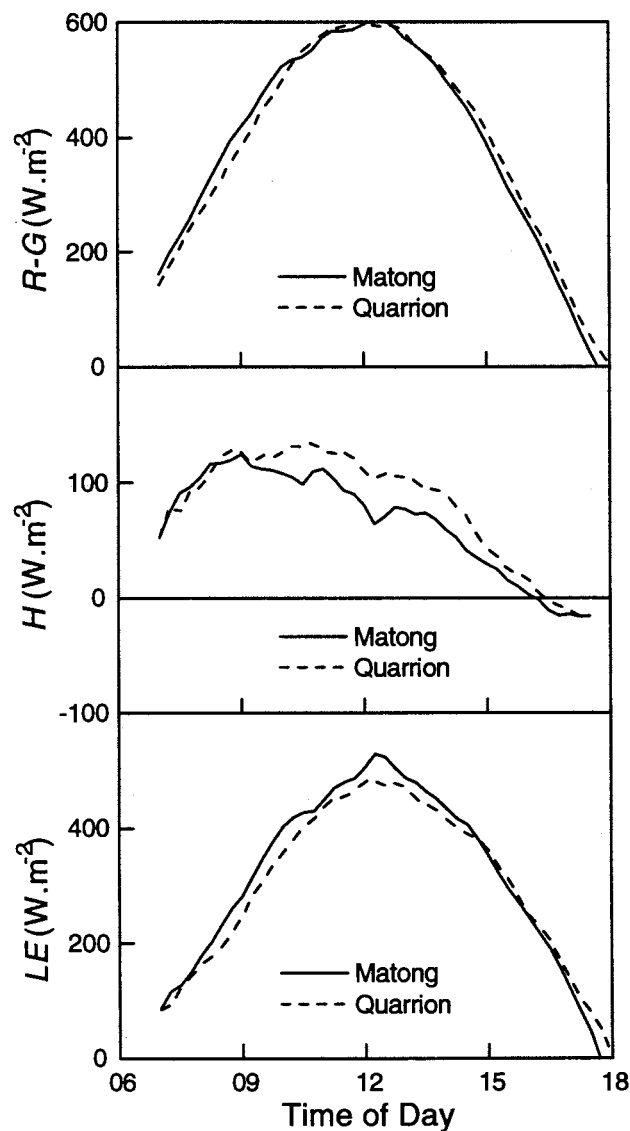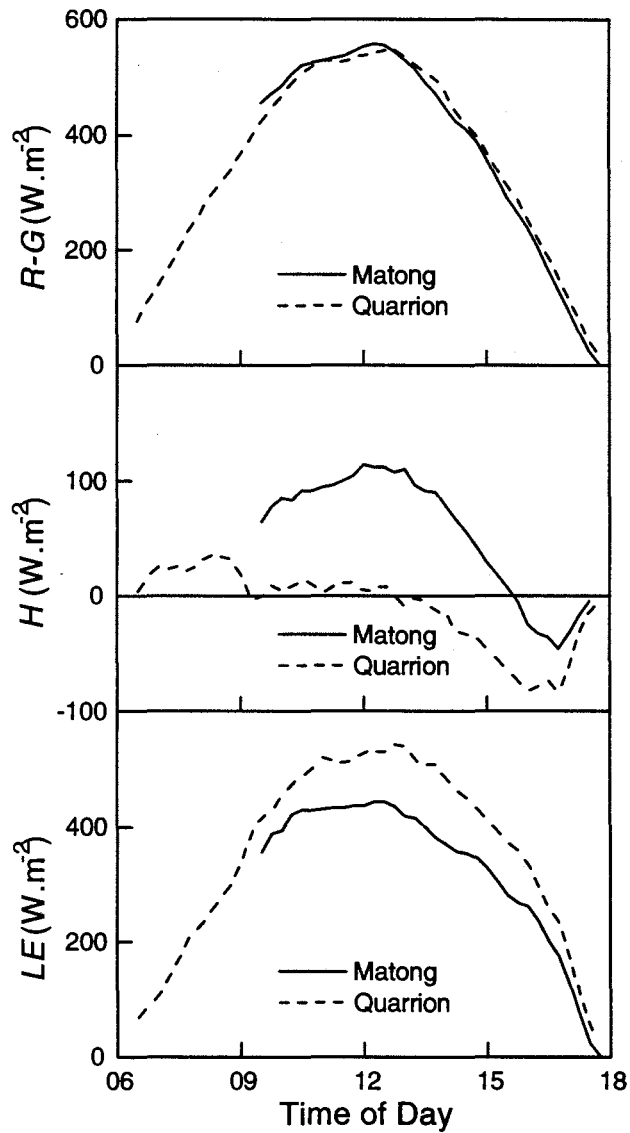

Figure 9.11 Available energy (R-G), sensible heat flux (H) and latent heat flux (LE) of the Matong (——) and Quarrion (- - -) crops on 30-Oct, measured with Bowen ratio systems.

Air and leaf temperature and D_l increased over Matong compared to Quarrion, but large variability in the humidity prevented any clear differences of humidity between the crops (figure 9.12). These observations are consistent with expected advection as the wind moved from Quarrion across the interface with Matong showing increasing air and surface temperature. The extreme temperatures and D_l combined with the low soil water status on this day resulted in more variation along the gradient, presumably due to variability in individual plants response to water stress.
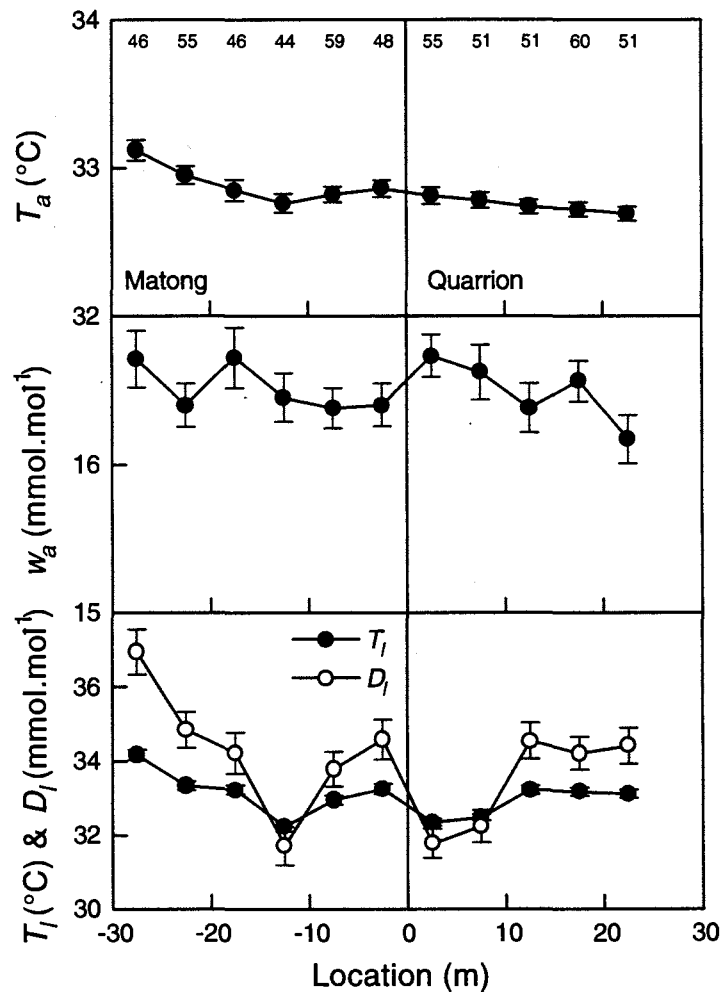
Figure 9.12 Variation of air temperature (T_a), humidity (w_a), surface radiative temperature (T_l) and leaf-to-air vapour concentration difference (D_l) across the interface between crops with wind blowing from a canopy with high conductance (Quarrion) onto a canopy with lower conductance (Matong) on 30-Oct between 11:00-12:00.

9.3.2. Transects with no contrast in Conductance

Data from 18-Oct were suitable for examining transects when both crops had similar conductances. The wind was steady from the north averaging 2-3 $m.s^{-1}$ (figure 9.13).
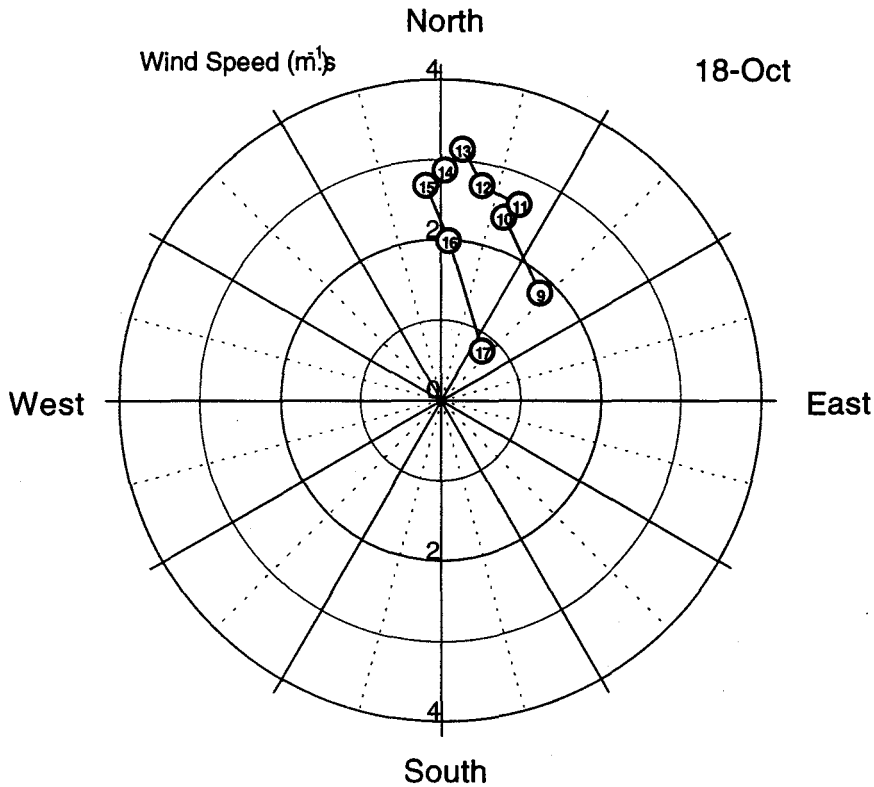
Figure 9.13 Diurnal variation of wind speed (0.5 m above crop height of 0.96 m) and direction on the 18-Oct.

The energy balance in the centre of each paddock on 18-Oct showed that both crops had similar fluxes of latent and sensible heat (figure 9.14), so that variation along the transect could not be attributed to advection.
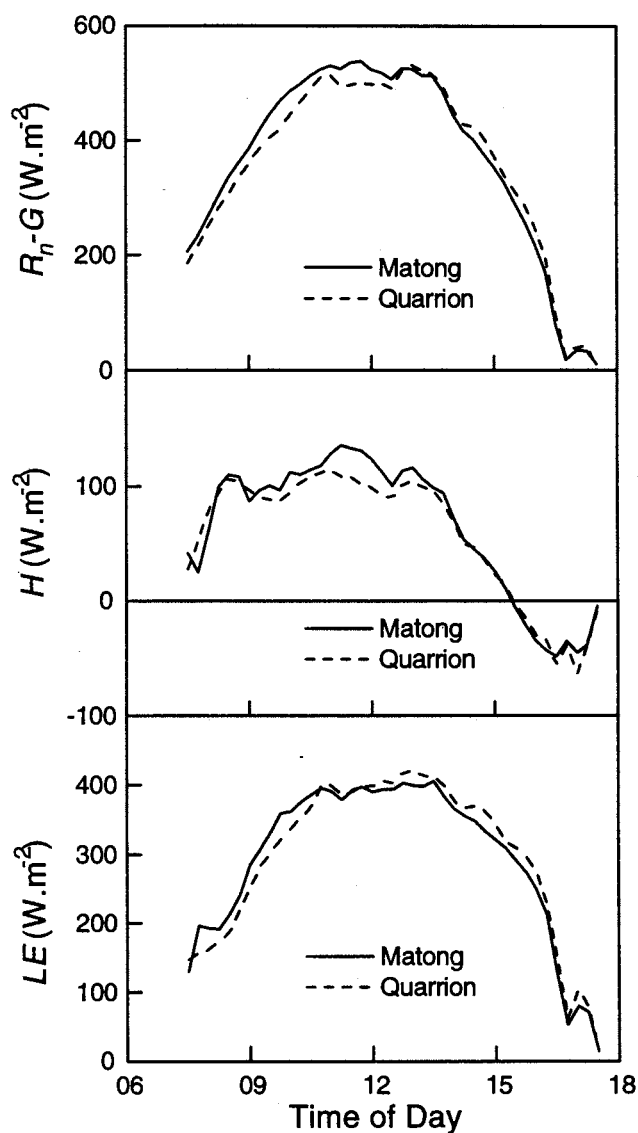
Figure 9.14 Available energy (*R-G*), sensible heat flux (*H*) and latent heat flux (*LE*) of the Matong (——) and Quarrion (- - -) crops on 18-Oct, measured with Bowen ratio systems.

High cloud caused some variation in the radiation load (figure 9.15) so that not all data could be used. Data from between 13:00-14:00 were selected after removing transects when the radiation varied more than 10% from the average.
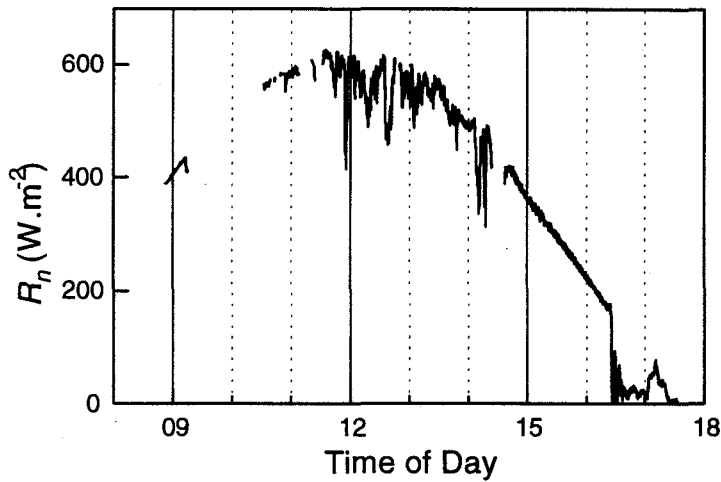
Figure 9.15 Diurnal variation of net radiation (R_n) measured at six second intervals measured in conjunction with the monorail data collection on 18-Oct.

Air temperature and humidity did not change significantly at the interface between the crops, but the surface temperature did increase causing an increase in D_l and the calculated canopy conductance and evaporation (figure 9.16). The sensible heat and latent heat fluxes, calculated from the wind and temperature profiles, were not significantly different between the two crops. The higher surface temperature of the Quarrion crop may have been due to a more open canopy (L_c = 2.26) than the Matong canopy (L_c = 3.36), so that the infra-red sensors would see a greater contribution from the soil, which would have been much warmer than the leaves, since the soil surface was dry on this day.
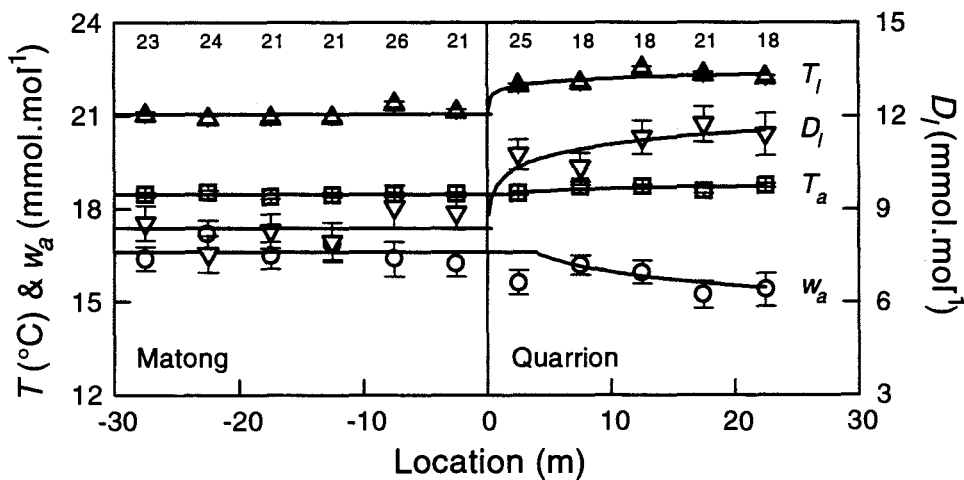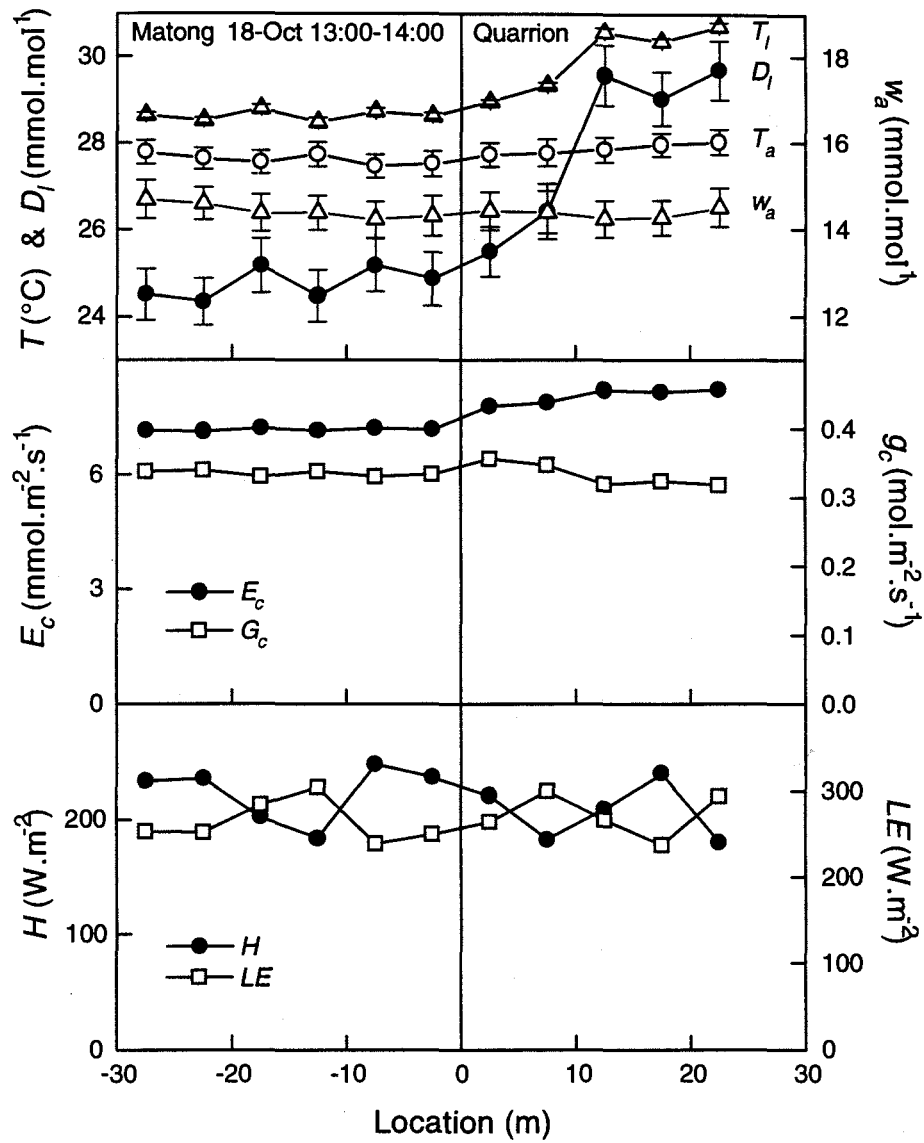
Figure 9.16 Variation of air temperature (T_a), humidity (w_a), surface radiative temperature (T_l), leaf-to-air vapour concentration difference (D_l), calculated canopy conductance (G_c), canopy transpiration (E_c), sensible heat (H) and latent heat (LE) fluxes across the interface between crops with wind blowing from a canopy with low conductance (Quarrion) onto a canopy with higher conductance (Matong).

9.4. Discussion

Small gradients of air temperature and humidity were detected along the transect between the crops when they had different conductances, which were not apparent when the conductances were similar. These gradients occurred when Matong had higher conductance than Quarrion and were reversed when the ranking of the crops' conductances were reversed, giving confidence to advection being the cause rather than some anomaly in the physical location.

Surface radiative temperature showed stronger gradients along the transect than air temperature or humidity. When the ranking of conductance of the crops reversed the surface temperature reflected this change (figure 9.12). However, when the conductances and evaporation rates of the crops were similar the surface temperature still indicated Quarrion to be 1 - 2° warmer than Matong (figure 9.16). This could be attributed to the more open canopy of Quarrion, resulting in a greater contribution from the soil to the measured surface radiative temperature. The difference in surface temperature between the crops was the main cause for large differences in the leaf-to-air vapour concentration difference.

Fluxes calculated from wind speed and temperature profiles were realistic in conditions of high wind, but too low in light wind. The fluxes were consistent with the differences in conductance between the crops, but did not clearly show evidence of advection from the edge of the crop with a different conductance. The lack of variation of fluxes with fetch was consistent with a step change of fluxes, but could not be conclusively distinguished from a step change in conductance or surface concentration. This was similar to the variation of sensible heat flux found at the interface between irrigated and dryland barley crops, which indicated a step change in surface flux (Itier *et al.*, 1994).

Variation of modelled conductance and evaporation rate along the transect showed a step change at the interface due to the different model coefficients for each crop. Some adjustment of conductance with increasing downwind distance from the interface was observed although this was mainly driven by the variation of surface temperature along the transect, which was shown to be somewhat overestimated. The adjustment of conductance and evaporation rate with distance from the leading edge was consistent with advection, although it was very small.

Differences between the variation of latent heat flux calculated from the wind and temperature profiles compared to the evaporation rate calculated from canopy conductance can be attributed to the different height at which the measurements were made. The calculated evaporation rate is the flux that occurs at the surface, whereas the latent heat flux is determined over the range of 0.25 - 0.50 m above the top of the canopy. The flux above a canopy does not directly relate to the flux at the surface immediately below, but has contributions from the surface fluxes over an area of crop upwind, known as the footprint area. Using a weighted averaging scheme of the upwind surface fluxes, similar to that indicated by the analysis of Schuepp *et al.* (1990), to correct for the footprint area, the variation of the surface flux with distance was similar to that calculated at 0.25 - 0.50 m above the crop.

Different fluxes of the two crops measured by the transect data were comparable to differences measured by the Bowen ratio systems at the centre of each paddock. The effect of advection on the fluxes was very small, if it occurred at all. This can be attributed to there being only a small contrast in the energy balance of the crops (Chapter Three). The reduced sensitivity of canopy transpiration to canopy conductance was attributed to the effect of canopy boundary layers and the modification of the air surrounding the canopy. The change in canopy conductance at the interface did result in lower rates of transpiration, but the change was sufficiently small that advection had minimal effect on the fluxes as a function of distance from the leading edge.

These results imply that advection between small plots with contrasting evaporation rates should not significantly affect total water use, in contrast to the estimates by Cowan (1988). Results obtained from small plots should be a reasonably accurate reflection of water use that would occur in extensive areas. In the field trial reported in this chapter, small plots of each of the varieties were grown embedded in the extensive paddocks of both varieties. Water use in the small plots was not significantly different from water use in the large plots (Condon, unpublished data), confirming the conclusions drawn from this study that advection was not significant. That is not to say that advection is never significant. Other advection studies have shown large variation of fluxes following changes in surface properties (Rider *et al.*, 1963; Lang *et al.*, 1974). Small plots grown in extensive areas of fallow, denuded of vegetation, or well irrigated plots in dry conditions would be much more affected by advection than this study. So long as small plots are grown in an area with similar vegetation, then advection between the plots should have minimal impact on water use.

9.5. Conclusions

Advection of heat was measured at the interface between two crops with contrasting conductances. The increase in air temperature was up to 0.5°C over 28 m downwind from the leading edge. Leaf temperature increased by several degrees in the crop with lower conductance, but substantial spatial variability along the transect prevented this from being attributed to advection. Change in air humidity was not observed in relation to the interface between the contrasting crops.

Calculated fluxes of sensible and latent heat showed a step change at the interface, but did not show any further variation with distance from the leading edge. Calculated canopy conductance and transpiration also showed a step change with some further minor readjustment over 10 m downwind from the leading edge.

These observations, although inconclusive, suggest that in this case advection did not significantly affect water use of crops at the interface with vegetation of different conductances. Advection may be more significant in situations with more marked contrasts such as irrigated and unirrigated crops. Water use measured in small plots should be representative of water use that would occur in extensive paddocks, so long as the small plots are surrounded by similar, though not necessarily identical, vegetation.

The novel system of travelling sensors provided direct observations of the spatial variation of the environment. There are difficulties in the analysis of these data in terms of advection, but further analysis by use of models may yet reveal whether advection was significant. Despite these problems, the technical approach presented in this chapter may in future be useful for investigating other problems of spatial variation of the environment.

CHAPTER TEN:

GENERAL DISCUSSION

10.1. Preamble

Scaling physiological processes has recently received considerable attention in the scientific literature, due to the need for a better understanding of the response of vegetation to increasing atmospheric CO_2 concentration and associated climate change (Carlson, 1991; Ehleringer & Field, 1993; Jarvis, 1995). The complexity of the interactions between vegetation and the environment requires the use of mathematical models to accurately describe canopy processes of photosynthesis and transpiration. Existing models adequately describe leaf photosynthesis (Farquhar *et al.*, 1980), conductance (Leuning, 1995) and radiation penetration through canopies (Goudriaan, 1977). Many researchers have presented frameworks for scaling conductance (Raupach & Finnigan, 1988; Kim & Verma, 1991b; Rochette *et al.*, 1990; Baldocchi, 1991; 1993; Raupach, 1995) and photosynthesis (Sellers *et al.*, 1992; Norman, 1993; Amthor, 1994), which have only recently been tested with suitable field experiments with concurrent measurements at leaf and canopy scales (Amthor *et al.*, 1994; Baldocchi & Harley, 1995). There remained a need to compare different approaches to scaling on different types of vegetation and under less than ideal conditions. This thesis has attempted to fill this gap with a thorough analysis of the scaling of photosynthesis and water use from leaves to canopies in dryland wheat crops. To conclude this thesis the main findings are presented in a broader context in the following discussion.

10.2. Models of Stomatal Conductance and Photosynthesis

Stomatal models which utilise the correlation between conductance and photosynthesis have been successfully applied in many experiments (Ball *et al.*, 1987; Leuning, 1990; 1995; Kim & Verma, 1991a; Aphalo & Jarvis, 1993), including the data in Chapter Four. While this is an elegant approach, use of photosynthesis as a variable in the model may be opening Pandora's proverbial box. For without measurements of photosynthesis the stomatal model must be coupled with a model of photosynthesis. The widely accepted Farquhar model of photosynthesis accurately describes the response of CO_2 exchange to short term variation of irradiance, CO_2 concentration and temperature. But the response of photosynthesis, and the appropriate parameters of a model, to long term changes of the environment such as acclimation to high CO_2, high temperature or water deficits, are not well described let alone predictable, as shown in Chapter Seven. Many empirical functions have been developed to describe stomatal response to soil water deficits independently of photosynthesis (Schulze, 1986; Inoue *et al.*, 1989).

When using the correlation of conductance with photosynthesis, functions relating conductance to soil water are redundant, but few functions exist that relate photosynthesis to soil water deficits. Periodic and terminal drought is typical of dryland agriculture, almost by definition, and will always affect photosynthesis and conductance whenever water-use efficiency is considered. Indeed, it is not the case that soil water deficits are exceptional conditions, but rather that they are more typical conditions for many crops, forests and natural ecosystems around the world (Lieth, 1973; Woodward, 1987).

So are we any further ahead? In some respects, utilising the correlation of conductance with photosynthesis is just circling the real issue of understanding plant response to real (non-ideal) environments. On the other hand, there are at least two benefits to this approach. Firstly, following recent technological developments, eddy correlation measurements of canopy CO_2 fluxes are becoming a routine micrometeorological measurement. Concurrent measurement of CO_2 and H_2O fluxes will allow testing of this type of stomatal model on a diverse range of canopies and under a range of conditions. Use of this model will overcome one of the main constraints for effective use of the Penman-Monteith model of canopy evaporation; obtaining accurate estimates of canopy conductance. As databases of canopy CO_2 fluxes expand, the use of models that link the CO_2 and H_2O fluxes will provide an extra constraint for valid predictions of vegetation response to climate change.

Secondly, a great deal more is known about the mechanistic nature of photosynthesis than stomatal behaviour. Many of the genes that control photosynthesis are known and are being used to manipulate photosynthesis through molecular techniques, (eg.; Stitt & Schulze, 1994). These may lead to a mechanistic understanding, and hence better models, of adaptation of photosynthesis to the environment. This will probably also involve better understanding of the coordination between photosynthesis and stomatal conductance. The validity of stomatal models that use this coordination will be tested as the underlying mechanism is elucidated.

In Chapter Four stomatal conductance of sunlit leaves was modelled simply as a function of photosynthesis and a response to humidity. The humidity variable was found to be the most important accounting for 70% of the variation in stomatal conductance. Yet, the sensitivity of stomatal conductance to humidity varied between days, decreasing with soil water deficit. Variation of stomatal model parameters was identified as a key

349

limitation to predicting stomatal conductance *a priori*. Perhaps, the model of optimisation of carbon gain with respect to water loss may yet provide a useful framework for analysing stomatal behaviour under increasing water stress (Cowan, 1982), even though it was not found to be the best model for the data in this thesis. The stomatal model, with parameters derived from leaf scale measurements, also adequately described the variation of canopy conductance, demonstrating the scaling of conductance from leaves to canopies (Chapter Five). Further measurements of CO_2 and H_2O fluxes on a range of canopies at high temperatures and under water stress may provide significant insight into the applicability of this type of model. With further testing this stomatal model may then be used in models of crop and forest growth or in models of global carbon cycling. Linking the water and carbon cycles of the globe through use of this stomatal model, with correlations of conductance and photosynthesis, will provide extra ways to constrain model predictions to realistic values.

Similarly, the decline in photosynthesis during each day is a fascinating but unresolved observation in this thesis (Chapter Seven). As previously stated it is unclear whether the decline is in electron transport, RuBP regeneration, Rubisco activity or steps leading to carbon export from the leaf. The tight coordination and regulation of the components of photosynthesis and carbon metabolism confound research into the mechanism of this phenomenon, although molecular approaches may soon provide some insight. It is also difficult to realistically reproduce in controlled environments the decline in soil water status that is observed in the field. New approaches to research on the effects of water stress on photosynthesis and stomatal behaviour are needed.

10.3.   Scaling and Canopy Photosynthesis Models

A great deal of research effort has gone into models of canopy photosynthesis over the last 30 years since the early work of de Wit (1965), Duncan *et al.* (1967), Lemon *et al.*, (1971), Sinclair (1976) and Norman (1979). They applied their models primarily to agricultural crops and demonstrated the importance of separating sunlit and shaded leaves as well as beam and diffuse radiation (Norman, 1980). Unfortunately, these widely accepted practices have not been taken up by canopy modellers working in other fields, such as those working on the optimal distribution of nitrogen in canopies (Hirose & Werger, 1987a; Anten *et al.*, 1995; Badeck, 1995; Sands, 1995) and those developing simple models for studying the response of vegetation to climate change (Sellers *et al.*, 1992; Amthor *et al.*, 1994; Wang & Jarvis, 1993; Lloyd *et al.*, 1995). These simple

models can introduce errors when tuned for canopies of particular leaf area index or leaf nitrogen content. For example, when a big leaf model tuned to accurately predict canopy photosynthesis at a leaf area index of 2.0 was applied to a canopy of leaf area index of 4.0 the model overestimated daily gross canopy photosynthesis by 25% (Chapter Six). Predictions are needed, but systematic biases from such models may lead to incorrect conclusions about the relative importance of different vegetation types in mitigating rising atmospheric CO_2 concentration.

A novel approach to modelling canopy photosynthesis was presented in Chapter Six. This involved use of separate single-layered models for the sunlit and shaded leaves, allowing incorporation of decreasing photosynthetic capacity in the canopy, and when combined with stomatal and energy balance models provided a computationally simple model that was as accurate as a multi-layered model (Chapter Eight). This new model fulfils the criteria of being mechanistically based on processes at a lower scale with corresponding parameters and functions with similar definitions at both scales (Norman, 1993; Raupach, 1995; Jarvis, 1995), while being sufficiently simple and accurate to be useful (Raupach & Finnigan, 1988). Modification of this model for use with canopies that require more complex light penetration models due either to clumping or penumbral effects will extend its use to forest canopies as well. Incorporation of this approach into models of photosynthesis of other ecosystems will simplify them and allow them to be more easily incorporated into higher level models.

Canopy models (such as presented in Chapter Eight) that combine the physiological processes of photosynthesis and stomatal behaviour with the physical processes of radiation penetration, energy partitioning and turbulent transport are very useful for investigating a range of issues. Use of mechanistic models to describe the component processes allows the non-linear interactions and feedback effects to be properly represented, so that extrapolation to new environmental conditions are more likely to be valid. For example, in Chapter Eight, model predictions were that transpiration efficiency and water-use efficiency (including soil fluxes) would be approximately 1.8 fold as much in response to doubling of atmospheric CO_2 concentrations, varying only slightly with leaf area index, although acclimation of photosynthesis may reduce this response. Incorporation of the effects of acclimation of plants to altered conditions will further enhance the utility of this model.

10.4.   Water-Use Efficiency

Carbon isotope discrimination (Δ) provided a practical means to link physiological traits to agronomic issues (Farquhar *et al.*, 1982; Farquhar & Richards, 1984). However, the link between Δ and water-use efficiency via physiological processes is not straight-forward (Farquhar *et al.*, 1989a; Hall *et al.*, 1994). Reduced sensitivity of transpiration to stomata conductance at increasing spatial scales (Jarvis & McNaughton, 1986), was seen as a potential limitation to improvements in water-use efficiency where changes came about from reduced stomatal conductance rather than increased photosynthetic capacity (Farquhar *et al.*, 1989b). Interactions between vegetation and the atmosphere and advection following a change in stomatal conductance of a crop were seen as possibly reversing benefits to water-use efficiency from reduced conductance (Cowan, 1988). Field experiments showed that the relationship between Δ and crop yields could be reversed in different conditions (Condon *et al.*, 1990), depending on water availability amongst other factors, suggesting that the canopy-atmosphere interactions may confound attempts to improve water-use efficiency through altered conductance. The Wagga Wagga field trials examined in this thesis were established as the definitive test of the relationship between Δ and water-use efficiency in the worst scenario where differences in Δ were mostly due to differences in conductance, rather than photosynthetic capacity.

Despite the effect of canopy boundary layers, reduced stomatal conductance in the Quarrion cultivar of wheat did result in higher water-use efficiency on individual days and over integrated over the entire 1990 growing season compared to Matong (Condon & Richards, 1993 Chapter Three). Low sensitivity of transpiration to stomatal conductance did reduce the benefit of lower stomatal conductance to canopy water-use efficiency, but did not obscure it entirely; 40% reduction of leaf conductance was estimated to result in 36% greater leaf transpiration efficiency and 19% greater canopy transpiration efficiency, but varied somewhat with the absolute conductance and the wind speed (Chapter Eight). Advection did not cause a reversal of water-use efficiency or appear to have much impact in the crops and conditions examined here (Chapter Nine), although it may play a significant role if small plots were grown in very contrasting surrounds such as bare ground. Unexpectedly, reduced stomatal conductance was associated with low early vigour in Quarrion, resulting in lower canopy leaf area index and greater soil evaporation, which partially offset the gains from reduced transpiration.

10.5.   Final Words

The modelling presented in this thesis will be useful in many different applications. The sun/shade canopy model has the same form as the leaf scale models facilitating comparison of the response of fluxes to the environment at both scales. This feature allowed the decline of photosynthesis during the day to be analysed at both the leaf and canopy scale. The mechanistic representation in this modelling of both physical and physiological processes should therefore assist in making predictions of the response of canopy fluxes to both altered physiological traits and climate change.

References

Acock, B., Charles-Edwards, D. A., Fitter, D. J., Hand, D. W., Ludwig, L. J., Warren Wilson, J., and Withers, A. C. (1978). The contribution of leaves from different levels within a tomato crop to canopy net photosynthesis: an experimental examination of two canopy models. *Journal of Experimental Botany* **29**, 815-827.

Amthor, J. S. (1989). 'Respiration and crop productivity.' (Springer-Verlag: New York.)

Amthor, J. S. (1991). Respiration in a future, higher-CO_2 world. *Plant, Cell and Environment* **14**, 13-20.

Amthor, J. S. (1994). Scaling CO_2-photosynthesis relationships from the leaf to the canopy. *Photosynthesis Research* **39**, 321-350.

Amthor, J. S., Goulden, M. L., Munger, J. W., and Wofsy, S. C. (1994). Testing a mechanistic model of forest-canopy mass and energy exchange using eddy correlation: carbon dioxide and ozone uptake by a mixed oak-maple stand. *Australian Journal of Plant Physiology* **21**, 623-651.

Anderson, J. P. E. (1982). Soil respiration. In 'Methods of soil analysis. Part 2. Chemical and microbiological properties.' (Eds. A. L. Page, R. H. Miller, & D. R. Keeney) (Second ed.) pp. 831-871. (American Society of Agronomy, Inc. Soil Science Society of America, Inc.: Madison.)

Anten, N. P. R., Schieving, F., and Werger, M. J. A. (1995). Patterns of light and nitrogen distribution in relation to whole canopy carbon gain in C_3 and C_4 mono- and dicotyledonous species. *Oecologia* **101**, 504-513.

Aphalo, P. J., and Jarvis, P. G. (1991). Do stomata respond to relative humidity? *Plant, Cell and Environment* **14**, 127-132.

Aphalo, P. J., and Jarvis, P. G. (1993). An analysis of Ball's empirical model of stomatal conductance. *Annals of Botany* **72**, 321-327.

Arya, S. P. (1988). 'Introduction to micrometeorology.' (Academic Press, Inc.: San Diego.)

Avissar, R. (1993). Observations of leaf stomatal conductance at the canopy scale: an atmospheric modeling perspective. *Boundary-Layer Meteorology* **64**, 127-148.

Avissar, R., and Pielke, R. A. (1991). The impact of plant stomatal control on mesoscale atmospheric circulations. *Agricultural and Forest Meteorology* **54**, 353-372.

Azcón-Bieto, J., and Osmond, C. B. (1983). Relationship between photosynthesis and respiration. *Plant Physiology* **71**, 574-581.

Badeck, F. W. (1995). Intra-leaf gradient of assimilation rate and optimal allocation of canopy nitrogen: a model on the implications of the use of homogeneous assimilation functions. *Australian Journal of Plant Physiology* **22**, 425-439.

Badger, M. R., and Collatz, G. J. (1977). Studies on the kinetic mechanism of ribulose-1,5-bisphosphate carboxylase and oxygenase reactions, with particular reference to the effect of temperature on kinetic parameters. *Carnegie Institute of Washington Yearbook* **76**, 355-361.

Bailey, W. G., and Davies, J. A. (1981). Bulk stomatal resistance control on evaporation. *Boundary-Layer Meteorology* **20**, 401-415.

Baldocchi, D., and Harley, P. (1995). Scaling carbon dioxide and water vapour exchange from leaf to canopy in a deciduous forest. II. Model testing and application. *Plant, Cell and Environment* **18**, 1157-1173.

Baldocchi, D. D. (1989). Turbulent transfer in a deciduous forest. *Tree Physiology* **5**, 357-377.

Baldocchi, D. D. (1991). Discerning the forest from the trees: an essay on scaling canopy stomatal conductance. *Agricultural and Forest Meteorology* **54**, 197-226.

Baldocchi, D. D. (1992). A lagrangian random-walk model for simulating water vapor, CO_2 and sensible heat flux densities and scalar profiles over and within a soybean canopy. *Boundary-Layer Meteorology* **61**, 113-144.

Baldocchi, D. D. (1993). Scaling water vapor and carbon dioxide exchange from leaves to a canopy: rules and tools. In 'Scaling physiological processes: leaf to globe.' (Eds. J. R. Ehleringer & C. B. Field) pp. 77-114. (Academic Press Inc.: San Diego.)

Baldocchi, D. D. (1994a). A comparative study of mass and energy exchange over a closed C_3 (wheat) and an open C_4 (corn) canopy: I. The partitioning of available energy into latent and sensible heat exchange. *Agricultural and Forest Meteorology* **67**, 191-220.

Baldocchi, D. D. (1994b). A comparative study of mass and energy exchange over a closed C_3 (wheat) and an open C_4 (corn) canopy: II. CO_2 exchange and water use efficiency. *Agricultural and Forest Meteorology* **67**, 291-321.

Baldocchi, D. D., Hicks, B. B., and Camara, P. (1987). A canopy stomatal resistance model for gaseous deposition to vegetated surfaces. *Atmospheric Environment* **21**, 91-101.

Baldocchi, D. D., Verma, S. B., Matt, D. R., and Anderson, D. E. (1986). Eddy-correlation measurements of carbon dioxide efflux from the floor of a deciduous forest. *Journal of Applied Ecology* **23**, 967-976.

Ball, J. T., Woodrow, I. E., and Berry, J. A. (1987). A model predicting stomatal conductance and its contribution to the control of photosynthesis under different environmental conditions. In 'Progress in Photosynthesis Research' (Ed. J. Biggens) Vol. IV, pp. 221-224. (Martinus Nijhoff: Dordrecht.)

Barnes, P. W., Beyschlag, W., Ryel, R., Flint, S. D., and Caldwell, M. M. (1990). Plant competition for light analyzed with a multispecies canopy model. III. Influence of canopy structure in mixtures and monocultures of wheat and wild oats. *Oecologia* **82**, 560-566.

Baver, L. D., Gardner, W. H., and Gardner, W. R. (1972). 'Soil Physics.' (John Wiley & Sons, Inc.: New York.)

Berry, J., and Björkman, O. (1980). Photosynthetic response and adaptation to temperature in higher plants. *Annual Review of Plant Physiology* **31**, 491-543.

Berry, J. A. (1992). Biosphere, atmosphere, ocean interactions: A plant physiologist's perspective. In 'Primary productivity and biogeochemical cycles in the sea.' (Eds. P. G. Falkowski & A. D. Woodhead) Vol. 43, pp. 441-454. (Plenum Press: New York.)

Bird, R. B., Stewart, W. E., and Lightfoot, E. N. (1960). 'Transport phenomena.' (John Wiley: New York.)

Björkman, O. (1981). Responses to different quantum flux densities. In 'Physiological plant ecology I. Responses to the physical environment.' (Eds. O. Lange, P. S. Nobel, C. B. Osmond, & H. Ziegler) Vol. 12A, (Springer-Verlag: Berlin.)

Björkman, O., Badger, M. R., and Armond, P. A. (1980). Response and adaptation of photosynthesis to high temperatures. In 'Adaptation of plants to water and high temperature stress.' (Eds. N. C. Turner & P. J. Kramer) pp. 233-249. (John Wiley & Sons. Inc.: New York.)

Black, T. A., Spittlehouse, D. L., Novak, M. D., and Price, D. T. (Eds.). (1989). 'Estimation of areal evapotranspiration.' (International Association of Hydrological Sciences: Wallingford.)

Black, T. A., Tanner, C. B., and Gardener, W. R. (1970). Evapotranspiration from a snap bean crop. *Agronomy Journal* **62**, 66-69.

Boote, K. J., and Loomis, R. S. (1991). The prediction of canopy assimilation. In 'Modeling crop photosynthesis - from biochemistry to canopy' (Eds. K. J. Boote & R. S. Loomis) Vol. Special Publication No. 19, pp. 109-140. (CSSA: Madison.)

Boyer, J. S., and Bowen, B. L. (1970). Inhibition of oxygen evolution in chloroplasts isolated from leaves with low water potentials. *Plant Physiology* **45**, 612-615.

Brooks, A., and Farquhar, G. D. (1985). Effect of temperature on the CO_2/O_2 specificity of ribulose-1,5-bisphosphate carboxylase/oxygenase and the rate of respiration in the light. *Planta* **165**, 397-406.

Brugnoli, E., Hubick, K. T., von Caemmerer, S., Wong, S. C., and Farquhar, G. D. (1988). Correlation between the carbon isotope discrimination in leaf starch and sugars of C_3 plants and the ratio of intercellular and atmospheric partial pressures of carbon dioxide. *Plant Physiology* **88**, 1418-1424.

357

Brunet, Y., Itier, B., McAneney, K. J., and Lagouarde, J. P. (1994). Downwind evolution of scalar fluxes and surface resistance under conditions of local advection. Part II: Measurements over barley. *Agricultural and Forest Meteorology* **71**, 227-245.

Brutsaert, W. H. (1982). 'Evaporation into the atmosphere.' (Reidel: Dordrecht, Holland.)

Bush, M. G., and Evans, L. T. (1988). Growth and development in tall and dwarf isogenic lines of spring wheat. *Field Crops Research* **18**, 243-270.

Caldwell, M. M., Meister, H.-P., Tenhunen, J. D., and Lange, O. L. (1986). Canopy structure, light microclimate and leaf gas exchange of *Quercus coccifera* L. in a Portuguese macchia: measurements in different canopy layers and simulations with a canopy model. *Trees* **1**, 25-41.

Campbell, G. S. (1977). 'An introduction to environmental biophysics.' (Springer-Verlag: New York.)

Carlson, T. N. (1991). Modeling stomatal resistance: an overview of the 1989 workshop at the Pennsylvania State University. *Agricultural and Forest Meteorology* **54**, 103-106.

Cheeseman, J. M. (1991). PATCHY: simulating and visualizing the effects of stomatal patchiness on photosynthetic CO_2 exchange studies. *Plant, Cell and Environment* **14**, 593-599.

Chen, J. L., Reynolds, J. F., Harley, P. C., and Tenhunen, J. D. (1993). Coordination theory of leaf nitrogen distribution in a canopy. *Oecologia* **93**, 63-69.

Collatz, G. J., Ball, T. J., Grivet, C., and Berry, J. A. (1991). Physiological and environmental regulation of stomatal conductance, photosynthesis and transpiration: a model that includes a laminar boundary layer. *Agricultural and Forest Meteorology* **54**, 107-136.

Condon, A. G., Farquhar, G. D., and Richards, R. A. (1990). Genotypic variation in carbon isotope discrimination and transpiration efficiency in wheat. Leaf gas exchange and whole plant studies. *Australian Journal of Plant Physiology* **17**, 9-22.

Condon, A. G., and Richards, R. A. (1993). Exploiting genetic variation in transpiration efficiency in wheat: an agronomic view. In 'Stable isotopes and plant carbon-water relations.' (Eds. J. R. Ehleringer, A. E. Hall, & G. D. Farquhar) pp. 435-450. (Academic Press, Inc.: San Diego.)

Condon, A. G., Richards, R. A., and Farquhar, G. D. (1987). Carbon isotope discrimination is positively correlated with grain yield and dry matter production in field-grown wheat. *Crop Science* **27**, 996-1001.

358

Condon, A. G., Richards, R. A., and Farquhar, G. D. (1993). Relationships between carbon isotope discrimination, water use efficiency and transpiration efficiency for dryland wheat. *Australian Journal of Agricultural Research* **44**, 1693-1711.

Cooper, P. J. M., Keatinge, J. D. H., and Hughes, G. (1983). Crop evapotranspiration - a technique for calculation of its components by field measurements. *Field Crops Research* **7**, 299-312.

Coppin, P. A., and Taylor, K. J. (1983). A three component sonic anemometer/thermometer system for general micrometeorological research. *Boundary-Layer Meteorology* **27**, 27-42.

Cowan, I. R. (1968a). The interception and absorption of radiation in plant stands. *Journal of Applied Ecology* **5**, 367-379.

Cowan, I. R. (1968b). Mass, heat and momentum exchange between stands of plants and their atmospheric environment. *Quarterly Journal of the Royal Meteorological Society* **94**, 523-544.

Cowan, I. R. (1977). Stomatal behaviour and environment. *Advances in Botanical Research* **4**, 117-228.

Cowan, I. R. (1982). Regulation of water use in relation to carbon gain in higher plants. In 'Physiological Plant Ecology II' (Eds. O. L. Lange, P. S. Nobel, C. B. Osmond, & H. Ziegler) Vol. 12B, pp. 589-613. (Springer-Verlag: Berlin.)

Cowan, I. R. (1986). Economics of carbon fixation in higher plants. In 'On the economy of plant form and function' (Ed. T. J. Givnish) pp. 133-170. (Cambridge University Press: Cambridge.)

Cowan, I. R. (1988). Stomatal physiology and gas exchange in the field. In 'Flow and transport in the natural environment: Advances and applications' (Eds. W. L. Steffen & O. T. Denmead) pp. 160-172. (Springer-Verlag: Canberra.)

Cowan, I. R., and Farquhar, G. D. (1977). Stomatal function in relation to leaf metabolism and environment. *Symposium of the Society for Experimental Biology* **31**, 471-505.

Davenport, D. C., and Hudson, J. P. (1967). Changes in evaporation rates along a 17-km transect in the Sudan Gezira. *Agricultural Meteorology* **4**, 339-352.

de Wit, C. T. (1965). 'Photosynthesis of leaf canopies'. (Agricultural Research Report No. 663). PUDOC, Wageningen.

de Wit, C. T. (1970). Dynamic concepts in biology. In 'Prediction and measurement of photosynthetic productivity' pp. 17-23. (PUDOC: Wageningen.)

de Wit, C. T., and et al (1978). 'Simulation of assimilation, respiration and transpiration of crops.' (PUDOC: Wageningen.)

DeJong, T. M., and Doyle, J. F. (1985). Seasonal relationships between leaf nitrogen content (photosynthetic capacity) and leaf canopy light exposure in peach (*Prunus persica*). *Plant, Cell and Environment* **8**, 701-706.

Denmead, O. T. (1969). Comparative micrometeorology of a wheat field and a forest of *Pinus radiata*. *Agricultural Meteorology* **6**, 357-371.

Denmead, O. T. (1976). Temperate cereals. In 'Vegetation and the atmosphere. Vol. 2. Case Studies' (Ed. J. L. Monteith) pp. 1-31. (Academic Press: London.)

Denmead, O. T. (1995). Novel meteorological methods for measuring trace gas fluxes. *Philosophical Transactions of the Royal Society of London. Series A* **351**, 383-396.

Denmead, O. T., and Bradley, E. F. (1985). Flux - gradient relationships in a forest canopy. In 'The forest - atmosphere interaction' (Eds. B. A. Hutchison & B. B. Hicks) pp. 421-442. (D. Reidel Pub.Co.: Dordrecht.)

Denmead, O. T., Dunin, F. X., Wong, S. C., and Greenwood, E. A. N. (1993). Measuring water use efficiency of eucalypt trees with chambers and micrometeorological techniques. *Journal of Hydrology* **150**, 649-664.

Denmead, O. T., and Raupach, M. R. (1993). Methods for measuring atmospheric gas transport in agricultural and forest systems. In 'Agricultural ecosystems effects on trace gases and global climate change.' Vol. ASA Special Publication no. 55, pp. 19-43. (American Society of Agronomy: Madison.)

Dolman, A. J., and Wallace, J. S. (1991). Lagrangian and K-theory approaches in modelling evaporation from sparse canopies. *Quarterly Journal of the Royal Meteorological Society* **117**, 1325-1340.

Dugas, W. A., Fritschen, L. J., Gay, L. W., Held, A. A., Matthias, A. D., Reicosky, D. C., Steduto, P., and Steiner, J. L. (1991). Bowen ratio, eddy correlation, and portable chamber measurements of sensible and latent heat flux over irrigated spring wheat. *Agricultural and Forest Meteorology* **56**, 1-20.

Duncan, W. G., Loomis, R. S., Williams, W. A., and Hanau, R. (1967). A model for simulating photosynthesis in plant communities. *Hilgardia* **38**, 181-205.

Dunin, F. X., Meyer, W. S., and Reyenga, W. (1989a). Seasonal change in water use and carbon assimilation of irrigated wheat. *Agricultural and Forest Meteorology* **45**, 231-250.

Dunin, F. X., Nulsen, R. A., Baxter, I. N., and Greenwood, E. A. N. (1989b). Evaporation from a lupin crop: A comparison of methods. *Agricultural and Forest Meteorology* **46**, 297-311.

Dunin, F. X., Reyenga, W., and McIlroy, I. C. (1991). Australian lysimeter studies of field evaporation. In 'Lysimeters for evapotranspiration and environmental measurements.' (Eds. R. G. Allen, T. A. Howell, W. O. Pruitt, I. A. Walter, & M. E. Jensen) pp. 237-245. (IR-Division/ASCE: Honolulu, HI.)

Dwyer, L. M., and Stewart, D. W. (1986). Effect of leaf age and position on net photosynthetic rates in maize (*Zea mays* L.). *Agricultural and Forest Meteorology* **37**, 29-46.

Dyer, A. J., and Hicks, B. B. (1970). Flux-gradient relationships in the constant flux layer. *Quarterly Journal of the Royal Meteorological Society* **96**, 715-721.

Edwards, N. T., and Sollins, P. (1973). Continuous measurement of carbon dioxide evolution from partitioned forest floor components. *Ecology* **54**, 406-412.

Ehleringer, J. R., and Field, C. B. (Eds.). (1993). 'Scaling physiological processes: leaf to globe.' (Academic Press, Inc.: San Diego.)

Ehleringer, J. R., Hall, A. E., and Farquhar, G. D. (Eds.). (1993). 'Stable isotopes and plant carbon-water relations.' (Academic Press, Inc.: San Diego.)

Evans, J. R. (1983). Nitrogen and photosynthesis in the flag leaf of wheat (*Triticum aestivum* L.). *Plant Physiology* **72**, 297-302.

Evans, J. R. (1986). The relationship between carbon-dioxide-limited photosynthetic rate and ribulose-1,5-bisphosphate-carboxylase content in two nuclear-cytoplasm substitution lines of wheat, and the coordination of ribulose-bisphosphate-carboxylation and electron-transport capacities. *Planta* **167**, 351-358.

Evans, J. R. (1987). The dependence of quantum yield on wavelength and growth irradiance. *Australian Journal of Plant Physiology* **14**, 69-79.

Evans, J. R., and Farquhar, G. D. (1991). Modelling canopy photosynthesis from the biochemistry of the C_3 chloroplast. In 'Modelling crop photosynthesis - from biochemistry to canopy' (Eds. K. J. Boote & R. S. Loomis) Vol. Special Publication No. 19, pp. 1-16. (CSSA: Madison.)

Evans, J. R., Sharkey, T. D., Berry, J. A., and Farquhar, G. D. (1986). Carbon isotope discrimination measured concurrently with gas exchange to investigate CO_2 diffusion in leaves of higher plants. *Australian Journal of Plant Physiology* **13**, 281-292.

Evans, J. R., von Caemmerer, S., Setchell, B. A., and Hudson, G. S. (1994). The relationship between CO_2 transfer conductance and leaf anatomy in transgenic tobacco with a reduced content of Rubisco. *Australian Journal of Plant Physiology* **21**, 475-495.

Evans, L. T., and Rawson, H. M. (1970). Photosynthesis and respiration by the flag leaf and components of the ear during grain development in wheat. *Australian Journal of Biological Science* **23**, 245-254.

Farquhar, G. D. (1978). Feedforward responses of stomata to humidity. *Australian Journal of Plant Physiology* **5**, 787-800.

Farquhar, G. D. (1989). Models of integrated photosynthesis of cells and leaves. *Philosophical Transactions of the Royal Society of London. Series B. Biological Sciences* **323**, 357-367.

Farquhar, G. D., Dubbe, D. R., and Raschke, K. (1978). Gain of the feedback loop involving carbon dioxide and stomata. *Plant Physiology* **62**, 406-412.

Farquhar, G. D., Ehleringer, J. R., and Hubick, K. T. (1989a). Carbon isotope discrimination and photosynthesis. *Annual Review of Plant Physiology and Plant Molecular Biology* **40**, 503-537.

Farquhar, G. D., Hubick, K. T., Condon, A. G., and Richards, R. A. (1989b). Carbon isotope fractionation and plant water-use efficiency. In 'Stable isotopes in ecological research' (Eds. P. W. Rundle, J. R. Ehleringer, & K. A. Nagy) Vol. 68, pp. 21-40. (Springer-Verlag: New York.)

Farquhar, G. D., O'Leary, M. H., and Berry, J. A. (1982). On the relationship between carbon isotope discrimination and the intercellular carbon dioxide concentration in leaves. *Australian Journal of Plant Physiology* **9**, 121-137.

Farquhar, G. D., and Richards, R. A. (1984). Isotopic composition of plant carbon correlates with water-use efficiency of wheat genotypes. *Australian Journal of Plant Physiology* **11**, 539-552.

Farquhar, G. D., Schulze, E.-D., and Küppers, M. (1980). Responses to humidity by stomata of *Nicotiana glauca* L. and *Corylus avellana* L. are consistent with the optimization of carbon dioxide uptake with respect to water loss. *Australian Journal of Plant Physiology* **7**, 315-327.

Farquhar, G. D., and Sharkey, T. D. (1982). Stomatal conductance and photosynthesis. *Annual Review of Plant Physiology* **33**, 317-345.

Farquhar, G. D., and von Caemmerer, S. (1982). Modelling of photosynthetic response to environmental conditions. In 'Physiological Plant Ecology II' (Eds. O. L. Lange, P. S. Nobel, C. B. Osmond, & H. Ziegler) Vol. 12B, pp. 549-587. (Springer-Verlag: Berlin.)

Farquhar, G. D., von Caemmerer, S., and Berry, J. A. (1980). A biochemical model of photosynthetic CO_2 assimilation in leaves of C_3 species. *Planta* **149**, 78-90.

Farquhar, G. D., and Wong, S. C. (1984). An empirical model of stomatal conductance. *Australian Journal of Plant Physiology* **11**, 191-210.

Field, C. (1981). Leaf age effects on the carbon gain of individual leaves in relation to microsite. In 'Components of productivity of Mediterranean regions: basic and applied aspects.' (Eds. N. S. Margaris & H. A. Mooney) pp. 41-50. (Dr. W. Junk: The Hague.)

Field, C. (1983). Allocating leaf nitrogen for the maximization of carbon gain: leaf age as a control on the allocation program. *Oecologia* **56**, 341-347.

Field, C., and Mooney, H. A. (1986). The photosynthesis - nitrogen relationship in wild plants. In 'On the economy of plant form and function.' (Ed. T. J. Givnish) pp. 25-55. (Cambridge University Press: Cambridge.)

Field, C. B., and Mooney, H. A. (1990). Leaf chamber methods for measuring photosynthesis under field conditions. *Remote Sensing Reviews* **5**, 117-139.

Finnigan, J. J., and Raupach, M. R. (1987). Transfer processes in plant canopies in relation to stomatal characteristics. In 'Stomatal function' (Eds. E. Zeiger, G. D. Farquhar, & I. R. Cowan) pp. 385-429. (Stanford University Press: Stanford, California.)

Fischer, R. A. (1979). Growth and water limitation to dryland wheat yield in Australia: a physiological framework. *Journal of the Australian Institute of Agricultural Science* **45**, 83-94.

French, R. J., and Schultz, J. E. (1984). Water use efficiency of wheat in a Mediterranean-type environment. I. The relation between yield, water use and climate. *Australian Journal of Agricultural Research* **35**, 743-764.

Garcia, R. L., Norman, J. M., and McDermitt, D. K. (1990). Measurements of canopy gas exchange using an open chamber system. *Remote Sensing Reviews* **5**, 141-162.

Garratt, J. R. (1990). The internal boundary layer - a review. *Boundary-Layer Meteorology* **50**, 171-203.

Garratt, J. R., and Hicks, B. B. (1973). Momentum, heat and water vapour transfer to and from natural and artificial surfaces. *Quarterly Journal of the Royal Meteorological Society* **99**, 680-687.

Gates, D. M. (1980). 'Biophysical ecology.' (Springer-Verlag: New York.)

Gerbaud, A., André, M., and Richaud, C. (1988). Gas exchange and nutrition patterns during the life cycle of an artificial wheat crop. *Physiologia Plantarum* **73**, 471-778.

Gimenez, C., Mitchell, V. J., and Lawlor, D. W. (1992). Regulation of photosynthetic rate of two sunflower hybrids under water stress. *Plant Physiology* **98**, 516-524.

Goudriaan, J. (1977). 'Crop micrometeorology: a simulation study.' (PUDOC: Wageningen.)

Goudriaan, J. (1986). A simple and fast numerical method for the computation of daily totals of crop photosynthesis. *Agricultural and Forest Meteorology* **38**, 257-262.

Graan, T., and Boyer, J. S. (1990). Very high CO_2 partially restores photosynthesis in sunflower at low water potentials. *Planta* **181**, 378-384.

Grace, J. (1977). 'Plant response to wind.' (Academic Press: London.)

Graham, D. (1980). Effects of light on "dark" respiration. In 'Metabolism and respiration.' (Ed. D. Davies) Vol. 2, pp. 526-579. (Academic Press: New York.)

363

Grant, R. F. (1992a). Interactions between carbon dioxide and water deficits affecting canopy photosynthesis: simulation and testing. *Crop Science* **32**, 1322-1328.

Grant, R. F. (1992b). Interactions between carbon dioxide and water deficits affecting leaf photosynthesis: simulation and testing. *Crop Science* **32**, 1313-1321.

Grantz, D. A. (1990). Plant response to atmospheric humidity. *Plant, Cell and Environment* **13**, 667-679.

Gunasekera, D., and Berkowitz, G. A. (1993). Use of transgenic plants with ribulose-1,5-bisphosphate carboxylase/oxygenase antisense DNA to evaluate the rate limitation of photosynthesis under water stress. *Plant Physiology* **103**, 629-635.

Hall, A. E., Richards, R. A., Condon, A. G., Wright, G. C., and Farquhar, G. D. (1994). Carbon isotope discrimination and plant breeding. *Plant Breeding Reviews* **4**, 81-113.

Hall, A. E., and Schulze, E.-D. (1980). Stomatal responses to environment and a possible interrelation between stomatal effects on transpiration and CO_2 assimilation. *Plant, Cell and Environment* **3**, 467-474.

Hall, A. J., Connor, D. J., and Whitfield, D. M. (1990). Root respiration during grain filling in sunflower: The effects of water stress. *Plant and Soil* **121**, 57-66.

Harley, P. C., and Tenhunen, J. D. (1991). Modeling the photosynthetic response of C_3 leaves to environmental factors. In 'Modeling crop photosynthesis - from biochemistry to canopy.' (Eds. K. J. Boote & R. S. Loomis) Vol. Special Publication No. 19, pp. 17-39. (CSSA: Madison.)

Harley, P. C., Thomas, R. B., Reynolds, J. F., and Strain, B. R. (1992). Modelling photosynthesis of cotton grown in elevated CO_2. *Plant, Cell and Environment* **15**, 271-282.

Haugen, D. A. (Ed.). (1973). 'Workshop on micrometeorology.' (American Meteorological Society: Boston, Mass.)

Held, A. A., Steduto, P., Orgaz, F., Matista, A., and Hsiao, T. C. (1990). Bowen ratio/energy balance technique for estimating crop net CO_2 assimilation, and comparison with a canopy chamber. *Theoretical and Applied Climatology* **42**, 203-213.

Herold, A. (1980). Regulation of photosynthesis by sink activity - The missing link. *New Phytologist* **86**, 131-144.

Hewitt, E. J., and Smith, T. A. (1975). 'Plant mineral nutrition.' (The English University Press: London.)

Hirose, T., and Werger, M. J. A. (1987a). Maximising daily canopy photosynthesis with respect to the leaf nitrogen allocation pattern in the canopy. *Oecologia* **72**, 520-526.

Hirose, T., and Werger, M. J. A. (1987b). Nitrogen use efficiency in instantaneous and daily photosynthesis of leaves in the canopy of a *Solidago altissima* stand. *Physiologia Plantarum* **70**, 215-222.

Hudson, G. S., Evans, J. R., von Caemmerer, S., Arvidsson, Y. B. C., and Andrews, T. J. (1992). Reduction of ribulose-1,5-bisphosphate carboxylase/oxygenase content by antisense RNA reduces photosynthesis in transgenic tobacco plants. *Plant Physiology* **98**, 294-302.

Inoue, Y., Jackson, R. D., Pinter, P. J., Jr, and Reginato, R. J. (1989). Influences of extractable soil water and vapour pressure deficit on transpiration and stomatal resistance in differentially irrigated wheat. *Japanese Journal of Crop Science* **58**, 430-437.

Iqbal, M. (1983). 'An introduction to solar radiation.' (Academic Press: Toronto.)

Itier, B., Brunet, Y., McAneney, K. J., and Lagouarde, J. P. (1994). Downwind evolution of scalar fluxes and surface resistance under conditions of local advection. Part I: A reappraisal of boundary conditions. *Agricultural and Forest Meteorology* **71**, 211-225.

Jahnke, E., and Emde, F. (1945). 'Tables of functions with formulae and curves.' (Dover Publications: New York.)

Jalota, S. K., and Prihar, S. S. (1990). Bare-soil evaporation in relation to tillage. In 'Advances in Soil Science' (Ed. B. A. Stewart) Vol. 12, pp. 187-216. (Springer Verlag: New York.)

Jarman, P. D. (1974). The diffusion of carbon dioxide and water vapour through stomata. *Journal of Experimental Botany* **25**, 927-936.

Jarvis, P. G. (1976). The interpretation of the variations in leaf water potential and stomatal conductance found in canopies in the field. *Philosophical Transactions of the Royal Society of London. Series B. Biological Sciences* **273**, 593-610.

Jarvis, P. G. (1993). Water losses of crowns, canopies and communities. In 'Water deficits: plant responses from cell to community.' (Eds. J. A. C. Smith & H. Griffiths) pp. 285-315. (BIOS Scientific Publishers: Oxford.)

Jarvis, P. G. (1995). Scaling processes and problems. *Plant, Cell and Environment* **18**, 1079-1089.

Jarvis, P. G., Edwards, W. R. N., and Talbot, H. (1981). Models of plant and crop water use. In 'Mathematics and plant physiology' (Eds. D. A. Rose & D. A. Charles-Edwards) pp. 151-194. (Academic Press: London.)

Jarvis, P. G., and McNaughton, K. G. (1986). Stomatal control of transpiration: Scaling up from leaf to region. *Advances in Ecological Research* **15**, 1-49.

Jarvis, P. G., Miranda, H. S., and Muetzelfeldt, R. I. (1985). Modelling canopy exchanges of water vapour and carbon dioxide in coniferous forest plantations. In 'The forest-atmosphere interaction.' (Eds. B. A. Hutchison & B. B. Hicks) pp. 521-542. (D. Reidel Publishing Company: Dordrecht.)

Johnson, I. R., Parsons, A. J., and Ludlow, M. M. (1989). Modelling photosynthesis in monocultures and mixtures. *Australian Journal of Plant Physiology* **16**, 501-516.

Johnson, I. R., and Thornley, J. H. M. (1984). A model of instantaneous and daily canopy photosynthesis. *Journal of Theoretical Biology.* **107**, 531-545.

Johnson, R. R., Frey, N. M., and Moss, D. N. (1974). Effect of water stress on photosynthesis and transpiration of flag leaves and spikes of barley and wheat. *Crop Science* **14**, 728-731.

Jones, F. E. (1992). 'Evaporation of water: with emphasis on applications and measurements.' (Lewis Publishers, Inc.: Chelsea, Michigan.)

Jones, H. G. (1976). Crop characteristics and the ratio between assimilation and transpiration. *Journal of Applied Ecology* **13**, 605-622.

Jones, H. G. (1992). 'Plants and microclimate.' (Cambridge University Press: Cambridge.)

Jones, H. G., and Higgs, K. H. (1989). Empirical models of the conductance of leaves in apple orchards. *Plant, Cell and Environment* **12**, 301-308.

Jordan, D. B., and Ogren, W. L. (1984). The CO_2/O_2 specificity of ribulose 1,5-bisphosphate carboxylase/oxygenase. Dependence on ribulosebisphosphate concentration, pH and temperature. *Planta* **161**, 308-313.

Kaiser, W. M. (1987). Effects of water deficit on photosynthetic capacity. *Physiologia Plantarum* **71**, 142-149.

Kanemasu, E. T., Powers, W. L., and Sij, J. W. (1974). Field chamber measurements of CO_2 flux from soil surface. *Soil Science* **118**, 233-237.

Keck, R. W., and Boyer, J. S. (1974). Chloroplast response to low leaf water potentials III. Differing inhibition of electron transport and photophosphorylation. *Plant Physiology* **53**, 474-479.

Kelliher, F. M., Leuning, R., Raupach, M. R., and Schulze, E.-D. (1995). Maximum conductances for evaporation of global vegetation types. *Agricultural and Forest Meteorology* **73**, 1-16.

Kim, J., and Verma, S. B. (1991a). Modeling canopy photosynthesis: scaling up from a leaf to canopy in a temperate grassland ecosystem. *Agricultural and Forest Meteorology* **57**, 187-208.

Kim, J., and Verma, S. B. (1991b). Modeling canopy stomatal conductance in a temperate grassland ecosystem. *Agricultural and Forest Meteorology* **55**, 149-166.

Kirschbaum, M. U. F., and Farquhar, G. D. (1984). Temperature dependence of whole-leaf photosynthesis in *Eucalyptus pauciflora* Sieb. ex Spreng. *Australian Journal of Plant Physiology* **11**, 519-538.

Kirschbaum, M. U. F., and Farquhar, G. D. (1987). Investigation of the CO_2 dependence of quantum yield and respiration in *Eucalyptus pauciflora*. *Plant Physiology* **83**, 1032-1036.

Körner, C., Scheel, J. A., and Bauer, H. (1978). Maximum leaf diffusive conductance in vascular plants. *Photosynthetica* **13**, 45-82.

Krömer, S. (1995). Respiration during photosynthesis. *Annual Review of Plant Physiology and Plant Molecular Biology* **46**, 45-70.

Kumura, A. (1968). Photosynthetic rate of soybean plant population as affected by proportion of diffuse light. *Proceedings of the Crop Science Society of Japan* **37**, 570-582.

Lang, A. R. G., Evans, G. N., and Ho, P. Y. (1974). The influence of local advection on evapotranspiration from irrigated rice in a semi-arid region. *Agricultural Meteorology* **13**, 5-13.

Lemon, E., Stewart, D. W., and Shawcroft, R. W. (1971). The sun's work in a cornfield. *Science* **164**, 371-378.

Leuning, R. (1983). Transport of gases into leaves. *Plant, Cell and Environment* **6**, 181-194.

Leuning, R. (1990). Modelling stomatal behaviour and photosynthesis of *Eucalyptus grandis*. *Australian Journal of Plant Physiology* **17**, 159-175.

Leuning, R. (1995). A critical appraisal of a combined stomatal-photosynthesis model for C_3 plants. *Plant, Cell and Environment* **18**, 339-355.

Leuning, R., Condon, A. G., Dunin, F. X., Zegelin, S., and Denmead, O. T. (1994). Rainfall interception and evaporation from soil below a wheat canopy. *Agricultural and Forest Meteorology* **67**, 221-238.

Leuning, R., Kelliher, F. M., de Pury, D. G. G., and Schulze, E.-D. (1995). Leaf nitrogen, photosynthesis, conductance and evaporation: scaling from leaves to canopies. *Plant, Cell and Environment* **18**, 1183-1200.

Lhomme, J. P. (1988). A generalized combination equation derived from a multi-layer micrometeorological model. *Boundary-Layer Meteorology* **45**, 103-115.

Lieth, H. (1973). Primary productivity: terrestrial ecosystems. *Human Ecology* **1**, 303-332.

Lloyd, J. (1991). Modelling stomatal responses to environment in *Macadamia integrifolia*. *Australian Journal of Plant Physiology* **18**, 649-660.

Lloyd, J., Grace, J., Miranda, A. C., Meir, P., Wong, S. C., Miranda, H. S., Wright, I. R., Gash, J. H. C., and McIntyre, J. (1995). A simple calibrated model of Amazon rainforest productivity based on leaf biochemical properties. *Plant, Cell and Environment* **18**, 1129-1145.

Lloyd, J., Syvertsen, J. P., Kriedemann, P. E., and Farquhar, G. D. (1992). Low conductances for CO_2 diffusion from stomata to the sites of carboxylation in leaves of woody species. *Plant, Cell and Environment* **15**, 873-899.

Lloyd, J., and Taylor, J. A. (1994). On the temperature dependence of soil respiration. *Functional Ecology* **8**, 315-323.

Lloyd, J., Trochoulias, T., and Ensbey, R. (1991). Stomatal responses and whole-tree hydraulic conductivity of orchard *Macadamia integrifolia* under irrigated and non-irrigated conditions. *Australian Journal of Plant Physiology* **18**, 661-671.

Lohammar, T., Larsson, S., Linder, S., and Falk, S. O. (1980). FAST - simulation models of gaseous exchange in Scots Pine. *Ecological Bulletins* **32**, 505-523.

Loreto, F., Harley, P. C., Di Marco, G., and Sharkey, T. D. (1992). Estimation of mesophyll conductance to CO_2 flux by three different methods. *Plant Physiology* **98**, 1437-1443.

Makino, A., Sakashita, H., Hidema, J., Mae, T., Ojima, K., and Osmond, B. (1992). Distinctive responses of ribulose-1,5-bisphosphate carboxylase and carbonic anhydrase in wheat leaves to nitrogen nutrition and their possible relationships to CO_2-transfer resistance. *Plant Physiology* **100**, 1737-1743.

Mansfield, T. A., Hetherington, A. M., and Atkinson, C. J. (1990). Some current aspects of stomatal physiology. *Annual Review of Plant Physiology and Plant Molecular Biology* **41**, 55-75.

Martin, B., and Ruiz-Torres, N. A. (1992). Effects of water-deficit stress on photosynthesis, its components and component limitations, and on water use efficiency in wheat (*Triticum aestivum* L.). *Plant Physiology* **100**, 733-739.

McCullough, D. E., and Hunt, L. A. (1993). Mature tissue and crop canopy respiratory characteristics of rye, triticale and wheat. *Annals of Botany* **72**, 269-282.

McMurtrie, R. E., Leuning, R., Thompson, W. A., and Wheeler, A. M. (1992). A model of canopy photosynthesis and water use incorporating a mechanistic formulation of leaf CO_2 exchange. *Forest Ecology Management* **52**, 261-278.

McNaughton, K. G. (1994). Effective stomatal and boundary-layer resistances of heterogenous surfaces. *Plant, Cell and Environment* **17**, 1061-1068.

McNaughton, K. G., and Jarvis, P. G. (1983). Predicting effects of vegetation changes on transpiration and evaporation. In 'Water deficits and plant growth' (Ed. T. T. Kozlowski) Vol. VII, pp. 1-47. (Academic Press: New York.)

McNaughton, K. G., and Jarvis, P. G. (1991). Effects of spatial scale on stomatal control of transpiration. *Agricultural and Forest Meteorology* **54**, 279-301.

McNaughton, K. G., and Van den Hurk, B. J. J. M. (1995). A 'Lagrangian' revision of the resistors in the two-layer model for calculating the energy budget of a plant canopy. *Boundary-Layer Meteorology* **74**, 261-288.

Meinzer, F. C., and Grantz, D. A. (1989). Stomatal control of transpiration from a developing sugarcane canopy. *Plant, Cell and Environment* **12**, 635-642.

Meister, H. P., Caldwell, M. M., Tenhunen, J. D., and Lange, O. (1987). Ecological implications of sun/shade-leaf differentiation in sclerophyllous canopies: assessment by canopy modeling. In 'Plant response to stress' (Eds. J. D. Tenhunen et al.) pp. 401-411. (Springer-Verlag: Berlin.)

Meyers, T., and Paw U, K. T. (1987a). Testing of a higher-order closure model for modeling airflow within and above plant canopies. *Agricultural and Forest Meteorology* .

Meyers, T. P., and Paw U, K. T. (1987b). Modelling the plant canopy micrometeorology with higher-order closure principles. *Agricultural and Forest Meteorology* **41**, 143-163.

Millar, B. D. (1964). Effect of local advection on evaporation rate and plant water status. *Australian Journal of Agricultural Research* **15**, 85-90.

Miller, A. J. (1990). 'Subset selection in regression.' (Chapman and Hall: London.)

Monsi, M., and Saeki, T. (1953). Über den lichtfaktor in den pflanzengesellschaften und seine bedeutung fur die stoffproduktion. *Japanese Journal of Botany* **14**, 22-52.

Monteith, J. L. (1963). Gas exchange in plant communities. In 'Environmental control of plant growth' (Ed. L. T. Evans) pp. 95-112. (Academic Press: New York.)

Monteith, J. L. (1965). Evaporation and environment. *Symposium of the Society for Experimental Biology* **19**, 205-234.

Monteith, J. L. (1973). 'Principles of environmental physics.' (Edward Arnold: London.)

Monteith, J. L. (1977). Climate and the efficiency of crop production in Britain. *Philosophical Transactions of the Royal Society of London. Series B. Biological Sciences* **281**, 277-294.

Monteith, J. L. (1995). A reinterpretation of stomatal responses to humidity. *Plant, Cell and Environment* **18**, 357-364.

Monteith, J. L., Szeicz, G., and Yabuki, K. (1964). Crop photosynthesis and the flux of carbon dioxide below the canopy. *Journal of Applied Ecology* **1**, 321-337.

Mooney, H. A., Field, C., Gulmon, S. L., and Bazzaz, F. A. (1981). Photosynthetic capacity in relation to leaf position in desert versus old-field annuals. *Oecologia* **50**, 109-112.

Morgan, J. A., LeCain, D. R., McCaig, T. N., and Quick, J. S. (1993). Gas exchange, carbon isotope discrimination, and productivity in winter wheat. *Crop Science* **33**, 178-186.

Morison, J. I. L., and Gifford, R. M. (1983). Stomatal sensitivity to carbon dioxide and humidity. *Plant Physiology* **71**, 789-796.

Mott, K. A. (1988). Do stomata respond to CO_2 concentrations other than intercellular? *Plant Physiology* **86**, 200-203.

Mott, K. A., and Parkhurst, D. F. (1991). Stomatal responses to humidity in air and helox. *Plant, Cell and Environment* **14**, 509-515.

Munro, D. S. (1989). Stomatal conductances and surface conductance modelling in a mixed wetland forest. *Agricultural and Forest Meteorology* **48**, 235-249.

Norman, J. M. (1979). Modeling the complete crop canopy. In 'Modification of the aerial environment of plants' (Eds. B. J. Barfield & J. F. Gerber) pp. 249-277. (American Society Agricultural Engineers: St.Joseph, Michigan.)

Norman, J. M. (1980). Interfacing leaf and canopy light interception models. In 'Predicting photosynthesis for ecosystem models' (Eds. J. D. Hesketh & J. W. Jones) Vol. II, pp. 49-67. (CRC Press, Inc.: Boca Raton, Florida.)

Norman, J. M. (1982). Simulation of microclimates. In 'Biometeorology in integrated pest management' (Eds. J. L. Hatfield & I. J. Thomason) pp. 65-99. (Academic Press: New York.)

Norman, J. M. (1993). Scaling processes between leaf and canopy levels. In 'Scaling physiological processes: leaf to globe.' (Eds. J. R. Ehleringer & C. B. Field) pp. 41-76. (Academic Press, Inc.: San Diego.)

Norman, J. M., Garcia, R., and Verma, S. B. (1992). Soil surface CO_2 fluxes and the carbon budget of a grassland. *Journal of Geophysical Research* **97**, 18845-18853.

Norman, J. M., and Polley, W. (1989). Canopy photosynthesis. In 'Photosynthesis' (Ed. W. R. Briggs) Vol. 8, pp. 227-241. (Alan R. Liss, Inc.: New York.)

Nulsen, R. A. (1984). Evapotranspiration of four major agricultural plant communities in the south-west of Western Australia measured with large ventilated chambers. *Agricultural Water Management* **8**, 191-202.

Passioura, J. B. (1977). Grain yield, harvest index and water use of wheat. *Journal of the Australian Institute of Agricultural Science* **43**, 117-120.

Passioura, J. B. (1979). Accountability, philosophy and plant physiology. *Search* **10**, 347-350.

Pattey, E., Rochette, P., Desjardins, R. L., and Dubé, P. A. (1991). Estimation of the net CO_2 assimilation rate of a maize (*Zea mays* L.) canopy from leaf chamber measurements. *Agricultural and Forest Meteorology* **55**, 37-57.

Paulson, C. A. (1970). The mathematical representation of wind speed and temperature profiles in the unstable atmospheric surface layer. *Journal of Applied Meteorology* **9**, 857-886.

Paw U, K. T., and Meyers, T. P. (1989). Investigations with a higher-order canopy turbulence model into mean source-sink levels and bulk canopy resistances. *Agricultural and Forest Meteorology* **47**, 259-271.

Penman, H. L. (1948). Natural evaporation from open water, bare soil and grass. *Proceedings of the Royal Society of London. Series A.* **193**, 120-145.

Penman, H. L. (1953). The physical basis of irrigation control. *Report of the 13th International Horticultural Congress.* **2**, 913-924.

Penning de Vries, F. W. T. (1972). A model for simulating transpiration of leaves with special attention to stomatal functioning. *Journal of Applied Ecology* **9**, 57-78.

Philip, J. R. (1959). The theory of local advection: I. *Journal of Meteorology* **16**, 535-547.

Philip, J. R. (1987). Advection, Evaporation, and Surface Resistance. *Irrigation Science* **8**, 101-114.

Pickering, N. B., Jones, J. W., and Boote, K. J. (1993). Evaluation of the portable chamber technique for measuring canopy gas exchange by crops. *Agricultural and Forest Meteorology* **63**, 239-254.

Pons, T. L., Schieving, F., Hirose, T., and Werger, M. J. A. (1989). Optimization of leaf nitrogen allocation for canopy photosynthesis in *Lysimachia vulgaris*. In 'Causes and consequences of variation in growth rate and productivity of higher plants.' (Eds. H. Lambers, M. L. Cambridge, H. Konings, & T. L. Pons) pp. 175-186. (SPB Academic Publishing bv: The Hague.)

Popper, K. R. (1982). 'The open universe. An argument for indeterminism.' (Hutchinson: London.)

Priestley, C. H. B., and Taylor, R. J. (1972). On the assessment of surface heat flux and evaporation using large-scale parameters. *Monthly Weather Review* **100**, 81-92.

Quick, W. P., Schurr, U., Scheibe, R., Schulze, E.-D., Rodermel, S. R., Bogorad, L., and Stitt, M. (1991). Decreased ribulose-1,5-bisphosphate carboxylase-oxygenase in transgenic tobacco transformed with "antisense" rbcS. *Planta* **183**, 542-554.

Raupach, M. R. (1989). Stand overstorey processes. *Philosophical Transactions of the Royal Society of London. Series B. Biological Sciences* **324**, 175-190.

Raupach, M. R. (1995). Vegetation-atmosphere interaction and surface conductance at leaf, canopy and regional scales. *Agricultural and Forest Meteorology* **73**, 151-179.

Raupach, M. R., Denmead, O. T., and Dunin, F. X. (1992). Challenges in linking atmospheric CO_2 concentrations to fluxes at local and regional scales. *Australian Journal of Botany* **40**, 697-716.

Raupach, M. R., and Finnigan, J. J. (1988). 'Single-layer models of evaporation from plant canopies are incorrect but useful, whereas multilayer models are correct but useless': Discuss. *Australian Journal of Plant Physiology* **15**, 715-726.

Raupach, M. R., and Finnigan, J. J. (1995). Scale issues in boundary-layer meteorology: Surface energy balances in heterogeneous terrain. *Hydrological Processes* **9**, 589-612.

Reicosky, D. C. (1990). Canopy gas exchange in the field: closed chambers. *Remote Sensing Reviews* **5**, 163-177.

Reicosky, D. C., Sharratt, B. S., Ljungkull, J. E., and Baker, D. G. (1983). Comparison of alfalfa evapotranspiration measured by a weighing lysimeter and a portable chamber. *Agricultural Meteorology* **28**, 205-211.

Reynolds, J. F., Chen, J. L., Harley, P. C., Hilbert, D. W., Dougherty, R. L., and Tenhunen, J. D. (1992). Modeling the effects of elevated CO_2 on plants: extrapolating leaf response to a canopy. *Agricultural and Forest Meteorology* **61**, 69-94.

Richards, R. A., and Condon, A. G. (1993). Challenges ahead in using carbon isotope discrimination in plant-breeding programs. In 'Stable isotopes and plant carbon-water relations.' (Eds. J. R. Ehleringer, A. E. Hall, & G. D. Farquhar) pp. 451-462. (Academic Press, Inc.: San Diego.)

Rider, N. E., Philip, J. R., and Bradley, F. E. (1963). The horizontal transport of heat and moisture - a micrometeorological study. *Quarterly Journal of the Royal Meteorological Society* **89**, 507-531.

Ritchie, J. T. (1972). Model for predicting evaporation from a row crop with incomplete cover. *Water Resources Research* **8**, 1204-1213.

Rochette, P., Desjardins, R. L., and Pattey, E. (1991). Spatial and temporal variability of soil respiration in agricultural fields. *Canadian Journal Soil Science* **71**, 189-196.

Rochette, P., Pattey, E., Desjardins, R. L., and Dwyer, L. M. (1990). Adjustment of leaf temperature measurements in Li-Cor 6200 assimilation chamber using energy balance calculations. *Agricultural and Forest Meteorology* **53**, 149-156.

Rochette, P., Pattey, E., Desjardins, R. L., Dwyer, L. M., Stewart, D. W., and Dubé, P. A. (1991). Estimation of maize (*Zea mays* L.) canopy conductance by scaling up leaf stomatal conductance. *Agricultural and Forest Meteorology* **54**, 241-261.

Ross, J. (1975). Radiative transfer in plant communities. In 'Vegetation and the atmosphere' (Ed. J. L. Monteith) Vol. 1. Principles, pp. 13-55. (Academic Press: London.)

Ross, J. (1981). 'The radiation regime and architecture of plant stands.' (Dr W.Junk Publishers: The Hague.)

372

Ross, J., and Nilson, T. (1967). The spatial orientation of leaves in crop stands and its determination. In 'Photosynthesis of productive systems' (Ed. A. A. Nichiporovich) pp. 86-99. (Academy of Sciences of the USSR: Jerusalem.)

Sadras, V. O., Hall, A. J., and Connor, D. J. (1993). Light-associated nitrogen distribution profile in flowering canopies of sunflower (*Helianthus annuus* L.) altered during grain growth. *Oecologia* **95**, 488-494.

Sage, R. F. (1994). Acclimation of photosynthesis to increasing atmospheric CO_2: the gas exchange perspective. *Photosynthesis Research* **39**, 351-368.

Sage, R. F., and Sharkey, T. D. (1987). The effect of temperature on the occurrence of O_2 and CO_2 insensitive photosynthesis in field grown plants. *Plant Physiology* **84**, 658-664.

Sands, P. J. (1995). Modelling canopy production. I. Optimal distribution of photosynthetic resources. *Australian Journal of Plant Physiology* **22**, 593-601.

Santrucková, H., and Straskraba, M. (1991). On the relationship between specific respiration activity and microbial biomass in soils. *Soil Biology and Biochemistry* **23**, 525-532.

Saugier, B., and Katerji, N. (1991). Some plant factors controlling evapotranspiration. *Agricultural and Forest Meteorology* **54**, 263-277.

Sayed, O. H., Earnshaw, M. J., and Emes, M. J. (1989). Photosynthetic responses of different varieties of wheat to high temperature. II. Effect of heat stress on photosynthetic electron transport. *Journal of Experimental Botany* **40**, 633-638.

Schieving, F., Pons, T. L., Werger, M. J. A., and Hirose, T. (1992). The vertical distribution of nitrogen and photosynthetic activity at different plant densities in *Carex acutiformis*. *Plant and Soil* **14**, 9-17.

Schlesinger, W. H. (1977). Carbon balance in terrestrial detritus. *Annual Review of Ecology and Systematics*. **8**, 51-81.

Schuepp, P. H., Leclerc, M. Y., MacPherson, J. I., and Desjardins, R. L. (1990). Footprint prediction of scalar fluxes from analytical solutions of the diffusion equation. *Boundary-Layer Meteorology* **50**, 355-373.

Schulze, E.-D. (1986). Carbon dioxide and water vapor exchange in response to drought in the atmosphere and in the soil. *Annual Review of Plant Physiology* **37**, 247-274.

Sellers, P. J., Berry, J. A., Collatz, G. J., Field, C. B., and Hall, F. G. (1992). Canopy reflectance, photosynthesis, and transpiration. III. A reanalysis using improved leaf models and a new canopy integration scheme. *Remote Sensing of Environment* **42**, 187-216.

Sharkey, T. D. (1985). O_2-insensitive photosynthesis in C_3 plants. Its occurrence and a possible explanation. *Plant Physiology* **78**, 71-75.

Sharkey, T. D., and Raschke, K. (1981). Separation and measurement of direct and indirect effects of light on stomata. *Plant Physiology* **68**, 33-40.

Shuttleworth, W. J. (1976). A one-dimensional theoretical description of the vegetation-atmosphere interaction. *Boundary-Layer Meteorology* **10**, 273-302.

Shuttleworth, W. J., and Gurney, R. J. (1990). The theoretical relationship between foliage temperature and canopy resistance in sparse crops. *Quarterly Journal of the Royal Meteorological Society* **116**, 497-519.

Shuttleworth, W. J., and Wallace, J. S. (1985). Evaporation from sparse crops - an energy combination theory. *Quarterly Journal of the Royal Meteorological Society* **111**, 839-855.

Sinclair, T. R., Murphy, C. E., and Knoerr, K. R. (1976). Development and evaluation of simplified models for simulating canopy photosynthesis and transpiration. *Journal of Applied Ecology* **13**, 813-829.

Smolander, H. (1984). Measurement of fluctuating irradiance in field studies of photosynthesis. *Acta Forestalia Fennica* **187**, 1-56.

Snedecor, G. W., and Cochran, W. G. (1980). 'Statistical methods.' (The Iowa State University Press: Ames, Iowa, U.S.A.)

Spiertz, J. H. J., and Ellen, J. (1978). Effects of nitrogen on crop development and grain growth of winter wheat in relation to assimilation and utilization of assimilates and nutrients. *Netherlands Journal of Agricultural Science* **26**, 210-231.

Stewart, B. A., and Nielsen, D. R. (Eds.). (1990). 'Irrigation of Agricultural Crops.' (ASA: Madison, Wisconsin.)

Stewart, J. B. (1983). A discussion of the relationships between the principal forms of the combination equation for estimating crop evaporation. *Agricultural Meteorology* **30**, 111-127.

Stitt, M., and Schulze, D. (1994). Does Rubisco control the rate of photosynthesis and plant growth? An exercise in molecular ecophysiology. *Plant, Cell and Environment* **17**, 465-487.

Stull, R. B. (1988). 'An introduction to boundary layer meteorology.' (Kluwer Academic Publishers: Dordrecht.)

Sud, Y. C., Sellers, P. J., Mintz, Y., Chou, M. D., Walker, G. K., and Smithe, W. E. (1990). Influence of the biosphere on the global circulation and hydrological cycle - a GCM simulation experiment. *Agricultural and Forest Meteorology* **52**, 133-180.

Tan, C. S., and Black, T. A. (1976). Factors affecting the canopy resistance of a Douglas-fir forest. *Boundary-Layer Meteorology* **10**, 475-488.

Tanner, C. B., and Sinclair, T. R. (1983). Efficient water use in crop production: Research or re-search? In 'Limitations to efficient water use in crop production' (Eds. H. M. Taylor, W. R. Jordan, & T. R. Sinclair) pp. 1-17. (ASA: Madison.)

Terashima, I. (1992). Anatomy of non-uniform leaf photosynthesis. *Photosynthesis Research* **31**, 195-212.

Terashima, I., Wong, S. C., Osmond, C. B., and Farquhar, G. D. (1988). Characterisation of non-uniform photosynthesis induced by abscisic acid in leaves having different mesophyll anatomies. *Plant and Cell Physiology* **29**, 385-394.

Thom, A. S. (1971). *Quarterly Journal of the Royal Meteorological Society* **97**, 414-428.

Thom, A. S. (1972). Momentum, mass and heat exchange of vegetation. *Quarterly Journal of the Royal Meteorological Society* **98**, 124-134.

Thom, A. S. (1975). Momentum, mass and heat exchange of plant communities. In 'Vegetation and the atmosphere. Vol. 1. Principals' (Ed. J. L. Monteith) pp. 57-109. (Academic Press: London.)

Thomas, B. A., and Spicer, R. A. (1987). 'The evolution and palaeobiology of land plants.' (Croom Helm: London.)

Thornley, J. H. M. (1976). 'Mathematical models in plant physiology.' (Academic Press: London.)

Thorpe, M. R., Warrit, B., and Landsberg, J. J. (1980). Responses of apple leaf stomata: a model for single leaves and a whole tree. *Plant, Cell and Environment* **3**, 23-27.

Valentini, R., Scarascia Mugnozza, G. E., De Angelis, P., and Bimbi, R. (1991). An experimental test of the eddy correlation technique over a Mediterranean macchia canopy. *Plant, Cell and Environment* **14**, 987-994.

Van den Hurk, B. J. J. M., and McNaughton, K. G. (1995). Implementation of near-field dispersion in a simple two-layer surface resistance model. *Journal of Hydrology* **166**, 293-311.

van Herwaarden, A. (1995) 'Carbon, nitrogen and water dynamics in dryland wheat, with particular reference to haying-off.'. Ph.D. Thesis, Australian National University.

Verma, S. B. (1989). Aerodynamic resistances to transfers of heat, mass and momentum. In 'Estimation of areal evapotranspiration' (Eds. T. A. Black, D. L. Spittlehouse, M. D. Novak, & D. T. Price) Vol. 177, pp. 13-20. (IAHS: Wallingford.)

von Caemmerer, S., and Evans, J. R. (1991). Determination of the average partial pressure of CO_2 in chloroplasts from leaves of several C_3 plants. *Australian Journal of Plant Physiology* **18**, 287-305.

von Caemmerer, S., Evans, J. R., Hudson, G. S., and Andrews, T. J. (1994). The kinetics of ribulose-1,5-bisphosphate carboxylase/oxygenase in vivo inferred from measurements of photosynthesis in leaves of transgenic tobacco. *Planta* **195**, 88-97.

von Caemmerer, S., and Farquhar, G. D. (1981). Some relationships between the biochemistry of photosynthesis and the gas exchange of leaves. *Planta* **153**, 376-387.

Wang, Y. P., and Jarvis, P. G. (1990). Description and validation of an array model - MAESTRO. *Agricultural and Forest Meteorology* **51**, 257-280.

Wang, Y. P., and Jarvis, P. G. (1993). Influence of shoot structure on the photosynthesis of Sitka spruce (*Picea sitchensis*). *Functional Ecology* **7**, 433-451.

Warren Wilson, J. (1960). Inclined point quadrats. *New Phytologist* **59**, 1-8.

Watanabe, N., Evans, J. R., and Chow, W. S. (1994). Changes in the photosynthetic properties of Australian wheat cultivars over the last century. *Australian Journal of Plant Physiology* **21**, 169-183.

Webb, E. K., Pearman, G. I., and Leuning, R. (1980). Correction of flux measurements for density effects due to heat and water vapour transfer. *Quarterly Journal of the Royal Meteorological Society* **106**, 85-100.

Weiss, A., and Norman, J. M. (1985). Partitioning solar radiation into direct and diffuse, visible and near-infrared components. *Agricultural and Forest Meteorology* **34**, 205-213.

Wesely, M. L., Lenschow, D. H., and Denmead, O. T. (1989). Flux measurement techniques. In 'Global tropospheric chemistry: Chemical fluxes in the global atmosphere' (Eds. D. H. Lenschow & B. B. Hicks) pp. 31-46. (National Centre for Atmospheric Research: Boulder, CO.)

Whisler, F. D., Acock, B., Baker, D. N., Fye, R. E., Hodges, H. F., Lambert, J. R., Lemmon, H. E., McKinion, J. M., and Reddy, V. R. (1986). Crop simulation models in agronomic systems. *Advances in Agronomy* **40**, 141-208.

Whitehead, D., Jarvis, P. G., and Waring, R. H. (1984). Stomatal conductance, transpiration, and resistance to water uptake in a *Pinus sylvestris* spacing experiment. *Canadian Journal Forest Research* **14**, 692-700.

Whitehead, D., Okali, D. U. U., and Fasehun, F. E. (1981). Stomatal response to environmental variables in two tropical forest species during the dry season in Nigeria. *Journal of Applied Ecology* **18**, 571-587.

Wong, S. C. (1979). Elevated atmospheric partial pressure of CO_2 and plant growth. I. Interactions of nitrogen nutrition and photosynthetic capacity in C_3 and C_4 plants. *Oecologia* **44**, 68-74.

Wong, S. C., Cowan, I. R., and Farquhar, G. D. (1978). Leaf conductance in relation to assimilation in *Eucalyptus pauciflora* Sieb. ex Spreng: Influence of irradiance and partial pressure of carbon dioxide. *Plant Physiology* **62**, 670-674.

Wong, S. C., Cowan, I. R., and Farquhar, G. D. (1979). Stomatal conductance correlates with photosynthetic capacity. *Nature* **282**, 424-426.

Wong, S. C., Cowan, I. R., and Farquhar, G. D. (1985a). Leaf conductance in relation to rate of CO_2 assimilation. I. Influence of nitrogen nutrition, phosphorus nutrition, photon flux density and ambient partial pressure of CO_2 during ontogeny. *Plant Physiology* **78**, 821-825.

Wong, S. C., Cowan, I. R., and Farquhar, G. D. (1985b). Leaf conductance in relation to rate of CO_2 assimilation. II. Effects of short-term exposures to different photon flux densities. *Plant Physiology* **78**, 826-829.

Wong, S. C., Cowan, I. R., and Farquhar, G. D. (1985c). Leaf conductance in relation to rate of CO_2 assimilation. III. Influences of water stress and photoinhibition. *Plant Physiology* **78**, 830-834.

Wong, S. C., and Dunin, F. X. (1987). Photosynthesis and transpiration of trees in a eucalypt forest stand: CO_2, light and humidity responses. *Australian Journal of Plant Physiology* **14**, 619-632.

Woodrow, I. E., and Berry, J. A. (1988). Enzymatic regulation of photosynthetic CO_2 fixation in C_3 plants. *Annual Review of Plant Physiology and Plant Molecular Biology* **39**, 533-594.

Woodward, F. I. (1987). 'Climate and plant distribution.' (Cambridge University Press: Cambridge.)

Wright, G. C., Hubick, K. T., and Farquhar, G. D. (1988). Discrimination in carbon isotopes of leaves correlates with water-use efficiency of field-grown peanut cultivars. *Australian Journal of Plant Physiology* **15**, 815-825.

Wright, G. C., Hubick, K. T., Farquhar, G. D., and Nageswara Rao, R. C. (1993). Genetic and environmental variation in transpiration efficiency and its correlation with carbon isotope discrimination and specific leaf area in peanut. In 'Stable isotopes and plant carbon-water relations.' (Eds. J. R. Ehleringer, A. E. Hall, & G. D. Farquhar) pp. 247-267. (Academic Press, Inc.: San Diego.)

Wu, R. L. (1993). Simulated optimal structure of a photosynthetic system: implication for the breeding of forest crop ideotype. *Canadian Journal Forest Research* **23**, 1631-1638.

Wullschleger, S. D. (1993). Biochemical limitations to carbon assimilation in C_3 plants - A retrospective analysis of the A/C_i curves from 109 species. *Journal of Experimental Botany* **44**, 907-920.

Zegelin, S. J., White, I., and Russell, G. F. (1992). A critique of the time domain reflectometry technique for determining field soil water content. In 'Advances in measurement of soil physical properties: bringing theory into practice.' (Eds. G. C. Topp, W. D. Reynolds, & R. E. Green) (Soil Science Society of America: Madison, Wisconsin.)

Zeiger, E., Farquhar, G. D., and Cowan, I. R. (Eds.). (1987). 'Stomatal function.' (Stanford University Press: Stanford, California.)